

Ultra-Wideband Ranging for Low-Complexity Indoor Positioning Applications

Ultra-Wideband Ranging for Low-Complexity Indoor Positioning Applications

PROEFSCHRIFT

ter verkrijging van de graad van doctor
aan de Technische Universiteit Delft;
op gezag van de Rector Magnificus prof.ir. K.C.A.M. Luyben;
voorzitter van het College voor Promoties
in het openbaar te verdedigen op maandag 17 januari 2011 om 10.00
uur

door

Giovanni BELLUSCI

Laurea di Dottore in Ingegneria delle Telecomunicazioni
Università degli Studi di Pisa
geboren te Terlizzi, Italië.

Dit proefschrift is goedgekeurd door de promotor:

Prof.dr.ir. I.G.M.M. Niemegeers

Samenstelling promotiecommissie :

Rector Magnificus	voorzitter
Prof.dr.ir. I.G.M.M. Niemegeers	Technische Universiteit Delft, promotor
Dr.ir. G.J.M. Janssen	Technische Universiteit Delft, copromotor
Prof.dr. Z. Tian	Michigan Technological University
Prof.dr.ir. P.G.M. Baltus	Technische Universiteit Eindhoven
Prof.dr.ir. A.J. van der Veen	Technische Universiteit Delft
Prof.dr. A. Yarovoy	Technische Universiteit Delft
Dr.ir. M.J. Bentum	Technische Universiteit Twente

Copyright © 2011 by Giovanni Bellusci

All rights reserved. No part of the material protected by this copyright notice may be reproduced or utilized in any form or by any means, electronic or mechanical, including photocopying, recording or by any information storage and retrieval system, without the prior permission of the author.

ISBN: 978-94-6108-133-9

Author e-mail: bellusci.giovanni@gmail.com

*To my Parents, Rocco and Lucia,
for their Generosity and Love*

Summary

Recently, indoor positioning is attracting considerable attention from both research and industry. Logistics, health-care applications, search and rescue, military services, tracking of objects and people, gaming and entertainment are a few examples of applications which can benefit from having precise localization information. However, in indoor environments, traditional services provided by e.g. GPS usually are not available, unreliable or inaccurate. For this reason, alternative solutions need to be developed.

In the last years, Ultra-Wideband (UWB) technology has been identified as an ideal candidate to provide positioning information in these environments. In fact, the use of sub-nanosecond duration UWB pulses with several GHz of bandwidth offers the unique possibility of distinguishing the different multipath components which compose the received signal and of accurately estimating its Time of Arrival (TOA), which contains the relevant information for positioning. In this way, centimeter level accuracy can be achieved, even in multipath rich indoor environments. However, before being able to fully exploit the potentials of this technology, some issues need first to be addressed:

- UWB signals exhibit complex propagation phenomena. Due to the large bandwidth of these systems, different frequency components show significantly different interactions with the environment. For this reason, new propagation models describing and predicting the interaction of the traveling waves with the surrounding environment are of absolute importance, since the wireless channel is the first aspect which determines performance

limits. However, available UWB channel models were developed with communications applications in mind, and they lack of relevant information for positioning.

- Similar considerations hold for most of the proposed TOA estimation algorithms, which are often considered a simple extension of well known channel impulse response estimation approaches developed for communication applications, in which the TOA of the received signal comes as a byproduct. These approaches are inherently suboptimal, since they do not address the unique properties of UWB and do not focus on the relevant information which needs to be retrieved; in addition, they can often be hardly implemented, since they have hardware or signal processing requirements far from what is currently available in the market.

Following these main motivations, the original contributions of this thesis can be divided in two parts. In the first part, a new channel characterization for ranging applications has been provided. The use of the proposed model is manifold. First, the concept of statistics based ranging is developed; it is shown that this method is able to exploit the unique properties of UWB and to achieve an accuracy of a few decimeters in Line of Sight (LOS), significantly better than traditional signal strength, but with similar system complexity. Then, a model for the range error achieved with TOA is provided and its relationship with relevant parameters, like system bandwidth and distance between transmitter and receiver, is investigated. It is shown that model knowledge allows to significantly improve the final positioning accuracy using weighted least squares approaches. Finally, A LOS/NLOS detection strategy is developed and validated on the collected data. In the second part of this thesis, a new low-complexity TOA estimation concept and principle of implementation is proposed. This solution capitalizes on the unique properties of pulsed based UWB transmissions and it is able to achieve centimeter level accuracy with sampling rates in the order of a few tens of MHz, avoiding the main limitations which currently make it difficult to practically build UWB positioning systems. In this context, a framework to evaluate impairments due to narrowband interference on the proposed algorithm has been developed; the suggested analysis is based on the first threshold crossing probability evaluation for Gaussian processes and time varying boundaries. It is shown that the proposed strategy exhibits a fair resistance to interference, allowing the system to operate with other licensed devices sharing the same bandwidth.

Giovanni Bellusci

April 2010



Contents

Summary	i
1 Introduction	1
1.1 Indoor positioning	1
1.2 Ultra-Wideband communications	2
1.2.1 History of ultra-wideband	3
1.2.2 Ultra-wideband properties	5
1.2.3 Ultra-wideband for positioning applications	8
1.3 Research context	12
1.4 Related available work	13
1.4.1 Ultra-wideband indoor propagation characterization	13
1.4.2 Ultra-wideband ranging	17
1.5 Motivations	21
1.6 "HERE: indoor positioning based on UWB radio signals" research project	23
1.7 Summary of the main contributions	24
1.8 Outline of the thesis	25
Bibliography	25
2 UWB Channel Measurements and Characterization for Statistics Based Ranging	33
2.1 The UWB measurement set-up	35

2.1.1	Pulse generator	35
2.1.2	Sampler unit and sampling oscilloscope	36
2.1.3	Reference channel	38
2.1.4	Antennas	38
2.2	Channel measurements motivations	39
2.2.1	Statistics for ranging applications	39
2.3	Fading characterization and choice of measurement procedure	40
2.3.1	Measurement locations	41
2.4	Data analysis and processing	42
2.4.1	Inverse filtering deconvolution	43
2.4.2	First peak detection and threshold setting	44
2.4.3	Bandwidth dependency	45
2.5	Modeling results for the full bandwidth	46
2.5.1	Path-loss for the total signal power	46
2.5.2	Statistical characterization of S_{TP} for the full bandwidth	46
2.5.3	Path-loss for the first path power	48
2.5.4	Statistical characterization of S_{FP} for the full bandwidth	49
2.6	Modeling results motivations	51
2.6.1	Nakagami-lognormal distribution for TP	52
2.6.2	Double Gaussian distribution for FP in LOS propagation	55
2.6.3	Double Nakagami-lognormal distribution for FP in NLOS propagation	57
2.7	Bandwidth dependency of path-loss	58
2.7.1	Bandwidth dependency of n_{TP}	59
2.7.2	Bandwidth dependency of n_{FP}	60
2.7.3	Bandwidth dependency of fading - LOS	60
2.7.4	Bandwidth dependency of fading - NLOS	64
2.7.5	Correlation between $S_{TP,0}$ and $S_{FP,0}$	65
2.8	Parameters' estimation dependency on the number of measurements	67
2.8.1	Dependency of \hat{n} on N_m	68
2.8.2	Dependency of $\hat{\sigma}_S$ on N_m	70
2.9	Chapter summary	72
	Bibliography	72

3	Statistics Based UWB Ranging	75
3.1	Range Estimation with TP and FP	75
3.2	LOS propagation	76
3.2.1	Unbiased range estimation for the full bandwidth	77
3.2.2	Environment differentiation and identification	81
3.2.3	Range estimation for smaller B_{if}	86
3.3	NLOS propagation	89
3.3.1	Unbiased range estimation	89
3.3.2	Best linear unbiased estimation	90
3.3.3	Standard deviation analytical evaluation	91
3.4	Effect of practical limitations on range estimation accuracy	91
3.4.1	Effect of limited number of measurements on range estimation accuracy	91
3.4.2	Antennas directional gain dependency	93
3.5	Weighted Least Squares Positioning	94
3.5.1	LOS positioning performance	96
3.5.2	LOS-NLOS and NLOS positioning performance	97
3.6	Chapter summary	98
	Bibliography	101
4	TOA Based Range Error Evaluation, Modeling, and Applications	103
4.1	TOA estimation and signal processing	104
4.2	Range error results, and modeling	105
4.2.1	Modeling of $m_{TOA}(B_{if}, d)$	106
4.2.2	Modeling of $S_{TOA}(B_{if}, d)$	107
4.3	LOS/NLOS detection	111
4.3.1	Maximum a posteriori LOS/NLOS decision rule	113
4.3.2	Analytical Evaluation of the MAP Performance	115
4.4	Weighted least squares positioning	118
4.5	Chapter summary	119
	Bibliography	120
5	Low-Complexity TOA Estimation	123
5.1	Signal model	125
5.2	TOA estimation	126

5.2.1	Receiver implementation	127
5.2.2	TOA estimation strategy	132
5.2.3	Performance evaluation - early false alarm	133
5.2.4	Performance evaluation - missed detection	136
5.2.5	Oscillator inaccuracies	139
5.3	Coarse acquisition	143
5.3.1	Coarse acquisition performance evaluation	145
5.4	Link Budget Evaluation	150
5.5	Chapter summary	152
	Bibliography	153
6	Narrowband Interference Impairments on Low-Complexity TOA Estimation	157
6.1	Narrowband interference signal model	159
6.2	NBI impairments - TOA estimation	159
6.2.1	Early False Alarm	159
6.2.2	Missed Detection	162
6.2.3	TOA performance evaluation under NBI	162
6.3	NBI impairments - coarse acquisition	163
6.3.1	Statistical characterization of the signal \times interference term	165
6.3.2	Probability of coarse acquisition under NBI	167
6.4	Chapter summary	168
	Bibliography	170
7	Conclusions and Recommendations	173
7.1	Conclusions	174
7.1.1	Channel characterization for positioning applications based on ranging	174
7.1.2	Performance evaluation of ranging based positioning	175
7.1.3	Low complexity TOA estimation receiver architecture and signal processing	178
7.1.4	impairments due to narrowband interference	179
7.2	Recommendations for future research	180
	List of Abbreviations	183

List of symbols	185
Publications by the Author	191
Samenvatting (Summary in Dutch)	195
Acknowledgments	199
Curriculum Vitae	201

Chapter 1

Introduction

This thesis focuses on *Ultra-Wideband* wireless signals for *positioning* applications in *indoor* environments. In the following, it will be assumed that the reader of this manuscript is familiar with the general theory of wireless communications. However, despite the fact that the use of ultra-wideband is gaining considerable interest both from research and from industry, we believe that not all the readers might have this specific background knowledge. For this reason, this chapter provides an overview of the main motivations, requirements and challenges which arise when using UWB signals for indoor positioning applications, prior to introduce the main original contributions and outline of this thesis.

1.1 Indoor positioning

The last decades have been characterized by a continuous increase of interest towards positioning information. The development of the Global Positioning System (GPS) has found a large number of applications, first for military operations (e.g. in weapon guidance, target tracking, attitude determination, aircraft stabilization), then for civilian uses. The dramatic decrease of costs and size of the most modern GPS receivers has allowed this technology to enter in the consumer electronics market, and this system is currently widely used for personal navigation. However, while GPS works in a satisfactory way in open space, it presents significant problems inside buildings in which the actual accuracy, typically between some tens and several hundreds of meters, is significantly lower than that

achievable in open space (in the order of a few meters). Indoor environments in fact pose unique challenges for the GPS system, due to their particular properties. The complex physical characteristics of these environments, and the presence of walls, obstructions, and heterogeneous obstacles cause severe multipath propagation. In fact, the received signal is typically composed by tens or hundreds or relevant paths very closely spaced to each other, due to reflections, scattering and diffraction of the signals transmitted from the satellites with the surrounding environment. Since the bandwidth of the GPS signal for civilian applications is only approximately 2 MHz, the different multipath components are typically completely overlapping each other¹, and it appears extremely problematic to accurately detect the Time of Arrival (TOA) of the *direct* path coming from the satellites, which contains the useful information for positioning determination, especially considering that the direct path often is not the strongest one. On the other hand, it is particularly in indoor environments that it would be possible to significantly profit by the availability of high accurate position information. It is not only the smaller environmental scale, compared to outdoor, which demands for an accordingly higher accuracy, but also the potentially larger number of possible applications which can benefit from accurate *indoor* positioning information to motivate the interest towards this issue. Besides the traditional seamless indoor-outdoor personal navigation, which has been the first application to require solutions to the "indoor positioning bottleneck" experienced by GPS, many other emerging areas are in fact currently demanding for sub-meter positioning service, and the rhetorical sentence: "It is your imagination which limits possible applications" perfectly reflects a lively and growing area which is identifying today emerging uses in: wireless sensor networks, health-care, logistics, location based services, automation, gaming, entertainment.

1.2 Ultra-Wideband communications

While particular applications, especially when not particularly demanding in terms of accuracy, can benefit from the integration of GPS with other technologies (e.g. inertial sensors) which can allow to mitigate the poor performance of traditional satellite navigation inside buildings, it has been recognized that the

¹In fact, the capability of resolving multipath components is directly related to the signal bandwidth; for example, using 2 MHz of bandwidth (B) provides a multipath resolvability capability of approximately $c/B = 150$ m, being c the speed of light in air.

most effective and reliable way to provide highly accurate positioning information in indoor environments is to rely on alternative wireless systems with larger bandwidths, since this directly affects the multipath resolvability capability. The technology which is able to provide the perfect answer to this requirement is represented by Ultra-Wideband (UWB) wireless signals, due to its unique and unmatched characteristics [1]-[8].

1.2.1 History of ultra-wideband

In its more general meaning, the history of ultra-wideband is as old as that of wireless communications and finds its birth in the late 1890s, in the spark gap transmission experiments performed by Marconi and Hertz. Thus, we can say that the very first wireless communication technique was based on the emission of short time domain pulses with very large bandwidth. Technological limitations however pushed the research towards the development of transmissions employing narrowband signals modulated with a carrier frequency typically some orders of magnitude larger than the signal bandwidth itself. Therefore, the attractive promise of Shannon in its pioneering work on the channel capacity [9], to make it potentially possible to achieve reliable and very high data rate transmission, even with extremely low Signal to Noise Ratio (SNR), provided a large signal bandwidth is used, found an insurmountable obstacle in the practical possibility of building electronic components able to properly work in large portions of the spectrum. It was only in the 1960s that baseband sub-nanosecond pulses found their applications for radar devices, due to their accurate spatial resolution, and because of the properties of low frequency components to penetrate objects. A few years later, in 1978, Bennet and Ross [1], when describing the applications of baseband radars, also proposed to use pulse techniques as the solution "to the problem of developing a short-range wireless communications link ... potentially providing the means for wireless transmission without licensing", showing a visionary intuition of what would have happened at the end of that century. However, the advances in digital signal processing and the consequent determinant rule of Analog to Digital Converters (ADC) in modern telecommunication systems, together with the increasing awareness of the radio spectrum as a "scarce" resource, made most of their contemporary engineers skeptic towards "ultra-wideband" pulse based wireless communication systems.

After a period of silence which lasted two decades, from the end of 20th century the first related works of Win and Scholtz [3]-[6], which appeared contemporary

to the rule making opened by the Federal Communications Commissions (FCC) for ultra-wideband communications [8], gave a huge boost to this technology, and already in the first years of the new century UWB was listed among the most impacting emerging communication technologies. In a handful of years, UWB gained the interest of both research and industry, as no other technology was able to do before. The unique potentials of UWB, with its premises to become a universal physical layer technique able to provide flexibility, high data rates, spectral efficiency, robustness towards interference, very low power transmission, accurate positioning capabilities, made this technology extremely attractive from a commercial point of view. At the same time, it also found the favor of the scientific world, always starving for research challenges to investigate [3]-[16]. UWB, in fact, required the scientific community to reconsider the common vision of the wireless transmission system. The use of a bandwidth: 1) of some GHz and 2) in the same order of magnitude as the central frequency, immediately appeared as a uniquely stimulating problem with huge implications in the overall system model, design, and principle of operation. The very large fractional bandwidth in fact required to reconsider traditional (narrowband or wideband) wireless channel models, since the different frequency components are effected in a significantly different way from the interaction with the propagation medium. Similar issues had to be addressed by antenna design engineers. From a system architecture point of view, the biggest challenge immediately appeared to be at the receiver side. On one hand, the huge signal bandwidth, allowing to resolve tens to hundreds of relevant multipath components, made the implementation of traditional rake receiver architectures extremely critical, not only for the number of branches required but also for the sub-nanosecond timing alignment needed for the replica in each branch. On the other hand, the maturity reached by digital signal processing techniques in traditional wireless communications could not be directly exploited due to the critical bottleneck of the analog to digital conversion step, which should be performed at several GHz rates to be able to rely on Nyquist based solutions. As a result of this stimulating context, while most of the big multinational companies immediately started to invest in a potentially impacting technology and several small and medium-sized enterprises focused on the development of wireless communication systems based on the impulse radio concept, several thousands of scientific papers related to UWB communications and some dedicated conferences appeared in the academic world.

This ideal situation, however, lasted for only a few years. The IEEE 802.15.3a

standardization group [17], after some years dedicated to the attempt to provide an UWB based physical layer enhancement to the IEEE 802.15.3 standard for high data rate applications, did not succeed in coming to an agreement choosing between two technology proposals, (multi-band orthogonal frequency division multiplexing and direct sequence UWB), and it was withdrawn in January 2006. At the same time, the optimistic promises which accompanied the birth of the modern concept of UWB, were not maintained. On one hand, effective performance in realistic conditions (e.g. accounting for power emission requirements and consequently link budget limitations, interference issues, multipath propagation effects) were far from the theoretical limits claimed in the early stage of investigation of this technology, and too close to or even worse than other competitor technologies already commercially available. On the other hand, significant implementation challenges were still unsolved and delayed the introduction in the market of UWB systems.

After a period of skepticism due to the failure of the original vision of UWB as a universal physical layer transmission technique, today a more mature and conscious understanding of the unique properties of this technology has identified two areas of use in which UWB can have a determinant rule: the first in very short range, very high data rates communications (e.g. wireless USB), the second, in localization applications. As motivated in the previous section, this thesis will focus on the potentials, challenges and open research issues for UWB when used for indoor positioning applications.

1.2.2 Ultra-wideband properties

Today there is not a univocal definition of UWB. On the contrary, different countries have proposed, at different times, different definitions of UWB for civilian uses. As mentioned in the previous section, the first official document providing a regulatory body for UWB transmissions was released by the FCC, the US frequency regulator, in its first report and order dated February 2002 [8]. Some years later, similar definitions were started to be adopted in other continents. These rules present some variations among each other, especially with respect to the bandwidth in which UWB transmissions are allowed in the different countries; however, the basic motivations and described principles of operation are similar. For this reason, in the following only the FCC regulations will be shortly discussed; consequently, when in this thesis it is necessary to refer to regulatory issues, we will only consider these rules. The reason for this choice is twofold; first, FCC

rules represent the regulatory body most often used and accepted in the scientific community; second and direct cause of the previous point, FCC provided regulations already in the early stage of UWB studies, while e.g. in Europe, the final documents provided by CEPT were issued only in April 2009. While the choice of some numerical values introduced in this thesis might require to be adapted to fit other regulatory bodies (e.g. the European ones [18]), the general validity of the proposed work continues to hold.

FCC definition of ultra-wideband

The great difference between UWB and previous wireless technologies is first of all reflected in the unique peculiarities of its definition. In fact, the original distinguishing feature for the deployment of UWB radios was their potential ability to transmit in an *unlicensed* way very *low power* over an *ultra wide* portion of the spectrum, allowing this technology to coexist with current and future licensed wireless systems. For this reason, the FCC does not directly specify any particular signal format or modulation technique for UWB; on the contrary, it strictly specifies the spectral and emission properties for this technology.

UWB is defined as any wireless system with bandwidth $B \geq 500$ MHz, or a fractional bandwidth $B_f \triangleq 2B/(f_H - f_L) \geq 0.2$, where f_H and f_L are the upper and lower frequencies of the -10 dB emission points respectively [8]. For communication and positioning applications, the operating band is limited in the portion of the spectrum between 3.1 and 10.6 GHz, provided that the emissions satisfy given limitations. These limitations have been defined with the pulse based ultra-wideband approach in mind, and distinguish between peak and average power:

- $P_{meas}^{pk} \leq 0$ dBm in any 50 MHz signal bandwidth
- $P_{meas}^{av} \leq -41.3$ dBm in any 1 MHz signal bandwidth

where P_{meas}^{pk} and P_{meas}^{av} are the peak and average measured EIRP power, respectively. As an example, Fig. 1.1 shows the FCC mask for the *average measured* power P_{meas}^{av} .

Power limitation implications

At first sight, the FCC power limitations might appear rather strict and justify the original idea of UWB, in which the transmitted signal is completely hidden

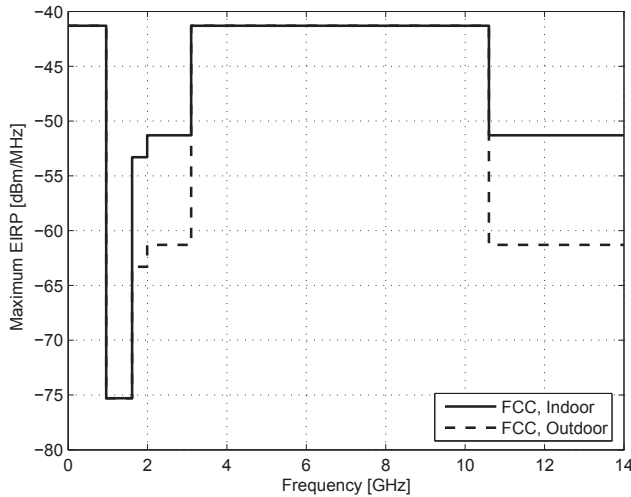


Figure 1.1: FCC mask for the average measured power, for UWB emissions in US.

by noise, to meet the emission requirements and to avoid interference to other systems. This prejudice has been common in the research community and has often driven the attention towards pulse repetition based transmission schemes, which have often been considered a necessary strategy in order to increase the effective SNR at the receiver by coherent processing of the received train of pulses. In this way however, the demand for very high sampling rates required to achieve combining gain and for very accurate (at a very small fraction of nanosecond level) timing need to be addressed, making most of the proposed solutions far from the state of the art of available technology. On the other hand, the FCC does not directly specify any limit on the effective power which can be transmitted during a single pulse; on the contrary, it provides limits on the peak and average power when *measured* with a spectrum analyzer with a resolution bandwidth B_R much smaller than the UWB signal bandwidth. While in general the relationship between the power P_T which can be effectively transmitted during a single pulse and the constraints on peak and average measured power given by the FCC depends on the different system parameters (e.g. pulse spectral characteristics and repetition frequency), it is relatively easy to provide an approximate evaluation of the *maximum* allowed transmitted power during a single pulse P_T^{MAX} , in the asymptotic condition in which the pulse repetition frequency is much smaller than the resolution bandwidth of the spectrum analyzer used for compliance

measurements. This is a particularly interesting case for positioning applications, which often use very low rate transmission schemes. Under this hypothesis, the emissions are only limited by the constraint on the peak power; the relationship between P_T and the peak measured power P_{meas}^{pk} , can be simply evaluated as [19]:

$$P_T = P_{meas}^{pk} \left(\frac{B}{B_R} \right)^2 \quad (1.1)$$

It is evident that a maximum power in the order of a watt can be transmitted in a single UWB pulse, depending on the particular signal bandwidth used (e.g., for $B = 3$ GHz, $P_T^{MAX} \approx 35.6$ dBm), for a very low pulse repetition frequency. This point will be further discussed in Chapter 5, and has a huge impact on the system design, receiver algorithms development, and performance evaluation.

1.2.3 Ultra-wideband for positioning applications

In this section, the most common methods which have been proposed in literature for positioning estimation using UWB signals are presented, and their main peculiarities are emphasized. The problem which is addressed here is to determine the unknown position of a target with respect to the known position of a network of dedicated reference nodes.

Time based methods

Time based positioning techniques rely on the measurement of the travel time of the signal propagating from the transmitter to the receiver. In the conceptually most simple situation in which two nodes have a common clock, the receiver node can determine the Time of Arrival (TOA) of the incoming signal and directly calculate its distance from the transmitter, by multiplying the estimated TOA (after subtracting the *known* time of transmission) by the speed of light [15]; in this way, the estimated range allows to draw a circle (in 2-dimensions) with the reference node in its center and radius equal to the estimated range. By collecting at least three measurements between the node with unknown position and some reference nodes with known position, and by intersecting the defined circles, it is possible (in the absence of noise and inconsistencies) to univocally determine the position of the node, as depicted in Fig. 5.9. This is equivalent to solving a system of three non-linear equations in two unknowns, the Cartesian coordinates of the node to be positioned.

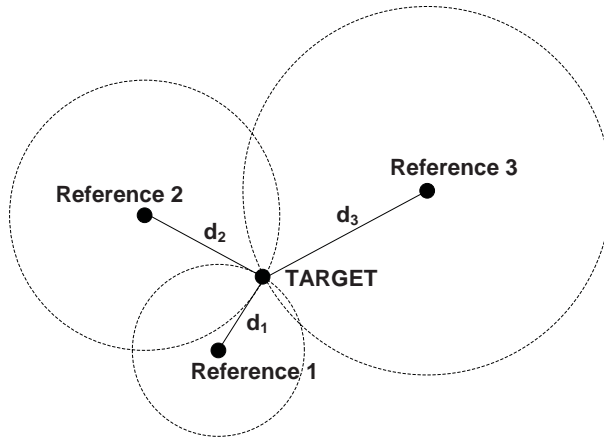


Figure 1.2: *Position estimation via ranging.*

If there is no synchronization between the target and the reference nodes, but there is synchronization among the reference nodes, then Time Difference of Arrival (TDOA) techniques can be employed [15]. In this case, the TDOA of two signals traveling between the target and two reference nodes is estimated; this determines an hyperbola, with foci at the two reference nodes. As an alternative, the time offset between the (synchronized) reference nodes and the target can be treated as an additional unknown in the non-linear system of positioning equations. In both cases, an additional reference node, compared to TOA, is needed to determine the position of the target, exploiting concepts similar to those previously described.

In the absence of a common clock between the nodes, the round trip time of flight between two nodes can be measured to estimate the distance between them. In this case the time of arrival of the received signal, referred to as the receiver clock, is sent back to the transmitter and then used to calculate the range between the two nodes, using two way ranging protocols [2].

The three different variants of time based approaches, above presented, have each specific advantages and drawbacks. The first approach in fact, while conceptually very simple, in practice can be hardly used, since usually the target can not share a common clock with the references. The second method is suboptimal in terms of performance, since it requires a larger number of references to calculate the position of the target; however, it is similar to the principle of working of GPS,

and has been widely used in the first commercially available UWB positioning systems [21]. The third approach appears definitively as the most interesting one because it does not require any synchronization, making the overall system more easily scalable, since the distance between any pair of nodes can be calculated in a completely independent way. However, it requires nodes which can operate both as transmitter and as receiver. This is particularly problematic to achieve, since current UWB receivers are big, power hungry, expensive and present significant practical implementation challenges, which makes it not possible to integrate both functionalities in small devices. As it will be further emphasized in the following sections, this consideration is at the basis of several of the original contributions presented in this thesis.

In the Additive White Gaussian Noise (AWGN) channel, the Cramer-Rao lower bound for the estimated distance standard deviation $\sigma_{\hat{d}}$ using TOA techniques is [15]:

$$\sigma_{\hat{d}} = \frac{c}{2\pi B_e \sqrt{2SNR}} \quad (1.2)$$

where B_e is the effective signal bandwidth. It is important to underline that the estimation accuracy can be improved by increasing the SNR or the effective signal bandwidth. Since UWB has a very large B_e , extremely accurate positioning can be obtained using time based techniques. For this reason, this technique has attracted the interest of the scientific community and the first commercially available UWB positioning systems are based on this approach. Since the achievable accuracy under ideal conditions is very high, clock synchronization between the nodes becomes an important factor affecting the TOA estimation accuracy [4]. For an expression of the Cramer-Rao lower bound for the standard deviation of the estimated distance in realistic multipath environments and for different signal formats employed, the interested reader is referred to [16].

Signal strength based methods

In signal strength based positioning techniques, the distance between two nodes is calculated by measuring the energy of the received signal. Having a-priory knowledge of the distance dependency of the received signal power and of the transmitted one, the range between the transmitter and the receiver can be roughly estimated [15]. Using the collected ranges, the position of the unknown node is then computed exploiting techniques similar to those previously discussed for TOA based positioning algorithms. To determine the range between two nodes using this approach, the channel characteristics need to be known; therefore, this

method requires an accurate calibration phase in order to be able to accurately estimate the path-loss exponent for the considered environments.

Under the classical lognormal shadowing assumption, the Cramer-Rao lower bound for the standard deviation of the estimated distance obtained using received signal strength is [15]:

$$\sigma_d = \frac{\ln 10 \sigma_S}{10n} d \quad (1.3)$$

where d is the distance between the two nodes, n is the path-loss exponent, and σ_S is the shadowing standard deviation. It is evident that the achievable accuracy depends on the channel parameters and on the distance between the two nodes. The very large bandwidth used by UWB signals, allows to significantly reduce the shadowing effects (which for narrowband systems can cause a variation of the received power in the order of some tens of dB, making this approach useless for indoor positioning). For this reason, acceptable performance is expected with this technique mainly for short distances between the nodes [5]-[24].

Angle of arrival based methods

In Angle of Arrival (AOA) based positioning, the position of the node is obtained by measuring the angles of the target node seen by the reference nodes, obtained by means of antenna arrays [15]. To determine the location of a node in 2-dimensions, it is sufficient to measure the angles of the straight lines that connect the node with unknown position with at least two reference nodes. The main limitation of this solution is related to the need of using expensive and relatively large array antennas to estimate the AOA of the received signal, and to the processing requirements.

Comments on the different methods

Among the three previously introduced approaches, the method which has received the largest attention is certainly time based positioning. This is due to the fact that this approach is immediately able to exploit the potential centimeter level positioning accuracy provided by the large bandwidth used by UWB. On the contrary, AOA techniques have received relatively little attention, since they do not exhibit specific benefits compared to time based methods, especially in the situations in which TOA is likely to fail, e.g. when the direct path is not detectable (a situation in which also AOA will fail). At the same time, AOA introduces some challenges in the system implementation, which appear to go in the opposite

direction with respect to the current efforts oriented to address complexity issues. Also signal strength methods received relatively little attention, since deviations even of only a few dB, common in indoor environments, can introduce large errors, voiding the unique benefits coming from UWB.

1.3 Research context

A PhD for its nature is a focused work part of a wider area of research, and the main aim of this activity should be to generate and to share novel knowledge with the scientific community circumscribed in a well accepted and more general framework. In this context, it is relevant 1) to narrow the angle of view of the scientific problem to be addressed, and 2) to gain a deep understanding of available related work in the literature, to identify problems which still lack satisfactory answers.

Due to the unique properties of UWB, particularly when used for positioning applications, a critical reconsideration of most of the system components and principle of operation is required. New technical challenges arise in the system design and traditional guidelines are insufficient, or not applicable. Architectural issues include circuitry for UWB signal generation, broadband antenna and radio-frequency components design. At the medium access control (MAC) layer, innovative energy-awareness protocols are desired, together with effective strategies to allow multiple access. New propagation models describing and predicting the interaction of the traveling waves with the surrounding environment are of absolute importance since the wireless channel is the first aspect which determines performance limits. Positioning algorithms should be developed considering the overall system specification and properties, and the simple adoption of approaches, coming from e.g. the GPS world, might be sub-optimal. Among these issues, this thesis specifically focuses on physical layer aspects related to UWB radio signals when used for positioning applications based on *ranging*. With "ranging" we intend the general operation of calculating the distance (range) between a pair of nodes of the system; as motivated in the previous section, this represents the basic operation both for time based and for received signal strength based methods.

1.4 Related available work

In this section, a short overview of relevant related work available in literature at the start of this Ph.D. research, is provided. The purpose is not to give any detailed description of specific solutions proposed, but instead to emphasize the general research trends and approaches and to offer a representative description of the knowledge available in literature during the research activity summarized in this thesis, as well as to report the main references in which interested reader can find more detailed information.

1.4.1 Ultra-wideband indoor propagation characterization

A correct understanding of the peculiarities of UWB indoor radio propagation is relevant both for signal strength based methods, since they directly exploit the information about some large scale channel parameters, and for time based methods, since it allows to relate the achievable performance in realistic situations with the different system parameters used.

UWB signals exhibit complex propagation phenomena. Due to the large bandwidth of these signals, different frequency components show significantly different interactions with the environment. The analysis and modeling of the diffraction at the edge of objects [25]-[28], the scattering on rough surfaces [29], and the reflection and transmission characterization from dielectric materials slabs of finite thickness [30]-[34] have received large attention, due to the significant impact which they can have on the overall system performance. Several related contributions, both based on specifically developed mathematical frameworks and on propagation measurement campaigns, can be found in the literature. The proposed works however, while fundamental for understanding the basic UWB indoor propagation mechanisms, have found little use in practice, due to the complexity of the problem formulation, and the extremely diverse geometrical properties of different indoor environments. On the contrary, *statistical* based characterization approaches [35]-[42] immediately appeared more suitable to describe UWB indoor radio propagation in a more compact and easily interpretable way. The goal in this case is to give a representation of the essential properties of the UWB channel as a function of a set of random variables, without trying to replicate the exact behavior of the specific channel. The significant efforts, necessary to collect and characterize a large variety of propagation scenarios and conditions, resulted in the standardized IEEE models [36]-[37], which are currently commonly used as

reference for algorithms simulation and performance evaluation. In the following, the most significant literature results concerning the statistical characterization of UWB channels is presented.

Path-loss model

The *frequency dependent* path loss for UWB channels is defined as [35]:

$$PL(f, d) = \frac{1}{\int_{f-\Delta f/2}^{f+\Delta f/2} |H(\tilde{f}, d)|^2 d\tilde{f}} \quad (1.4)$$

where Δf is chosen small enough so that the environmental characteristics can be considered constant in that bandwidth, and $H(f, d)$ is the channel transfer function. The total path loss is obtained by integrating $PL(f, d)$ over the whole bandwidth of interest. To simplify the model it is common to separate the path loss in a part which depends on the frequency and in a part which depends on the distance only [35]:

$$PL(f, d) = PL(f)PL(d) \quad (1.5)$$

The distance dependency of the path loss in dB is usually modeled as:

$$PL(d) = PL(d_0) - 10n \log_{10} \frac{d}{d_0} + S \quad (1.6)$$

where the reference distance d_0 needs to be in the far-field of the used antenna, $PL(d_0)$ is the path loss at the reference distance, n is the path loss exponent and accounts for the cumulative effect of heterogeneous obstacles in the link between the transmitter and the receiver; realistic values for different environments can be found in [36]. The shadowing term S represents the variation of the local mean around the path loss; it is related to diffraction, refraction and reflection effects, and it is usually modeled as a zero mean log-normal random variable. The frequency dependency of the path loss is usually modeled as:

$$\sqrt{PL(f)} \propto f^{-k_{PL}} \quad (1.7)$$

Typical values of k_{PL} range between 0 and 1.8 ($k_{PL} = 0$ corresponds to the spherical spreading of free space propagation); this can be explained considering the larger attenuation for higher frequencies introduced by common walls and obstacles encountered by UWB signals, when propagating. A substantial difference is found in industrial environments since, due to the presence of large metallic reflectors, k_{PL} is usually negative [41]. It is worth to note that the assumption

in (1.5) implies that the effect of the frequency dependency is equivalent to a variation of only $PL(d_0)$ in (1.6), for different f .

Time domain impulse response model

The classical Turin model [43] of the received signal as the sum of the contributions of the different multipath components propagating in the environment, developed for narrowband communications, has been widely adopted also for UWB. However, due to the large bandwidth used by these signals and to the frequency dependent interaction of electromagnetic waves with the environment, each path has its own frequency transfer characteristic and each multipath component undergoes distortions; therefore a commonly accepted representation of the channel impulse response (CIR) is:

$$h(t) = \sum_0^{L_{ch}-1} h_l \exp(j\phi_l) \zeta_l(t - \tau_l) \quad (1.8)$$

where L_{ch} is the number of multipath components, h_l their amplitude, $\phi_l \in \{0, \pi\}$ their random phase (due to the inherently baseband UWB transmission nature, the real passband model is considered for convenience), and τ_l their delay (normalized to $\tau_0 = 0$). ζ_l denotes the distortion undergone by the l -th multipath component.

Power delay profile and path arrival time models

The path arrival time is evaluated with respect to τ_0 , which is the delay of the LOS component. The arrivals are usually distributed in clusters, which are related to the dominant reflections with the main obstacles in the surrounding environment. This characterization was first introduced in the Saleh-Valenzuela model [44], and with some improvements and refinements it is widely accepted today. The power delay profile of each cluster is usually modeled as a one-sided exponential decay, and the cluster arrivals follow a Poisson process [35]. A similar model holds for the paths power decay in each cluster, while their inter-arrival is often modeled as a mixture of two Poisson processes to adequately fit the measured data. For more details related to this model, as well as for realistic values of its parameters, we refer to [35].

Small scale fading

The small scale fading describes the variation of h_l over small areas, caused by the overlapping of unresolvable multipath components. The typical approach to characterize the small scale fading statistics is to test some well known distributions and to determine the best one, using some goodness fitting criteria as the Kolmogorov-Smirnov or the Chi-square hypothesis tests. In the following, the most commonly used distributions are reported.

- **Rayleigh distribution:** In mobile radio channels, the Rayleigh distribution is the most accepted model for small-scale rapid amplitude fluctuations in absence of the LOS component. However, its validity for UWB is questionable, due to the fact that multipath components can usually be largely resolved. To this purpose, an exception is represented by industrial environments [41], due to the extremely dense multipath which characterizes them. The Rayleigh pdf is:

$$f(x) = \frac{x}{\sigma^2} \exp\left(-\frac{x^2}{2\sigma^2}\right) \quad (1.9)$$

where σ^2 is the average power of h_l and can be both fixed or variable with the path delay.

- **Nakagami distribution:** It was first proposed in [45] and it has been adopted in the IEEE 802.15.4a standard [36]. Its pdf is:

$$f(x) = \frac{2m^m x^{2m-1}}{\Gamma(m)\Omega^m} \exp\left(-\frac{mx^2}{\Omega^2}\right) \quad (1.10)$$

where $\Gamma(m) \triangleq \int_0^\infty t^{m-1} \exp(-t) dt$ is the Gamma function, $\Omega = E\{x^2\}$ is the amplitude mean square value, and $m = \Omega^2 / \text{Var}\{x^2\} \geq 0.5$ is the Nakagami m -factor, which provides a quantitative information of the fading severity. As special cases, (1.10) reduces to a Gaussian distribution for $m = 0.5$, and to a Rayleigh distribution for $m = 1$.

- **Lognormal distribution:** It is adopted in the standard proposal IEEE 802.15.3a [17]. The pdf is:

$$f(x) = \frac{1}{x\sigma\sqrt{2\pi}} \exp\left(-\frac{(\ln x - \mu)^2}{2\sigma^2}\right) \quad (1.11)$$

where $\ln x$ has a Gaussian distribution with mean and standard deviation given respectively by: μ and σ .

Other proposed distributions include Rice, Suzuki, and Weibull.

1.4.2 Ultra-wideband ranging

In this section, the main approaches to range estimation using UWB are proposed. After a very short discussion related to the signal strength approach, this section will focus on time based methods, since they received the largest attention both from research and from industry.

Signal strength based ranging

While it has been immediately recognized that the use of very large bandwidths is beneficial also for the signal strength method, since it allows to significantly reduce the fading variations due to unresolvable multipath, the overall accuracy provided by this method still appears unsatisfactory for most positioning applications [15]. The main reason is that in typical indoor environments, the location dependency of the received power can cause variations of a few dB of this statistic, which causes errors of some meters in the final position estimation. The contributions related to this method are currently limited to some theoretical evaluations of the performance of this approach in realistic propagation scenarios [24], and to some results based on real channel measurements [5]. However, an in depth investigation and understanding of the potentials of this approach is still missing.

TOA estimation using matched-filtering

When the autocorrelation of the transmitted pulse resembles a Dirac delta function, the matched filter output can be considered an approximation of the CIR. This solution has been widely adopted for UWB ranging, due to the temporally narrow pulses employed. The authors in [46] correlate the received waveform with a template signal, measured under ideal free-space propagation. The TOA of the direct path is then estimated by detecting the first peak above a dynamic threshold. Similar approaches can be found in [47]-[48]. Some refinements to this strategy are introduced in [49], in which the authors make use of the noise and the LOS/NLOS statistical characterization to improve the TOA estimation reliability.

TOA estimation using the matched filter output appears a straightforward approach. However, it presents some critical issues when used in practice. In fact, a fully digital filter implementation appears unfeasible, due to the very large signal bandwidths used. In case the matched filter is implemented in the analog domain, the problem of the first peak *detection* at its output still needs to be

solved; this would require again, a Nyquist based sampling of the filter output. The solution proposed in Chapter 5, will specifically address this issue.

TOA estimation using CIR estimation algorithms

Several solutions described in literature use traditional CIR estimation algorithms proposed for narrowband communications. As byproduct, these approaches also provide information about the TOA of the first path, which is the only relevant information for ranging.

A classical approach to estimate the CIR is to deconvolve the received signal in the frequency domain using the inverse filtering technique. The spectrum of the received signal is divided by the one of the template pulse; the division is done only for the parts of the spectrum in which the power of the template is different from zero and within the frequency band of interest (an overview of the problems related to this technique is provided by [50]). By taking the inverse Fourier transform, the impulse response of the channel is obtained. The time of arrival of the first path is then estimated by choosing the first local maximum above a threshold.

A time domain deconvolution technique is provided by the CLEAN algorithm [51]. In computing the CIR, the CLEAN algorithm cycles through the following steps. First the autocorrelation $R_{tt}(\tau)$ of the template pulse and the cross-correlation $R_{tr}(\tau)$ between the template pulse and the received signal are computed. The iterative process then begins by searching the maximum correlation peak of $R_{tr}(\tau)$, finding the time delay τ_k associated with the peak, and then normalizing this peak by the one of $R_{tt}(\tau)$, to give the amplitude of the first detected path a_k . The autocorrelation $R_{tt}(\tau)$ is then scaled by a_k and subtracted from $R_{tr}(\tau)$ at the time delay τ_k . At the same time a path with amplitude a_k and delay τ_k is added to a clean map (initialized to zero). A second iteration is done to find and remove the next strongest correlation peak. The iterative process continues until a given threshold is reached. The TOA is then estimated as the time delay of the first path of the clean map. CLEAN is considered a time domain super-resolution CIR estimation algorithm, since it is potentially able to detect paths separated by less than the pulse width. For this reason, better performance compared to the more simple solutions based on matched filtering, is expected.

The authors in [52] proposed a derivation of the Generalized Maximum Likelihood (GML) criterion to detect the TOA of the first path. First, the TOA of the strongest path is estimated (selecting for example the matched-filter output peak).

Then an iterative search is performed to estimate the TOA of the first path using a modification of the GML criterion (the proposed algorithm is a more general case of the CLEAN deconvolution technique previously described). The search stops according to a threshold determined so that the sum of the probability of missed direct path and of false alarm are minimized.

In [53], the authors derive a data-aided ML estimation of the TOA of the first path for the realistic scenario in which the received pulse shapes are unknown, to take into account the distortions undergone by each path. The pulse received in each single path is approximated by a truncated Fourier series expansion. The TOA estimation and its Cramer-Rao lower bound are derived and simulated using the IEEE 802.15.3a channel model. The authors show that the proposed solution significantly outperforms other algorithms available in literature, especially in NLOS channels. However concerns arise about its practical implementation.

To improve the accuracy of the TOA estimation in dense multipath, some papers presented frequency-domain super-resolution techniques. Considering the frequency domain representation of the channel impulse response in (1.8) and neglecting for the sake of the example the distortions undergone by each path:

$$H(f) = \sum_0^{L_{ch}-1} h_l \exp(-j2\pi f\tau_l + j\phi) \quad (1.12)$$

by exchanging the role of time and frequency variables, the problem of the estimation of h_l and τ_l becomes the classical estimation of the amplitudes and frequencies of closely spaced sinusoidal signals immersed in noise, which is a well known problem in the field of spectral estimation [54]-[55]. This problem, applied to the context of ranging, has been well explained in [56]; the super-resolution technique used in this reference is the MUSIC algorithm [55], which is based on the eigenvalue decomposition of the autocorrelation matrix of the vector containing the samples of $H(f)$. These approaches, however, did not receive much attention apart from a few references, for several reasons. First, the use of these techniques, which could be justified and advantageous for narrowband signals, appears redundant when using UWB. In fact, due to the extremely large signal bandwidth used, improvements coming from the use of these methods are negligible even in ideal situations, since multipath is already largely resolvable with UWB. Moreover, these approaches perform well for very high SNR (in the order of 40 dB or more), and small (and often a-priori known) number of multipath components, which does not reflect practical indoor propagation conditions.

In [57], the authors capitalize on the concept of innovation rate, defined as

the number of degrees of freedom per unit of time [58]. The received signal is projected onto a lower dimensional subspace via band-pass filtering and sampling below the classical Nyquist rate. The information about the time delays are extracted from the roots of the annihilating filter² for the vector of the frequency domain samples of the CIR. Also in this case, concerns arise when the algorithm is applied to realistic UWB channels.

TOA estimation using low-complexity energy detection algorithms

To address the complexity issue, sub-optimal and lower complexity approaches, in which part of the potential accuracy is sacrificed to reduce the system demands, have been investigated in the literature. For example, the authors in [59] recognize that due to the very large bandwidth of UWB systems, the ADC appears as the bottleneck in realizing practical UWB receivers. In the proposed solution, the received signal is first squared; the observation window is divided in small time bins and the energy of each bin is collected using frame-rate samples. Different techniques useful for TOA estimation are proposed and compared. It is shown that the "maximum energy selection" algorithm, which simply estimates the TOA as the center of the bin with largest energy, while robust at low SNR, is not able to provide sufficient accuracy, since the delay between the TOA of the first path and of the strongest one can be of some tens of nanoseconds. For this reason, different threshold comparison algorithms are derived. In this case, the TOA is estimated as the center of the first threshold exceeding bin. Theoretical expressions for the mean error are derived for the fixed threshold case, while the dependency of the optimum threshold on the SNR and the channel model are investigated and compared via simulation. Errors at meter level can be achieved with this solution. In [60] it is shown that the same principle, with slight modifications, can be used with transmitted-reference systems [61]-[63], while in [64] the kurtosis³ of the collected samples is used as a metric for the threshold selection. In this way it is possible to capture both the statistics of individual channel realizations, and the SNR. The same approach of [59] has been adopted in [65], which proposes a complete low-complexity transceiver which is able to achieve 5-ns TOA estimation accuracy; in [66] a similar concept is exploited; the authors propose an energy-based TOA estimation; the accuracy depends on the sampling rate used; e.g. it is at meter level using a 500 MHz ADC.

²The annihilating filter is: $A(z) = \sum_{k=0}^K A[k]z^{-k}$ which satisfies $(H * A)[m] = 0$

³The kurtosis of the collected samples is defined as: $\kappa(z[n]) = E\{z[n]^4\}/E^2\{z[n]^2\}$.

These techniques, while attractive since they are able to relax requirements in terms of complexity, are not able to fully exploit the centimeter level accuracy provided by UWB; moreover, they are more sensitive to noise and interference, since they are based on energy detection.

1.5 Motivations

The unique advantages coming from the use of UWB when applied to positioning applications, together with a constantly increasing demand for accurate indoor localization information, determined a strong interest of the scientific community. After the first paper by Lee and Scholtz dated 2002 [52], which specifically investigated positioning performance of UWB ranging in indoor environments, a large number of contributions appeared. However, at the start of my research activity, in February 2006, in spite of about four years of related works available in literature, several issues were still unsolved.

The main point which appeared evident was that, with few exceptions, most of the solutions proposed did not try to deal with the unique properties and challenges which arise when using UWB *specifically* for positioning applications; on the contrary, they simply "borrowed" well known concepts and ideas coming from the traditional communications world, and applied them to the new context of ranging. This approach on one hand caused an only partial understanding of the specific problems introduced by positioning applications; on the other hand, limited potentially interesting solutions, due to a scarce and often not adequate available and commonly accepted framework.

The IEEE 802.15.4a channel model, even if specifically developed with ranging applications in mind, still lacks of relevant information to the purpose. In fact for ranging, the information about the *direct* path is determinant; however, a deep understanding of its dependency on the distance is completely neglected, and it is simply assumed that the direct path has the same path loss exponent as the total power. The same consideration holds for its fading, which is not accurately modeled as a function of the different system parameters. In this context, it appears fundamental to investigate the distance dependency of the statistics of interest, especially for ranging based on signal strength; however, also this point was not addressed in available models.

A realistic evaluation of TOA based ranging performance can not be made with IEEE models, because they do not contain any information about the *true*

distance between transmitter and receiver. For this reason, only the unresolvable multipath source of error can be investigated in this way (with some limits, e.g. the impossibility of investigating its distance dependency). The undetectable direct path situation, as well as the additional delay due to propagation through dielectric materials, which can happen in NLOS propagation and are often the most consistent source of inaccuracy in TOA methods, on the contrary can not be analyzed. At the same time and for similar reasons, most of the information contained in IEEE models appears redundant and cause of unwanted complications for ranging applications. For example, models for the cluster statistics, or (multi)paths inter-arrival and fading, is usually not relevant; on the contrary, this information could be "condensed" in some large scale statistics, e.g. (distance dependent) RMS, maximum or mean excess delay spread models.

Accurate models for the statistics of interest are relevant not only for the pure range estimation operation, but also for other tasks which are relevant for these applications. For example, the possibility of distinguishing between LOS and NLOS propagation, can certainly be of interest for communication applications; however it becomes fundamental for positioning applications, since these two conditions provide a significantly different ranging accuracy. The use of IEEE models, which have not been specifically developed for these applications in mind, usually provide results which are far from those achievable in practice, and could lead to system designs which in practice do not work, because of the points previously highlighted.

Similar considerations hold for most of the proposed TOA estimation algorithms, which are often considered a simple extension of well known CIR estimation approaches in which the time of the received signal comes as a byproduct. These approaches are inherently suboptimal, since they do not address the unique properties of UWB and do not focus on the relevant information which needs to be retrieved. The main limitation of these methods is that they usually rely on Nyquist sampling rates and for this reason they can be hardly implemented, since they are particularly demanding in terms of hardware and signal processing requirements. The approaches based on lower complexity energy detection algorithms on the contrary, while able to relax complexity issues, need to sacrifice part of the potential accuracy provided by UWB; in addition, they are particularly sensitive to noise and interference.

1.6 "HERE: indoor positioning based on UWB radio signals" research project

"This research was supported by the Technology Foundation STW, applied science division of NWO and the technology program of the Ministry of Economic Affairs."

The work presented in this thesis has been conducted within the research project: "HERE: indoor positioning based on UWB radio signals", supported by the Dutch Technological Foundation STW (project no. 0.7343). This four years project has been carried out in a team composed by two Ph.D. candidates and two supervisors, in a cooperation between the Wireless and Mobile Communications Group of the Faculty of Electrical Engineering of the Delft University of Technology, and the Mathematical Geodesy and Positioning Group of the Faculty of Aerospace Engineering of the same university.

The main research questions which the project aimed to answer can be summarized in the following points:

1. Identification of characteristic parameters of the UWB multipath channel in typical indoor environments, for the purpose of positioning.
2. Determination of statistical UWB channel models for these parameters based on measurements, and verification of the models.
3. Investigation of transmitter and receiver architectures, and signal processing algorithms for extraction of the required channel parameter information.
4. Design and development of a real-time ultra wideband positioning system testbed based on acoustic signals.
5. Investigation of system non-linearity and the feasibility of applying non-linear positioning algorithms, in typical indoor environments.
6. Analysis of existing positioning algorithms and development of possible improvements aiming lower computational load or higher positioning accuracy.
7. Development of positioning model hypothesis tests for outlier/bias detection, based on the developed statistical ranging models.

The overall outcome of the project is the results of the strict cooperation among all the people involved in the project; however, this thesis specifically presents results related to the points 1-4 of the list, which represent the main research focus of this thesis. The issues 4-7 are covered by the research carried out by the Ph.D. candidate Junlin Yan of the Mathematical Geodesy and Positioning Group in his thesis entitled "Algorithms for indoor positioning systems using ultra-wideband signals".

1.7 Summary of the main contributions

Following the main motivations shortly highlighted in Section 1.5, the research activity presented in this thesis can be summarized with the following contributions:

- Based on a large database of measured UWB channel impulse responses in indoor environments, a new statistical channel characterization for ranging applications has been provided. The distance and bandwidth dependency of the considered statistics is investigated, and insight in the obtained results is given.
- Exploiting the proposed characterization, the traditional idea of ranging based on measured signal strength, has been extended. The concept of statistics based ranging is developed; it is shown that this method is able to exploit the unique properties of UWB and to achieve an accuracy of a few decimeters in LOS, significantly better than traditional signal strength based positioning, but with a similar system complexity.
- A model for the range error achieved with TOA based ranging is provided and its relationship with relevant parameters, like system bandwidth and distance between transmitter and receiver, is investigated. It is shown that model knowledge allows to significantly improve the final positioning accuracy using weighted least squares approaches.
- A LOS/NLOS detection approach based on the introduced statistics is developed and validated on the collected data; the proposed solution exhibits a reliability of about 99%.
- A new low-complexity TOA estimation concept and principle of implementation has been proposed and patented. This solution capitalizes on the

unique properties of pulsed based UWB transmissions and it is able to achieve centimeter level accuracy with sampling rates in the order of a few tens of MHz, avoiding the main limitations which currently make it difficult to practically build UWB positioning systems.

- A framework to evaluate impairments due to narrowband interference on first peak based TOA estimation has been developed; the suggested analysis is based on the first threshold crossing probability evaluation for Gaussian processes and time varying boundaries.

1.8 Outline of the thesis

In Chapter 2, the UWB radio frequency setup used to collect the CIR measurements database employed in this thesis is shortly described, and the measurement locations and data-processing are presented. A statistical channel characterization for ranging applications is then provided, and the obtained results are motivated. In Chapter 3, the concept of "statistics based ranging" is introduced, and the achieved performance evaluated using the available measurements. Different strategies to improve the plain accuracy achievable with the direct use of these statistics are then presented. Chapter 4 provides an evaluation of the TOA estimation performance in the considered indoor environments. The distance and bandwidth dependency of the obtained results is then discussed and motivated. An application of the overall models for the introduced statistics to LOS/NLOS detection is described. In Chapter 5, a new low-complexity TOA estimation strategy and receiver implementation is proposed, and its performance evaluated; a coarse acquisition method, developed considering the specific requirements that arise when the proposed TOA estimation approach is used, is then presented. Chapter 6 evaluates the impairments on the concept proposed in the previous chapter, due to narrowband interference. Finally, Chapter 7 summarizes the author's general conclusions, and it indicates possible directions for future research.

Bibliography

- [1] A. Molisch, I. Oppermann, M. G. Di Benedetto, D. Porcino, C. Politano, T. Kaiser, *UWB Communication Systems - A Comprehensive Overview*, Hindawi Publishing Corporation, New York, 2006.

- [2] I. Oppermann, M. Hmlinen, J. Inatti, *UWB theory and applications*", John Wiley and Sons, Nov. 2004.
- [3] M. Z. Win and R. A. Scholtz, *Ultra-wide bandwidth time-hopping spreads spectrum impulse radio for wireless multiple-access communications*", IEEE Transaction on Communications, vol. 48, no. 4, pp. 679-691, Apr. 2000.
- [4] R. A. Scholtz, D. M. Pozar, and W. Namgoong, *Ultra-wideband radio*", EUR-ASIP Journal on Applied Signal Processing, pp. 252-272, 2005.
- [5] M.Z. Win, R.A. Scholtz, *Impulse radio: how it works*", IEEE Communications Letters, vol. 2, no. 2, pp. 36-38, Feb. 1998.
- [6] R.A. Scholtz, *Multiple access with time-hopping impulse modulation*", IEEE MILCOM 1993, vol. 2, pp. 447-450, 11-14 Oct. 1993.
- [7] Liuqing Yang, G.B. Giannakis, *Ultra-wideband communications: an idea whose time has come*", IEEE Signal Processing Magazine, vol. 21, no. 6, pp. 26-54, Nov. 2004.
- [8] FCC, Office of Engineering and Technology, *Revision of Part 15 of the Commission's Rules Regarding Ultra-Wideband Transmission Systems*", ET Docket, no. 98-153, 2002.
- [9] C.E. Shannon, *A mathematical theory of communication*", Bell System Technical Journal, vol. 27, pp. 379-423, 623-656, 1948.
- [10] C.L. Bennett and G.F. Ross, *Time-domain electromagnetics and its applications*", Proceedings of the IEEE, vol. 66, no. 3, pp. 299-318, 1978.
- [11] M.Z. Win and R. A. Scholtz, *On the robustness of ultra-wide bandwidth signals in dense multipath environments*", IEEE Communication Letters, vol. 2, pp. 51-53, Feb. 1998.
- [12] M.Z. Win and R. A. Scholtz, *On the energy capture of ultra-wide bandwidth signals in dense multipath environments*", IEEE Communication Letters, vol. 2, pp. 245-247, Sept. 1998.
- [13] S. Roy, J. R. Foerster, V. S. Somayazulu, and D. G. Leeper, *Ultrawideband radio design: The promise of high-speed, short-range wireless connectivity*", IEEE Proceedings, vol. 92, pp. 295-311, Feb. 2004.

-
- [14] Y. C. Yoon and R. Kohno, *Optimum multi-user detection in ultra-wideband (UWB) multiple-access communication systems*, IEEE ICC, vol. 2, pp. 812-816, 2002.
- [15] S. Gezici, Zhi Tian, G. B. Giannakis, H. Kobayashi, A. F. Molisch, H. V. Poor, Z. Sahinoglu, *Localization via ultra-wideband radios: a look at positioning aspects for future sensor networks*, IEEE Signal Processing Magazine, vol. 22, no. 4, pp. 70-84, July 2005.
- [16] R. Cardinali, L. De Nardis, M. G. Di Benedetto, P. Lombardo, *UWB ranging accuracy in high- and low-data-rate applications*, IEEE Transactions on Microwave Theory and Techniques, vol. 54, no. 4, pp. 1865-1875, April 2006.
- [17] J. Foerster, *IEEE 802.15.SG3a channel modeling sub-committee report final*.
- [18] CEPT ECC document, *ECC decision of 24 march 2006 on the harmonized conditions for devices using ultra-wideband (UWB) technology in bands below 10.6 ghz* Tech. Rep. Doc. ECC/DEC/(06)04.
- [19] R.J. Fontana, E.A. Richley, *Observations on Low Data Rate, Short Pulse UWB Systems*, IEEE ICUWB 2007, pp. 334-338, Sep. 2007.
- [20] R. Roberts, *Ranging subcommittee final report*, Nov. 2004.
- [21] Time Domain Corporation: www.timedomain.com.
- [22] Y. Shimizu, Y. Sanada, *Accuracy of relative distance measurement with ultra wideband system*, IEEE ICUWST 2003, pp. 374-378, 16-19 Nov. 2003.
- [23] T. Gigl, G. J. M. Janssen, V. Dizdarevic, K. Witrisal and Z. Irahhtauten, *Analysis of a UWB Indoor Positioning System Based on Received Signal Strength*, IEEE WPNC 2007, Mar. 2007.
- [24] Y. Qi and H. Kobayashi, *On relation among time delay and signal strength based geolocation methods*, IEEE GLOBECOM 2003, vol. 7, pp. 4079-4083, Dec. 2003.
- [25] M. Born, E. Wolf, *Principles of optics*, Cambridge U. Press, 1999.
- [26] R.C. Qiu, *A study of the ultra-wideband wireless propagation channel and optimum UWB receiver design*, IEEE Journal on Selected Areas in Communications, vol. 20, no. 9, pp. 1628-1636, December 2002.

- [27] R.C. Qiu, "A generalized time domain multipath channel and its application in ultra-wideband (UWB) wireless optimal receiver design-Part II: physics-based system analysis", IEEE Transaction on Wireless Communications, vol. 3, no. 6, pp. 2312-2324, November 2004.
- [28] R.C. Qiu, "A theoretical study of the ultra-wideband wireless propagation channel based on the scattering centers", IEEE 48th VTC 1998, vol. 1, pp. 308-312, 18-21 May 1998.
- [29] R.D. De Roo, F.T. Ulaby, "Bistatic scattering from rough dielectric surfaces", IEEE Transaction on Antennas and Propagation, vol. 42, no. 2, pp. 220-231, February 1994.
- [30] O.S. Heavens, "Optical properties of thin solid films", Dover Publications Inc., 1991.
- [31] Zenqiu Clien, R. Yao, Zihua Guo, "The characteristics of UWB signal transmitting through a lossy dielectric slab", IEEE 60th VTC 2004, vol. 1, pp. 134-138, 26-29 September 2004.
- [32] Ray-Rong Lao, Jenn-Hwan Tarnq, Chiuder Hsiao, "Transmission coefficients measurement of building materials for UWB systems in 3-10 GHz", IEEE 57th VTC 2003, vol. 1, pp. 11-14, 22-25 April 2003.
- [33] A. Muqaibel, "Characterization of Ultra Wideband Communication Channels", Ph.D. dissertation.
- [34] A. Muqaibel, A. Safaai-Jazi, "A new formulation for characterization of materials based on measured insertion transfer function", IEEE Transaction on Microwave Theory and Techniques, vol. 51, no. 8, pp. 1946-1951, August 2003.
- [35] A.F. Molisch, "Ultrawideband propagation channels - theory, measurements, and modeling", IEEE Transaction on Vehicular Technologies, vol. 54, no. 5, pp. 1528-1545, Sept. 2005.
- [36] A.F. Molisch, D. Cassioli, Chia-Chin Chong, S. Emami, A. Fort, B. Kannan, J. Karedal, J. Kunisch, H.G. Schantz, K. Siwiak, M.Z. Win, "A comprehensive standardized model for ultrawideband propagation channels", IEEE Transaction on Antennas and Propagation, vol. 54, no. 11, pp. 3151-3166, Nov. 2006.

-
- [37] A.F. Molisch, K. Balakrishnan, D. Cassioli, Chia-Chin Chong, S. Emami, A. Fort, J. Karedal, J. Kunisch, H.G. Schantz, U. Schuster, K. Siwiak, "*IEEE 802.15.4a channel model - final report*", 2005, available at: <https://mentor.ieee.org/802.15/dcn/04/15-04-0662-04-004a-channel-model-final-report-r1.pdf>.
- [38] A. Muqaibel, A. Safaai-Jazi, A. Attiya, B. Woerner, S. Riad, "*Path-loss and time dispersion parameters for indoor UWB propagation*", IEEE Transactions on Wireless Communications, vol. 5, no. 3, pp. 550-559, March 2006.
- [39] D. Cassioli, M.Z. Win, A.F. Molisch, "*The ultra-wide bandwidth indoor channel: from statistical model to simulations*", IEEE Journal on Selected Areas in Communications, vol. 20, no. 6, pp. 1247-1257, August 2002.
- [40] W. Ciccognani, A. Durantini, D. Cassioli, "*Time domain propagation measurements of the UWB indoor channel using PN-sequence in the FCC-compliant band 3.6-6 GHz*", IEEE Transactions on Antennas and Propagation, vol. 53, no. 4, pp. 1542-1549, April 2005.
- [41] J. Karedal, S. Wyne, P. Almers, F. Tufvesson, A. F. Molisch, UWB channel measurements in an industrial environment, IEEE GLOBECOM 2004, vol. 6, pp. 3511-3516, 29 November- 3 December 2004.
- [42] Chia-Chin Chong, Su Khiong Yong, "*A generic statistical-based UWB channel model for high-rise apartment*", IEEE Transactions on Antennas and Propagation, vol. 53, no. 8, pp. 2389-2399, August 2004.
- [43] G.L. Turin, "*A statistical model of urban multipath propagation*", IEEE Transaction on Vehicular Technology, vol. 21, pp. 1-9, Feb. 1972.
- [44] A.A.M. Saleh, R.A. Valenzuela, "*A statistical model for indoor multipath propagation*", IEEE Journal on Selected Areas in Communications, vol. SAC-5, no. 2, pp. 128-137, February 1987.
- [45] M. Nakagami, "*The m-distribution - a general formula of intensity distribution of rapid fading*", Statistical Methods in Radio Wave Propagation, pp. 336, 1960.
- [46] Z.N. Low, J.H. Cheong, C. L. Law, W. T. Ng, Y. J. Lee, "*Pulse detection algorithm for line-of-sight (LOS) UWB ranging applications*", IEEE Antennas and Wireless Propagation Letters, vol. 4, pp. 63-67, 2005.

- [47] Woo Cheol Chung, Dong Ha, "*An accurate ultra wideband (UWB) ranging for precision asset location*", IEEE Conference on Ultra Wideband Systems and Technologies 2003, pp. 389-393, 16-19 November 2003.
- [48] J. Schroeder, S. Galler, K. Kyamakya, "*A low-cost experimental ultra-wideband positioning system*", IEEE ICU 2005, pp. 632-637, 5-8 September 2005.
- [49] A.H. Tewfik, S. Srirangarajan, "*Localization in non line-of-sight environments for wireless sensor networks*", IEEE European Workshop on Wireless Sensor Networks 2005, pp. 410-414, 31 January-2 February 2005.
- [50] S.M. Riad, "*The deconvolution problem, an overview*", IEEE Proceedings, vol. 74, no. 1, pp. 82-85, January 1986.
- [51] R.G. Vaughan, N.L. Scott, "*Super-resolution of pulsed multipath channels for delay spread characterization*", IEEE Transactions on Communications, vol. 47, no. 3, pp. 343-347, March 1999.
- [52] Joon-Yong Lee, R. A. Scholtz, "*Ranging in dense multipath environment using an UWB radio link*", IEEE Journal on Selected Areas in Communications, vol. 20, no. 9, pp. 1677-1683, December 2002.
- [53] S. Aedudodla and T.F. Wong, "*On time-of-arrival estimation in dense ultra-wideband channels*", IEEE ICCAS 2006, vol. 2, pp. 1315-1320, 25-28 June 2006.
- [54] R. Roy, T. Kailath, "*ESPRIT estimation of signal parameters via rotational invariance techniques*", IEEE Transactions on Acoustics, Speech, and Signal Processing, vol. 37, no. 7, pp. 984-995, July 1989.
- [55] R. Schmidt, "*Multiple emitter location and signal parameter estimation*", IEEE Transactions on Antennas and Propagation, vol. 34, no. 4, pp. 276-280, Mar 1986.
- [56] Xinrong Li, K. Pahlavan, "*Super-resolution TOA estimation with diversity for indoor geolocation*", IEEE Transactions on Wireless Communications, vol. 3, no. 1, pp. 224-234, January 2004.
- [57] I. Maravic, J. Kusuma, M. Vetterli, "*Low-sampling rate UWB channel characterization and synchronization*", Journal on Communications and Networks, vol. 5, no. 4, pp. 319-327, 2003.

-
- [58] M. Vetterli, P. Marziliano, T. Blu, "*Sampling rate with finite rate of innovation*", IEEE Transactions on Signal Processing, vol. 50, no. 6, pp. 1417-1428, June 2002.
- [59] I. Guvenc, Z. Sahinoglu, "*Threshold-based TOA estimation for impulse radio UWB systems*", IEEE ICU 2005, pp. 420-425, 5-8 September 2005.
- [60] I. Guvenc, Z. Sahinoglu, P.V. Orlik, "*TOA estimation for IR-UWB systems with different transceiver types*", IEEE Transactions on Microwave Theory and Techniques, vol. 54, no. 4, pp. 1876-1886, April 2006.
- [61] R. Hoctor and H. Tomlinson, "*Delay-hopped transmitted-reference RF communications*", IEEE Conference on Ultra Wideband Systems and Technologies, Baltimore, MD, May 2002, pp. 265-270.
- [62] J. Choi and W. Stark, "*Performance of ultra-wideband communications with suboptimal receivers in multipath channels*", IEEE Journal on Selected Areas in Communications, vol. 20, no. 9, pp. 1754-1766, Dec. 2002.
- [63] C. Rushforth, "*Transmitted-reference techniques for random or unknown channels*", IEEE Transaction on Information Theory, vol. 10, pp. 39-42, Jan. 1964.
- [64] I. Guvenc, Z. Sahinoglu, "*Threshold selection for UWB TOA estimation based on kurtosis analysis*", IEEE Communications Letters, vol. 9, no. 12, pp. 1025-1027, December 2005.
- [65] L. Stoica, A. Rabbachin, I. Oppermann, "*A low-complexity noncoherent IR-UWB transceiver architecture with TOA estimation*", IEEE Transactions on Microwave Theory and Techniques, vol. 54, no. 4, pp. 1637-1646, April 2006.
- [66] A.A. D'Amico, U. Mengali, L. Taponecco, "*Energy-based TOA estimation*", IEEE Transaction on Wireless Communications, vol. 7, no. 3, pp. 838-847, Mar. 2008.

UWB Channel Measurements and Characterization for Statistics Based Ranging

A proper characterization of the radio propagation channel is fundamental for any wireless system. A common way to characterize the channel is to use a statistical approach based on measurements; by performing a measurement campaign for typical propagation environments, it is possible to extract parameters from the collected data which can be used to describe in a statistical way the wireless channel.

To provide a *good* statistical channel model for UWB indoor propagation is a challenging task. In fact, indoor radio propagation takes place via hundreds of multipath components due to reflections, diffraction, and scattering of the transmitted waveform with obstacles and objects which are typically present in these environments. The interaction of electromagnetic waves with the environment is frequency dependent; since UWB uses very large bandwidths, similar as the central frequency of the spectrum, the different frequency components are affected in a significantly different way by the environment. Therefore, a statistical model for UWB signals is typically figment of compromise: on one hand, the extremely complex UWB indoor propagation phenomena; on the other hand, system or practical limitations in the measurement campaign (e.g. time to collect a proper

number of data required to make the extracted statistics reliable), and the need to provide a model which is simple enough to be useful for theoretical analysis and performance evaluation. In recent years, as shortly discussed in the previous chapter, there has been a great effort to provide adequate UWB indoor channel models, which resulted in the IEEE standardized models [1]-[3]. However, these models have been developed with communications applications in mind; when used for ranging and positioning applications, most of the contained information appears redundant, resulting in an undesired complexity. For example, for TOA based ranging applications, the relevant information is contained in the *first* path of the received signal, while the remaining part of the channel contains information which can be hardly exploited. At the same time, useful information for these applications is neglected; e.g. IEEE models fail to provide an accurate statistical model for the attenuation of the direct path, as well as a model for its fading, as a function of the distance.

Another point is relevant to address as well. The use of extremely large bandwidths implies that the different paths which compose the received signal can be largely resolved, and are affected by very little fading when compared to narrowband or traditional wideband signals. This means that the use of the total received power can be sufficiently reliably related to the distance traveled by the signal, and used for range estimation, when the required target accuracy is at meter level. At the same time, the direct path itself is likely to be clearly distinguishable and affected by negligible overlap with late multipath components, particularly in LOS propagation. This unique peculiarity coming from UWB offers the possibility of using only the power of the direct path for ranging, even in a rich multipath environment. However, to properly exploit these possibilities, it is relevant to provide adequate models for the suggested statistics, which relate them to the relevant channel and system parameters, like the used bandwidth or the distance between transmitter and receiver. Again, IEEE models fail to give an answer to this need.

This chapter investigates in detail issues related to statistics based ranging, when UWB signals are used. The radio frequency measurement set-up used to perform UWB channel measurements is shortly introduced, and the measurement locations and the signal processing used to extract the relevant parameters are described. A comprehensive model for the total power and for the first path power of the received signal are proposed, based on the collected data. The bandwidth and distance dependency of the retrieved statistics is investigated and modeled;

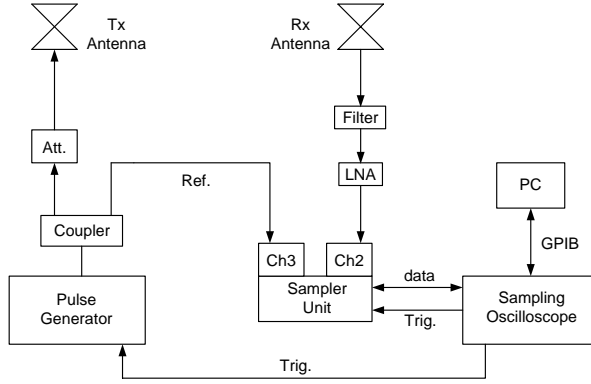


Figure 2.1: *System setup for UWB channel measurements.*

finally, the dependency of the parameters' estimation accuracy on the number of collected measurements is analyzed.

2.1 The UWB measurement set-up

The UWB channel measurements presented in this thesis are performed using a time domain measurement technique. This technique employs a narrow time domain pulse to probe the channel. The setup consists of two main parts: the transmitter and receiver. The transmitter part is composed of a pulse generator, resistive coupler and a transmit antenna. The receiver part has the same type of antenna, band-pass filter, a wideband resistive attenuator, a wideband Low Noise Amplifier (LNA), a sampler unit, a sampling oscilloscope and a PC. Using a General Purpose Information Bus (GPIB), the measured time signal is transferred to a PC where the data are stored for later processing and analysis. The whole measurement set-up is depicted in Fig. 2.1. In the following, a short overview of the main components is provided; for a more detailed description we refer to [4]-[5].

2.1.1 Pulse generator

The generator used for the measurements fires a Gaussian-like pulse with a maximum amplitude equal to 25 V and a width of about 50 ps. The measured generator output and its spectrum are shown in Fig. 2.2.

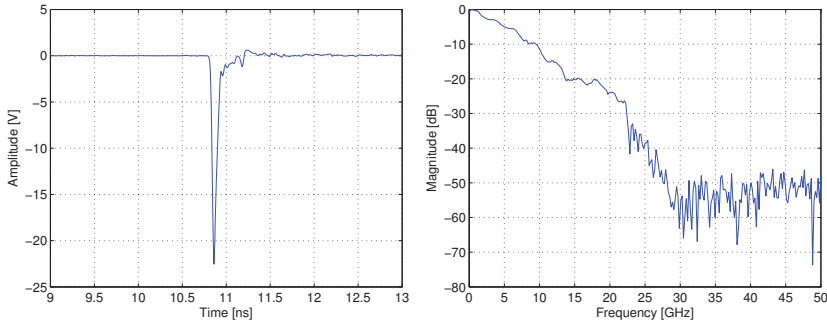


Figure 2.2: *The pulse generator output (left) and its frequency response (right).*

2.1.2 Sampler unit and sampling oscilloscope

Maximum frequency of the measurements

The sampling oscilloscope can measure four channels simultaneously:

- 2 channels up to 6 GHz
- 2 channels up to 18 GHz

This means that, using the second pair of channels, the system is suitable to carry out measurements in the full UWB band of interest. The important characteristics of the sampling oscilloscope are given in Table 2.1.

Maximum delay of the measurements

The pulse generator has a repetition frequency $f_{pr} = 100$ kHz. Therefore, the maximum delay which can be retrieved is $T_{md} = 1/f_{pr} = 10$ μ s. This value is significantly larger than the maximum delay spread of indoor wireless channels, which is typically on the order of 100 ns.

Stroboscopic sampling

The sampling unit performs a stroboscopic sampling of the received signal. To recover one complete received signal, a train of pulses with repetition frequency f_{pr} is transmitted. The sampling unit receives a sequence of waveforms with period $T_{pr} = 1/f_{pr}$ and it takes one sample per waveform. The time difference between two successive samples is equal to $T_{pr} + T_{vs}$, where T_{vs} is the virtual sampling period. In the collected data, $T_{vs} = 10$ ps is chosen. This corresponds to an

Table 2.1: *Characteristics of the sampling oscilloscope*

Parameters	Value
Number of channels	4
Bandwidth	2 x (1-6 GHz), 2 x (1-18 GHz)
Noise (RMS)	± 1.0 mV (1-6 GHz), 4.0 mV (1-18 GHz)
Max. input voltage	± 1.0 V
A/D converter	12 bit
Number of samples	256, 512, 1024
Max. averaging	256
Min. sampling time	0.1 ps
Jitter	≤ 2.0 ps
Measurement Range	10 ps - 10 μ s

oversampling factor of about 5 compared to the minimum Nyquist rate for signals with bandwidth smaller than 10.6 GHz, and allows to accurately reconstruct the received continuous waveform from the collected samples.

Number of samples

The maximum number of samples $N_{s,os}$ which can be recorded is 1024. Therefore, the total signal time which can be recorded is limited to $T_{s,os} = (N_{s,os} - 1)T_{vs} = 10.23$ ns. This value is significantly smaller than a typical UWB indoor channel impulse response; for this reason, for each channel, measurements are repeated $N_{w,os}$ times, and a corresponding number of adjacent time windows $T_{s,os}$ is recorded. Since the setting of the delay in the oscilloscope is not exact, the starting time of consecutive time windows is chosen such that they partly overlap each other; the overlap time interval T_{oti} has been chosen equal to 1.23 ns (about 12% of $T_{s,os}$). The correct value of the time delay in each time window is reconstructed at the receiver by maximizing the cross-correlation between the overlapping signal parts belonging to successive windows.

In the collected measurements, $N_{w,os} = 16$ is chosen. In this way, the maximum delay which can be recorded is of about 144 ns and allows to collect all the significant channel multipath components.

2.1.3 Reference channel

For time based ranging applications, eventual inaccuracies in the reference oscillator need to be addressed. Errors in time-domain measurements can be divided into two groups: short-term errors and long-term errors [6]. The former are due to thermal noise, jitter and quantization noise. Only jitter is discussed here because this error source is specific for time-domain measurements. Jitter can be explained as the non-deterministic variation in the sample position which results into a voltage error. Long-term error sources are due to changes in the position and shape of the measurement pulse. These long-term variations are mainly induced by imperfections in the measurement system. The variations in the pulse shape lead to amplitude variations and the variation in the pulse position (drift) results in phase errors. The measurement results showed a drift of almost 20 ps over three hours. To compensate for these effects, a reference channel, shown in Fig. 2.1 is used.

2.1.4 Antennas

The antenna characteristics affect the radio propagation conditions. For conventional narrowband or wideband systems, the fractional bandwidth is small, and consequently the antenna frequency response can be assumed constant in it. However, this is typically not the case for UWB; when estimating the channel, the antenna frequency characteristics should be taken into consideration.

More problematic for channel modeling purposes appears to be the antenna angular dependency. In fact, for a given frequency f , the antenna frequency response $H_{ant}(f, \theta, \phi)$ is dependent on the azimuth angle θ and elevation angle ϕ . To exclude from the channel model the effect of the antenna angular dependency would require knowledge of the departure angle from the transmit antenna and arrival angle to the receive antenna for each channel multipath component, which is unfeasible in practice. For this reason, the obtained results become antenna dependent, meaning that a general characterization of the channel can be obtained only for a specific pair of antennas used in the measurements. The effect of using directive or omni-directional antennas on the channel parameters like delay spread and path-loss is investigated in [7]-[8]. In the measurement campaign carried out, omni-directional, vertically polarized bi-conical antennas, have been used.

2.2 Channel measurements motivations

The measurement campaign has been performed with the following purposes in mind:

- Identify and model suitable statistics, other than TOA, which can be used for range estimation. The concept behind this point is that if a particular statistic retrieved from the received signal exhibits a dependency with respect to the distance between transmitter and receiver, it can be used for ranging, since measuring its value directly provides an estimate for the distance itself. We refer to this generic approach as *statistics based ranging*. A typical example of statistics based ranging is the classical signal strength method. It appears worthwhile to investigate this issue since, given the extremely large signal bandwidth used by UWB [9]-[12], variations of the determined statistics due to non-resolvable multipath are expected to be very small.
- Investigate and model the range estimation accuracy which can be achieved with traditional TOA based methods, and its relationship with relevant system parameters, like distance between transmitter and receiver, and used signal bandwidth.

This chapter focuses on channel modeling for statistics based ranging applications (the proposed model will be explicitly used for ranging in Chapter 3), while results and applications related to TOA based ranging are presented in Chapter 4.

2.2.1 Statistics for ranging applications

The statistics which are identified and modeled in this chapter are the total power of the received signal (TP), and the power of the first path of the received signal (FP). As previously motivated, very little fading in the total received signal power is expected, which makes this statistic usable for the purpose of range estimation, when the target accuracy is at decimeter-meter level. In addition, the huge signal bandwidth used by UWB also offers the unique possibility to accurately distinguish the direct path from late multipath components in the received signal; at least in LOS, the first path is expected to provide a higher accuracy than the total power, since only the signal component which is directly related to the distance traveled between transmitter and receiver is used for range estimation.

2.3 Fading characterization and choice of measurement procedure

A fundamental information for statistics based ranging is represented by the characterization of the random deviations of the statistics of interest from the determined model fit; in fact, these deviations do directly relate to the accuracy which can be achieved, when using this approach for ranging.

For the total power statistic, traditional approaches to model these deviations for UWB channels usually distinguish between (small-scale) fading and (large-scale) shadowing [1]-[3]. This differentiation reflects the diverse nature of the two phenomena. In fact, fading is due to changes in the received signal power due to different constructive or destructive time overlap of unresolvable multipath components, which happen with small changes in the position of transmitter or receiver. Shadowing on the contrary, is due to the location dependency of the received signal power, and accounts for the different physical propagation characteristics of the environment, when changing significantly the location of transmitter and receiver (in a more strict meaning, shadowing is related to the power drop due to the presence of obstacles between the transmitter and receiver; in this thesis, however, the extended meaning of shadowing, previously introduced, is adopted). To characterize the small scale fading, measurements in a grid of closely spaced points with spacing in the same order of magnitude as the signal wavelengths are usually collected for each location, while the large scale fading is evaluated after averaging out the small scale fading variation.

The approach followed in the measurement campaign reported in this thesis is different. In fact, transmitter and receiver have been placed at random locations, and for each location, only a single measurement is collected. In this way, it is not possible to distinguish between small scale fading and large scale shadowing, which conceptually have different causes. On the contrary, it is only possible to model the *global* fading (from this moment on, simply denoted as fading, keeping in mind other specific meanings that this term can have), which in this thesis is defined as the variation in the measured received power (total, or of the first path), from the determined fit, independently on the source of variation (multipath or location dependency). This choice is justified by complexity issues. In fact, the proposed characterization is developed for statistics based ranging applications; a differentiation in the model among the different sources of error would significantly complicate the mathematical analysis and make analytical deriva-

tions hardly feasible. On the other hand, one of the purposes of the proposed measurement campaign is to investigate any possible dependency of the fading on the distance itself (this point is completely neglected in IEEE models [1]-[3]); as it will be shown in detail in the next chapter, this information is important for weighted least squares localization, and it allows to significantly improve the achieved position estimation accuracy. To extract in a reliable way distance dependent parameters, it is necessary to collect measurements for a sufficiently large number of *random* locations (e.g. at least 20 different locations for each meter distance variation). Therefore, it would be extremely time consuming to follow the traditional approach which separately models large scale shadowing and small scale fading, and to collect a few tens of grid measurements for each different location. In addition to this, to distinguish between shadowing and multipath fading would not introduce a significant improvement in the ranging accuracy, as it will be better justified in the next chapter. However, insight and justification of the proposed model, using available data from an independent and previously conducted measurement campaign, which allows to retrieve the different sources of parameters' deviations, is provided.

2.3.1 Measurement locations

The measurements, which were carried out in the EEMCS faculty building of the Delft University of Technology at different floors, cover LOS and NLOS propagation and are representative of typical indoor office environments. In NLOS, there is a physical obstruction, represented by one wall between the transmitter and the receiver. The walls are made of brick or concrete and have a thickness between 15 and 30 cm, while the floors are made of reinforced concrete. A total of about 400 measurement in LOS, and 250 measurement in NLOS have been collected. The distance between transmitter and receiver varies between 2 and 13 m for LOS, and between 3 and 15 m for NLOS. To allow for distance dependency modeling, the measurements have been approximately uniformly distributed between the minimum and maximum distance in both cases, and the location of transmitter and receiver have been randomly chosen. The choice of limiting the measurements in this range of distances and of considering only propagation through a single wall is related to practical system operation issues. In fact, for power based ranging, the accuracy decreases with the distance between transmitter and receiver; therefore, a real system is expected to work with a satisfactory accuracy for short to medium distances only; therefore, this propagation condition represents the most

interesting and realistic one to consider. For the same reason, in NLOS, propagation through only a single wall is considered. Finally, both the transmit and receive antennas have been placed at 1.5 m high and with the H-plane parallel to the floor. The true distance between transmitter and receiver has been measured with a Leica DISTO laser meter, able to provide an accuracy of $\pm 1\text{mm}$, and with the support of triangulation techniques in NLOS.

2.4 Data analysis and processing

To extract the channel impulse response from the measured signal, an appropriate data analysis technique is required. The received signal $r(t)$ is affected by the transmit and receive antenna characteristics, and by the measurement system, and can be expressed as:

$$r(t) = p(t) \otimes h_{sys}(t) \otimes h_{ant,tx}(t, \theta_{tx}, \phi_{tx}) \otimes h_{ch}(t) \otimes h_{ant,rx}(t, \theta_{rx}, \phi_{rx}) \quad (2.1)$$

where $p(t)$ is the generator output, $h_{sys}(t)$ characterizes the measurement system (e.g. cables, filter and LNA), $h_{ant,tx}(t, \theta_{tx}, \phi_{tx})$ is the transmit antenna impulse response along the generic departure angle (θ_{tx}, ϕ_{tx}) , $h_{ant,rx}(t, \theta_{rx}, \phi_{rx})$ is the receive antenna impulse response along the generic arrival angle (θ_{rx}, ϕ_{rx}) , and $h_{ch}(t)$ is the channel impulse response.

As motivated in Section 2.1.4, to estimate $h_{ch}(t)$ from $r(t)$ requires not only knowledge of $p(t)$ and $h_{sys}(t)$, but also of the antenna characteristics for the departure angle from the transmit antenna and arrival angle at the receive antenna for each channel multipath component. This is unfeasible in practice; for this reason, in (2.1) the following simplifications are considered:

$$h_{ant,tx}(t, \theta_{tx}, \phi_{tx}) \approx h_{ant,tx}(t, \theta_{tx|_{los}}, \phi_{tx|_{los}}) \quad (2.2)$$

and

$$h_{ant,rx}(t, \theta_{rx}, \phi_{rx}) \approx h_{ant,rx}(t, \theta_{rx|_{los}}, \phi_{rx|_{los}}) \quad (2.3)$$

where $h_{ant,tx}(t, \theta_{tx|_{los}}, \phi_{tx|_{los}})$ and $h_{ant,rx}(t, \theta_{rx|_{los}}, \phi_{rx|_{los}})$ are the transmit and receive antenna impulse responses for the angle corresponding to the straight LOS connection between the two antennas. Under this simplification, it is possible to extract from $r(t)$ the propagation channel $h_{ch}(t)$ with a simple calibration measurement and deconvolution operation. In fact, indicating with $r_{fs}(t)$ the received signal for ideal free space propagation, from (2.1) and using (2.2), (2.3),

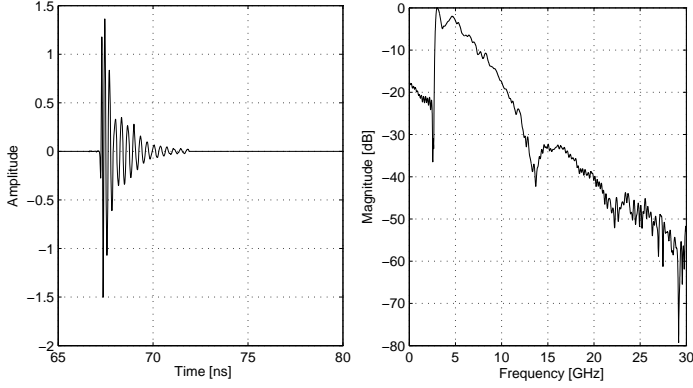


Figure 2.3: Reference signal $r_{fs}(t)$ (left) and its frequency response (right).

results:

$$r_{fs}(t) = p(t) \otimes h_{sys}(t) \otimes h_{ant,tx}(t, \theta_{tx|los}, \phi_{tx|los}) \otimes \delta(t - \tau_{fs}) \otimes h_{ant,rx}(t, \theta_{rx|los}, \phi_{rx|los}) \quad (2.4)$$

where $\delta(t)$ is the Dirac delta function and τ_{fs} is the free space delay for the signal propagation from transmitter to receiver in the calibration measurement. Therefore, $r(t)$ can be expressed as:

$$r(t) = r_{fs}(t + \tau_{fs}) \otimes h_{ch}(t) \quad (2.5)$$

The signal $r_{fs}(t)$ has been obtained with a calibration measurement by placing the transmitter and receiver at a reference distance d_0 of one meter, and with objects and obstacles far enough from the straight line of sight path; in this way, late multipath components in the received signal do not overlap with the direct path and can be easily gated out. Fig. (2.3) shows $r_{fs}(t)$, and its spectrum.

2.4.1 Inverse filtering deconvolution

To solve (2.5) with respect to $h_{ch}(t)$ requires a deconvolution operation; this operation can be easily performed in the frequency domain [13]; in fact, in the frequency domain (2.5) can be written as:

$$R(f) = R_{fs}(f) H_{ch}(f) \exp(j2\pi f \tau_{fs}) \quad (2.6)$$

where $R(f)$, $R_{fs}(f)$ and $H_{ch}(f)$ are the Fourier transforms of $r(t)$, $r_{fs}(t)$, and $h_{ch}(t)$, respectively. Therefore, the channel frequency response can be estimated

as:

$$\hat{H}_{ch}(f) = \frac{R(f)}{R_{fs}(f)} \exp(-j2\pi f\tau_{fs}) \quad (2.7)$$

The estimated channel impulse response $\hat{h}_{ch}(t)$ is then simply obtained by calculating the inverse Fourier transform of (2.7). It is worthwhile to mention that, to give consistent results, the division in (2.7) needs to be performed only inside the frequency band of interest B_{if} . Therefore, zeros are added to $\hat{H}_{ch}(f)$ at frequencies outside B_{if} ; this windowing operation is equivalent to convolve the ideal impulse response with a *sinc* function with the same bandwidth B_{if} in time domain. This has two consequences: first, that the multipath resolvability of the proposed solution is equal to the inverse of the used bandwidth; second, that side-lobes are present in the estimated impulse response. The first side-lobe of a *sinc* function has an amplitude of about 13 dB smaller than the main lobe; this may lead to erroneous detection of side-lobes as multipath components, depending on the chosen threshold, especially in NLOS propagation. To prevent this problem, a Hamming window, which provides side-lobes of -43 dB, is used [14]; in this way, however, the width of the main lobe is increased by a factor of about 48%, which worsens the multipath resolvability; therefore, specific modeling results will be affected by this choice. The differences between the two situations have been evaluated by comparing modeling results in the two cases for LOS propagation, in which the direct path is usually the strongest path, and can be easily detected, also without the use of the additional Hamming window. Variations are always smaller than 10% in absolute value (e.g. when using the Hamming window the first path power fading standard deviation in LOS increases from 0.59 to 0.62, while the total power fading standard deviation decreases from 0.88 to 0.84).

2.4.2 First peak detection and threshold setting

The first path of $\hat{h}_{ch}(t)$ is detected as the first local maximum of the envelope of $\hat{h}_{ch}(t)$, within a given threshold from the strongest peak. The threshold is an important key parameter to determine the first path, and its setting is a critical issue. In fact, choosing a high threshold (from the strongest path - i.e. a low absolute value) might lead to the wrong detection of noise components, especially in NLOS propagation, where the useful signal is significantly attenuated, while a low threshold could cause the missed detection of the direct path, especially when it is significantly smaller than the strongest one; again, NLOS is the most critical situation.

In the following, a threshold of 13 dB from the strongest peak of the envelope of $\hat{h}_{ch}(t)$ is chosen. For the considered environments, this value is adequate to correctly detect the direct path.

2.4.3 Bandwidth dependency

A proper model for the bandwidth dependency of the described statistics is fundamental for ranging applications. In fact, the proposed statistics are typically dependent on the used bandwidth; this means that they can be properly used for range estimation only if an accurate model for them is provided for the particular bandwidth used by the system. For example, errors in the evaluation of the path-loss exponent immediately reflect in errors in the estimated distance; however, this information is not satisfactory provided in IEEE models [2]. In fact, in this model it is *assumed* that the global path-loss can be decomposed in the product of a term only dependent on the distance, and in a term only dependent on the frequency. This is equivalent to assume that the channel frequency dependency affects the path-loss only in terms of an additive constant in dB, while the path-loss exponent itself remains constant, or, equivalently, to assume that the frequency dependency only affects the power measurement at the *reference* distance, while the propagation itself is not frequency dependent; this assumption, clearly appears unrealistic, and in practical statistics based ranging system operation would result in significant errors. A similar problem holds for the standard deviation of the fading, which in IEEE models is assumed constant and has been obtained by combining heterogeneous data coming from measurement campaigns which used different signal bandwidths.

In this thesis we limit the modeling to the bandwidth dependency, while the central frequency is considered constant. This is justified with the fact that it is the signal bandwidth which directly affects the multipath resolvability of the used signal and the reliability of the considered statistics. However, it is clear that the retrieved parameters are in general dependent also on the particular choice of the central frequency; the interested reader can refer to [2], [15] for an investigation of the path-loss frequency dependency.

To model the bandwidth dependency, the estimated frequency response $\hat{H}_{ch}(f)$ is windowed within different portions of the spectrum, centered at the same central frequency $f_{B,0} = 6.85$ GHz and with bandwidth B_{if} varying from 0.5 GHz to 7.5 GHz in steps of 0.5 GHz; the described statistics are accordingly evaluated; $f_{B,0}$ represents the central frequency of the portion of the spectrum between 3.1 and

Table 2.2: Channel model parameters for TP and FP, for the full bandwidth, both for LOS and for NLOS propagation

	n_{TP}	n_{FP}	σ_{TP} [dB]	σ_{FP} [dB]	$\rho_{TP,FP}$
LOS	1.38	1.92	0.84	0.62	0.38
NLOS	2.11	2.91	1.59	2.93	0.82

10.6 GHz in which UWB transmission is allowed by FCC.

2.5 Modeling results for the full bandwidth

In this section, a statistical model for the total power, and for the power of the first path of $\hat{h}(t)$ is proposed, when the full 7.5 GHz bandwidth is used.

2.5.1 Path-loss for the total signal power

The total power in the received signal decreases on average with the distance d between the transmitter and the receiver, according to the law: $1/d^{n_{TP}}$, where n_{TP} is the path-loss exponent for TP. Therefore, the power $P_{TP}(d)$ received at distance d can be written as:

$$P_{TP}(d) = \bar{P}_{0,TP} - 10n_{TP} \log_{10} \frac{d}{d_0} + S_{TP} \quad (2.8)$$

where d_0 is the reference distance, $\bar{P}_{0,TP}$ is the average measured power at the reference distance, and the total power global fading term S_{TP} is a random variable in dB with standard deviation $\sigma_{S_{TP}}$. The path-loss exponent n_{TP} is obtained by least-squares fitting. Table 2.2 reports the values of n_{TP} and $\sigma_{S_{TP}}$ both for LOS and for NLOS propagation. As an example, Fig. 2.4 shows in its left part the scatter-plot of the received power vs. the logarithm of the distance, both for LOS and for NLOS propagation, and their respective fit.

2.5.2 Statistical characterization of S_{TP} for the full bandwidth

Both for LOS, and for NLOS, a lognormal random variable models very well S_{TP} ; moreover, no distance dependency of the fading has been observed. Therefore, S_{TP} is modeled as a zero mean Gaussian random variable in dB with standard deviation $\sigma_{S,TP}$ independent of the distance. Fig. 2.5 shows the *cdf* of S_{TP} from

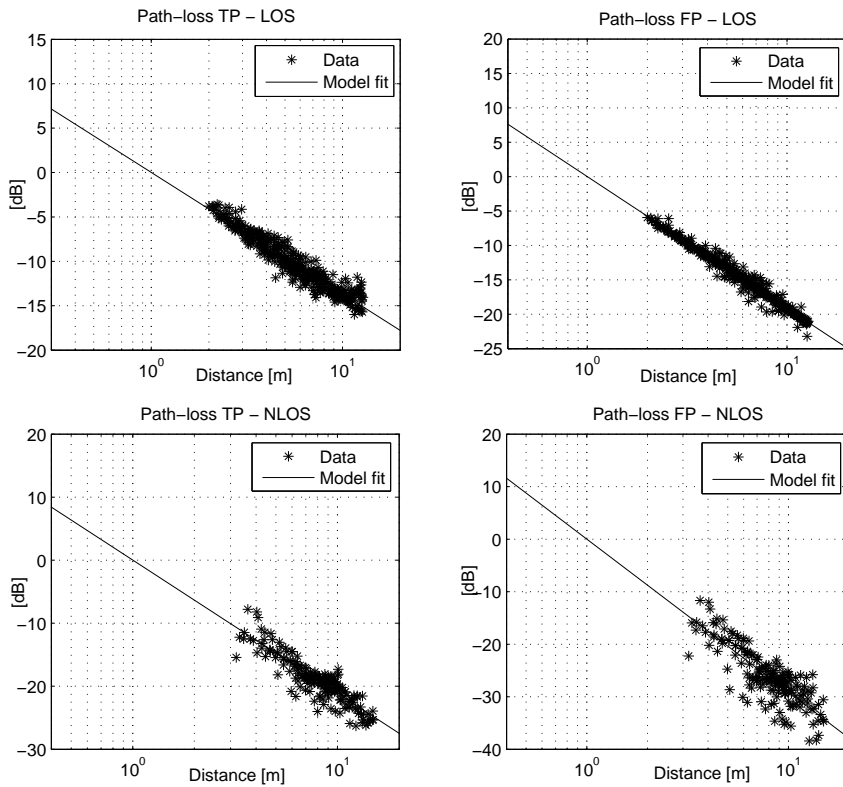


Figure 2.4: path-loss and model fit for the total signal power (left) and first path power (right), both for LOS and NLOS propagation.

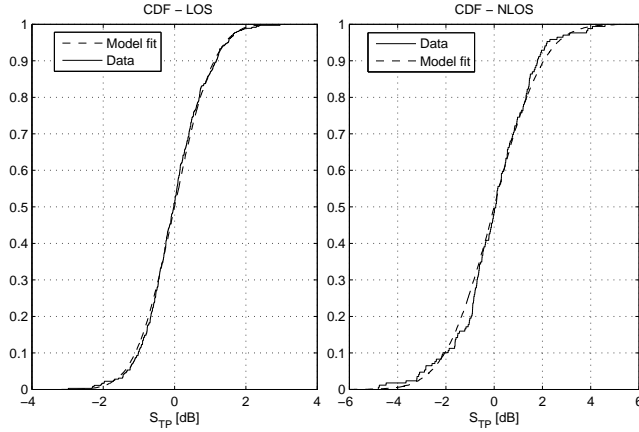


Figure 2.5: Cumulative distribution function obtained from the data, and model fit for S_{TP} , in LOS (left) and in NLOS (right).

the data and its Gaussian fit, for comparison, both for LOS (on the left) and for NLOS (on the right).

2.5.3 Path-loss for the first path power

The first path of the CIR is defined here as the first local maximum of the envelope of $\hat{h}_{ch}(t)$, with amplitude within 13 dB from the strongest peak. As explained in Section 2.4.2, this particular choice of the threshold allows to always correctly detect the direct path, both in LOS, and in NLOS propagation. Also the first path power has been modeled with a linear decrease on a logarithmic scale of the distance:

$$P_{FP}(d) = \bar{P}_{0,FP} - 10n_{FP} \log_{10} \frac{d}{d_0} + S_{FP} \quad (2.9)$$

where $\bar{P}_{0,FP}$ is the average measured first path power at the reference distance and S_{FP} is a random variable in dB with standard deviation $\sigma_{S_{FP}}$. The values of n_{FP} and $\sigma_{S_{FP}}$ both for LOS and for NLOS propagation are reported in the same Table 2.2. As an example, Fig. 2.4 shows in its right part the scatter-plot of the first path power vs the logarithm of the distance, both for LOS and for NLOS propagation, and their respective fit.

2.5.4 Statistical characterization of S_{FP} for the full bandwidth

For the first path power, a difference in the statistical characterization of S_{FP} arises between LOS and NLOS; therefore, the two propagation conditions are separately considered in the following.

LOS propagation

By observing the empirical histogram, S_{FP} in LOS has been modeled as a combination of two Gaussian *pdf*:

$$f_{S_{FP}}(s) = p_{FP}f_{S_{FP,1}}(s) + (1 - p_{FP})f_{S_{FP,2}}(s) \quad (2.10)$$

with $0 \leq p_{FP} \leq 1$; $f_{S_{FP,1}}(s)$ and $f_{S_{FP,2}}(s)$ are the *pdf* of two independent zero mean Gaussian random variables with standard deviation $\sigma_{S_{FP,1}}$ and $\sigma_{S_{FP,2}} = k_{FP}\sigma_{S_{FP,1}}$, respectively, with $k_{FP} \geq 1$. The standard deviation of S_{FP} is $\sigma_{S_{FP}} = \sigma_{S_{FP,1}}\sqrt{p_{FP} + (1 - p_{FP})k_{FP}^2}$. This model has a clear physical interpretation, since the *pdf* in (2.10) can be obtained generating a random variable as:

$$S_{FP} = P_{FP}S_{FP,1} + (1 - P_{FP})S_{FP,2} \quad (2.11)$$

where P_{FP} is a binary random variable equal to 1 or 0 with probability p_{FP} and $1 - p_{FP}$, respectively, and $S_{FP,1}$ and $S_{FP,2}$ are two independent zero mean Gaussian random variables with standard deviation $\sigma_{S_{FP,1}}$ and $\sigma_{S_{FP,2}}$, respectively. Thus, the model in (2.10) reflects the practical situation in which the direct path can experience very little fading with probability p_{FP} , since late multipath components are largely separated from it, or significant fading with probability $(1 - p_{FP})$, since there is a clear overlap of multipath components with the direct path itself. This phenomenon becomes evident by plotting the scatter-plot of S_{FP} vs. distance, shown in Fig. 2.6. Fig. 2.7 shows in its left part the *cdf* of S_{FP} from the data, and its fit using (2.10), for $p_{FP} = 0.35$ and $k_{FP} = 5$; these values have been determined by least-squares fitting.

NLOS propagation

Also for NLOS propagation, a simple Gaussian distribution in dB does not provide a satisfactory fit. In fact, by observing the empirical histogram of S_{FP} , shown in Fig. 2.8, an asymmetric distribution is found, with the negative tail larger than the positive one. This phenomenon is clearly visible also by observing the corresponding scatter-plot in Fig 2.4, in which the majority of the points in the

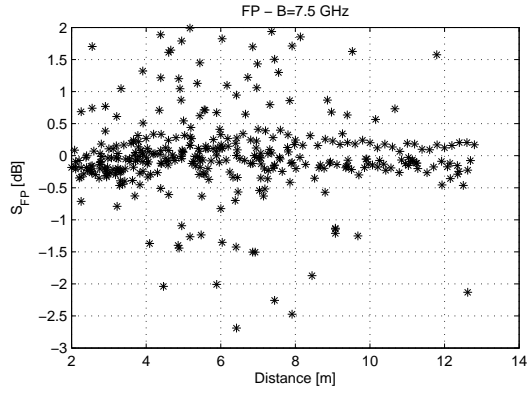


Figure 2.6: Scatter-plot of S_{FP} vs. distance for LOS propagation.

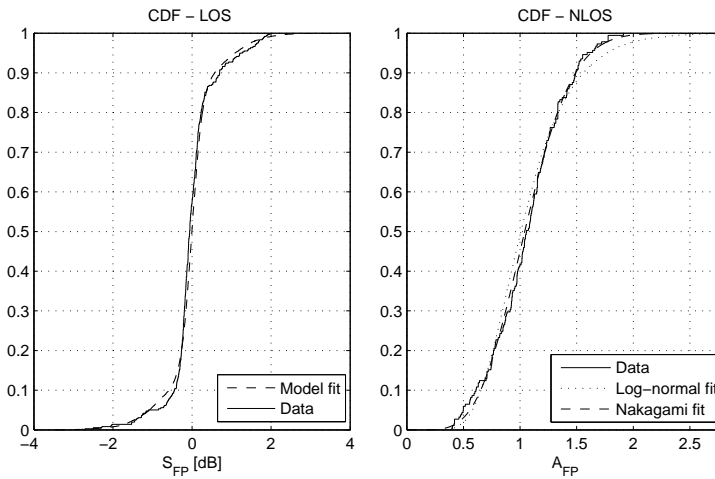


Figure 2.7: Cumulative distribution function obtained from the data, and model fit, for S_{FP} in LOS (left), and A_{FP} in NLOS.

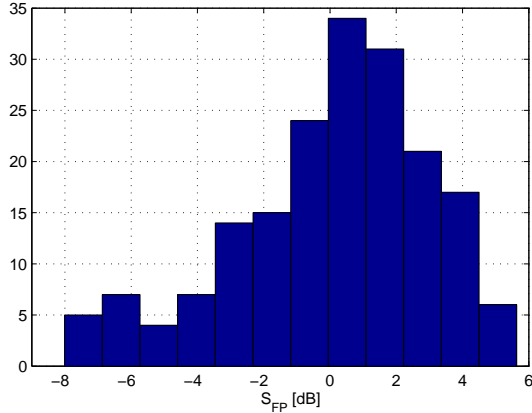


Figure 2.8: Empirical histogram for S_{FP} in NLOS.

plane are above the fit line and very close to it, while the remaining ones are below the curve and further from it.

For this reason, the linear amplitude fading, defined as:

$$A_{TP} \triangleq 10^{\frac{S_{TP}}{20}} \quad (2.12)$$

is introduced. It is found that a Nakagami distribution [3] provides a better fit for A_{TP} than a lognormal one; also in this case, no evident distance dependency of the fading has been observed. The m and Ω parameters of the Nakagami distribution have been found by least-squares fitting and are equal to 2.75 and 1.23, respectively. Fig. 2.7 shows in its right part the *cdf* of A_{TP} from the data, and its Nakagami fit. For comparison, also the lognormal fit is shown; the better fit of the Nakagami model is evident, especially in correspondence of the distribution tails.

2.6 Modeling results motivations

In this section, some comments on the proposed statistical characterization are provided. To address this issue, we explicitly consider the two terms which compose the global fading $S_{\{\cdot\}}$, namely the contribution due to the location dependency, $S_{\{\cdot\},L}$, and that due to unresolvable multipath, $S_{\{\cdot\},M}$:

$$S_{\{\cdot\}} = S_{\{\cdot\},L} + S_{\{\cdot\},M} \quad (2.13)$$

where the symbol $\{\cdot\}$ stands for TP or FP .

To support results proposed in this section, we use UWB channel measurements collected in a previously conducted campaign [4]; these measurements were performed using a grid of 49 points (each separated by 5 cm) for each location in which transmitter and receiver were placed (a total of 11 locations in LOS and 18 locations in NLOS were measured), and for similar environments as those described in Section 2.3.1 (for details about this measurement campaign we refer to [4]). In this way, it is possible to separately characterize $S_{\{\cdot\},L}$, and $S_{\{\cdot\},M}$. The location dependent term is modeled considering the average power received at each location (averaged over the 49 grid points), while the unresolvable multipath contribution is evaluated considering the power deviation for each grid point, around the average power for the specific location. Similar processing as described in Section 2.4 is used.

2.6.1 Nakagami-lognormal distribution for TP

For the total power, the classical lognormal distribution for $S_{TP,L}$ and Nakagami distribution for $A_{TP,M} = 10^{S_{TP,M}/20}$ have been found; this is in line with available literature in the field [2], [17]. Fig. 2.9 shows $S_{TP,L}$ and $S_{TP,M}$, both for LOS and NLOS propagation, and their respective fits. The specific model parameters: $\sigma_{S_{TP,L}} = 0.88$, $m_{A_{TP,L}} = 87.5$ and $\Omega_{A_{TP,L}} = 1.01$ in LOS, and $\sigma_{S_{TP,L}} = 2.50$, $m_{A_{TP,L}} = 103.2$ and $\Omega_{A_{TP,L}} = 1.01$ in NLOS, can be in general measurement dependent, and, in particular for $\sigma_{S_{TP,L}}$, variations can be expected, depending on the particular set of locations (e.g., for NLOS, measurements with up to three walls are considered in [4], while the proposed measurement campaign considers only propagation through a single wall). Therefore, these specific values can not be directly used to characterize the different sources of error for the model proposed in Section 2.5 (which, on the other hand, is not the purpose of this analysis), but in this way it is possible to provide motivations for the statistical model provided in the previous section for the global fading S_{TP} .

From the *pdf* transformation role for the product of random variables, and observing that $S_{TP,L}$ and $S_{TP,M}$ are independent, results:

$$f_{A_{TP}}(s) = \int_{-\infty}^{\infty} \frac{1}{|s|} f_{A_{TP,M}}\left(\frac{s}{y}\right) f_{A_{TP,L}}(y) dy \quad (2.14)$$

where $A_{TP} = 10^{S_{TP}/20}$ is the linear amplitude global fading, and $A_{TP,L} = 10^{S_{TP,L}/20}$. By substituting the expressions for $f_{A_{TP,M}}(s)$ and $f_{A_{TP,L}}(s)$ in (2.14),

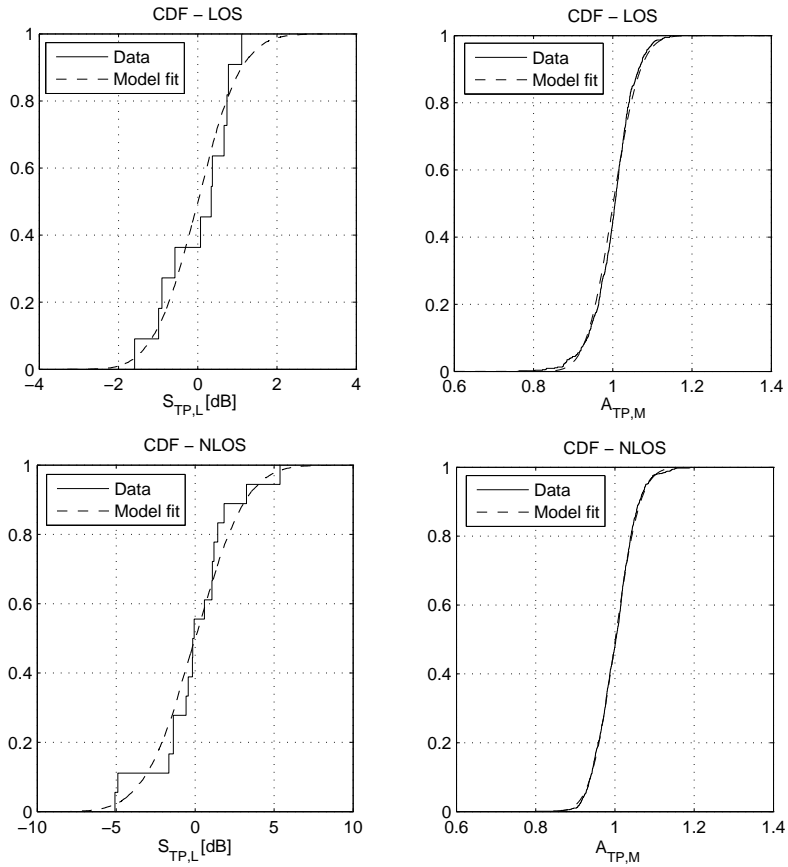


Figure 2.9: $S_{TP,L}$ and $A_{TP,M}$, both for LOS (above) and NLOS (below) propagation, and respective fits, from the measurements in [4].

results:

$$f_{A_{TP}}(s) = \frac{2m_{A_{TP,L}}^{m_{A_{TP,L}}} s^{2m_{A_{TP,L}}-1}}{\Gamma(m_{A_{TP,L}})\Omega^{m_{A_{TP,L}}}\sigma_{S_{TP,L}}\sqrt{2\pi}} \int_0^\infty \frac{\exp\left(-\frac{m_{A_{TP,L}}s^2}{\Omega y^2} - \frac{\ln^2 y}{2\sigma_{S_{TP,L}}}\right)}{y^{2m_{A_{TP,L}}+1}} dy \quad (2.15)$$

The *pdf* in (2.15) is usually referred in literature as Nakagami-lognormal distribution [18]¹.

Lognormal approximation

The expression in (2.15) can not be further simplified, unless for specific values of the parameters of interest (a typical approach to derive the statistics of interest of (2.15) is to approximate $f_{A_{TP,L}}$ with a gamma distribution [19]). However, it is intuitively clear that $f_{A_{TP}}(s)$ can be well approximated with a lognormal or Nakagami distribution depending on the values of the parameters (when the location dependency, or the unresolvable multipath is dominant, respectively). To investigate this issue, (2.15) is numerically evaluated, and the empirical distribution is tested versus a Nakagami, and a lognormal one; Fig. 2.10 shows the Kolmogorov-Smirnov (KS) test significance level ξ_{KS} , in the two cases; ξ_{KS} provides a quantitative information about the similarity of the tested distribution and the hypothesized *pdf*. Values of ξ_{KS} smaller than 0.03 indicate a very good match of the two distributions, while the hypothesized *pdf* is usually rejected for $\xi_{KS} \geq 0.05$. The parameters space is: $0.2 \leq \sigma_{S_{TP,L}} \leq 6$, and $0.5 \leq m_{A_{TP,M}} \leq 100$, while $\Omega_{A_{TP,M}}$ is chosen constant and equal to 1, since this value has been found in the collected set of measurements, and similar results are available in literature [4], [17]. From the figure, it can be seen that the lognormal approximation hypothesis is accepted at level 0.05 for every $\sigma_{S_{TP,L}}$, for $m_{A_{TP,M}} \geq 2.5$; clearly, the requirement for the minimum $m_{A_{TP,M}}$ decreases for increasing $\sigma_{S_{TP,L}}$; this can be intuitively motivated, since $m_{A_{TP,M}}$ is inversely proportional to the spreading of $A_{TP,M}$ around $\Omega_{A_{TP,M}}$; large values of $m_{A_{TP,M}}$ mean that $A_{TP,M}$ is almost deterministic and $f_{A_{TP}}(s)$ can be approximated as a lognormal random variable. Vice-versa, the Nakagami approximation is accepted at level 0.05 for $\sigma_{S_{TP,L}} \leq 2.5$,

¹It is worthwhile to note that in some papers, the Nakagami-lognormal distribution is defined as: $f_{A_{TP}}(s) = \int_{-\infty}^{\infty} f_{A_{TP,M}}(s|y)f_{A_{TP,L}}(y)dy$. This definition is suitable for traditional approaches to mobile communications channel modeling in which the fading is divided in a slow lognormal process, which defines the average received power, and a fast process which models the fast deviations (due to movement) around the average power itself [19].

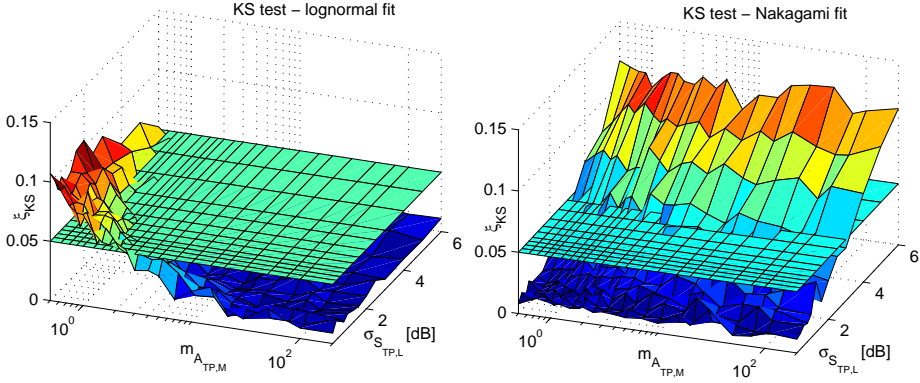


Figure 2.10: *KS test significance level value vs. $\sigma_{S_{TP,L}}$ and $m_{A_{TP,M}}$, both for lognormal (left) and for Nakagami (right) fit.*

independently on $m_{A_{TP,M}}$. From the figure, with the parameters of interest previously determined, a lognormal approximation provides a very good fit, both in LOS and in NLOS. The Nakagami approximation is also suitable, especially in LOS, while in NLOS it provides an acceptance level close to the critical one of 0.05. For this reason, a lognormal approximation can be employed for $f_{ATP}(s)$; this is in line with results obtained in Section 2.5.4.

2.6.2 Double Gaussian distribution for FP in LOS propagation

Considering the first path power global fading: $S_{FP} = S_{FP,L} + S_{FP,M}$, for LOS propagation $S_{FP,L}$ is expected to be very small, since the direct path in LOS should be affected in a very minor way by the location dependency. Fig. 2.11 shows the empirical *cdf* of $S_{FP,L}$ in LOS propagation, in its left hand part; the plot confirms this hypothesis, since $S_{FP,L}$ is of only a fraction of dB, for all the locations. It is worthwhile to mention that since this term is extremely small, eventual sources of error introduced during the measurement (e.g. deviations in the effective transmitted power from the nominal value, or noise in the measured signal) can affect its value; for this reason, these variations are not necessarily completely related to physical propagation phenomena. The same figure shows also a Gaussian fit, with $\sigma_{S_{FP,L}} = 0.21$ dB.

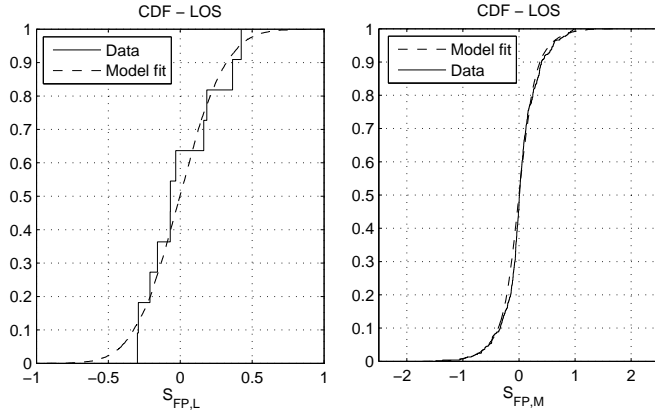


Figure 2.11: $S_{FP,L}$ (left) and $S_{FP,M}$ (right), for LOS propagation, and respective fits, from the measurements in [4].

On the right hand part of Fig. 2.11, the *cdf* of $S_{FP,M}$ is shown; by analyzing the empirical histogram, $S_{FP,M}$ has been modeled as a double Gaussian distribution:

$$f_{S_{FP,M}}(s) = p_{FP,M} f_{S_{FP,M,1}}(s) + (1 - p_{FP,M}) f_{S_{FP,M,2}}(s) \quad (2.16)$$

$f_{S_{FP,M,1}}(s)$ and $f_{S_{FP,M,2}}(s)$ are the *pdf* of two independent zero mean Gaussian random variables with standard deviation $\sigma_{S_{FP,M,1}}$ and $\sigma_{S_{FP,M,2}} = k_{FP,M} \sigma_{S_{FP,M,1}}$, respectively; the figure also shows the *cdf* fit obtained for $k_{FP,M} = 2.5$ and $p_{FP,M} = 0.35$; the obtained standard deviation of $S_{FP,M}$ is $\sigma_{S_{FP,M}} = 0.39$ dB. This model can be motivated with arguments similar as those provided in Section 2.5.4.

The *pdf* of the global fading for FP is then:

$$f_{S_{FP}}(s) = p_{FP,M} f_{S_{FP,1}}(s) + (1 - p_{FP,M}) f_{S_{FP,2}}(s) \quad (2.17)$$

where $f_{S_{FP,1}}$ and $f_{S_{FP,2}}$ are two Gaussian distributions with variance equal to $\sigma_{S_{FP,1}}^2 = \sigma_{S_{FP,M,1}}^2 + \sigma_{S_{FP,L}}^2$ and $\sigma_{S_{FP,2}}^2 = \sigma_{S_{FP,M,2}}^2 + \sigma_{S_{FP,L}}^2$, respectively. The *pdf* in (2.17) is the same as that found in (2.10).

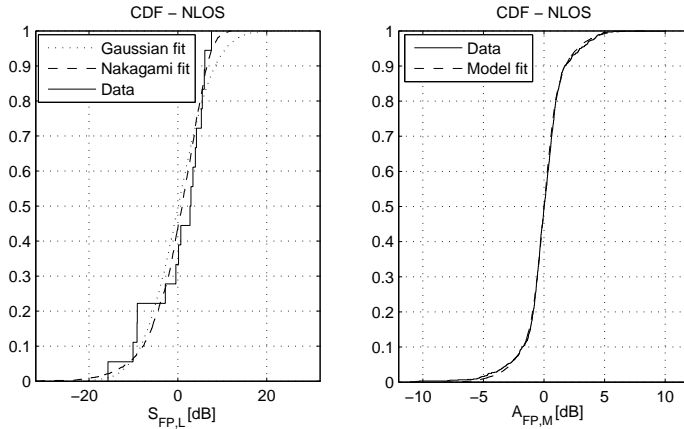


Figure 2.12: $S_{FP,L}$ (left) and $S_{FP,M}$ (right), for NLOS propagation, and respective fits, from the measurements in [4].

2.6.3 Double Nakagami-lognormal distribution for FP in NLOS propagation

Fig. 2.12 shows the empirical *cdf* of $S_{FP,L}$ in NLOS propagation, in its left hand part; from the figure, $S_{FP,L}$ exhibits an asymmetric behavior, with the negative tail larger than the positive one; for this reason, the location dependent term in NLOS has been modeled with a Nakagami distribution; the same figure also shows the Nakagami fit (with the *cdf* converted in dB scale) with parameters $m_{A_{FP,L}} = 0.89$ and $\Omega_{A_{FP,L}} = 1.93$. We believe that, given the difficulty of accurately estimating a 2-parameters distribution with a limited number of measurements, this point deserves further investigation with a larger number of measurement locations. An intuitive explanation for the diverse model for NLOS shadowing between TP and FP can be explained with different mechanisms for the two statistics; in fact, the total power shadowing results from the contribution of *several* random multipath components; from the central limit theorem, the global variation can be well approximated as Gaussian; the first path power shadowing on the contrary, is due to variations of the direct path only; an asymmetric distribution in dB appears reasonable, since for some NLOS locations the direct path can experience a significant drop, due to heavy obstructions, making the distribution in dB asymmetric around its mean.

As for LOS, also for NLOS $S_{FP,M}$ has been modeled as the combination of

two Gaussian $pdfs^2$, with $k_{FP,M} = 2.5$ and $p_{FP,M} = 0.3$; its standard deviation results: $\sigma_{S_{FP,M}} = 1.83$ dB. The cdf of $S_{FP,M}$ and its model fit are shown in the same Fig. 2.12.

Using the proposed model, the pdf of the global first path power fading in NLOS is:

$$f_{S_{FP}}(s) = p_{FP,M} f_{S_{FP,1}}(s) + (1 - p_{FP,M}) f_{S_{FP,2}}(s) \quad (2.18)$$

where $f_{S_{FP,1}}(s) = \int_{-\infty}^{\infty} 1/|s| f_{S_{FP,M,1}}(s/y) f_{S_{FP,L}}(y) dy$ and $f_{S_{FP,2}}(s) = \int_{-\infty}^{\infty} 1/|s| f_{S_{FP,M,2}}(s/y) f_{S_{FP,L}}(y) dy$ are two Nakagami-lognormal distributions, with parameters as previously given.

Nakagami approximation

Also in this case, the possibility of modeling (2.18), with a simpler distribution, is investigated. To this purpose, (2.18) is numerically evaluated, and the empirical distribution is tested versus a Nakagami, and a lognormal one. Fig. 2.13 shows the KS test significance level ξ_{KS} , in the two cases. The parameters space is: $0.2 \leq \sigma_{S_{FP,L}} \leq 6$ dB, and $0.5 \leq m_{AFP,M} \leq 100$; $\Omega_{AFP,M}$ is chosen constant and equal to 1.93, while $k_{FP,M} = 2.5$ and $p_{FP,M} = 0.3$, as previously determined; testing results, however, change in a very minor way by changing $k_{FP,M}$ and $p_{FP,M}$. From the figure, it can be seen that the Nakagami approximation hypothesis is accepted at level 0.05 for $m_{AFP,M} \approx 1$, when $\sigma_{S_{FP,L}} \leq 3$ dB. Vice-versa, the lognormal approximation is accepted at level 0.05 when $\sigma_{S_{FP,L}} \geq 3$, for $m_{AFP,M} \approx 1$. These results can be motivated with arguments similar as those provided in Section 2.6.1. For this reason, a Nakagami approximation can be employed for $f_{AFP}(s)$ for the values of interest; this is in line with results obtained in Section 2.5.4.

2.7 Bandwidth dependency of path-loss

In this section, the bandwidth dependency of the proposed statistical characterization is discussed. It will be shown that, when using smaller bandwidths, in LOS the fading becomes dependent on the distance between transmitter and receiver.

²Modeling $S_{FP,M,2}$ as a Gaussian random variable provides accurate results for the bandwidths of interest for UWB; however, for smaller B_{if} a Nakagami approximation provides a better matching (this also holds for LOS, and for the measurements in Section 2.5).

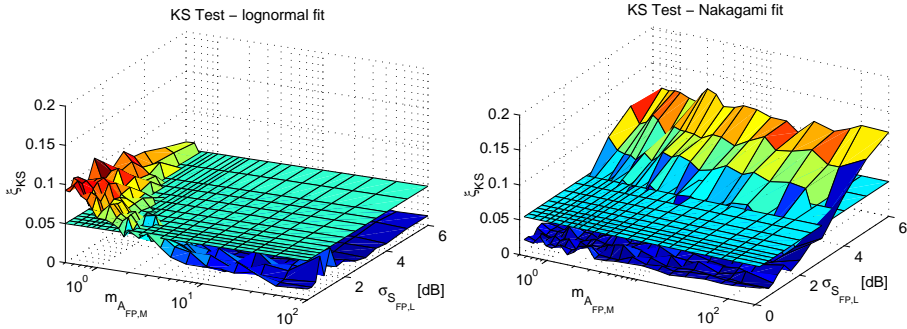


Figure 2.13: *KS test significance level value vs. $\sigma_{S_{FP,L}}$ and $m_{A_{FP,M}}$, both for lognormal (left) and for Nakagami (right) fit.*

2.7.1 Bandwidth dependency of n_{TP}

Both for LOS, and for NLOS, n_{TP} increases when decreasing B_{if} . Fig. 2.14 shows n_{TP} vs. B_{if} , for the two propagation conditions. Even if the actual values of the path-loss exponent depend on several factors (type of antennas, dielectric properties of the environment, polarization and angle of incidence of each multipath component with objects (typically walls) in the environment), a qualitative motivation for the obtained result can be provided. In fact, the total power path-loss exponent can also be considered as a quantitative measure of the global capability of the environment of "keeping" the radiated energy; the smaller the path-loss exponent, the higher is the capability of the environment of not dispersing the energy. In the considered environments, interaction of electromagnetic waves with the environment is mainly due to reflections with the walls (interaction with the floors are less significant, since the antenna gains of the considered biconical antennas are significantly smaller in this direction). The interaction of UWB signals with walls can be described considering results for the transmission and reflection coefficients for a lossy dielectric slab of finite thickness. For typical lossy dielectric slabs, the modulo of the reflection coefficient decreases with frequency less than linearly in the UWB band of interest (see e.g. [20]). This means that when decreasing the bandwidth and keeping constant the central frequency, the reflected energy from a dielectric lossy slab will be smaller. This explains the

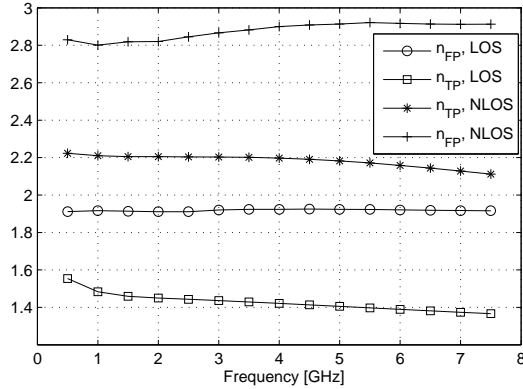


Figure 2.14: n_{TP} and n_{FP} vs. B_{if} , both for LOS, and for NLOS.

larger n_{TP} when decreasing B_{if} .

2.7.2 Bandwidth dependency of n_{FP}

The same Fig. 2.14 also shows n_{FP} vs. B_{if} , both for LOS, and for NLOS. From the figure, it can be seen that for LOS propagation, n_{FP} remains practically constant (it varies between 1.91 and 1.93); this is reasonable, since in LOS the direct path is affected in a very minor way by the environment. In NLOS n_{FP} seems to slightly decrease for decreasing B_{if} ; the deviations, however, are smaller than 5% in the full range of variation of B_{if} .

2.7.3 Bandwidth dependency of fading - LOS

Bandwidth dependency modeling of S_{TP}

When decreasing the bandwidth, the same lognormal fading model as for $B_{if} = 7.5$ GHz has been found, with an increasing $\sigma_{S_{TP}}$. This is straightforward, since the multipath resolvability is reduced. However, an other phenomenon is observed as well. In fact, while for the full bandwidth no distance dependency of the fading has been observed, this is not true anymore for smaller bandwidths, in which the fading tends to increase with the distance itself. This point can be intuitively explain with the following reasoning. In LOS, for increasing d , the direct path tends to have less weight with respect to the total signal, since n_{FP} is close to 2, while n_{TP} is smaller; this means that the most reliable part of the received signal

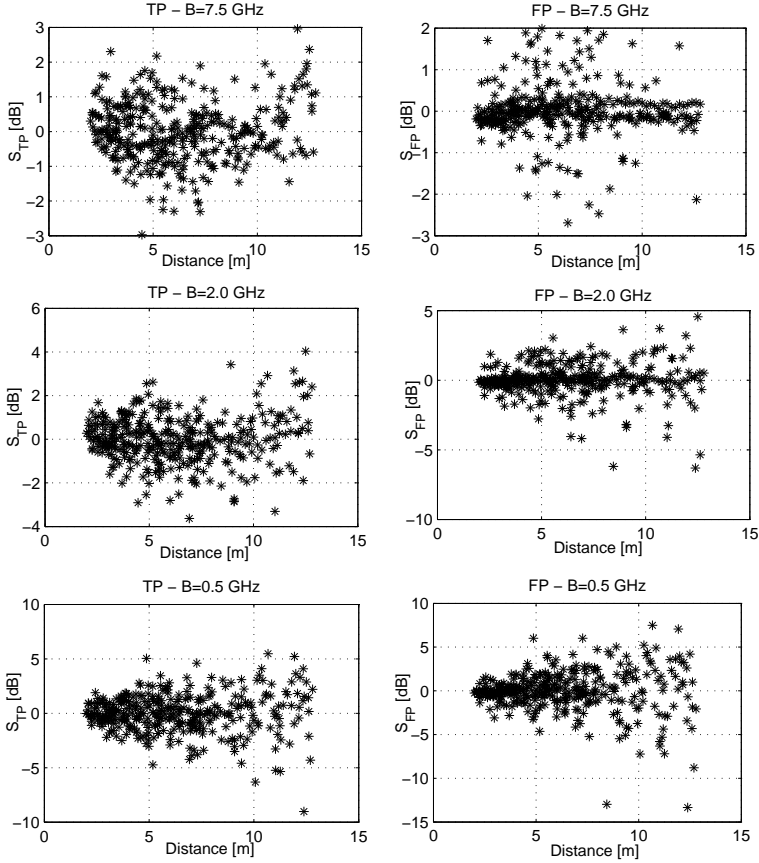


Figure 2.15: Scatter-plot of S_{TP} (left) and S_{FP} (right) vs. d , for different bandwidths.

represents a less significant part of it, for larger d . Moreover, by increasing d , the distance difference between the different path components tends to decrease, making the non-resolvable multipath more dense. Fig. 2.15 shows S_{TP} vs. d for $B_{if} = 7.5$ GHz, $B_{if} = 2$ GHz, and $B_{if} = 0.5$ GHz, for comparison.

To characterize the dependency of S_{TP} on d and B_{if} , its standard deviation has been modeled as an increasing function of d ; the slope of the fit increases with decreasing B_{if} :

$$\sigma_{S_{TP}}(B_{if}, d) = \sigma_{S_{TP},0}(g_{B_{if},TP}(B_{if})g_{d,TP}(d) + 1) \quad (2.19)$$

with $\sigma_{S_{TP},0}$ independent on B_{if} and d . $g_{B_{if},TP}$ and $g_{d,TP}$ account for the bandwidth and distance dependency, respectively; by analyzing the obtained results,

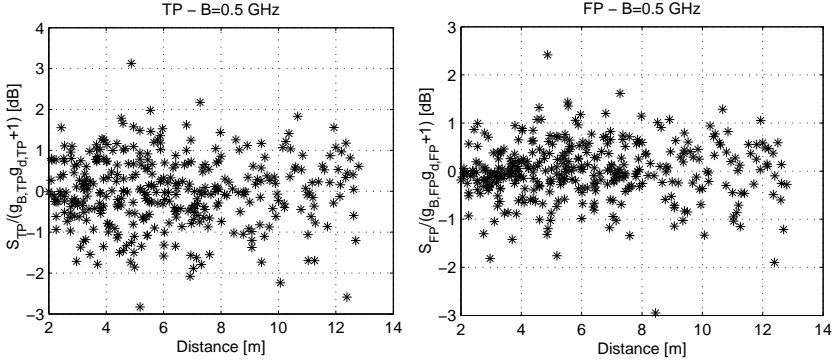


Figure 2.16: Scatter-plot of S_{TP} (left) and S_{FP} (right) vs. d , for $B_{if} = 0.5$ GHz, and normalized to their distance and bandwidth dependent terms.

they have been modeled as:

$$g_{B_{if},TP} = g_{B_1,TP} \left(\exp \left(-\frac{B_{if}^{g_{B_2,TP}}}{g_{B_3,TP}} \right) - \exp \left(-\frac{7.5g_{B_2,TP}}{g_{B_3,TP}} \right) \right) \quad (2.20)$$

$$g_{d,TP} = d^\alpha. \quad (2.21)$$

The model parameters $g_{B_1,TP} = 0.17$, $g_{B_2,TP} = 0.55$, $g_{B_3,TP} = 0.64$, and $\alpha_{TP} = 1.5$ have been obtained by least-squares fitting. It is worth to note that since $g_{B_{if},TP}(B_{if})|_{B_{if}=7.5\text{GHz}} = 0$, $\sigma_{S_{TP},0}$ represents the fading standard deviation when the full bandwidth is used. As an example, Fig. 2.16 shows on the left the scatter-plot of S_{TP} for $B_{if} = 0.5$ GHz, normalized to its bandwidth and distance dependent terms.

Using (2.19) it is possible to simply analytically evaluate the *global* fading standard deviation on the total set of collected measurements, by averaging over the distribution of the distance:

$$\sigma_{S_{TP}}(B_{if}) = \sqrt{\int_d \sigma_{S_{TP},0}^2 (g_{B_{if},TP}(B_{if})g_{d,TP}(d) + 1)^2 f_d(d) dd} = \quad (2.22)$$

$$\sigma_{S_{TP},0} \sqrt{g_{B_{if},TP}^2(B_{if}) E\{d^{2\alpha}\} + 2g_{B_{if},TP}(B_{if}) E\{d^\alpha\} + 1}$$

where $f_d(d)$ is the *pdf* of the distance between transmitter and receiver, and $E\{\cdot\}$ is the expectation operation. Fig. 2.17 shows the global fading vs. B_{if} , for TP, both from the total set of data, and using (2.22), for comparison. For plotting (2.22), $E\{d^{2\alpha}\} = 402.15$ and $E\{d^\alpha\} = 16.9$ have been obtained from the collected set of measurements.

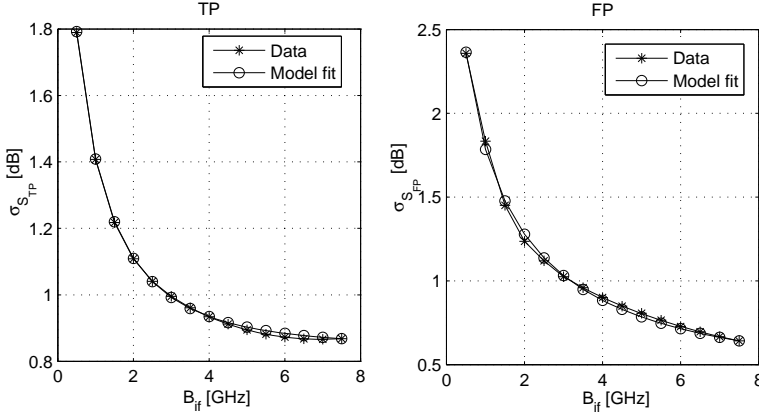


Figure 2.17: Global fading standard deviation of the total set of data for TP (left) and for FP right, both from the data, and with the model in (2.22), for comparison.

Bandwidth dependency modeling of S_{FP}

When decreasing the bandwidth, a similar behavior for $\sigma_{S_{FP}}$ vs. d and B_{if} , as for $\sigma_{S_{TP}}$, has been found. This dependency can be qualitatively explained with similar arguments as in the previous section. Fig. 2.15 also shows S_{FP} for $B_{if} = 7.5$ GHz, $B_{if} = 2$ GHz, and $B_{if} = 0.5$ GHz, for comparison.

The dependency of S_{FP} on d and B_{if} , is characterized with the same model as in (2.19). The model parameters $g_{B_1,FP} = 0.53$, $g_{B_2,FP} = 0.35$, $g_{B_3,FP} = 0.67$, and $\alpha_{FP} = 1.5$ have been obtained by least-squares fitting. As an example, Fig. 2.16 shows on the right the scatter-plot of S_{FP} for $B_{if} = 0.5$ GHz, normalized to its bandwidth and distance dependent terms.

The global fading standard deviation on the total set of collected measurements can be derived similarly as in (2.22), and it is shown on the right part of Fig. 2.17. To complete the model characterization, the variation of p_{FP} and k_{FP} vs. B_{if} and d needs to be addressed. By analyzing the data, $p_{FP}(B_{if}, d) = p_{FP}(B_{if}) = p_{1,FP} \exp(-B_{if}/p_{2,FP})$, while k_{FP} can be considered constant with the bandwidth and distance. The values of $p_{1,FP} = 0.9$ and $p_{2,FP} = 7.5$ have been obtained by least squares fitting. The intuitive explanation for this model is immediate: when decreasing B_{if} , the probability that the direct path is affected by significant fading increases.

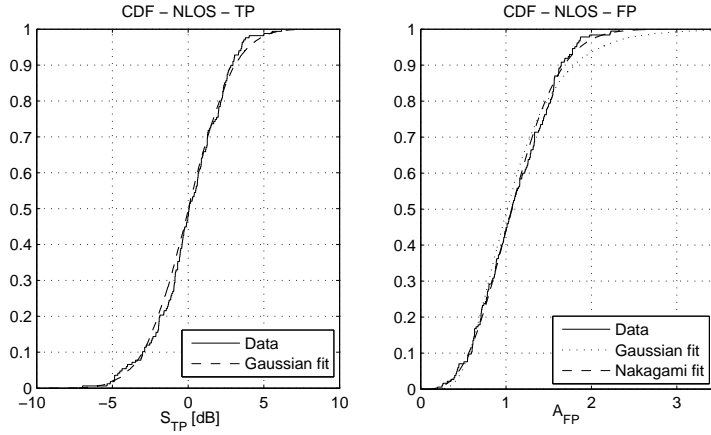


Figure 2.18: *cdf* of S_{TP} (left) and of A_{FP} (right) and model fits, for $B_{if} = 0.5$ GHz.

2.7.4 Bandwidth dependency of fading - NLOS

Bandwidth dependency of S_{TP}

In NLOS, when decreasing B_{if} , the same Gaussian model for S_{TP} has been found. As an example, Fig. 2.18 shows the *cdf* of S_{TP} for $B_{if} = 0.5$ GHz, and its Gaussian fit. Differently as for LOS, no distance dependency of $\sigma_{S_{TP}}$ has been observed. In this case, the same model as in (2.20) is valid, with $\alpha_{\{\cdot\}} = 0$. The other model parameters $g_{B_1,TP} = 0.026$, $g_{B_2,TP} = 1$, and $g_{B_3,TP} = 2.74$ have been obtained by least-squares fitting. Fig. 2.19 shows $\sigma_{S_{TP}}$ vs. B_{if} and the model fit.

Bandwidth dependency of S_{FP}

Also for decreasing B_{if} , A_{FP} can be modeled as a Nakagami random variable. Fig. 2.18 shows the *cdf* of A_{FP} for $B_{if} = 0.5$ GHz, and its Gaussian and Nakagami fits for comparison. Also in this case, the Nakagami fit exhibits a better match, especially in correspondence of the distribution tail. The m and Ω parameters vs. B_{if} are plotted in Fig. 2.19, together with $\sigma_{S_{FP}}$, and its model fit obtained for $g_{B_1,TP} = 0.022$, $g_{B_2,TP} = 1$, and $g_{B_3,TP} = 2.64$. As it can be seen, for $B_{if} = 0.5$ GHz an irregular behavior of $\sigma_{S_{FP}}$ is experienced; this is likely due to very large irregular deviations of this statistic in some NLOS measurements.

Table 2.3 shows a summary of the proposed modeling results for S_{TP} and

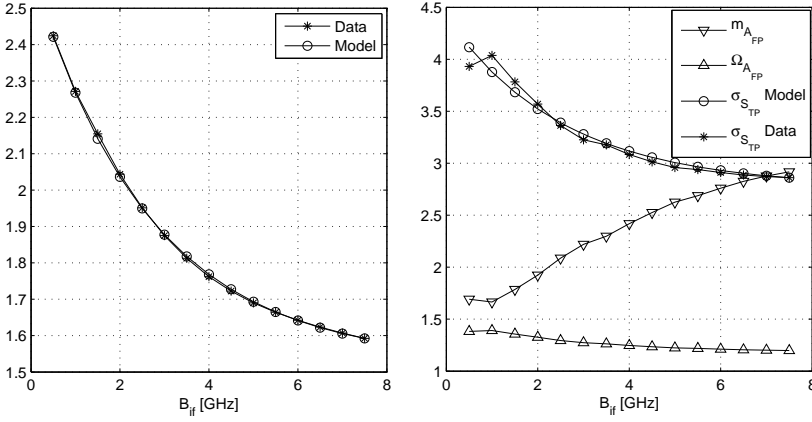


Figure 2.19: Global fading standard deviation of the total set of data for TP (left) and for FP (right), both from the data, and with the model in 2.22, for comparison.

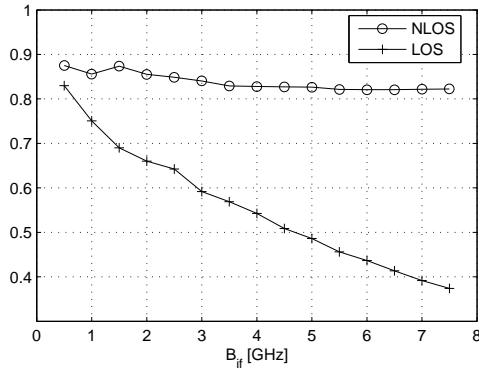
S_{FP} , both for LOS, and for NLOS.

2.7.5 Correlation between $S_{TP,0}$ and $S_{FP,0}$

The other relevant parameter to model is the correlation $\rho_{TP,FP,0}$ between the normalized fading of TP and FP, as a function of the bandwidth. Fig. 2.20 shows $\rho_{TP,FP,0}$ vs. B_{if} , both for LOS, and for NLOS. It can be seen that for NLOS propagation, the correlation coefficient is significantly higher than for LOS. This is due to the fact that in NLOS the fading of the direct path is much higher than in LOS and constitutes a significant part of the total signal power fading. The significant increase of $\rho_{TP,FP,0}$ for LOS, by decreasing B_{if} , is due to the fact that in this case a larger number of (non-resolvable) paths, and thus a higher percentage of the total signal power, composes the first detectable path. For NLOS, the fading correlation is mainly due to the presence of obstructions between the transmitter and the receiver and the bandwidth has a much less noticeable effect on it.

Table 2.3: Overview of modeling results for S_{TP} and S_{FP}

Full Bandwidth $B_{if}=7.5$ GHz:	Fading Model (approx.)	Fading Model (exact)	Distance dependency
<i>TP</i>			
LOS	lognormal	Nakagami-lognormal	No
NLOS	lognormal	Nakagami-lognormal	No
<i>FP</i>			
LOS	double lognormal	double lognormal	No
NLOS	Nakagami	double Nakagami-lognormal	No
<hr/>			
$0.5 \leq B_{if} \leq 7.5$ GHz:	Fading Model (approx.)	Fading Model (exact)	Distance dependency
<i>TP</i>			
LOS	lognormal	Nakagami-lognormal	Yes: $\sigma_{S_{TP}}(B_{if}, d) = \sigma_{S_{TP},0}(g_{B_{if},TP}(B_{if})g_{d,TP}(d) + 1)$
NLOS	lognormal	Nakagami-lognormal	No
<i>FP</i>			
LOS	double lognormal	double-lognormal	Yes: $\sigma_{S_{FP}}(B_{if}, d) = \sigma_{S_{FP},0}(g_{B_{if},FP}(B_{if})g_{d,FP}(d) + 1)$
NLOS	Nakagami	double Nakagami-lognormal	No

**Figure 2.20:** Correlation between the normalized fading of TP and FP , as a function of the bandwidth, both for LOS and for $NLOS$.

2.8 Parameters' estimation dependency on the number of measurements

In the previous paragraphs, models for n_{TP} , n_{FP} , S_{TP} , and S_{FP} have been proposed, based on a large set of collected measurements. In practical situations, for statistics based ranging applications, knowledge of the propagation parameters for the particular environment in which the system needs to operate is required. To this purpose, two different solutions can be employed. The first is to use parameters proposed in a previously developed model. The second is to perform a set of calibration measurements, in order to estimate the required propagation parameters for the specific environment. The first solution is attractive since it does not require any effort from the user of the system; however, it might lead to inaccurate knowledge of the propagation parameters. In the second solution, it is relevant to know how many measurements need to be performed, in order to retrieve in a reliable way the desired parameters. In this case, it is relevant to know:

- how the error in the parameters' estimation is related to the number of measurements.
- how the error in the parameters' estimation affects the range estimation accuracy.

In this section, we provide an answer to the first issue. Capitalizing on the results obtained in this section, the second issue will be addressed in the next chapter. Since the proposed path-loss model for the total signal power and first path power is formally the same, we omit the subscript TP and FP in (2.8) and (2.9), respectively, and we consider the equation:

$$P(d) = \overline{P}_0 - 10n \log_{10} \frac{d}{d_0} + S \quad (2.23)$$

The proposed analysis is general; however, we explicitly address only the case of the full bandwidth, in which no distance dependency of the fading has been found. The derivations for the case of smaller B_{if} can be obtained in a similar way.

In the following, we investigate how the estimates \hat{n} and $\hat{\sigma}_S$ of the path-loss exponent and fading standard deviation, respectively, are affected by the number N_m of collected measurements of the power P_i , for $1 \leq i \leq N_m$.

2.8.1 Dependency of \hat{n} on N_m

By estimating n in a least-squares sense, results:

$$\hat{n} = \frac{1}{10} \frac{\sum_{i=1}^{N_m} (P_0 - P_i) \log_{10} \frac{d_i}{d_0}}{\sum_{i=1}^{N_m} \log_{10}^2 \frac{d_i}{d_0}} = n - \frac{1}{10} \frac{\sum_{i=1}^{N_m} S_i \log_{10} \frac{d_i}{d_0}}{\sum_{i=1}^{N_m} \log_{10}^2 \frac{d_i}{d_0}} \quad (2.24)$$

where P_i is the received power in the i -th measurement, d_i is the distance between transmitter and receiver for the i -th measurement, and S_i is the fading in dB for the i -th measurement. The equation in (2.24) is a non-linear combination of $2N_m$ random variables: $\{d_1, d_2, \dots, d_{N_m}, S_1, S_2, \dots, S_{N_m}\}$ and can be formally written as:

$$\hat{n} = F_{\hat{n}}\{\mathbf{d}, \mathbf{S}\} \quad (2.25)$$

where $\mathbf{d} = [d_1, d_2, \dots, d_{N_m}]$ and $\mathbf{S} = [S_1, S_2, \dots, S_{N_m}]$ are the vectors of the distances and fading of the set of the N_m measurements. Using the variance propagation law for $F_{\hat{n}}$, approximated till the second order and evaluated around the mean of \mathbf{d} and \mathbf{S} , it is possible to evaluate the mean and variance of (2.24). This results in:

$$E\{\hat{n}\} \approx F_{\hat{n}}\{E\{\mathbf{d}\}, E\{\mathbf{S}\}\} + \frac{1}{2} \text{trace} \left\{ \delta_{[\mathbf{d}, \mathbf{S}][\mathbf{d}, \mathbf{S}]^T}^2 F_{\hat{n}}\{E\{\mathbf{d}\}, E\{\mathbf{S}\}\} \mathbf{Q}_{[\mathbf{d}, \mathbf{S}]} \right\} = n \quad (2.26)$$

$$\begin{aligned} \text{Var}\{\hat{n}\} \approx & \delta_{[\mathbf{d}, \mathbf{S}]^T} F_{\hat{n}}\{E\{\mathbf{d}\}, E\{\mathbf{S}\}\} \mathbf{Q}_{[\mathbf{d}, \mathbf{S}]} [\delta_{[\mathbf{d}, \mathbf{S}]^T} F_{\hat{n}}\{E\{\mathbf{d}\}, E\{\mathbf{S}\}\}]^T = \\ & \frac{\sigma_S^2}{100 N_m \log_{10}^2 \left(\frac{E\{d\}}{d_0} \right)} \end{aligned} \quad (2.27)$$

where the apex T indicates the vector transpose operation, $\delta_{[\mathbf{d}, \mathbf{S}]^T}^2 F_{\hat{n}}\{E\{\mathbf{d}\}, E\{\mathbf{S}\}\}$ is the Hessian matrix of $F_{\hat{n}}\{\mathbf{d}, \mathbf{S}\}$ evaluated around the mean of \mathbf{d} and \mathbf{S} , $\mathbf{Q}_{[\mathbf{d}, \mathbf{S}]}$ is the variance matrix of the $2N_m$ length vector $[d_1, d_2, \dots, d_{N_m}, S_1, S_2, \dots, S_{N_m}]$, and $\delta_{[\mathbf{d}, \mathbf{S}]^T} F_{\hat{n}}\{E\{\mathbf{d}\}, E\{\mathbf{S}\}\}$ is the vector of the partial derivatives of $F_{\hat{n}}\{\mathbf{d}, \mathbf{S}\}$ evaluated around the mean of \mathbf{d} and \mathbf{S} . To calculate the previous expressions, it has been used that the $2N_m$ random variables $\{\mathbf{d}, \mathbf{S}\}$ are independent and that by definition \mathbf{S} is zero mean. Defining:

$$R_{j,0} = \frac{S_j \log_{10} \frac{d_j}{d_0}}{\sum_{i=1}^{N_m} \log_{10}^2 \frac{d_i}{d_0}} \quad (2.28)$$

(2.24) can be written as:

$$\hat{n} = n - \frac{R_{N_m}}{10} \quad (2.29)$$

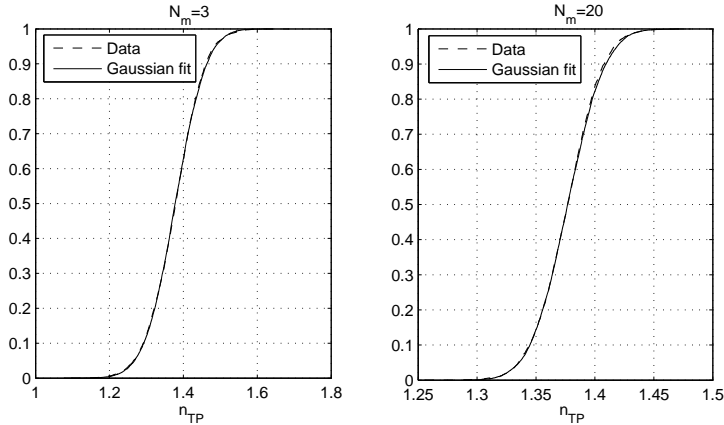


Figure 2.21: *cdf of n_{TP} for LOS, from the data, and Gaussian fit, for $N_m = 3$ and $N_m = 20$.*

with $R_{N_m} = \sum_{j=1}^{N_m} R_{j,0}$. The mean of \hat{n} is n , indicating that the estimate of the path-loss exponent is unbiased. Using the central limit theorem, (2.24) can be modeled as a Gaussian random variable. From simulation, the approximation gives accurate results already for $N_m \geq 3$. As an example, Fig. 2.21 shows the *cdf* of \hat{n} for LOS and *TP*, for $N_m = 3$ and 20, obtained both from the model, and directly from a random selection of the data.

For evaluation purposes, it can be more convenient to introduce the standard deviation of the error in the normalized path-loss exponent, defined as:

$$\sigma_{\Delta_{\hat{n}}} \triangleq \text{std}\{\hat{n}/n\} = \frac{\sigma_S}{10n\sqrt{N_m} \log_{10}\left(\frac{E\{d\}}{d_0}\right)} \quad (2.30)$$

where $E\{d\}$ can be evaluated from the collected data. From (2.30) it can be seen that for having for example $\sigma_{\Delta_{\hat{n}_{TP}}} \leq 1/30$ (this is equivalent to require that with 99.9% probability $(\hat{n} - n)/n \leq 0.1$), it is necessary to have $N_m \geq 6$ in LOS and $N_m \geq 13$ in NLOS. Similar requirements can be obtained for the case of n_{FP} .

As an example, Fig. 2.22 shows the standard deviation of the error in evaluation of the normalized path-loss exponent as a function of N_m , for *TP* and for *FP*, both empirically, and using (2.30), for LOS propagation. It is evident that a significantly smaller number of calibration measurements is required to correctly estimate n_{FP} , than for n_{TP} ; this is due to the smaller fading for *FP* and to the larger value of n_{FP} , compared to n_{TP} .

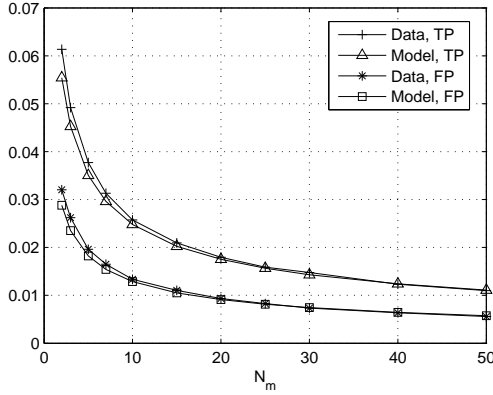


Figure 2.22: $\sigma_{\Delta_{\hat{n}}}$ vs. N_m , for LOS and for TP and FP, both from the data, and using (2.30).

2.8.2 Dependency of $\hat{\sigma}_S$ on N_m

Similarly, the dependency of $\hat{\sigma}_S$ on N_m can be determined. Using the previously calculated \hat{n} , the following relationship holds, for the generic i -th measurement:

$$P_i = P_0 - 10n \log_{10} \frac{d}{d_0} + S_i = P_0 - 10\hat{n} \log_{10} \frac{d}{d_0} + \hat{S}_i \quad (2.31)$$

where \hat{S}_i is the fading term for the i -th measurement, when the fit is done with the estimated path-loss exponent \hat{n} instead of the true one n . It immediately follows:

$$\hat{S}_i = -10(n - \hat{n}) \log_{10} \frac{d_i}{d_0} + S_i = \quad (2.32)$$

$$S_i - \frac{\sum_{j=1}^{N_m} S_j \log_{10} \frac{d_j}{d_0}}{\sum_{j=1}^{N_m} \log_{10}^2 \frac{d_j}{d_0}} \log_{10} \frac{d_i}{d_0} = S_i - R_{N_m} \log_{10} \frac{d_i}{d_0}$$

Given the set of N_m fading terms \hat{S}_i for $1 \leq i \leq N_m$, it is possible to evaluate the estimated variance $\hat{\sigma}_S^2$. Considering the following estimator for σ_S^2 :

$$\hat{\sigma}_S^2 = \frac{1}{N_m - 1} \sum_{i=1}^{N_m} \left(\hat{S}_i - E\{\hat{S}_i\} \right)^2 = \quad (2.33)$$

$$\frac{1}{N_m - 1} \sum_{i=1}^{N_m} \hat{S}_i^2 = \frac{1}{N_m - 1} \sum_{i=1}^{N_m} \left(S_i - R_{N_m} \log_{10} \frac{d_i}{d_0} \right)^2$$

where it has been used that \hat{S}_i is zero mean (this is evident from (2.32)). After some calculation, results:

$$\hat{\sigma}_S^2 = \frac{1}{N_m - 1} \left(\sum_{i=1}^{N_m} S_i^2 - \frac{\left(\sum_{i=1}^{N_m} S_i \log_{10} \frac{d_i}{d_0} \right)^2}{\sum_{i=1}^{N_m} \log_{10}^2 \frac{d_i}{d_0}} \right) = F_{\hat{\sigma}_S^2} \{ \mathbf{d}, \mathbf{S} \} \quad (2.34)$$

The mean value of (2.34) can be evaluated in the same way as in (2.26), giving:

$$E\{\hat{\sigma}_S^2\} \approx \sigma_S^2 \quad (2.35)$$

Therefore, also the estimator of the fading variance is unbiased. To evaluate the variance of the estimator for the fading variance, it is necessary to consider an approximation till the third order of (2.34):

$$\begin{aligned} Var\{\hat{\sigma}_S^2\} &\approx \delta_{[\mathbf{d}, \mathbf{S}]^T} F_{\hat{\sigma}_S^2} \{E\{\mathbf{d}\}, E\{\mathbf{S}\}\} \mathbf{Q}_{[\mathbf{d}, \mathbf{S}]} [\delta_{[\mathbf{d}, \mathbf{S}]^T} F_{\hat{\sigma}_S^2} \{E\{\mathbf{d}\}, E\{\mathbf{S}\}\}]^T + \\ &\frac{1}{2} trace \left\{ \left(\delta_{[\mathbf{d}, \mathbf{S}]^T}^2 F_{\hat{\sigma}_S^2} \{E\{\mathbf{d}\}, E\{\mathbf{S}\}\} \mathbf{Q}_{[\mathbf{d}, \mathbf{S}]} \right)^2 \right\} = \frac{2}{N_m} \sigma_S^4 \end{aligned} \quad (2.36)$$

Also in this case, we can introduce the standard deviation of the error in the normalized fading variance, defined as:

$$\sigma_{\Delta_{\hat{\sigma}_S^2}} \triangleq std\{(\hat{\sigma}_S^2 - \sigma_S^2)/\sigma_S^2\} = \sqrt{\frac{2}{N_m}} \quad (2.37)$$

which does not depend on the channel parameters (as for the case of \hat{n}), but only on N_m . From(2.37) it is evident that an accurate estimate of $\hat{\sigma}_S^2$ requires a significantly higher N_m , compared to \hat{n} . On the other hand, as it will be shown in the next chapters, for ranging applications an accurate estimate of $\hat{\sigma}_S^2$ is usually not required.

The statistical characterization of (2.34) deserves further discussion. Considering the terms inside the brackets in (2.34), it can be immediately seen that the first term: $\sum_{i=1}^{N_m} S_i^2$ dominates over the second one: $(\sum_{i=1}^{N_m} S_i \log_{10}(d_i/d_0))^2 / \sum_{i=1}^{N_m} \log_{10}^2(d_i/d_0)$. This can be understood observing that the first and second term are two correlated random variables with mean and variance, respectively equal to (using a second order approximation for the mean and a third order approximation for the variance, as previously discussed): $N_m \sigma_S^2$ and $2N_m \sigma_S^4$ in the first case, and σ_S^2 and $(2/N_m) \sigma_S^4$ in the second case. Using the central limit theorem, the first term in (2.34), can be modeled as a Gaussian random variable, for N_m large enough; therefore, the overall expression in (2.34) can be approximated as a Gaussian random variable for N_m large enough.

2.9 Chapter summary

In this chapter, a short overview of the time domain measurement set-up, employed to collect the UWB channel measurements used in this thesis, is preliminarily presented, and the measurement locations and signal processing are briefly described. The concept of *statistics based ranging* is then introduced. This approach uses statistics retrieved from the received signal in order to estimate the distance between transmitter and receiver. It is shown that both the traditional total power of the received signal, and the power of the first path of the received signal exhibit very little fading when the total bandwidth allowed by FCC for UWB transmissions is used, making these statistics attractive for low-complexity ranging applications. Path-loss models for *TP* and *FP* are provided and justified; it is shown that the considered statistics are in general dependent on the system bandwidth and on the distance between transmitter and receiver. Knowledge of an accurate and complete model is relevant to be able to fully exploit the estimation accuracy provided by this method; on the other hand, these issues are neglected in traditional IEEE models, which have been developed with communication applications in mind. Therefore, the contribution of this chapter allows to overcome practical limitations experienced by traditional UWB channel modeling, when used for statistics based ranging purposes.

Bibliography

- [1] A.F. Molisch, "*Ultrawideband propagation channels - theory, measurements, and modeling*", IEEE Transaction on Vehicular Technologies, vol. 54, no. 5, pp. 1528-1545, Sept. 2005.
- [2] A.F. Molisch, D. Cassioli, Chia-Chin Chong, S. Emami, A. Fort, B. Kannan, J. Karedal, J. Kunisch, H.G. Schantz, K. Siwiak, M.Z. Win, "*A Comprehensive Standardized Model for Ultrawideband Propagation Channels*", IEEE Transaction on Antennas and Propagation, vol. 54, no. 11, pp. 3151-3166, Nov. 2006.
- [3] A.F. Molisch, K. Balakrishnan, D. Cassioli, Chia-Chin Chong, S. Emami, A. Fort, J. Karedal, J. Kunisch, H.G. Schantz, U. Schuster, K. Siwiak, "*IEEE 802.15.4a channel model - final report*", 2005, available at: <https://mentor.ieee.org/802.15/dcn/04/15-04-0662-04-004a-channel-model-final-report-r1.pdf>.

-
- [4] Z. Irahhauten, "*Ultra-wideband wireless channel: measurements, analysis and modeling*", Ph.D. dissertation, Jan. 2008, Delft University of Technology, The Netherlands.
- [5] Z. Irahhauten, A. Yarovoy, H. Nikookar, G. J. M. Janssen, and L. Ligthart, "*Measurement setup for ultra wideband indoor radio channel characterization*", IEEE SCVT 2004, Nov. 2004.
- [6] R.V. de Jongh, M. Hajian, and L.P. Ligthart, "*Time domain antenna measurement: implementation and verification of a novel technique*", European Microwave Conference, vol. 1, pp. 470-475, Oct. 1997.
- [7] A. Muqaibel, A. Safaai-Jazi, A. Attiya, B. Woerner, S. Riad, "*Path-loss and time dispersion parameters for indoor UWB propagation*", IEEE Transactions on Wireless Communications, vol. 5, no. 3, pp. 550-559, Mar. 2006.
- [8] A. Muqaibel, "*Characterization of ultra wideband communication channels*", Ph.D. dissertation, 2003, Virginia Tech University, U.S..
- [9] M.Z. Win, R.A. Scholtz, "*Impulse radio: how it works*", IEEE Communications Letters, vol. 2, no. 2, pp. 36-38, Feb. 1998.
- [10] FCC, Office of Engineering and Technology, "*Revision of part 15 of the commissions rules regarding ultra-wideband transmission systems*", ET Docket, no. 98-153, 2002.
- [11] M.Z. Win, R.A. Scholtz, "*Ultra-wide bandwidth time-hopping spread-spectrum impulse radio for wireless multiple-access communications*", IEEE Transaction on Communications, vol. 48, no. 4, pp. 679-689, Apr. 2000.
- [12] Liuqing Yang, G.B. Giannakis, "*Ultra-wideband communications: an idea whose time has come*", IEEE Signal Processing Magazine, vol. 21, no. 4, pp. 26-54, Nov. 2004.
- [13] S.M. Riad, "*The deconvolution problem, an overview*", IEEE Proceedings, vol. 74, no. 1, pp. 82-85, Jan. 1986.
- [14] F.J. Harris, "*On the use of windows for harmonic analysis with the discrete Fourier transform*", IEEE Proceedings, vol. 66, no. 1, pp. 51-83, Jan. 1978.
- [15] P. Pajusco, P. Pagani, "*Frequency dependence of the UWB indoor propagation channel*", IEEE EUCAP 2007, pp. 1-7, Nov. 2007.

- [16] M. Nakagami, "*The m-distribution - a general formula of intensity distribution of rapid fading*", Statistical Methods in Radio Wave Propagation, pp. 336, 1960.
- [17] J. Romme and B. Kull, "*On the relation between bandwidth and robustness of indoor UWB communication*", IEEE UWBST, pp. 255-259, Nov. 2003.
- [18] T.T. Tjhung, C.C. Chai, "*Fade statistics in Nakagami-lognormal channels*", IEEE Transaction on Communications, vol. 47, no. 12, pp. 1769-1772, Dec. 1999.
- [19] I.M. Kostic, "*Analytical approach to performance analysis for channel subject to shadowing and fading*", IEEE Communications Proceedings, vol. 152, no. 6, pp. 821-827, Dec. 2005.
- [20] Wang Yang, Zhang Qinyu, Zhang Naitong, "*Time domain calculation of UWB impulse signal transmitting through a finitely conducting slab*", IEEE International Symposium on Microwave, Antenna, Propagation and EMC Technologies for Wireless Communications 2007, pp. 822-825, Aug. 2007.

Statistics Based UWB Ranging

In this chapter, the models proposed in Chapter 2 for the total signal power and first path power, are used for range estimation. The obtained standard deviation range error is derived, and a discussion on the achieved performance is provided. The possibility to further improve the estimation accuracy, by combining the results obtained with total power and first path power in an optimal way, is then investigated. The bandwidth dependency of the achieved range error is derived, and a method to mitigate outliers in the range estimation for LOS, which arise when small bandwidths are used, is proposed. A strategy to recognize the environment in which transmitter and receiver are placed, making use of the proposed statistical characterization is discussed. The effect on ranging of errors in channel parameters' estimation is derived. Finally, an application of the model to weighted least squares positioning is proposed, and improvements compared to the classical signal power based approach are evaluated.

3.1 Range Estimation with TP and FP

Range estimation using the total signal power is performed as:

$$\hat{d}_{TP} = d_0 10^{\frac{P_{0,TP} - P_{TP}(d)}{10n_{TP}}} = d \exp\left(-\frac{S_{TP} \ln 10}{10n_{TP}}\right) \quad (3.1)$$

The expression for range estimation using the first path power is formally the same as (3.1). In the following, for practical convenience we distinguish between LOS and NLOS propagation.

3.2 LOS propagation

In LOS, using TP , the estimated range as given by (3.1) is a log-normal random variable with mean and variance:

$$\mu_{\hat{d}_{TP}} = d \exp\left(\frac{\sigma_{S,TP} \ln 10}{10\sqrt{2}n_{TP}}\right)^2 \quad (3.2)$$

$$\sigma_{\hat{d}_{TP}}^2 = d^2 \exp\left(\frac{\sigma_{S,TP} \ln 10}{10n_{TP}}\right)^2 \left(\exp\left(\frac{\sigma_{S,TP} \ln 10}{10n_{TP}}\right)^2 - 1\right) \quad (3.3)$$

In a similar way, for range estimation using the first path power, applying the *pdf* transformation rule to (3.1) and using the model in Section 2.5 gives:

$$\hat{d}_{FP} = d \left(p_{FP} \exp\left(-\frac{S_{FP,1} \ln 10}{10n_{FP}}\right) + (1 - p_{FP}) \exp\left(-\frac{S_{FP,2} \ln 10}{10n_{FP}}\right) \right) \quad (3.4)$$

which is the sum of two log-normal random variables; this gives:

$$\mu_{\hat{d}_{FP}} = d \left(p_{FP} \exp\left(\frac{\sigma_{S,FP,1} \ln 10}{10\sqrt{2}n_{FP}}\right)^2 + (1 - p_{FP}) \exp\left(\frac{\sigma_{S,FP,2} \ln 10}{10\sqrt{2}n_{FP}}\right)^2 \right) \quad (3.5)$$

$$\sigma_{\hat{d}_{FP}}^2 = d^2 p_{FP} \exp\left(\frac{\sigma_{S,FP,1} \ln 10}{10n_{FP}}\right)^2 \left(\exp\left(\frac{\sigma_{S,FP,1} \ln 10}{10n_{FP}}\right)^2 - 1\right) + \quad (3.6)$$

$$d^2 (1 - p_{FP}) \exp\left(\frac{\sigma_{S,FP,2} \ln 10}{10n_{FP}}\right)^2 \left(\exp\left(\frac{\sigma_{S,FP,2} \ln 10}{10n_{FP}}\right)^2 - 1\right)$$

Fig. 3.1 shows the mean and standard deviation range error obtained from the *total* set of measurement data (as described in the previous chapter), using (3.1) and applied to both TP and FP , as a function of the bandwidth used. The range error:

$$\epsilon_{\{\cdot\}} \triangleq \hat{d}_{\{\cdot\}} - d \quad (3.7)$$

is defined as the difference between the estimated distance $\hat{d}_{\{\cdot\}}$ and the true distance d , where $\{\cdot\}$ stands for TP or FP . It can be seen that for large bandwidths and LOS, the first path power outperforms the total signal power by a factor of about 2; in fact, for $B_{if} = 7.5$ GHz, the standard deviation of the range error using FP is $\sigma_{\epsilon_{FP}} = 0.53$ m, while for using TP is $\sigma_{\epsilon_{FP}} = 1.07$ m. This result appears reasonable, since the used bandwidth is extremely large and the direct path is affected in a very minor way by later multipath components; therefore, this method exploits in this case the most reliable part of the received signal. For

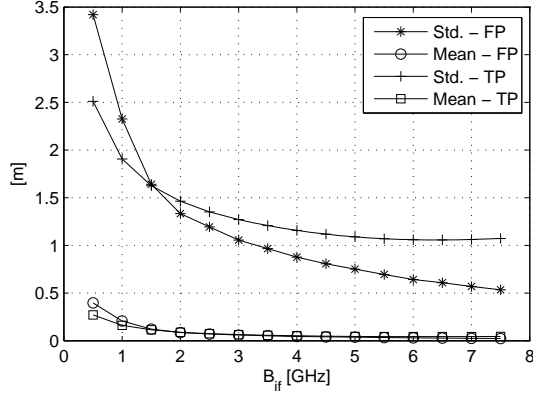


Figure 3.1: Mean and standard deviation range error vs. B_{if} in LOS, both for TP, and for FP.

$B_{if} \leq 1.5$ GHz, on the contrary, the total power outperforms the first path power. This is due to the larger increase of $\sigma_{S_{FP}}$ with respect to $\sigma_{S_{TP}}$, when decreasing B_{if} .

The mean range error is 0.04 and 0.02 m for TP and FP, when the full bandwidth is used; it increases up to 0.27 and 0.40 m, respectively, for $B_{if} = 0.5$ GHz.

3.2.1 Unbiased range estimation for the full bandwidth

As shown in the previous chapter, when using the full bandwidth, no distance dependency of the fading has been experienced in LOS. Therefore, it is possible to normalize the range estimate by dividing the estimated distance with TP and FP by the terms:

$$\mu_{\hat{d}_{TP}}^{(n)} = \exp\left(\frac{\sigma_{S_{TP}} \ln 10}{10\sqrt{2}n_{TP}}\right)^2 \quad (3.8)$$

$$\mu_{\hat{d}_{FP}}^{(n)} = p_{FP} \exp\left(\frac{\sigma_{S_{FP,1}} \ln 10}{10\sqrt{2}n_{FP}}\right)^2 + (1 - p_{FP}) \exp\left(\frac{\sigma_{S_{FP,2}} \ln 10}{10\sqrt{2}n_{FP}}\right)^2 \quad (3.9)$$

respectively, to obtain an unbiased estimate of d , given by:

$$\hat{d}_{TP}^{(n)} = \hat{d}_{TP} / \mu_{\hat{d}_{TP}}^{(n)} \quad (3.10)$$

and

$$\hat{d}_{FP}^{(n)} = \hat{d}_{FP} / \mu_{\hat{d}_{FP}}^{(n)} \quad (3.11)$$

in the two cases. Improvements are however modest, due to the very small values of $\mu_{\hat{d}_{TP}}^{(n)}$, and $\mu_{\hat{d}_{FP}}^{(n)}$ (equal respectively to 1.011 and 1.003); in fact, the mean and standard deviation of the normalized range error are: $\mu_{\epsilon_{TP}}^{(n)} = -0.01$ m and $\sigma_{\epsilon_{TP}}^{(n)} = 1.05$ m for TP , and $\mu_{\epsilon_{FP}}^{(n)} \approx 0$ and $\sigma_{\epsilon_{FP}}^{(n)} = 0.52$ m for FP .

It is also worthwhile to note that approximating S_{FP} as Gaussian, does not introduce any noticeable difference in ranging results for the full bandwidth case either; this can be formally explained by observing that differences in the statistical characterization of S_{FP} only reflect in differences in the second and higher order terms of \hat{d}_{FP} (this can be immediately seen by considering the variance propagation law applied to the Taylor expansion of (3.1)). Since $((\sigma_{S_{FP}} \ln 10)/(10n_{FP}))^2 \approx 0.01$, for the purpose of ranging, S_{FP} can be approximated as a Gaussian random variable without any impairment; this is equivalent to assume $p_{FP} = 1$ and $k_{FP} = 0$. This approximation allows to simplify the theoretical analysis as well as modeling efforts.

Estimator variance and Cramer-Rao lower bound

Capitalizing on the observation that: $((\sigma_{S_{\{i,j\}}} \ln 10)/(10n_{\{i,j\}}))^2 \ll 1$, both for TP and for FP , neglecting the second and higher order terms of the variance of (3.10), (3.11), results in, respectively:

$$\sigma_{\hat{d}_{TP}}^2 \approx d^2 \left(\frac{\sigma_{S_{TP}} \ln 10}{10n_{TP}} \right)^2 \quad (3.12)$$

and:

$$\sigma_{\hat{d}_{FP}}^2 \approx d^2 \left(\frac{\sigma_{S_{FP}} \ln 10}{10n_{FP}} \right)^2 \quad (3.13)$$

which equal the Cramer-Rao lower bound for power based ranging [1]. Therefore, for the full bandwidth, the minimum estimator variance can be achieved from the power measurement with the a-priori knowledge of only the path loss exponent and fading standard deviation; moreover without knowledge of the second parameter, deviations are only minor.

Best linear unbiased estimation

Having knowledge of the correlation $\rho_{\hat{d}_{TP}, \hat{d}_{FP}}^{(n)}$ between $\hat{d}_{TP}^{(n)}$ and $\hat{d}_{FP}^{(n)}$, it is possible to calculate a Best Linear Unbiased Estimator (BLUE) of the distance d_{BLUE} [2], by combining in an optimum way the estimated distances of the two methods. d_{BLUE} is optimum in the sense that it is unbiased, and it achieves the minimum

variance among the estimators which exploit the moments till the second order of the used statistics. Exploiting the Gaussian approximation for S_{FP} previously introduced, the fading of TP and FP has a bivariate Gaussian distribution, and the normalized estimated distance has a bivariate log-normal distribution; this allows to simply calculate $\rho_{\hat{d}_{TP}^{(n)}, \hat{d}_{FP}^{(n)}}$ as:

$$\rho_{\hat{d}_{TP}^{(n)}, \hat{d}_{FP}^{(n)}} = \frac{\exp(\rho_{S_{TP}, S_{FP}} \sigma_{S, TP} \sigma_{S, FP} (\ln 10/10)^2 / (n_{TP} n_{FP})) - 1}{\sqrt{(\exp(\sigma_{S, TP} \ln 10 / (10 n_{TP}))^2 - 1)(\exp(\sigma_{S, FP} \ln 10 / (10 n_{FP}))^2 - 1)}} \quad (3.14)$$

The variance matrix \mathbf{Q}_d can then be calculated as:

$$\mathbf{Q}_d = \begin{pmatrix} \sigma_{\hat{d}_{TP}^{(n)}}^2 & \rho_{\hat{d}_{TP}^{(n)}, \hat{d}_{FP}^{(n)}} \sigma_{\hat{d}_{TP}^{(n)}} \sigma_{\hat{d}_{FP}^{(n)}} \\ \rho_{\hat{d}_{TP}^{(n)}, \hat{d}_{FP}^{(n)}} \sigma_{\hat{d}_{TP}^{(n)}} \sigma_{\hat{d}_{FP}^{(n)}} & \sigma_{\hat{d}_{FP}^{(n)}}^2 \end{pmatrix} \quad (3.15)$$

It is worth to note that the distance dependent term d^2 which appears in each element of the matrix in (3.15) is immaterial for the calculation of the BLUE. The BLUE of the distance results in:

$$\hat{d}_{BLUE} = (\mathbf{a}^T \mathbf{W}_{BLUE} \mathbf{a})^{-1} \mathbf{a}^T \mathbf{W}_{BLUE} [\hat{d}_{TP}^{(n)}, \hat{d}_{FP}^{(n)}]^T = \quad (3.16)$$

$$(\mathbf{a}^T \mathbf{Q}_d^{-1} \mathbf{a})^{-1} \mathbf{a}^T \mathbf{Q}_d^{-1} [\hat{d}_{TP}^{(n)}, \hat{d}_{FP}^{(n)}]^T$$

where $\mathbf{a} = [1, 1]^T$ and $\mathbf{W}_{BLUE} = \mathbf{Q}_d^{-1}$ is the BLUE weight matrix. Using the BLUE, the achieved standard deviation range error is $\sigma_{\hat{d}_{BLUE}} = 0.50$ m; the modest improvement is due to the correlation between the fading of TP and FP and to the significantly better accuracy of FP , which then dominates the performance.

Estimator variance analytical evaluation

It is interesting to analytically evaluate the standard deviation of the range error on the total set of measurements and to compare it with empirical results obtained on the total set of data. Considering e.g. the total power, using (3.1), (3.7), (3.8), and (3.10), the normalized error in a generic measurement is:

$$\epsilon_{TP}^{(n)} = d \left(\exp \left(-\frac{\ln 10}{10 n_{TP}} S_{TP} - \frac{1}{2} \left(\frac{\ln 10 \sigma_{S, TP}}{10 n_{TP}} \right)^2 \right) - 1 \right) \quad (3.17)$$

which is a non-linear combination of two random variables, d and S ; its standard deviation $\sigma_{\epsilon_{TP}^{(n)}}$ is given by:

$$\sigma_{\epsilon_{TP}^{(n)}} = \sqrt{\int_d \int_s (\epsilon_{TP}^{(n)})^2 f_d(d) f_{S,TP}(s) dd, ds} \quad (3.18)$$

where it has been used that $\epsilon_{TP}^{(n)}$ is zero mean. After some calculation it follows:

$$\sigma_{\epsilon_{TP}^{(n)}} = \sqrt{E\{d^2\} \left(\exp \left(\frac{\ln 10}{10n_{TP}} \sigma_{S_{TP}} \right)^2 - 1 \right)} \approx \sqrt{E\{d^2\}} \frac{\ln 10}{10n_{TP}} \sigma_{S_{TP}} \quad (3.19)$$

where $E\{d^2\}$ can be evaluated from the data, and in the last approximation, it has been used that $((\ln 10 \sigma_{S_{TP}})/(10n_{TP}))^2 \ll 1$. Eq. (3.19) can be also used to correctly dimension the positioning network by imposing given requirements on the maximum standard deviation range error $\sigma_{\epsilon_{TP}}^{max}$; e.g., in the simplest case in which d is uniformly distributed between 0 and a maximum distance d_{max} , it immediately follows:

$$d_{max} \leq \sqrt{3} \sigma_{\epsilon_{TP}}^{max} \frac{10n_{TP}}{\ln 10 \sigma_{S_{TP}}} \quad (3.20)$$

In a similar way, using the previously introduced Gaussian approximation, the standard deviation of the range error using FP, $\sigma_{\epsilon_{FP}^{(n)}}$, can be evaluated (the expression is formally the same as (3.19)). To evaluate the average BLUE standard deviation range error $\sigma_{\epsilon_{BLUE}}$, we can observe that the theoretical BLUE variance is:

$$\sigma_{\epsilon_{BLUE}}^2 = (\mathbf{a}^T \mathbf{W}_{BLUE} \mathbf{a})^{-1} \quad (3.21)$$

By averaging over d and substituting the parameters of interest:

$$\begin{aligned} \sigma_{\hat{d}_{BLUE}} &= \quad (3.22) \\ &= \sqrt{\frac{E\{d^2\} (\exp(\frac{\sigma_{S_{TP}} \ln 10}{10n_{TP}})^2 - 1) (\exp(\frac{\sigma_{S_{FP}} \ln 10}{10n_{FP}})^2 - 1) (1 - \rho_{\hat{d}_{TP}^{(n)}, \hat{d}_{FP}^{(n)}})}{\exp(\frac{\sigma_{S_{TP}} \ln 10}{10n_{TP}})^2 + \exp(\frac{\sigma_{S_{FP}} \ln 10}{10n_{FP}})^2 - 2 \sqrt{\rho_{\hat{d}_{TP}^{(n)}, \hat{d}_{FP}^{(n)}} (\exp(\frac{\sigma_{S_{TP}} \ln 10}{10n_{TP}})^2 - 1) (\exp(\frac{\sigma_{S_{FP}} \ln 10}{10n_{FP}})^2 - 1) - 2}}}} \\ &\approx \frac{\sqrt{E\{d^2\} (1 - \rho_{\hat{d}_{TP}^{(n)}, \hat{d}_{FP}^{(n)}}) \frac{\sigma_{S_{TP}} \sigma_{S_{FP}} \ln 10}{10n_{TP} n_{FP}}}}{\sqrt{\left(\frac{\sigma_{S_{TP}}}{n_{TP}}\right)^2 + \left(\frac{\sigma_{S_{FP}}}{n_{FP}}\right)^2 - 2 \sqrt{\rho_{\hat{d}_{TP}^{(n)}, \hat{d}_{FP}^{(n)}}} \frac{\sigma_{S_{TP}} \sigma_{S_{FP}}}{n_{TP} n_{FP}}}} \end{aligned}$$

where to derive the last approximate expression, it has been used that $((\ln 10 \sigma_{S_{TP}})/(10n_{TP}))^2 \ll 1$ and $((\ln 10 \sigma_{S_{FP}})/(10n_{FP}))^2 \ll 1$.

The evaluation of (3.19) and (3.22) for TP , FP , and BLUE gives 1.03, 0.52 m, and 0.51 m, in the three cases; these values are in line with results previously reported, and obtained directly from the data.

Table 3.1: Channel parameters and ranging results for each single LOS environment

Environment #	1	2	3	4	5	6
n_{TP}	1.23	1.42	1.40	1.60	1.50	1.25
n_{FP}	1.92	1.92	2.01	1.92	1.92	1.87
$\sigma_{S_{TP}}$	0.59	0.80	0.67	0.57	0.46	0.20
$\sigma_{S_{FP}}$	0.48	0.66	1.08	0.61	0.21	0.07
$\rho_{S_{TP}, S_{TP}}$	0.15	0.44	0.81	0.61	0.28	0.31
$\sigma_{\hat{d}_{TP}^{(n)}}$	0.92	1.19	0.63	0.47	0.54	0.14
$\sigma_{\hat{d}_{FP}^{(n)}}$	0.38	0.80	0.79	0.42	0.15	0.04
$\sigma_{\hat{d}_{BLUE}}$	0.35	0.75	0.60	0.40	0.13	0.03

3.2.2 Environment differentiation and identification

In this section, the possibility of further improving the estimation accuracy obtained in LOS and for the full bandwidth, by distinguishing among the different environments in which the measurements have been collected, is investigated. The idea behind this approach is that, if knowledge about the channel parameters for the specific environment in which transmitter and receiver are placed is available, it is possible to exploit a much more reliable model, in which the considered statistics exhibit a smaller deviation from their model fit. In this way, the range estimation accuracy can be potentially higher. Since this possibility requires knowledge of the environment in which transmitter and receiver are located, a possible way to identify it by using the statistical characterization itself, is then proposed.

The environments in which the previously described LOS measurements have been performed are: a laboratory room, two different corridors, an office, a corridor to office and a meeting room; For easiness of notation, the environments are named: 1, 2, 3, 4, 5, and 6, respectively, and to denote the model parameters for the particular environment, the apex (e) is used. Table 3.1 shows the obtained channel parameters previously presented, for the considered environments. Also in this case, a Gaussian approximation for S_{FP} is used.

A-priori knowledge of the environment

The same table 3.1 also shows in the last three lines the obtained standard deviation range errors when a-priori knowledge of the environment in which transmitter

and receiver are placed is available (and therefore it is possible to use the correct channel parameters), for *TP* and *FP*, and *BLUE*. The global range error standard deviation using *TP* is 0.79 m, significantly smaller than that obtained without environment differentiation. This is reasonable, since the path loss exponent for *TP* changes in a noticeable way among different environments. On the contrary, the standard deviation range error using the first path power is 0.50, almost the same as that obtained in Section 3.2.1, since n_{FP} changes in a negligible way among the different environments. Using the BLUE it is possible to further improve the estimation accuracy ($\sigma_{\hat{d}_{BLUE}} = 0.43$ m), gaining a factor about 15% compared to results obtained without the environment differentiation.

Environment identification strategy

In the previous section, it has been assumed that the environment in which transmitter and receiver are located is known. However, this might not be the case in a real positioning system, even when knowledge of the transmitter ID is available.

In this section, we show how the statistical characterization of *TP* and *FP* can be used to identify the environment in which the transmitter and receiver are located. In this way, the only a priori information which is required by the described approach is the accurate modeling of the previously presented statistics for the environments of interest.

Considering the test statistic:

$$\delta_d^{(e)} = \hat{d}_{TP}^{(e)} - \hat{d}_{FP}^{(e)} \quad (3.23)$$

The decision approach is the following:

- The different $\delta_d^{(e)}$ are computed for the different possible environments of interest (environment testing).
- The environment (e) is chosen as:

$$\arg \min_{(e)} \left\{ \frac{1}{p_{(e)}} |\delta_d^{(e)}| \right\} \quad (3.24)$$

where $p_{(e)}$ is the a-priori probability that we are in the environment (e). The intuitive explanation of this decision strategy is the following: if we are testing the right environment, (and thus we use the correct channel parameters), $|\delta_d^{(e)}|$ is small, since both $\hat{d}_{TP}^{(e)}$ and $\hat{d}_{FP}^{(e)}$ are close to the true distance; if we are testing

the wrong environment, it is likely that $\hat{d}_{TP}^{(e)}$ and $\hat{d}_{FP}^{(e)}$ give significantly different values and $|\delta_d^{(e)}|$ is large.

In formulas, denoting with $\hat{d}|_c$ the estimated distance (with total power or first path power) in case of correct test of the environment, and with $\hat{d}|_i$ the same estimated distance in case of incorrect test of the environment:

$$\hat{d}|_c = d_0 10^{\frac{P_0 - P(d)}{10n}} = d_0 10^{\frac{P_0 - (P_0 - 10n \log_{10} d/d_0 + S)}{10n}} \quad (3.25)$$

$$\hat{d}|_i = d_0 10^{\frac{P'_0 - P(d)}{10n'}} = d_0 10^{\frac{P_0 - (P_0 - 10n \log_{10} d/d_0 + S)}{10n'}} \quad (3.26)$$

where the apex to P_0 and n indicates that these parameters are related to an environment different from the true one (wrong test of the environment), and the fact has been used that by definition: $P_0 = P'_0$. This expression is formally the same for the power of the first path and for the total power, and for this reason in (3.25) and (3.26) the subscripts "FP" and "TP" have been omitted.

Using (3.23) and (3.25), after some calculation, denoting with $\delta_d|_c$ the test statistic under the case of correct choice of the environment (and omitting the apex (e)), we have:

$$\delta_d|_c \approx d \left(\frac{S_{TP}}{10n_{TP}} - \frac{S_{FP}}{10n_{FP}} \right) \ln 10 \quad (3.27)$$

The expression has been obtained using a first order approximation around zero for the exponential terms (for the purpose of the analysis, this is a good approximation). In a similar way, using (3.23) and (3.26), denoting with $\delta_d|_i$ the test statistic under the case of incorrect choice of the environment, results:

$$\delta_d|_i \approx d \left(\frac{S_{TP}}{10n'_{TP}} - \frac{S_{FP}}{10n'_{FP}} + \left(\frac{\Delta n_{TP}}{n'_{TP}} - \frac{\Delta n_{FP}}{n'_{FP}} \right) \log_{10} \frac{d}{d_0} \right) \ln 10 \approx \quad (3.28)$$

$$d \left(\frac{S_{TP}}{10n'_{TP}} - \frac{S_{FP}}{10n'_{FP}} + \frac{\Delta n_{TP}}{n'_{TP}} \log_{10} \frac{d}{d_0} \right) \ln 10$$

where: $\Delta n_{TP} = n_{TP} - n'_{TP}$ and it has been used that $\Delta n_{FP} = n_{FP} - n'_{FP} \approx 0$. The expression has been obtained using a first order approximation around zero for the exponential terms (also for this statistic this is a good approximation for the purpose of the analysis). Under the considered approximations, $\delta_d|_c$ and $\delta_d|_i$ are two correlated Gaussian random variables (by substituting in (3.27)-(3.28) the values of interest reported in Table 3.1 and using the variance propagation law, results in $\rho_{r|c,r|i} \approx 1$ for all the environments.), the first with zero mean, the second with a mean different from zero given by: $\Delta n_{TP}/n'_{TP} \log_{10} \frac{d}{d_0} \ln 10$

(normalizing $r|_c$ and $r|_i$ by a factor d which is not relevant for the decision strategy). For this reason, with the proposed decision strategy, it is likely to choose the test statistic for the correct environment, which corresponds to the zero mean random variable $r|_c$. The mean increases with the distance; therefore, the decision strategy becomes more robust for larger distances.

Decision test optimality conditions

To summarize the problem, and derive the situation in which the proposed approach is optimum, we can analyze the following simple example in which only two environments, named (e_1) and (e_2) and with equal a-priori probability $p_{(e_1)} = p_{(e_2)} = 1/2$, are considered. Denoting with H_1 and H_2 the hypotheses in which we are in the environment (e_1) and (e_2) respectively, from the previous considerations:

$$\text{Under } H_1 : \delta_d^{(1)} \sim N(0, \sigma_1^2); \delta_d^{(2)} \approx v^{(1)}\delta_d^{(1)} + u^{(1)} \quad (3.29)$$

$$\text{Under } H_2 : \delta_d^{(2)} \sim N(0, \sigma_2^2); \delta_d^{(1)} \approx v^{(2)}\delta_d^{(2)} + u^{(2)} \quad (3.30)$$

which is, in the two situations, the most general way to express two perfectly correlated Gaussian random variables; $v^{(i)}$, $u^{(i)}$ and σ_i , for $i = 1, 2$, can be obtained for comparison with (3.27)-(3.28). Under the good hypothesis that $|\delta_d^{(i)}(v^{(i)} - 1)| \ll |2v^{(i)}u^{(i)}|$ (in fact, it is easy to see with some substitution that in our measurements: $v^{(i)} \approx 1$ and $u^{(i)}$ of the same order of magnitude of σ_i), defining: $\Delta\delta_d = (\delta_d^{(1)})^2 - (\delta_d^{(2)})^2$ and using (3.27)-(3.28):

$$\Delta\delta_d \approx \begin{cases} -2u^{(1)}r^{(1)} - (u^{(1)})^2 & | H_1 \\ 2u^{(2)}r^{(2)} + (u^{(2)})^2 & | H_2 \end{cases} \quad (3.31)$$

If $|u^{(1)}| \approx |u^{(2)}|$ and $\sigma_1 \approx \sigma_2$ the optimal decision rule for $\Delta\delta_d$ is obtained by placing the critical value of the test in zero. In this way the test becomes exactly the one proposed in (3.24), reduced to the case of only two environments. Therefore, the test in (3.24) is a maximum a posteriori test and accounts for the more general situation of multiple environments and different a-priori probability of being in each environment. Under the introduced approximations, the critical value does not depend on the distance (which is unknown, and we can not correctly estimate it, since we still do not have knowledge of the environment). It is worthwhile to mention that the last approximation $\sigma_1 \approx \sigma_2$ does not hold in our measurements; for this reason the used test is not optimum. On the other hand, if we remove some of the last simplifying hypotheses it is not trivial anymore to

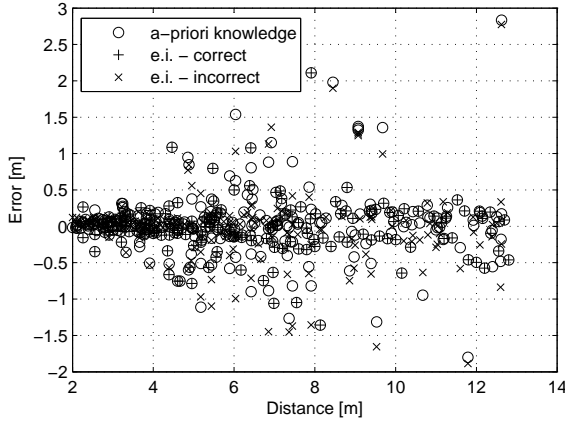


Figure 3.2: Scatter-plot of range error vs. distance obtained with environment differentiation, both with a-priori knowledge of the environment and with the developed identification approach.

derive the optimum decision rule, since we have, under the two hypotheses, two random variables with different standard deviation and mean which depends on the unknown distance. Using the test strategy in (3.24) the achieved standard deviation range error is of about 0.44 m, slightly worse than that obtained with the a-priori knowledge of the environment.

It is worth to underline that the situation in which it is likely that the test is wrong and large errors are produced, is the one in which $\Delta n_{TP}/n'_{TP} \log_{10} d/d_0 \approx 0$ and at the same time Δn_{TP} is significantly different from zero. On the contrary, if $\Delta n_{TP}/n'_{TP} \log_{10} d/d_0 \approx 0$ but Δn_{TP} is also close to zero, the test is likely to be wrong, but range estimation performance is not significantly affected, since the right environment is confused with one with similar parameters. This explains the high failure ratio of the proposed test, which for the considered environments is high (about 41%), and the achieved accuracy, which on the contrary is not significantly affected. This is due to the presence of some environments (e.g. (e_2) and (e_3)) with similar parameters. In the case in which the parameters of the channel are different on the contrary, the test is able to correctly identify the environment. Therefore, the proposed strategy can only be used to improve range estimation accuracy, but not to effectively *identify* the environment in which transmitter and receiver are actually placed.

3.2.3 Range estimation for smaller B_{if}

For smaller B_{if} , making (3.1) unbiased would allow to improve the accuracy in a more consistent way, compared to the case of the full bandwidth, due to the significant increase of $\mu_{\hat{d}_{TP}}$ and $\mu_{\hat{d}_{FP}}$. However, this solution is not practically feasible, since it would be necessary to know the fading variance, which in this case depends on the unknown distance itself (see e.g. eq. (2.19)). In this section, we propose an alternative option which, capitalizing on the model properties, allows to significantly improve the estimation accuracy by mitigating the large positive errors in the range estimates.

Outliers mitigation

Considering for example the total power, we can replace the unknown real distance which appears in the normalization factor (see eq. (2.19), (3.8), (3.10)), by the (biased) *estimated* distance with the total power itself \hat{d}_{TP} , obtained using (3.1):

$$\hat{d}_{TP}^{(n)} = d_0 10^{\frac{P_{0,TP} - P_{TP}(d)}{10n_{TP}}} \exp \left(- \left(\frac{\sigma_{S_{TP,0}} (1 + g_{B_{if},TP} \hat{d}_{TP}^{\alpha_{TP}}) \ln 10}{10\sqrt{2}n_{TP}} \right)^2 \right) \quad (3.32)$$

The obtained range error is now:

$$\epsilon_{TP}^{(n)} = d \left(\exp \left(- \frac{\ln 10}{10n_{TP}} S_{TP} \right) \exp \left(- \left(\frac{\ln 10}{\sqrt{2}10n_{TP}} \sigma_{S_{TP,0}} \left(1 + g_{B_{if},TP} (d \exp \left(- \frac{\ln 10}{10n_{TP}} S_{TP} \right))^{\alpha_{TP}} \right) \right)^2 \right) - 1 \right) \quad (3.33)$$

The same formal equation holds also for FP (relying on the Gaussian approximation for S_{FP}). The multiplicative term used for estimated distance normalization:

$$\exp \left(- \left(\frac{\ln 10}{\sqrt{2}10n_{TP}} \sigma_{S_{TP,0}} \left(1 + g_{B_{if},TP} (d \exp \left(- \frac{\ln 10}{10n_{TP}} S_{TP} \right))^{\alpha_{TP}} \right) \right)^2 \right) \quad (3.34)$$

depends on the value of S_{TP} itself; for large positive S_{TP} , the additional term tends to one, and the estimate is similar to the not-normalized case. For negative S_{TP} on the contrary, the additional term allows to correct for the error itself; this is a very interesting point, since it is possible to reduce the positive distance errors, which are the most consistent ones in energy based range estimation (the $\exp(S)$ function in (3.1) is asymmetric with respect to 0). Fig. 3.3 explains this point by comparing the range error obtained both using the a-priori knowledge of the exact distance in the range estimation, and the formula introduced in (3.33) (for the first path power, $B_{if} = 0.5$ GHz, and a distance $d = 10$ m, as an example); on the

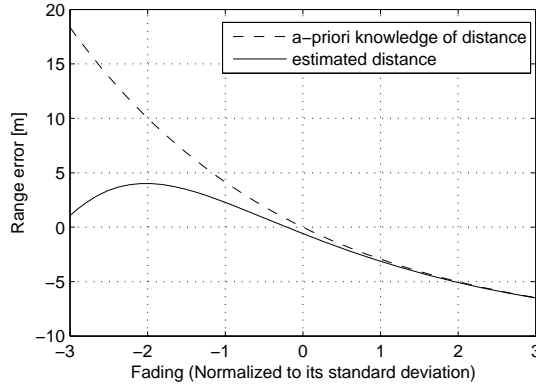


Figure 3.3: Range error vs. normalized fading, for FP , $B_{if}=0.5$ Ghz and $d=10$ m, both using the a-priori knowledge of the distance and by replacing it with the estimated distance with FP , as an example.

x-axis, the fading has been normalized to its standard deviation. The capability of the approach to mitigate the larger positive errors is evident (also note that negative errors are always limited to $-d$). As a further example, Fig. 3.4 shows a scatter-plot of the range error vs. distance, for the collected measurements, for FP and $B_{if}=0.5$ Ghz, both using a-priori knowledge of the distance and by replacing it with the estimated distance with FP itself.

Fig. 3.5 shows the mean and standard deviation of the range error as a function of the used bandwidth, for the proposed method, obtained from the collected set of measurements. It can be seen that for large bandwidths differences with respect to the results in Fig. 3.1 are negligible, as expected. For small bandwidths, on the contrary, the proposed approach allows to reduce in a significant way the range error standard deviation; for example, for FP and $B_{if} = 0.5$ GHz, the standard deviation decreases from 3.42 m down to 1.76 m, i.e. a factor about 2 smaller. This possibility makes it attractive and justifies to provide an accurate distance dependent fading model for the considered statistics. The mean range error remains similar in modulo (it passes from 0.40 m to -0.42 m), but becomes negative; as previously motivated, this is due to the principle of working of the outliers mitigation approach. It is also remarkable to note that the proposed method allows FP based ranging to outperform TP based ranging, for all bandwidths.

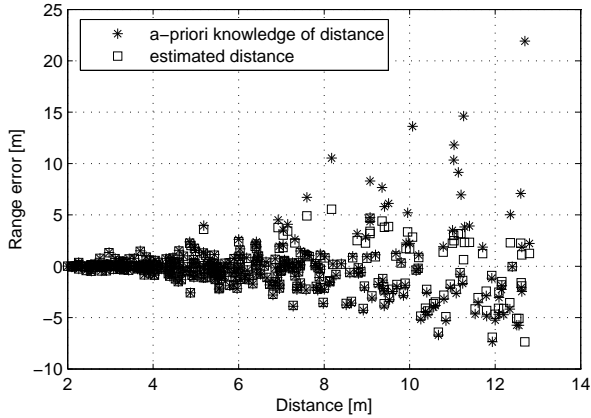


Figure 3.4: Scatter-plot of the range error vs. distance for FP and $B_{if}=0.5$ Ghz, both using the a-priori knowledge of the distance and by replacing it with the estimated distance with FP.

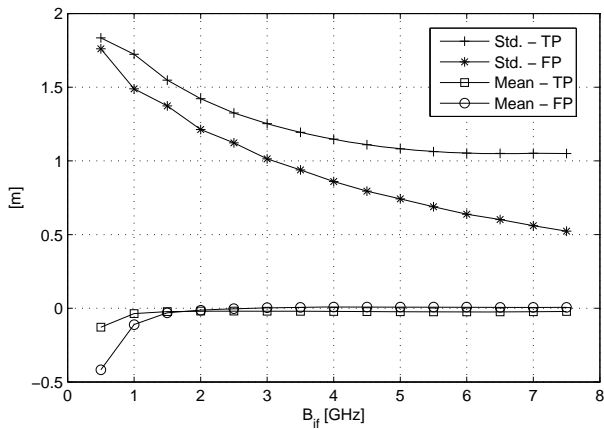


Figure 3.5: Mean and standard deviation range error vs. B_{if} in LOS, both for TP, and for FP, using the model information and the outliers mitigation strategy.

Since the outliers mitigation approach makes the estimated distances biased, the BLUE has not been evaluated in this case.

3.3 NLOS propagation

In NLOS, the same formulas as in (3.1)-(3.3) hold for the estimated distance using *TP*. For the first path power based ranging, it follows:

$$\hat{d}_{FP} = d_0 10^{\frac{P_{0,FP} - P_{FP}(d)}{10n_{FP}}} = d A_{FP}^{-\frac{2}{n_{FP}}} \quad (3.35)$$

Observing that for a Nakagami [3] random variable X and for $m + k/2$ strictly larger than zero, the following relation holds:

$$E\{X^k\} = \frac{\Gamma(m + k/2)}{\Gamma(m)} \left(\frac{\Omega}{m}\right)^{\frac{k}{2}} \quad (3.36)$$

then the mean and variance of (3.35) are, respectively:

$$\mu_{\hat{d}_{FP}} = E\left\{A_{FP}^{-\frac{2}{n_{FP}}}\right\} = \frac{\Gamma(m_{AFP} - 1/n_{FP})}{\Gamma(m_{AFP})} \left(\frac{\Omega_{AFP}}{m_{AFP}}\right)^{-\frac{1}{n_{FP}}} \quad (3.37)$$

$$\sigma_{\hat{d}_{FP}}^2 = E\left\{A_{FP}^{-\frac{4}{n_{FP}}}\right\} - E\left\{A_{FP}^{-\frac{2}{n_{FP}}}\right\}^2 = \quad (3.38)$$

$$\left(\frac{\Omega_{AFP}}{m_{AFP}}\right)^{-\frac{2}{n_{FP}}} \left(\frac{\Gamma(m_{AFP} - 2/n_{FP})}{\Gamma(m_{AFP})} - \left(\frac{\Gamma(m_{AFP} - 1/n_{FP})}{\Gamma(m_{AFP})}\right)^2\right)$$

The expressions in (3.37) and (3.38) can be evaluated for $n_{FP} > 2/m_{AFP}$; from the values in Chapter 2, this relation holds for all B_{if} .

3.3.1 Unbiased range estimation

Similarly as in Section 3.2.1, also in NLOS an unbiased estimate of d can be provided. Since no distance dependency of the fading has been experienced in NLOS for all bandwidths, having knowledge of the model proposed in the previous chapter, it is possible to obtain the estimated distances with the two statistics $\hat{d}_{TP}^{(n)}$ and $\hat{d}_{FP}^{(n)}$, normalized to their mean values, respectively.

Figure 3.6 shows the achieved mean and standard deviation range error using *TP* and *FP*, as a function of B_{if} . From this figure, it can be seen that in NLOS the classical total power always outperforms the first path power. This is intuitively clear, since in this case the exploited information is directly corrupted by the

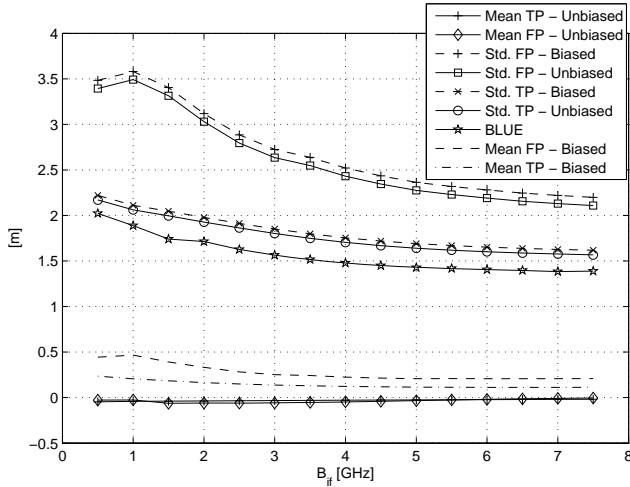


Figure 3.6: Mean and standard deviation range error vs. B_{if} in NLOS for TP, FP, and BLUE.

presence of physical obstructions between transmitter and receiver. For example, for $B_{if} = 7.5$ GHz, $\sigma_{\epsilon_{TP}}^{(n)} = 1.57$ m, while $\sigma_{\epsilon_{FP}}^{(n)} = 2.11$ m. By comparing results between the biased and unbiased range estimation, differently from LOS, normalizing the estimated distances by the respective mean terms allows to improve ranging results in a noticeable way, in terms of a decreased mean and standard deviation of the range error.

Also in NLOS a Gaussian approximation for S_{FP} can be employed; this solution would be interesting since it allows to make the model simpler and to use for S_{FP} a single parameter distribution. However, compared to the LOS case, this solution affects the ranging accuracy. This can be immediately noted considering that the second order term in the Taylor expansion of (3.1) can assume non-negligible values (e.g, normalized to d , for $S_{FP} = 3\sigma_{S_{FP}}$ and $B_{if} = 0.5$ GHz it is approximately equal to 0.25). Variations in ranging results are however limited to less than 10% in all cases.

3.3.2 Best linear unbiased estimation

Also in this case, a BLUE of the distance can be calculated. The correlation between the estimated distances with TP and FP can be obtained from $\rho_{S_{TP}, S_{FP}}$ using the variance propagation law approximated till the second order for the

system of equations:

$$\begin{cases} \hat{d}_{TP}^{(n)} = d \exp\left(-\frac{S_{TP} \ln 10}{10n_{TP}}\right) / \mu_{\hat{d}_{TP}} \\ \hat{d}_{FP}^{(n)} = d A_{FP}^{-\frac{1}{n_{FP}}} / \mu_{\hat{d}_{FP}} \end{cases} \quad (3.39)$$

and results: $\rho_{\hat{d}_{TP}^{(n)}, \hat{d}_{FP}^{(n)}} \approx \rho_{S_{TP}, S_{FP}}$. The BLUE of the distance d_{BLUE} can then be calculated using (3.16).

In NLOS, the BLUE of the distance allows to noticeably improve the estimation accuracy obtained with each single method; e.g. $\hat{d}_{BLUE} = 1.39$ m for $B_{if} = 7.5$ GHz. This is due to the high correlation between the two statistics, and the difference between their estimation accuracy.

3.3.3 Standard deviation analytical evaluation

Also in this case, it is possible to analytically evaluate the range error standard deviation on the total set of measurements. The expression for TP is the same as (3.19). For the first path power, using (3.35) and (3.37), results in:

$$\sigma_{\epsilon_{TP}} = \sqrt{E\{d^2\} \left(\frac{\Gamma(m_{FP} + 2/n_{TP})\Gamma(m_{FP})}{\Gamma^2(m_{FP} + 1/n_{TP})} - 1 \right)} \quad (3.40)$$

The average BLUE standard deviation range error, can be calculated from (3.21) and is equal to:

$$\sigma_{\hat{d}_{BLUE}} = \sqrt{\frac{E\{d^2\} \left(\exp\left(-\frac{\sigma_{S_{TP}} \ln 10}{10n_{TP}}\right)^{2-1} \left(\frac{\Gamma(m_{FP} + 2/n_{FP})\Gamma(m_{FP})}{\Gamma^2(m_{FP} + 1/n_{FP})} - 1 \right) (1 - \rho_{S_{TP}, S_{FP}}) \right)}{\exp\left(-\frac{\sigma_{S_{TP}} \ln 10}{10n_{TP}}\right)^{2-1} + \frac{\Gamma(m_{FP} + 2/n_{FP})\Gamma(m_{FP})}{\Gamma^2(m_{FP} + 1/n_{FP})} - 2 \sqrt{\rho_{S_{TP}, S_{FP}} \left(\exp\left(-\frac{\sigma_{S_{TP}} \ln 10}{10n_{TP}}\right)^{2-1} \left(\frac{\Gamma(m_{FP} + 2/n_{FP})\Gamma(m_{FP})}{\Gamma^2(m_{FP} + 1/n_{FP})} - 1 \right) - 2}} \right)} \quad (3.41)$$

3.4 Effect of practical limitations on range estimation accuracy

In this paragraph, the effects of different non-idealities which typically arise in practical statistics based ranging system operation, are shortly discussed.

3.4.1 Effect of limited number of measurements on range estimation accuracy

To evaluate the effect on the ranging accuracy of a limited number of measurements used in the preliminary calibration step required for parameters estimation,

range estimation as in (3.1) is considered, and the full bandwidth case only is explicitly addressed. The estimated distance is calculated as:

$$\hat{d} = d_0 10^{\frac{P_0 - P(d)}{10\hat{n}}} \quad (3.42)$$

where $\hat{n} = n - R_{N_m}/10$ (see also Section 2.8) is the estimated path loss exponent from the set of N_m preliminary calibration measurements, with:

$$R_{N_m} \triangleq \frac{\sum_{j=1}^{N_m} S_j \log_{10} \frac{d_j}{d_0}}{\sum_{i=1}^{N_m} \log_{10}^2 \frac{d_i}{d_0}} \quad (3.43)$$

where the index i represents that the parameters are referred to the generic i -th calibration measurement; now (3.42) becomes:

$$\begin{aligned} \hat{d} &= d_0 10^{\frac{P_0 - P(d)}{10\hat{n}}} = d_0 \exp\left(\frac{10n \log_{10} \frac{d}{d_0} - S}{10\hat{n}} \ln 10\right) \approx \\ &d_0 \exp\left(\left(\frac{10n \log_{10} \frac{d}{d_0} - S}{10n}\right) \left(1 + \frac{R_{N_m}}{10n}\right) \ln 10\right) \approx \\ &d \exp\left(\frac{R_{N_m} \log_{10} \frac{d}{d_0} - S}{10n} \ln 10\right) = d \exp\left(-\frac{\hat{S} \ln 10}{10n}\right) \end{aligned} \quad (3.44)$$

with

$$\hat{S} \triangleq S - R_{N_m} \log_{10} \frac{d}{d_0} \quad (3.45)$$

To obtain the last expression in (3.44), the second and higher order terms in the Taylor expansion for the exponential term have been neglected; this approximation is accurate if $R_{N_m}/(10n) \ll 1$, which e.g. for TP is true for $N_m \geq 5$ in LOS and $N_m \geq 13$ in NLOS, as discussed in Section 2.8.1. The expression found is formally the same as (3.1). Using the variance propagation law applied to (3.45), and evaluated around the mean of \mathbf{S} , \mathbf{d} , and d , and observing that all these random variables are independent, results in:

$$\sigma_{\hat{S}} \approx \sigma_S \sqrt{1 + 1/N_m} \quad (3.46)$$

The term $\sqrt{1 + 1/N_m}$, which only depends on N_m , represents the relative increase in σ_S with respect to the case in which the path loss exponent is perfectly known. With (3.46), impairments of the standard deviation range error on the global set of data can be evaluated. From (3.19), $\sqrt{1 + 1/N_m}$ also represents the relative increase in σ_ϵ ; e.g., for $N_m = 10$, the increase is of about 5%. Therefore, only a very limited amount of calibration measurements is required to be able to completely exploit the accuracy provided by TP and FP . This is a very important conclusion for practical uses of statistics based ranging.

3.4.2 Antennas directional gain dependency

In this section, the effect of the transmit and receive antennas' directional gain dependency on the ranging accuracy is shortly discussed. The main purpose of this paragraph is not to provide an in depth analysis of the problem, but instead, to highlight some issues which from the antenna design perspective are relevant in the context of statistics based ranging.

The antennas directional gain dependency can be relatively easy addressed for *FP* based ranging, since, particularly for very large bandwidths, the direct path is completely resolvable and the considered signal is transmitted (received) along a unique direction at the transmit (receive) antenna. On the contrary, to address this issue for *TP* based ranging appears more problematic, since the total signal comes from multiple departure and arrival angles at the two antennas; however, it is intuitively clear that this problem for *TP* is expected to be less severe than for *FP*, since reception of the total energy along different angles allows to partly average out angular variations. Therefore, in this section only impairments in first path power based ranging are evaluated, keeping in mind that this appears to be the most critical situation.

Denoting with $\sigma_{FP, Ant_{TX}}$ and $\sigma_{FP, Ant_{RX}}$ the standard deviation of the angular power deviations for the transmit and receive antennas, the total first path power standard deviation is given by:

$$\sigma_{FP, Tot} = \sqrt{\sigma_{FP}^2 + \sigma_{FP, Ant_{TX}}^2 + \sigma_{FP, Ant_{RX}}^2} = \sqrt{\sigma_{FP}^2 + 2\sigma_{FP, Ant}^2} \quad (3.47)$$

where the last equality holds if transmit and receive antennas are equal, and it has been used that these deviations are independent of each other, and independent of the fading deviations. Usually, antenna designers provide the radiation patterns in different planes, or the difference between the minimum and the maximum antenna gain for the planes of interest, while in (3.47) knowledge of the standard deviation of the antenna angular power deviations is required. To address this issue, antenna angular variations are assumed Gaussian (this hypothesis is not justified, but only introduced for convenience of the simplified analysis); in this case, observing that $1 - \Phi(3) \approx 10^{-3} \approx 0$, where $\Phi(x)$ is the standard Gaussian *cdf*, the standard deviation of the antenna angular variations can be related to the maximum radiations variation ΔP_{Ant} by the empirical relation: $\sigma_{FP, Ant} \approx \Delta P_{Ant}/6$. For example, considering variations of typical omni-directional antennas in the H-plane in the order of 1 dB [4]-[6], impairments in ranging results are less than 5%, by evaluating (3.47) for LOS propagation and $B_{if} = 7.5$ GHz. This means

that the potential accuracy provided by this solution can be fully exploited for systems which require positioning information in planes only. More critical appears the situation considering typical angular variations on the other planes. For example, for the omni-directional antenna in [6], variations in the other two planes are limited to 6 dB within each of the two 120 degrees angles around the two main radiation lobes; this corresponds to a performance worsening by a factor 2.5, compared to the ideal case (this impairment can be compensated e.g. by reducing the maximum achievable distance by the same factor, as shown in (3.19)). Impairments are significantly less severe for NLOS, due to the larger σ_{SFP} ; in this case the evaluation of (3.47) gives a decrease in accuracy of about 10% for the same 6 dB maximum variation. Therefore, the antennas' directional gain dependency is a particularly critical issue to address in order to be able to *fully* exploit the potential accuracy provided by statistics based ranging. The design of antennas with improved omni-directionality properties especially around the main lobe (this solution appears preferable with respect to antennas with two-lobes radiation pattern), as well as proper placement of the antennas and system planning, can be beneficial in order to mitigate these impairments.

3.5 Weighted Least Squares Positioning

As shown in the previous sections, having knowledge of a proper fading model is fundamental both to provide accurate error models (this information can be useful for dimensioning of the system infrastructure for example) and to improve the achievable range estimation accuracy. In this section, another possible application of the model, namely to improve the classical least-squares positioning, is investigated. To this purpose, positioning results which can be obtained in LOS propagation are presented in detail, and improvements deriving from the proposed LOS model knowledge are exploited. This is a particularly relevant situation to investigate, since, as shown in the previous sections, the statistics based ranging approach provides accurate results particularly in LOS propagation, therefore, for practical applications, this is the most interesting situation to analyze. The global performance of statistics based ranging in mixed LOS-NLOS propagation, and NLOS are also presented.

From the total set of measurements, a subset of N_p of them is randomly chosen. A pair (θ, ϕ) is associated to each of the N_p selected ranges. In this way, a reference point with spherical coordinates (d_i, θ_i, ϕ_i) , with $1 \leq i \leq N_p$, in

the three-dimensional space is associated to each measurement, and a simulated positioning system with N_p reference stations is obtained from the N_p selected ranges. θ_i is the angle between the z-axis and the i -th reference point, ϕ_i is the angle between the x-axis and the projection of the i -th reference point on the x-y plane. The axis origin represents the unknown position to be estimated using the set of N_p corresponding range estimates $\hat{\mathbf{d}}$. The general system model can be written as:

$$\hat{\mathbf{d}} = \mathbf{A}(\mathbf{x}_u) + \boldsymbol{\epsilon} \quad (3.48)$$

where $\mathbf{A}(\cdot)$ is a mapping from R^3 to R^{N_p} , $\hat{\mathbf{d}}$ and $\boldsymbol{\epsilon} \in R^{N_p}$, and $\mathbf{x}_u = (0, 0, 0)$. From the vector of estimated distances, an estimate $\hat{\mathbf{x}}_u$ of \mathbf{x}_u can be obtained. The performance of the positioning algorithm is evaluated by calculating $\epsilon_{\hat{\mathbf{x}}_u} = E\{\|\hat{\mathbf{x}}_u\|\}$, which represents the root mean square error in the position estimation.

The weighted least squares (WLS) coordinates estimation is performed as:

$$\hat{\mathbf{x}}_u^{WLS} = \arg \min_{\mathbf{x}_u} \left\| \hat{\mathbf{d}} - \mathbf{A}(\mathbf{x}_u) \right\|_{\mathbf{V}_d^{-1}}^2 \quad (3.49)$$

where \mathbf{V}_d is the variance matrix (a diagonal matrix containing as the $[j, j]$ element the variance of the j -th measured distance), and its inverse represents the WLS weight matrix. Since \mathbf{V}_d depends on the real distance which is unknown, the estimated distance, instead of the unknown real distance, has been used for their evaluation in (3.49). This simplification in general determines a worsening in performance of the WLS estimator, with respect to the ideal case of exact knowledge of the distance. For comparison, also the un-weighted case has been evaluated. This is simply obtained by replacing \mathbf{V}_d with the identity matrix.

To solve the non-linear equation (3.49) with respect to \mathbf{x}_u is a challenging problem, particularly for statistics based indoor ranging, due to the small system scale, and the relatively large errors experienced. The interested reader is referred to [7]-[??] for an overview of the main problems from the positioning perspective when UWB signals are used for ranging. These issues go beyond the scope of this section, therefore, the standard Gauss-Newton iterative method has been used to solve (3.49), even if more sophisticated (or a combination of different) techniques could provide globally better results. The initial guess used to iteratively solve (3.49) has been chosen as the true position \mathbf{x}_u ; performance has been evaluated in terms of achieved standard deviation of the positioning error $\sigma_{\epsilon_{\hat{\mathbf{x}}_u}}$ and percentage of rank deficient solutions p_{nc} . This last event is detected when $\det\{\mathbf{A}^T \mathbf{V}_d^{-1} \mathbf{A}\} \leq 10^{-17}$.

Two different scenarios have been simulated: $N_p=4$ and $N_p=8$. Denoting with r_1 ($x \geq 0, y \geq 0, z \geq 0$), r_2 ($x \leq 0, y \geq 0, z \geq 0$), r_3 ($x \leq 0, y \leq 0, z \geq 0$), r_4 ($x \geq 0, y \leq 0, z \geq 0$), r_5 ($x \geq 0, y \geq 0, z \leq 0$), r_6 ($x \leq 0, y \geq 0, z \leq 0$), r_7 ($x \leq 0, y \leq 0, z \leq 0$), r_8 ($x \geq 0, y \leq 0, z \leq 0$), the 8 regions in which the total space is divided by the x-y, y-z and x-z planes, two different geometries have been analyzed in both cases. In the first one, denoted as 'good' geometry, the simulated reference nodes have been placed each in a different of the regions: r_1, r_3, r_6, r_8 in the first scenario, and $r_1, r_2, r_3, r_4, r_5, r_6, r_7, r_8$, in the second scenario. In the second one, denoted as 'bad' geometry, all the reference nodes have been placed only in r_1 and r_2 , in both scenarios.

The good geometry has been used to evaluate the accuracy which can be achieved in case of correct convergence of the algorithm; on the contrary, with the second bad geometry it is possible to investigate the positioning algorithm convergence rate, for the different methods. Results are finally averaged over 10000 repetitions.

3.5.1 LOS positioning performance

Table 3.2 shows the obtained positioning results for LOS propagation, for the two scenarios, both for $B_{if} = 7.5$ GHz and for $B_{if} = 0.5$ GHz. Different methods are compared: the classical *TP* with un-weighted least squares, *TP* and *FP* based ranging with WLS but without knowledge of the fading model (distance is estimated as in eq. (3.1), with only knowledge of the path-loss exponent), and *TP* and *FP* based ranging with WLS and knowledge of the fading model proposed in Section 3.2.

It can be seen that for all cases, the worst performance is provided by classical *TP* without WLS; this is clear, since the algorithm is not able to satisfactorily exploit the redundancy coming from the set of used range measurements. Traditional *TP*, with WLS which only exploits information about distance between transmitter and receiver achieves better performance than non-WLS; this is due to the fact that the simplistic assumption of constant fading (which for small bandwidths is not accurate), already allows to give more weight to range measurements with small distance between transmitter and receiver, which are the most reliable ones in statistic based ranging. Depending on B_{if} and N_p , improvements with respect to *TP* based un-weighted positioning range between about 10% and 37%; clearly, the gain is higher for larger N_p . Knowledge of the proposed fading model allows to significantly gain in terms of positioning accuracy; this is due

Table 3.2: Final position estimation accuracy for different scenarios, in LOS

LOS	$N_p = 4$	$N_p = 4$	$N_p = 8$	$N_p = 8$
	$\sigma_{\epsilon_{\hat{x}_u}}$	p_{nc}	$\sigma_{\epsilon_{\hat{x}_u}}$	p_{nc}
$B = 7.5$ GHz				
<i>TP</i> - LS - no fading model	1.61	0.092	1.12	0.023
<i>TP</i> - WLS - no fading model	1.44	0.097	0.87	0.025
<i>FP</i> - WLS - no fading model	0.69	0.040	0.41	0.002
<i>TP</i> - WLS - fading model	1.11	0.061	0.71	0.009
<i>FP</i> - WLS - fading model	0.54	0.013	0.35	0
$B = 0.5$ GHz				
<i>TP</i> - LS - no fading model	2.73	0.275	2.29	0.327
<i>TP</i> - WLS - no fading model	2.26	0.271	1.44	0.264
<i>FP</i> - WLS - no fading model	2.40	0.280	1.48	0.281
<i>TP</i> - WLS - fading model	2.05	0.188	1.17	0.209
<i>FP</i> - WLS - fading model	1.69	0.123	0.94	0.187

to the higher accuracy in the collected range estimates, and to the use of more accurate weights in \mathbf{V}_d^{-1} ; improvements are up to 50% for $B_{if} = 0.5$ GHz and $N_p = 8$. Using *FP* and the model knowledge, allows to always outperform in a significant way all the other methods; e.g., using the full bandwidth, $\sigma_{\epsilon_{\hat{x}_u}} = 0.54$ m for $N_p = 4$ and $\sigma_{\epsilon_{\hat{x}_u}} = 0.35$ m for $N_p = 8$ have been found, which is a factor of about 3 better than traditional *TP* based positioning. Similar considerations hold for p_{nc} , which is significantly smaller when using *FP* and the model knowledge.

3.5.2 LOS-NLOS and NLOS positioning performance

Table 3.3 shows obtained positioning results both for NLOS propagation, and for mixed LOS/NLOS propagation; in this last case, 2 or 4 distance measurements belong to LOS, and the remaining to NLOS, for $N_p = 4$ and $N_p = 8$, respectively. Also in this case, results for both scenarios, and for $B_{if} = 7.5$ GHz and $B_{if} = 0.5$ GHz are reported, for comparison. The classical *TP* with un-weighted least squares, and *TP* and *FP* based ranging with WLS and knowledge of the fading model proposed in Chapter 2, are compared.

From the table, it can be seen that the results in this case are more heterogeneous, compared to those reported in Table 3.2; however, some general comments

Table 3.3: Final position estimation accuracy for different scenarios, in NLOS

	$N_p = 4$ $\sigma_{\varepsilon_{x_u}}$ LOS/NLOS	$N_p = 4$ p_{nc} LOS/NLOS	$N_p = 8$ $\sigma_{\varepsilon_{x_u}}$ LOS/NLOS	$N_p = 8$ p_{nc} LOS/NLOS	$N_p = 4$ $\sigma_{\varepsilon_{x_u}}$ NLOS	$N_p = 4$ p_{nc} NLOS	$N_p = 8$ $\sigma_{\varepsilon_{x_u}}$ NLOS	$N_p = 8$ p_{nc} NLOS
<i>B = 7.5 GHz</i>								
<i>TP</i> - no WLS - no fad. m.	1.92	0.103	1.34	0.023	2.23	0.101	1.54	0.031
<i>TP</i> - WLS - fad. m.	1.61	0.091	0.94	0.016	1.99	0.102	1.40	0.044
<i>FP</i> - WLS - fad. m.	1.80	0.117	0.52	0.007	2.78	0.203	1.97	0.174
<i>B = 0.5 GHz</i>								
<i>TP</i> - no WLS - no fad. m.	2.99	0.247	2.29	0.138	3.16	0.181	2.34	0.120
<i>TP</i> - WLS - fad. m.	2.49	0.211	1.57	0.109	2.72	0.181	2.04	0.166
<i>FP</i> - WLS - fad. m.	2.69	0.250	1.47	0.103	3.58	0.316	2.66	0.341

can be provided. The use of larger N_p also in this case allows to improve performance in terms of $\sigma_{\varepsilon_{x_u}}$ and p_{nc} . Improvements are especially remarkable for mixed LOS/NLOS, in which redundancy in measurements is particularly beneficial since it allows to rely in a stronger way on the LOS measurements, which exhibit smaller range errors. By comparing WLS results for LOS/NLOS and $N_p = 8$ with those of LOS and $N_p = 4$, it can be seen that the gain due to the additional 4 NLOS measurements is very limited, and mainly affects the convergence rate of the positioning algorithm; therefore, having knowledge of the fading model and propagation condition, redundancy added by NLOS measurements brings modest additional useful information. With the exception of LOS/NLOS and $N_p = 8$, in which the positioning performance is dominated by the 4 LOS measurements, in all the other cases WLS *FP* based positioning exhibits worse performance than the WLS *TP* based one, both in terms of accuracy, and in terms of convergence rate.

3.6 Chapter summary

In this chapter, the performance of statistics based ranging has been evaluated, exploiting the models proposed in Chapter 2 for the total signal power and first path power of the received signal. Relevant points and conclusions, which can be drawn from the presented results, are summarized in the following:

- The contribution of this chapter has been to develop a framework for statistics based ranging; it is shown that this approach can be used for indoor positioning applications, when the target accuracy is at decimeter to meter level. This possibility comes from the unique peculiarities of UWB signals; in fact, the use of extremely large bandwidths allows to achieve very small

variations due to unresolvable multipath in the used statistics, and limits these variations to their location dependency, as justified in detail in Chapter 2.

- Different solutions can be employed in order to improve the accuracy provided by traditional total power based ranging; given the propagation condition (LOS or NLOS), actual improvements depend on the particular method used. A straightforward conclusion is that higher accuracy can be achieved with a larger amount of information used; for example, in LOS and for the full bandwidth, it is possible to gain a factor about 2.5 by *differentiating* and *identifying* the particular environment in which transmitter and receiver are placed (Section 3.2.2); this gain, however, comes at the cost of a significantly higher amount of a-priori model information, since it is necessary to have accurate prior knowledge of the path-loss exponent and fading for TP and FP , and their correlation, for *each* environment. This requirement contrasts with demands for solutions which require a limited amount of prior setup and operation from the end-user.
- For the same reason, while for research purposes it is certainly appealing to investigate the *potential* accuracy provided by a particular solution, for practical applications it is relevant to investigate the best compromise between complexity and performance. From this point of view, the most appealing solution appears the use of this approach in LOS only, and to rely on the first path power statistic, in conjunction with the use of very large bandwidths. The use of large bandwidths has in fact two advantages: to make the used statistics very reliable, and to make the model characterization extremely simple (no distance dependency). In LOS propagation, FP based ranging is able to achieve a standard deviation range error of about 50 cm, and no a-priori information *at all* is required; in fact, its path loss exponent can be approximated with 2 (representing free space propagation), and the direct use of (3.1) introduces negligible difference with respect to the unbiased solution, given the already very small fading deviations. This solution, combined with good positioning system geometries and depending on the number of reference stations, can provide a final positioning accuracy of a few decimeters, for a system with maximum distance between transmitter and receiver up to 13 m.
- To combine TP with FP appears advantageous in NLOS propagation (and

in mixed LOS/NLOS positioning scenarios). When using also *TP*, knowledge of the channel parameters is needed. As shown in Section 3.5, a very limited amount of calibration measurements is needed to correctly estimate them; e.g. 10 random measurements allow to make the additional range error due to incorrect parameters estimation smaller than 5%.

- From the issues previously motivated, a vision of the system which is able to cope with the peculiarities and requirements of statistics based ranging is represented by 1) *a very dense* network of 2) *uncoordinated* and 3) *extremely simple* nodes.

1) A very dense network allows each location to have a sufficient number of LOS references at short distance (e.g. smaller than 10 m); this condition is required to make estimated ranges reliable. 2) The absence of demand for coordination among system nodes is the point which makes statistics based ranging most appealing, when compared to e.g. time based approaches. This possibility is a key factor for drastically decreasing the system complexity and to make the overall network easily scalable, which is an implicit requirement needed by the previous point. 3) The first path power can be estimated with a low-complexity receiver implementation [9]. In fact, the same circuit proposed in Section 5.2 for low-complexity TOA estimation can be also used for estimating the first path power in an inexpensive way, allowing to overcome current UWB system complexity bottlenecks.

- The antennas angular gain dependency appears the most critical issue to address in order to be able *to fully* exploit the potential accuracy provided by statistics based ranging. Design of antennas with improved omnidirectionality properties especially around the main beam, as well as proper placement of the antennas and system planning, can be practical solutions towards this issue.
- For proper operation, statistics based ranging requires a prior LOS/NLOS identification. This task appears challenging to achieve without relying on time of arrival methods (see also the next chapter); for this reason, this issue should be addressed at positioning level, when a redundant data-set of range measurements is available.

Bibliography

- [1] Y. Qi and H. Kobayashi, "On relation among time delay and signal strength based geolocation methods", IEEE GLOBECOM 2003, vol. 7, pp. 4079-4083, Dec. 2003.
- [2] K.R. Koch, "Parameters estimation and hypothesis testing in linearmodels", par. 3.2.2, Springer Verlag, 1999.
- [3] M. Nakagami, "The m -distribution - a general formula of intensity distribution of rapid fading", Statistical Methods in Radio Wave Propagation, pp. 336, 1960.
- [4] Lau Pui Yi, G.S. Lamba, A. Gupta, E.K.N. Yung, "A small omni-directional patch antenna with ultra wide impedance bandwidth", IEEE APMC 2008, pp. 1-4, Dec. 2008.
- [5] Qi Wu, Ronghong Jin, Junping Geng, Min Ding, "Printed Omni-Directional UWB Monopole Antenna With Very Compact Size", IEEE Transactions on Antennas and Propagation, vol. 56, no. 3, pp. 896-899, Mar. 2008.
- [6] T. Wakabayashi, H. Matsui, "Omni-directional characteristics over frequency range for UWB of modified planar antenna with an elliptical element on the dielectric substrate", IEEE ISWCS 2009, pp. 463-467, Sep. 2009.
- [7] J. Yan, C.C.J.M. Tiberius, P.J.G. Teunissen, G. Bellusci, G.J.M. Janssen, "A Framework for Low-Complexity Least-Squares Localization with High Accuracy", submitted to IEEE Transaction on Signal Processing.
- [8] J. Yan, C.C.J.M. Tiberius, G. Bellusci, G.J.M. Janssen, "A Novel Non-Iterative Localization Solution", IEEE GLOBECOM 2009, Honolulu.
- [9] G. Bellusci, G.J.M. Janssen, J. Yan, C.C.J.M. Tiberius, "Low complexity ultra-wideband ranging in indoor multipath environments", IEEE/ION PLANS 2008, pp. 394-401, May 2008.

TOA Based Range Error Evaluation, Modeling, and Applications

Time of Arrival (TOA) estimation appears the most suitable UWB ranging technique for indoor positioning applications which require centimeter to decimeter level accuracy, due to the very high time resolution provided by UWB signals. For this reason, in recent years, this technique has received large attention both from industry, and from research [1]-[5]. A fundamental issue to address in this context is the investigation of the accuracy which can be achieved with this technique, in indoor multipath environments. While it appears trivial to provide the lowest bound for the ranging accuracy in ideal additive white Gaussian noise channel conditions [2], a theoretical investigation of TOA based ranging performance in *realistic* environments appears extremely challenging. This is due to the complexity of indoor propagation phenomena, as discussed in the previous chapters, and to the current lack of channel models specifically developed for ranging applications in mind. Recently, there has been significant effort in order to address potential accuracy which can be achieved with this technique [5]-[8] taking into account the severe indoor multipath conditions; however, provided theoretical results are often far from the accuracy which is experienced in actual measurements. For this reason, together with papers which approached this issue theoretically, there has been significant activity focused on statistical TOA based range error modeling from collected data sets of measurements, in order to be able to relate ranging performance with relevant system parameters [9]-[15]. However, related

work reported in literature still lacks of a complete and coherent understanding of the different factors which affect the range estimation accuracy and of good statistical error models. In [9], we proposed a preliminary investigation of UWB ranging capabilities in indoor environments; however no modeling for the error was provided; reference [10] shows the same limitation. Results in [11] and [12] are based on ray tracing tools instead of real channel measurements. In [13], only a fixed bandwidth is considered, while in [14] only a preliminary analysis is conducted to investigate the effect of bandwidth on different types of error and no explicit model is provided; in addition, the maximum considered bandwidth is limited to 3 GHz. Recently, the authors in [15] proposed a model limited to the absolute mean range error using TOA, as a function of the bandwidth used. However no statistical characterization is given. In addition, no distance dependency has been experienced; this appears in contrast with previous references.

In this chapter, a better understanding of the types of range error usually experienced in indoor environments is given, and a new statistical model for the error obtained by TOA-based UWB range estimation is provided, using the collected data as described in Chapter 3. Unlike previous literature, the distance and the bandwidth dependency of both the bias of the range error, and of the term which accounts for its random variations have been investigated and statistically modeled. Finally, a closed form expression for the global mean and standard deviation of the range error obtained from the total set of measurements, as a function of the bandwidth used, is derived and compared with the experimental data. Two different applications of the model are investigated; the first, to distinguish between LOS and NLOS propagation. The second, to weighted least square positioning; it will be shown that, having knowledge of the error model, and using the introduced LOS/NLOS detection algorithm, it is possible to significantly improve global TOA-based positioning performance.

4.1 TOA estimation and signal processing

Also in this case, as in the previous chapter, the range error:

$$\epsilon_{TOA} \triangleq \hat{d}_{TOA} - d \quad (4.1)$$

is defined as the difference between the estimated distance $\hat{d}_{TOA} = c\hat{\tau}_{TOA}$ and the true distance d , where c is the speed of light in air and $\hat{\tau}_{TOA}$ is the estimated TOA. As described in Section 3.1, the TOA is estimated as the time delay of the

first peak of the envelope of the estimated signal using the inverse filtering technique. The particular TOA estimation algorithm used clearly is directly related to the achieved ranging accuracy, and therefore, to the modeling results. Inverse filtering represents the most intuitive method to estimate the unknown channel impulse response, given knowledge of the transmitted pulse and of the received signal. The multipath resolvability provided by this technique is equal to the inverse of the signal bandwidth used; as discussed in Chapter 2, this property comes from the windowing operation required to perform the division in the frequency domain only within the bandwidth in which the signal is different from zero, and it is equivalent to convolve the ideal infinite bandwidth channel impulse response with a *sinc* function in the time domain with the same bandwidth (neglecting the additional Hamming window used). Therefore, the choice of this technique for range error modeling purposes, is motivated by the intention of providing results which are not dependent on the particular choice and mechanisms of the TOA estimation algorithm used (or information required by it), but on the contrary are simply representative for the accuracy which can be achieved given a multipath resolvability capability equal to the inverse of the bandwidth used. The use of more sophisticated approaches (e.g. maximum likelihood or super-resolution) would require to develop a complete framework to evaluate the achievable performance, (depending among other things, on the error statistics assumption, whose development itself is the purpose of this section), which is clearly out of the scope of this chapter; the interested reader can refer to e.g. [2] and included references or to [16] for different TOA estimation approaches.

4.2 Range error results, and modeling

In this section, a statistical model for the range error obtained from the measured data, is provided. The range error is expressed as the sum of a bias m_{TOA} , plus a zero mean random variable S_{TOA} which accounts for the random variations around m_{TOA} . The proposed model explicitly considers the distance and bandwidth dependency of these two quantities. Thus, the range error can be written as:

$$\epsilon_{TOA}(B_{if}, d) = m_{TOA}(B_{if}, d) + S_{TOA}(B_{if}, d) \quad (4.2)$$

In the following, a characterization for $m_{TOA}(B_{if}, d)$ and $S_{TOA}(B_{if}, d)$ valid for both LOS and NLOS propagation is proposed.

4.2.1 Modeling of $m_{TOA}(B_{if}, d)$

In LOS, the bias $m_{TOA}(B_{if}, d)$ is due to multipath and reflects the fact that the paths due to reflections always arrive later than the direct one. In NLOS, $m_{TOA}(B_{if}, d)$ is due to both multipath, as for LOS, and to the additional delay introduced by the propagation through dielectric materials. By analyzing the data, $m_{TOA}(B_{if}, d)$ has been modeled as a linearly increasing function of d ; the slope of the linear fit increases by decreasing B_{if} :

$$m_{TOA}(B_{if}, d) = m_{B_{if}}(B_{if})d + m_0 \quad (4.3)$$

$m_{B_{if}}(B_{if})$ accounts for the bandwidth dependency of $m_{TOA}(B_{if}, d)$ and it has been modeled as:

$$m_{B_{if}}(B_{if}) = m_1 \exp(-B_{if}/m_2) + m_3 \quad (4.4)$$

The coefficients m_0 , m_1 , m_2 , and m_3 have been obtained by fitting the data corresponding to different bandwidths in a least squares sense, and are reported in Table I.

For LOS, by plotting the function $m_{B_{if}}(B_{if})$, it can be seen that $m_{B_{if}}(B_{if}) \cong 0$ starting from about $B_{if} = 3$ GHz, which means that the distance dependency of $m_{TOA}(B_{if}, d)$ can be neglected in this case; on the contrary, it becomes larger for smaller B_{if} . At the same time, the bandwidth dependency becomes more evident with increasing d . This behavior for $m_{TOA}(B_{if}, d)$ can be intuitively justified. By decreasing B_{if} , the number of overlapping multipath components which follow the direct path increases, resulting in more bias. To explain the distance dependency, the following consideration can be provided. In LOS propagation, by increasing d , the direct path tends to have less weight with respect to the total signal. This can be intuitively explained by observing that, as shown in Chapter 3, in LOS the path loss exponent corresponding to the first path power is close to 2, while that corresponding to the total power is usually between 1 and 2, thus smaller; this means that multipath is more deteriorating for the resolvability of the direct path for larger d . In addition, by increasing d , the distance difference between the direct path and the reflected ones tends to decrease, making the multipath more dense. For NLOS, the distance and bandwidth dependency of $m_{TOA}(B_{if}, d)$ can be explained with arguments similar to those provided so far for LOS. The significantly larger values of $m_{TOA}(B_{if}, d)$ compared to LOS, even for larger B_{if} , are due to the additional delay introduced by the propagation through dielectric materials.

Table 4.1: Parameters for the characterization of $m_{TOA}(B_{if}, d)$ and of $S_{TOA}(B_{if}, d)$

$m_{TOA}(B_{if}, d)$:	m_0 [m]	m_1	m_2 [GHz]	m_3
LOS	0	0.0148	0.48	0
NLOS	0.019	0.027	0.47	0.013
$S_{TOA}(B_{if}, d)$:	σ_{S_0} [m]	α	g_1 [m ^{-α}]	g_2 [GHz]
LOS	0.016	1.5	0.64	0.60
NLOS	0.049	1.5	0.21	0.73

4.2.2 Modeling of $S_{TOA}(B_{if}, d)$

The deviation from the mean, $S_{TOA}(B_{if}, d)$, has been modeled as a random variable with standard deviation $\sigma_{S_{TOA}}(B_{if}, d)$ which depends on both B_{if} and d . As for $m_{TOA}(B_{if}, d)$, also $\sigma_{S_{TOA}}(B_{if}, d)$ becomes larger by decreasing B_{if} . In addition, to reflect the fact that when using the full bandwidth no distance dependency of $\sigma_{S_{TOA}}(B_{if}, d)$ has been observed while when using smaller bandwidths $\sigma_{S_{TOA}}(B_{if}, d)$ significantly increases with d , the following model for $\sigma_{S_{TOA}}(B_{if}, d)$ is proposed:

$$\sigma_{S_{TOA}}(B_{if}, d) = \sigma_{S_{TOA,0}}(s_{B_{if}}(B_{if})s_d(d) + 1) \quad (4.5)$$

with:

$$s_{B_{if}}(B_{if}) = s_1 \exp(-B_{if}/s_2) \quad (4.6)$$

and:

$$s_d(d) = d^\alpha \quad (4.7)$$

The parameters: $\sigma_{S_{TOA,0}}$, α , s_1 , and s_2 have been obtained by fitting the data in a least-squares sense; their values are also reported in Table I. It is worth to underline that for LOS, since both $s_{B_{if}}(B_{if})|_{B_{if}=7.5\text{GHz}}$ and $m_{TOA}(B_{if}, d)|_{B_{if}=7.5\text{GHz}}$ are approximately zero, $\sigma_{S_{TOA,0}}$ represents the standard deviation of the global range error obtained using the total bandwidth of 7.5 GHz. Fig. 4.1 shows the scatter-plot of the range error vs. distance both for the LOS measurements (above) and for the NLOS ones (below), for $B_{if} = 7.5$ GHz and for $B_{if} = 0.5$ GHz, for comparison.

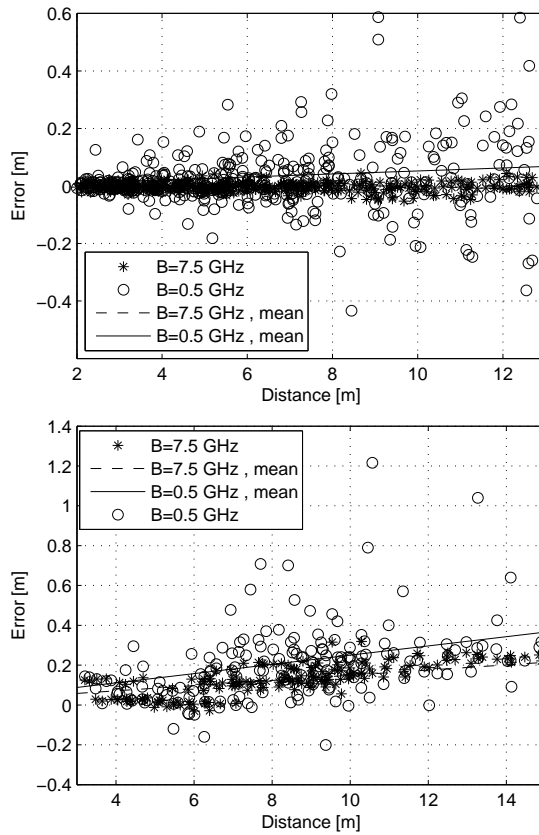


Figure 4.1: Range error vs. d for LOS (above) and NLOS (below), both for $B_{if} = 7.5$ GHz, and $B_{if} = 0.5$ GHz for comparison.

Statistical characterization of $S_{TOA}(B_{if}, d)$

For the statistical characterization of $S_{TOA}(B_{if}, d)$, a difference between the two propagation conditions arises. We introduce the new random variable:

$$S_{TOA,0} = \frac{S_{TOA}(B_{if}, d)}{s_{B_{if}}(B_{if})s_d(d) + 1} \quad (4.8)$$

which represents $S_{TOA}(B_{if}, d)$ normalized to the terms which model its bandwidth and distance dependency. By analyzing the histogram of $S_{TOA,0}$, for LOS it has been modeled as a zero mean Gaussian random variable with standard deviation $\sigma_{S_{TOA,0}}$. For NLOS, we notice an asymmetric distribution around the zero mean, for all bandwidths. In fact, the tail corresponding to the positive values of the histogram of $S_{TOA,0}$ is longer than that corresponding to the negative ones. The physical explanation of this aspect is the following: in NLOS, with strong multipath conditions, there are situations in which several reflected paths may arrive closely after the direct one; this can move the detected first path to a delay which is significantly larger than $1/B_{if}$. On the contrary, the negative errors due to multipath are always limited to approximately $1/B_{if}$. Fig. 4.2 explains this point. This phenomenon was not experienced in LOS due to the less dense multipath; however we think that this point deserves further investigation on a larger data set obtained in different environments and for larger distances. To account for this aspect, $S_{TOA,0}$ has been modeled as the sum of two independent random variables, the first one Gaussian distributed, as for the case of LOS, the second one exponentially distributed. Thus, for NLOS $S_{TOA,0}$ can be expressed as:

$$S_{TOA,0} = s_G G_0 + s_E E_0 + s_0 \quad (4.9)$$

where G_0 is a standard Gaussian random variable and E_0 is a standard exponentially distributed random variable with unit mean and standard deviation. The coefficients: $s_G = w_S \sigma_{S_{TOA,0}}$, $s_E = \sqrt{1 - w_S^2} \sigma_{S_{TOA,0}}$, and $s_0 = -s_E = -\sqrt{1 - w_S^2} \sigma_{S_{TOA,0}}$, can be expressed as functions of only one variable w_S ($0 \leq w_S \leq 1$), which are necessary to weight the two distributions with the constraints for the mean and the standard deviation of $S_{TOA,0}$ (equal to 0 and σ_{S_0} respectively). By fitting the data, we obtained: $w_S = 0.6$. It is worth to note that this model can be applied also to the LOS measurements presented so far, by choosing $w_S = 1$. Fig. 4.3 shows the *cdf* of $S_{TOA,0}$ in NLOS, using the data for $B_{if} = 7.5$ GHz and $B_{if} = 0.5$ GHz and the model proposed in (4.9), for comparison.

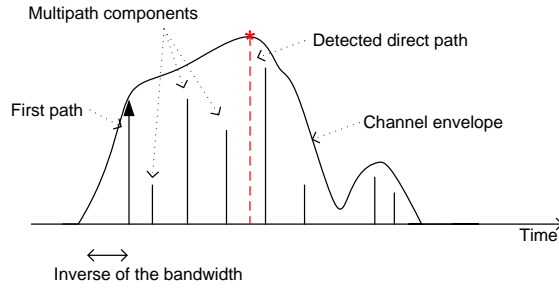


Figure 4.2: *NLOS range error behavior.*

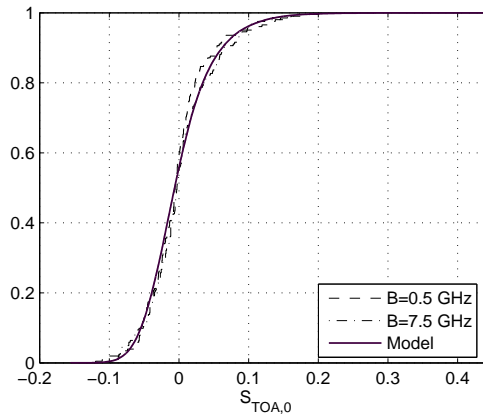


Figure 4.3: *cdf of S_0 in NLOS, for $B_{if} = 0.5$ GHz and $B_{if} = 7.5$ GHz, and for the model proposed in (4.9).*

Global mean and standard deviation range error

From the described model, it is possible to derive the global mean and standard deviation of the range error obtained from the total set of measurements, as a function of B_{if} . From (4.2) and (4.3), the global mean range error $\mu_{\epsilon_{TOA}}(B_{if})$ results as:

$$\mu_{\epsilon_{TOA}}(B_{if}) = m_{B_{if}}(B_{if})E[d] + m_0 \quad (4.10)$$

where the fact has been used that $S_{TOA}(B_{if}, d)$ is zero mean. For the standard deviation of the range error $\sigma_{\epsilon_{TOA}}(B_{if})$, using (4.2), (4.3), (4.7), and (4.8), $\epsilon_{TOA}(B_{if}, d)$ can be expressed as:

$$\epsilon_{TOA}(B_{if}, d) = m_{B_{if}}(B_{if})d + S_0(g_{B_{if}}(B_{if})d^\alpha + 1) \quad (4.11)$$

which is a non linear function of two independent random variables, d and S_0 . Using the variance propagation law applied to (4.11), linearized around the mean of d and $S_{TOA,0}$, and approximated to its second order gives:

$$\sigma_{\epsilon_{TOA}}(B_{if}) \approx \sqrt{(m_{B_{if}}(B_{if})\sigma_d)^2 + (\sigma_{S_{TOA,0}}(s_{B_{if}}(B_{if})(E[d])^\alpha + 1))^2} \quad (4.12)$$

Fig. 4.4 shows the mean and the standard deviation of the global range error directly obtained using the total set of data, and the model proposed in (4.10)-(4.12) for comparison, both for LOS and for NLOS. For LOS, using the full bandwidth, the global mean and standard deviation of the range error result $-0.001 \cong 0$ m and 0.018 m respectively; for $B_{if} = 0.5$ GHz, they increase up to 0.038 m and 0.124 m, respectively. Also in NLOS, ranging performance provided by UWB is very good, due to the high penetration capability of these signals and to the absence in our measurement scenarios of large metallic reflectors which might cause the complete blockage of the direct ray in the received signal. From the figure, bandwidths larger than about 4 GHz do not allow to further increase noticeably the range estimation accuracy, while bandwidths in excess of 2 GHz provide only modest gain in achieved performance.

4.3 LOS/NLOS detection

In this section, a possible use of the model for LOS/NLOS detection, is described. This issue appears extremely interesting, since e.g. it allows to improve the overall positioning accuracy, as shown in the next section. However, in literature only a few publications related to this point are available. For example, the authors in

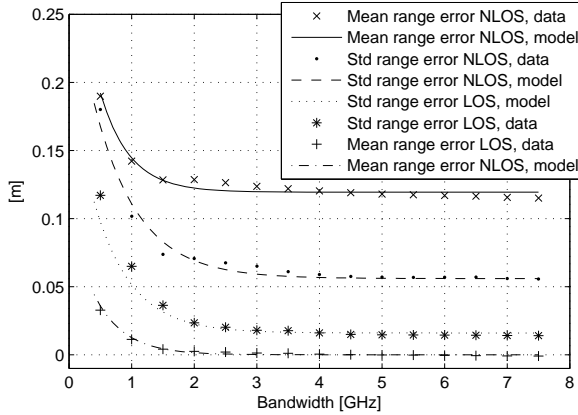


Figure 4.4: Mean and standard deviation of the global range error for both LOS and NLOS, as a function of B_{if} .

[17] propose a LOS/NLOS identification approach based on different statistics retrieved from the received signal (RMS delay spread, mean excess delay, kurtosis). However, this approach has been only validated with IEEE models, which do not provide satisfactory and accurate information to this purpose. For example, in [18] it is shown that the mean excess delay is in general dependent on the distance, and can have very similar values in LOS and NLOS, making this approach not viable in realistic situations.

The idea behind the proposed approach is depicted in Fig. 4.5, which shows the same total power and first path power path-loss models as in Fig. 2.4 of Chapter 2, but with the scatter-plots related to LOS and NLOS in the same figure. From the figure, it is clear that both for TP and for FP , the scatter-plots for LOS and NLOS propagation tend to increase their separation for increasing d , as an effect of the different path-loss exponents. Therefore, having knowledge of the *true* distance d between transmitter and receiver, it is possible to draw a vertical line with x-axis value d on the same scatter-plot. Focusing in this example on TP , it is also possible, when having knowledge of the total *measured* power P_{TP} , to draw an horizontal line, with y-value equal to P_{TP} . In the ideal case of no fading for TP , the two lines would intersect on the scatter-plot fit for LOS or NLOS, under the two propagation conditions, respectively. Since in general the measured received signal is affected by fading, the intersection point will deviate from the corresponding fit. However, from Fig. 4.5, it is clear that

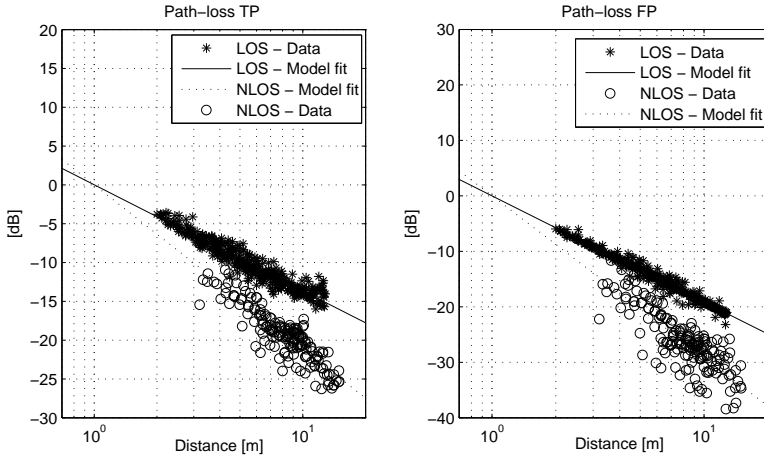


Figure 4.5: Path-loss and model fit for the total signal power (left) and first path power (right), both for LOS and NLOS propagation.

the separation of the LOS and NLOS scatter-plots is typically larger than the fading deviations; for this reason, it is likely to be able to correctly recognize the propagation condition by observing the considered statistic, and deciding among the two different hypotheses in a proper way. It is also clear that the approach can be easily extended to *FP*. In practice, the true distance is unknown; however, as shown in the previous section, errors provided by TOA estimation are significantly smaller than those provided by *TP* or *FP*; for this reason, it appears reasonable to use this technique, and to replace the true and unknown distance between transmitter and receiver, used as reference, with the distance estimated with TOA, in order to perform LOS/NLOS detection.

4.3.1 Maximum a posteriori LOS/NLOS decision rule

A Maximum a Posteriori (MAP) decision framework is developed in this section in order to perform LOS/NLOS identification, and its performance is analytically evaluated. This is the decision rule which minimizes the overall probability of erroneous detection, giving equal weight to the two types of error (LOS detection when NLOS is true, and NLOS detection when LOS is true).

For shortness, we omit from this moment on the prefix *TP* or *FP* to the statistics of interest. Denoting with p_{LOS} and p_{NLOS} the a-priori probabilities of

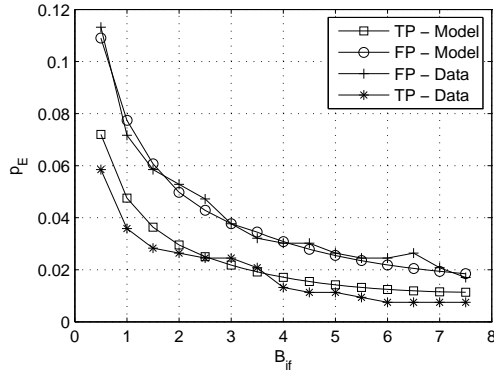


Figure 4.6: p_E vs. B_{if} , for TP and FP , both from the data, and using the analytical derivation proposed in Section 4.3.2.

being in LOS or NLOS, and with H_{LOS} and H_{NLOS} the hypotheses of being in LOS or NLOS, respectively, the MAP test is given by:

$$\text{Reject } H_{LOS} \text{ if: } \frac{f(P - P|_{LOS}(\hat{d}_{TOA}))p_{LOS}}{f(P - P|_{NLOS}(\hat{d}_{TOA}))p_{NLOS}} \leq 1 \quad (4.13)$$

where P is the measured power (with TP or FP), $P|_{LOS}(\hat{d}_{TOA})$ is the expected power under H_{LOS} at distance \hat{d}_{TOA} , and similarly $P|_{NLOS}(\hat{d}_{TOA})$ is the expected power under H_{NLOS} at distance \hat{d}_{TOA} . $f(P - P|_{LOS}(\hat{d}_{TOA}))$ is the *pdf* of the difference between measured and expected power under H_{LOS} and $f(P - P|_{NLOS}(\hat{d}_{TOA}))$ is the *pdf* of the difference between measured and expected power under H_{NLOS} . The evaluation of (4.13) from the data for $B_{if} = 7.5$ GHz gives a probability of error $p_E \approx 0.008$ for TP and $p_E \approx 0.017$ for FP . Fig. 4.6 shows the obtained results, as a function of the bandwidth used, both for TP , and FP . It can be seen that the error probability increases with decreasing B_{if} ; this appears logical, since in this case the fading both in LOS and in NLOS, and the error in the distance estimated with TOA, used as reference, increase. However, also for smaller bandwidths, it is possible to achieve a rather good LOS/NLOS detection, especially with TP . It is also worthwhile to note that TP based detection always outperforms the FP based one. This is due the significantly larger fading of this statistic in NLOS, which makes the use of this statistics for LOS/NLOS detection less reliable. As an example, Fig. 4.7 shows the evaluation of $f(P - P|_{LOS}(\hat{d}_{TOA}))p_{LOS}$ and $f(P - P|_{NLOS}(\hat{d}_{TOA}))p_{NLOS}$ for each particular measurement, under LOS propagation, for $B_{if} = 7.5$ GHz,

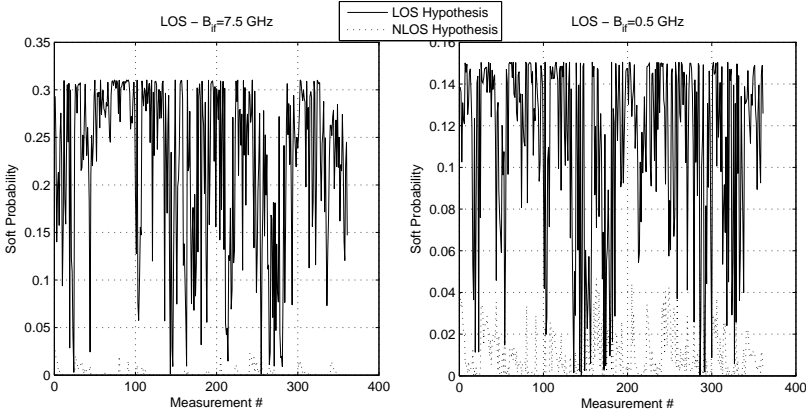


Figure 4.7: Evaluation of $f_{LOS}(S)p_{LOS}$ and $f_{NLOS}(S)p_{NLOS}$ vs. measurement number, under LOS propagation, for $B_{if} = 7.5$ (left) GHz, and $B_{if} = 0.5$ GHz (right), for comparison.

and $B_{if} = 0.5$ GHz, for comparison (the results for the two tests under NLOS are similar). In this case, errors happen when for a given measurement $f(P - P|_{LOS}(\hat{d}_{TOA})) p_{LOS} < f(P - P|_{NLOS}(\hat{d}_{TOA})) p_{NLOS}$; it can be seen that the occurrence of errors is limited, and most of the times the detection is reliable, since $f_{LOS}(S)p_{LOS} \gg f_{NLOS}(S)p_{NLOS}$. These values can be used e.g. as soft weights in weighted least-squares positioning, to take into account the reliability of each hypothesized propagation condition. It is clear that a soft approach can provide potentially better performance than a hard approach (as used in the next Section 4.4) in which detection is performed *before* positioning. To keep the focus of this chapter on TOA error modeling and applications, this issue is not further addressed.

4.3.2 Analytical Evaluation of the MAP Performance

Performance of the decision approach in (4.13) can be evaluated theoretically. To make the analytical derivation feasible, we introduce a Gaussian approximation for the fading terms (in dB) and for ϵ_{TOA} . This makes models for TP and FP formally the same. At this stage, for easiness of notation, we also assume to have perfect knowledge of the *true* distance d ; this hypothesis will be removed in the next subsection.

Denoting with:

$$m_{LOS} = P_0 - 10n_{LOS} \log_{10}(d/d_0) \quad (4.14)$$

and

$$m_{NLOS} = P_0 - 10n_{NLOS} \log_{10}(d/d_0) \quad (4.15)$$

the average received power at distance d under H_{LOS} and H_{NLOS} , respectively (with $m_{LOS} > m_{NLOS}$), and similarly with σ_{LOS} and σ_{NLOS} the fading in the two situations (with $\sigma_{LOS} < \sigma_{NLOS}$), the condition in (4.13) can be expressed as:

$$2 \ln \frac{p_{LOS}\sigma_{LOS}}{p_{NLOS}\sigma_{NLOS}} - \frac{(P - m_{LOS})^2}{\sigma_{LOS}^2} + \frac{(P - m_{NLOS})^2}{\sigma_{NLOS}^2} \leq 0 \quad (4.16)$$

Defining:

$$\Delta \triangleq \sigma_{LOS}^2 \sigma_{NLOS}^2 \left((m_{LOS} - m_{NLOS})^2 + 2(\sigma_{NLOS}^2 - \sigma_{LOS}^2) \ln \frac{p_{LOS}\sigma_{LOS}}{p_{NLOS}\sigma_{NLOS}} \right) \quad (4.17)$$

and observing that Δ is strictly larger than zero for the values of interest, the *two* critical values of the MAP test are:

$$\xi_1 = \frac{\sigma_{NLOS}^2 m_{LOS} - \sigma_{LOS}^2 m_{NLOS} - \sqrt{\Delta}}{\sigma_{NLOS}^2 - \sigma_{LOS}^2} \quad (4.18)$$

and

$$\xi_2 > \xi_1 = \frac{\sigma_{NLOS}^2 m_{LOS} - \sigma_{LOS}^2 m_{NLOS} + \sqrt{\Delta}}{\sigma_{NLOS}^2 - \sigma_{LOS}^2} \quad (4.19)$$

It immediately follows that the overall probability of error is:

$$\begin{aligned} p_E &= p_{LOS} \left(1 - Q \left(\frac{\xi_1 - m_{LOS}}{\sigma_{LOS}} \right) + Q \left(\frac{\xi_2 - m_{LOS}}{\sigma_{LOS}} \right) \right) + \\ & p_{NLOS} \left(Q \left(\frac{\xi_1 - m_{NLOS}}{\sigma_{NLOS}} \right) - Q \left(\frac{\xi_2 - m_{NLOS}}{\sigma_{NLOS}} \right) \right) \approx \\ & p_{LOS} Q \left(\frac{m_{LOS} - \xi_1}{\sigma_{LOS}} \right) + p_{NLOS} Q \left(\frac{\xi_1 - m_{NLOS}}{\sigma_{NLOS}} \right) \end{aligned} \quad (4.20)$$

where the last approximation holds since it is easy to see that:

$$1 - Q \left(\frac{\xi_1 - m_{LOS}}{\sigma_{LOS}} \right) \gg Q \left(\frac{\xi_2 - m_{LOS}}{\sigma_{LOS}} \right) \quad (4.21)$$

and

$$Q \left(\frac{\xi_1 - m_{NLOS}}{\sigma_{NLOS}} \right) \gg Q \left(\frac{\xi_2 - m_{NLOS}}{\sigma_{NLOS}} \right) \quad (4.22)$$

The approximation in (4.20) makes p_E only dependent on the single critical value $m_{NLOS} < \xi_1 < m_{LOS}$. The global probability of error can be simply obtained by averaging over the distribution of the distance:

$$p_E = \int (p_E|d) f_d(d) dd \quad (4.23)$$

where $p_E|d$ is the probability calculated as in (4.20) conditioned to a given value of d and $f_d(d)$ is the *pdf* of the distance between transmitter and receiver.

Effect of errors in the estimated distance with TOA

It is easy now to extend these results to the case in which the reference distance provided by TOA estimation is affected by an error itself. With respect to (4.20), errors in the evaluation of the true reference distance, reflect in errors in m_{LOS} and m_{NLOS} ¹; considering for example m_{LOS} :

$$\hat{m}_{LOS} = P_0 - 10n_{LOS} \log_{10} \frac{\hat{d}_{TOA}}{d_0} \approx \quad (4.24)$$

$$P_0 - 10n_{LOS} \log_{10} \frac{d}{d_0} - 10n_{LOS} \frac{\epsilon_{TOA}}{d} = m_{LOS} - 10n_{LOS} \frac{\epsilon_{TOA}}{d}$$

where \hat{m}_{LOS} represents the mean expected power in LOS, when the distance estimated with TOA instead of the true one is used. To derive the second expression in (4.24), capitalizing on the small ϵ_{TOA} with respect to d , only the zero and first order terms of the Taylor expansion of the logarithm have been considered. Considering the formal equality:

$$P_{LOS} = P_0 - m_{LOS} + S_{LOS} = P_0 - \hat{m}_{LOS} + \hat{S}_{LOS} \quad (4.25)$$

where

$$\hat{S}_{LOS} \triangleq S_{LOS} - 10n_{LOS} \frac{\epsilon_{TOA}}{d} \quad (4.26)$$

errors in TOA estimation are equivalent to an increase in the standard deviation of S_{LOS} ; in fact, \hat{S}_{LOS} is a Gaussian random variable (capitalizing on the introduced simplifications) with:

$$\sigma_{\hat{S}_{LOS}} = \sqrt{\sigma_{S_{LOS}}^2 + (10 \frac{n_{LOS}}{d} \sigma_{\epsilon_{TOA}})^2 - 10 \frac{n_{LOS}}{d} \sigma_{S_{LOS}} \sigma_{\epsilon_{TOA}} \rho_{TP, TOA}} \quad (4.27)$$

¹For small bandwidths, errors in the considered reference distance also affect the evaluation of the correct σ_{LOS} required in (4.20), since the fading standard deviation is dependent on the distance itself, in this last case. The analysis can be extended accounting also for this point; however, these deviations are negligible. Therefore, this case is not considered in this paragraph.

which represents the standard deviation of the equivalent fading which allows to analyze the case in which the reference distance is affected by an error ϵ_{TOA} with the same formula as in (4.23). In (4.27), $\rho_{TP,TOA}$ is the correlation between ϵ_{TOA} and S_{TP} , and it has been evaluated empirically. The evaluation of m_{NLOS} is similar. The same Fig. 4.6 also shows results using the developed analytical framework in order to evaluate the probability of wrong LOS/NLOS identification. In this case, $f_d(d)$ required in (4.23) has been evaluated from the empirical histogram of the recorded distances. It can be seen that the match between theoretical results and experimental data is good. Fluctuations for the empirical case are likely due to the limited amount of data, which is not large enough to reliably estimate error probabilities in the order of a few percentages.

4.4 Weighted least squares positioning

In this section, a possible application of the proposed model to improve the classical least-squares (LS) positioning, is investigated. We refer to Section 3.6 for a detailed formal presentation of the weighted least-squares (WLS) positioning problem, while in this section we focus on results. Two different situations are compared: the first in which positioning is performed using traditional least-squares (the variance matrix \mathbf{V}_d in (4.46) is an identity matrix), the second in which:

1. estimated distance with TOA is made unbiased exploiting the model information
2. the variance matrix is built using TOA error model knowledge
3. LOS/NLOS propagation is detected as described in the previous section.

In this second case, since both $m(B_{if}, d)$ and \mathbf{V}_d depend on the real distance which is unknown, the estimated distance, instead of the unknown real one, is used for their evaluation. Since TOA errors are small compared with d , this practical simplification does not affect performance.

Also in this case, the following scenarios have been simulated: LOS and $N_p=4$, LOS and $N_p=8$, NLOS and $N_p=4$, NLOS and $N_p=8$, $N_p=4$ with 2 measurements in LOS and 2 in NLOS, and $N_p=8$ with 4 measurements in LOS and 4 in NLOS. The N_p reference nodes have been placed each in a different of the height regions in which the space is divided by the x-y, x-z, and y-z planes ('good' geometry,

Table 4.2: Final position estimation accuracy for different scenarios

	LOS $N_p = 4$	LOS $N_p = 8$	NLOS $N_p = 4$	NLOS $N_p = 8$	LOS/NLOS $N_p = 4$	LOS/NLOS $N_p = 8$
$B_{if} = 7.5$ GHz						
LS	0.025 [m]	0.017 [m]	0.143 [m]	0.093 [m]	0.167 [m]	0.064 [m]
WLS	0.025 [m]	0.017 [m]	0.091 [m]	0.068 [m]	0.058 [m]	0.025 [m]
$B_{if} = 0.5$ GHz						
LS	0.211 [m]	0.147 [m]	0.322 [m]	0.210 [m]	0.308 [m]	0.180 [m]
WLS	0.183 [m]	0.103 [m]	0.237 [m]	0.1620 [m]	0.209 [m]	0.122 [m]

as defined in Section 3.6), and only the standard deviation positioning error $\sigma_{\epsilon_{\mathbf{x}_u}}$ is evaluated. The convergence rate evaluation is not addressed, since differently from power based methods, TOA errors are small with respect to d , and the convergence problem is less critical in this case. Table 4.2 shows obtained results, using the same simulation procedure as in Section 3.6, and averaged over 10000 repetitions, for $B_{if} = 7.5$ GHz and $B_{if} = 0.5$ GHz, for comparison. It can be seen that positioning accuracy ranges from a few centimeters for $B_{if} = 7.5$ GHz, down to a few decimeters for $B_{if} = 0.5$ GHz. Also in this case, increasing N_p allows to improve positioning performance. Only for the case of LOS and $B_{if} = 7.5$ GHz there is no improvement using the range error model knowledge, since the error is unbiased and it does not depend on the distance. For all the other scenarios, model knowledge always allows to improve the final position estimation accuracy; relative improvements are similar for the case of $N_p = 4$ and $N_p = 8$ (with the exception of LOS and $B_{if} = 0.5GHz$), and are larger for mixed LOS/NLOS scenarios, in which they reach about 300% when comparing the weighted and un-weighted case. For example, for $B_{if} = 7.5GHz$ and $N_p = 4$, $\sigma_{\epsilon_{\mathbf{x}_u}} = 0.167$ m for traditional LS; the use of WLS, together with the proposed range error model and the LOS/NLOS detection algorithm previously introduced, allows to reduce it down to about 0.058 m.

4.5 Chapter summary

In this chapter, the performance of TOA based ranging has been evaluated, and a model for the obtained range error has been proposed. Two different applications of the model have been described; the first, to LOS/NLOS detection, the second to weighted least-squares positioning. Relevant points and conclusions which can

be drawn from the results presented herein are summarized in the following:

- This chapter gives a comprehensive investigation and modeling of the range error ϵ_{TOA} experienced with TOA based ranging, and relates it to relevant system parameters. A statistical characterization of ϵ_{TOA} has been proposed; it is shown that both the mean range error, and the random deviations from it, are in general dependent on LOS/NLOS propagation, signal bandwidth and transmitter-receiver separation distance. The range error can be modeled as a Gaussian random variable in LOS, and the combination of a Gaussian and an exponential random variable in NLOS.
- TOA estimation is suited for applications which demand for highly accurate positioning information. In fact, when using the full bandwidth, centimeter level accuracy has been found in LOS. The error increases in NLOS due to the additional delay caused by propagation through dielectric materials and to the more dense multipath.
- Reliable LOS/NLOS detection can be achieved by combining TOA and received total power (or first path power) information. This knowledge can be used to improve in a significant way global positioning results, especially in mixed LOS/NLOS scenarios.
- Increasing B_{if} above 2 GHz does not provide a significant increase in TOA estimation accuracy. Larger bandwidth are however beneficial for LOS/NLOS detection, since TP and FP fading decrease in a noticeable way for bandwidths larger than 2 GHz.

Bibliography

- [1] M.Z. Win, R.A. Scholtz, "Ranging in a dense multipath environment using an UWB radio link", IEEE Journal on Selected Areas in Communications, vol. 20, no. 9, pp. 1677-1683, Dec. 2002.
- [2] S. Gezici, Zhi Tian, G. B. Giannakis, H. Kobayashi, A. F. Molisch, H. V. Poor and Z. Sahinoglu, "Localization via ultra-wideband radios: a look at positioning aspects for future sensor networks", IEEE Signal Processing Magazine, vol. 22, no. 4, pp. 70-84, July 2005.

-
- [3] A.A. D'Amico, U. Mengali, L. Taponecco, "*Energy-based TOA estimation*", IEEE Transaction on Wireless Communications, vol. 7, no. 3, pp. 838-847, Mar. 2008.
- [4] S. Gezici, H.V. Poor, "*Position estimation via ultra-wideband signals*", IEEE Proceedings, vol. 97, no. 2, pp. 386-403, Feb. 2009.
- [5] D. Dardari, A. Conti, U. Ferner, A. Giorgetti, M.Z. Win, "*Ranging with ultra-wide bandwidth signals in multipath environments*", IEEE Proceedings, vol. 97, no. 2, pp. 404-426, Feb. 2009.
- [6] D. Jourdan, D. Dardari, M.Z. Win, "*Position error bound for UWB localization in dense cluttered environments*", IEEE Transactions on Aerospace and Electronic Systems, vol. 44, no. 2, pp. 613-628, Apr. 2008.
- [7] D. Dardari, M.Z. Win, "*Ziv-Zakai bound on time-of-arrival estimation with statistical channel knowledge at the receiver*", IEEE ICUWB 2009, pp. 624-629, Sep. 2009.
- [8] Yiyin Wang, G. Leus, A.J. van der Veen, "*Cramr-Rao bound for range estimation*", IEEE ICASSP 2009, pp. 3301-3304, Apr. 2009.
- [9] Z. Irahauten, G. Bellusci, G. J. M. Janssen, H. Nikookar and C. C. J. M. Tiberius, "*Investigation of UWB ranging in dense indoor multipath environments*", IEEE ICCS 2006, pp. 1-5, 30 Oct.-1 Nov. 2006.
- [10] C. Gentile, A. Kik, "*An evaluation of ultra wideband technology for indoor ranging*", IEEE GLOBECOM 2006, pp. 1-6, Nov. 2006.
- [11] B. Alavi, K. Pahlavan, "*Modeling of the distance error for indoor geolocation*", IEEE WCNC 2003, pp. 668-672, Mar. 2003.
- [12] B. Alavi, K. Pahlavan, "*Bandwidth effect on distance error modeling for indoor geolocation*", IEEE PIMRC 2003, pp. 2198-2202, Sep. 2003.
- [13] B. Alavi, K. Pahlavan, "*Modeling of TOA-based distance measurement error using UWB indoor radio measurements*", IEEE Communication Letters, vol. 10, no. 4, pp. 275-277, Apr. 2006.
- [14] B. Alavi, K. Pahlavan, "*Studying the effect of bandwidth on performance of UWB positioning systems*", IEEE WCNC 2006, vol. 2, pp. 884-889, Apr. 2006.

- [15] Chia-Chin Chong, Fujio Watanabe, M.Z. Win, "*Effect of bandwidth on UWB ranging errors*", IEEE WCNC 2007, pp. 1559-1564, Mar. 2007.
- [16] R.G. Vaughan, N.L. Scott, "*Super-resolution of pulsed multipath channels for delay spread characterization*", IEEE Transactions on Communications, vol. 47, no. 3, pp. 343-347, March 1999.
- [17] I. Guvenc, C.C. Chong, F. Watanabe, "*NLOS identification and mitigation techniques for UWB localization systems*", IEEE WCNC 2007, pp. 1571-1576, 11-15 Mar. 2007.
- [18] G. Bellusci, G.J.M. Janssen, J. Yan, C.C.J.M. Tiberius, "*Novel ultra wide-band low complexity ranging using different channel statistics*", IEEE WCNC 2008, pp. 290-295, Apr. 2008.

Low-Complexity TOA Estimation

The use of sub-nanosecond duration UWB pulses offers the unique possibility of distinguishing the different multipath components which compose the received signal and of accurately estimating the TOA of the *first* path, which contains the relevant information for ranging. In this way, as shown in the previous chapter, centimeter level positioning accuracy can be potentially achieved, even in the multipath rich indoor environments, when UWB signals are used.

However, the use of these signals, while it allows for the aforementioned benefit, introduces significant problems in a practical system implementation. In particular, the main challenges are on the receiver side, since it is necessary to process GHz bandwidth waveforms. Most of the proposed solutions available in literature rely on samples of the received signal collected at least at Nyquist rate [1]-[3]. For example, 20.5 GHz sampling rate is used for the generalized maximum likelihood TOA estimator proposed in [3]. The requirements for extremely performing analog-to-digital converters (ADC), together with the very high hardware demands needed for processing the collected data samples in order to extract the timing information, have been identified as the major limiting factors towards the use of UWB technology for a wide range of applications, which typically have strict requirements on costs, complexity, and power consumption.

To address this issue, sub-optimal and lower complexity approaches, in which part of the potential accuracy is sacrificed to reduce system complexity and power consumption demands, have been investigated in literature. For example, the authors in [4] propose an energy-based TOA estimation; the accuracy depends

on the sampling rate used; e.g. it is at meter level using a 500 MHz ADC. A conceptually similar approach is proposed in [5]-[7]. The time window in which the received signal is observed is divided in small time bins; the center of the first bin whose energy exceeds a given threshold is detected as the signal TOA. This last solution, while attractive since it avoids the need for high sampling rates, presents some drawbacks; first, since the approach is based on bin energy detection, its TOA estimation accuracy is particularly sensitive to noise and interference; second, the potential centimeter accuracy provided by UWB technology is not fully exploited, since performance is limited by the bin size which is typically of a few nanoseconds, resulting in a decimeter to meter additional bin quantization error.

In this chapter, a new low-complexity TOA estimation approach is proposed. The considerations behind this work are the following. When using short duration UWB pulses, the received signal can be considered as an approximation of the Channel Impulse Response (CIR) (neglecting the sign value of each path) with potential time resolution given by the inverse of the signal bandwidth; the proposed solution capitalizes on this idea. The proposed receiver consists of an analog peak detector, working directly on the received signal, followed by two RC filters with different time-constants. From the two different exponentially decaying signals, which are sampled with a low rate, the first peak TOA is calculated (the principle of operation is illustrated in Fig. 5.2). It is shown that very simple signal processing and a sampling rate of only a few tens of MHz, about two orders of magnitude less than the Nyquist rate, are needed. At the same time, the additional sources of error specifically introduced by the proposed receiver implementation are negligible; therefore, the accuracy of the proposed approach is practically the same as an ideal first peak detector based on Nyquist sampling and perfect reconstruction of the received signal envelope. In this way, the final range error achieved with this solution is at centimeter level. Together with the principle of concept, a possible hardware implementation is suggested (see Fig. 5.1).

Since the proposed receiver estimates the TOA directly from the instantaneous received signal without further processing, it is not possible to increase the effective Signal to Noise Ratio (SNR) by performing an average *before* TOA estimation, to allow for performance and reliability flexibility. For this reason, a different strategy to combine multiple TOA estimates is proposed; even if the approach is particularly suited for the presented receiver concept, the proposed

analysis is general and can be used for other peak detection based TOA estimation algorithms. Finally, a preliminary coarse acquisition scheme [8]-[10], required for correct operation of the proposed TOA strategy, is described. To keep the system complexity low, coarse acquisition is based on energy detection. The presented theoretical framework to calculate the statistics of the maximum energy time window in closed-form, allows to evaluate the performance of the scheme in terms of probability of acquisition and to relate it to the relevant system and channel parameters. Also this step is developed considering the specific requirements that arise when the proposed TOA estimation concept is used; however, the analysis is general and the approach can be employed in other systems. Evaluation of the link budget of the proposed solution under the power requirements imposed by the FCC for UWB transmissions [1], shows that the maximum achievable distance of the described strategy is a few hundred meters in LOS, making this approach ideal for short to medium distance low-complexity indoor positioning applications which require centimeter level accuracy.

5.1 Signal model

The received UWB pulse-type signal in a multipath channel for a single user and without narrowband interference can be represented as:

$$r(t) = \sum_{j=-\infty}^{\infty} c_j w_{mp}(t - jT_f) + n(t) \quad (5.1)$$

where $c_j \in \{\pm 1\}$ is a random-polarity code only used to avoid the presence of spikes in the power spectral density of the received signal, T_f is the frame repetition period, and $n(t)$ is AWGN with zero mean and power spectral density N_0 . The received multipath signal $w_{mp}(t)$, which corresponds to the transmission of a single pulse $w(t)$ with energy E_w , is expressed as:

$$w_{mp}(t) = \sum_{l=0}^{L_{ch}-1} h_l w_l(t - \tau_l) \quad (5.2)$$

where h_l and τ_l are the amplitude coefficients and delays of the l -th channel multipath component, respectively, and $w_l(t)$ is the waveform received along the l -th path; L_{ch} is the number of multipath components. This is the most general indoor multipath propagation model in which each single path undergoes distortion. τ_0 represents the unknown TOA of the received signal. Without loss of generality,

we can assume $\tau_0 \in [0, T_f]$, since we are interested in the determination of TOA with respect to the receiver clock. The determination of the absolute value of τ_0 can be performed with higher layer protocols (e.g. two way ranging), or with a TDOA scheme.

In the analysis and simulation results presented in the next sections, $w(t)$ is chosen as a Gaussian pulse modulated with a carrier:

$$w(t) = A_0 \cos(2\pi f_0 t) \exp(-t^2/(2T_g^2)) \quad (5.3)$$

where A_0 is a normalization factor, $f_0 = 4.6$ GHz is the central frequency of the spectrum, and $T_g = 0.16$ ns, which corresponds to a -10 dB bandwidth B of 3 GHz, between 3.1 and 6.1 GHz. An additional bandpass filter is used to further cut off emissions outside the specified bandwidth and to satisfy the FCC mask imposed for UWB transmissions [1]. The results proposed in the next sections, however, are general and can be applied to different pulse shapes.

5.2 TOA estimation

In this section, a low-complexity receiver implementation to accurately estimate the TOA of the first peak of the received signal is proposed, and the sources of inaccuracy specifically introduced by the suggested implementation are analyzed. To allow for performance flexibility, a strategy to combine multiple TOA estimates, is then described and evaluated.

It is assumed that an estimate T_0 of the frame starting time, provided by a preliminary coarse acquisition step, is available. In this way, the TOA of the received signal τ_0 can be expressed as: $\tau_0 = T_0 + \tau$. In this section we focus on the estimation of τ ; for proper operation, the proposed approach requires that $0 \leq \tau \leq T_f - \tau_{cds}$, where τ_{cds} is the delay spread of the channel. This condition is needed to avoid that the described TOA estimation receiver will wrongly detect late multipath components belonging to the tail of a previous frame, and it is equivalent to the requirement that the received signal in the observed window starts with a noise only part of duration τ , followed by the useful signal part (of duration τ_{cds}) which goes to zero before the end of the frame. This condition is assumed in the following and it is satisfied by the coarse acquisition scheme discussed in Section 5.3.

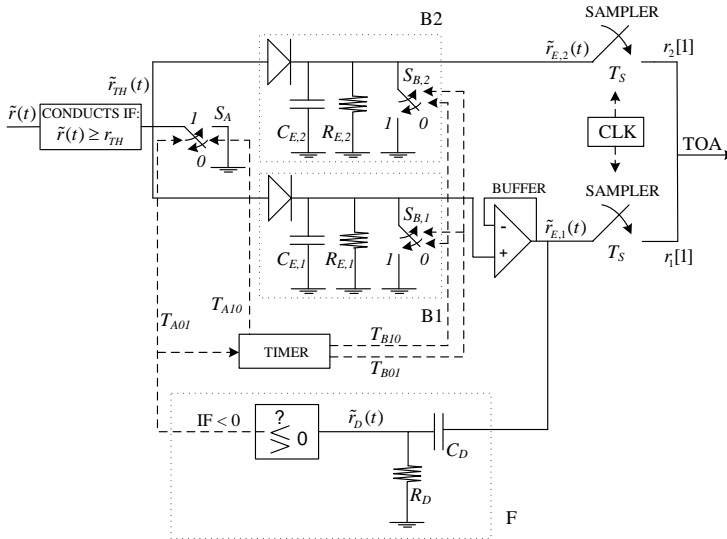


Figure 5.1: The proposed low-complexity receiver to estimate the TOA of the received signal.

5.2.1 Receiver implementation

The proposed TOA estimation receiver, a possible implementation is depicted in Fig. 5.1, exploits the fact that, when using extremely short duration UWB pulses, the received signal can be considered a good approximation of the channel impulse response (neglecting the sign value of each path). In the described strategy, the received signal is directly passed through two analog branches, the first of which keeps at the output the power of the first path of the received signal, the second whose output decreases exponentially with time from the first path power. Only at this point the two outputs are sampled with a very low sampling rate, as shown in Fig. 5.2, which illustrates the principle of operation of the described receiver in a qualitative way. From the collected samples, it is possible to precisely reconstruct the original TOA of the first path with a simple interpolation operation. In the following, we describe in detail this principle of operation and the proposed hardware implementation.

Referring to Fig. 5.1, the received signal $r(t)$ is passed through a filter matched to the transmitted pulse $w(t)$. The matched filter is only used for noise filtering and to simplify the theoretical analysis; in a practical implementation it can be

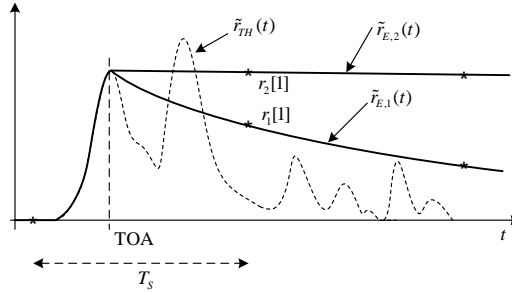


Figure 5.2: Principle of working of the proposed receiver.

realized with a bandpass filter causing a performance degradation of a fraction of a dB. The envelope $\tilde{r}(t)$ of the filter output is then calculated. Also the calculation of the envelope, used in the following, is not strictly required for the described principle of operation. $\tilde{r}(t)$ goes to a threshold device with input-output law given by:

$$\tilde{r}_{TH}(t) = \begin{cases} \tilde{r}(t) & \text{if } \tilde{r}(t) \geq r_{TH} \\ 0 & \text{otherwise} \end{cases} \quad (5.4)$$

which cuts off noise and signal components smaller than the defined threshold r_{TH} . The receiver is composed of a control timer and three blocks: the blocks $B1$ and $B2$ perform similar operations; the third block, called F , is a feedback circuit. $\tilde{r}_{TH}(t)$ goes to $B1$ and $B2$. The buffer amplifier placed between $B1$ and F prevents the circuits from loading each other. The default position of the switches S_A , $S_{B,1}$, and $S_{B,2}$ is "0" (open-circuit). Focusing on $B1$, after S_A there is an envelope detector composed of a diode followed by an RC circuit. The values of $R_{E,1}$ and $C_{E,1}$ are set to affect the output signal with the "diagonal clipping" phenomenon [12]; the time constant of the circuit $\tau_{E,1} = R_{E,1}C_{E,1}$ in fact is chosen larger than the inverse of the signal bandwidth; in this way, the output, instead of following the envelope of the signal, tends to decrease slowly from the detected peak value. The importance of this point will be clear in the following. $B2$ works in the same way. The output of $B1$, $\tilde{r}_{E,1}(t)$, is used by F ; this is an RC circuit used as differentiator; to work properly, its time constant, $\tau_D = R_D C_D$, should be smaller than $1/B$. The switch of S_A from "0" to "1" (short-circuit) is controlled by the sign of the output of F ; when $\tilde{r}(t)$ goes from positive to negative, corresponding to the occurrence of the first peak of the channel envelope, S_A is switched to the short circuit position at time T_{A01} ; at the

same time, the timer is set. This is the only control element of the circuit and it is used to pilot the subsequent switches of S_A , $S_{B,1}$, and $S_{B,2}$. For easiness of notation, and without loss of generality, we assume: $T_{A_{01}} = 0$. From this moment on, $\tilde{r}_{TH}(t)$ does not influence anymore $\tilde{r}_{E,1}(t)$ and $\tilde{r}_{E,2}(t)$ since the input of the envelope detectors is connected to ground. Thus, $\tilde{r}_{E,1}(t)$ and $\tilde{r}_{E,2}(t)$ decrease from the first peak value with time constants $\tau_{E,1}$ and $\tau_{E,2}$, respectively, and are sampled with sampling rate T_s . If $\tau_{E,2} \gg \tau_{E,1}$ (this can be simply obtained by replacing $R_{E,2}$ with an open circuit, which implies $\tau_{E,2} \rightarrow \infty$), the TOA can be reconstructed from the first pair of samples, as shown in Fig. 5.2. In this case, calling $r_1[1]$ and $r_2[1]$ the first sample at the output of the samplers of $B1$ and $B2$, respectively, the random delay t_0 of them with respect to the (unknown) TOA of the first peak (t_0 is uniformly distributed in $[0, T_s]$) can be determined by simply solving the equation:

$$r_2[1] \exp(-t_0/\tau_{E,1}) = r_1[1] \quad (5.5)$$

At time $T_{B_{01}}$, a reset pulse is sent from the timer to the switches $S_{B,1}$ and $S_{B,2}$, to reset them to their initial short-circuit position, allowing an instantaneous discharge of $C_{E,1}$ and $C_{E,2}$. At time $T_{B_{10}}$, $S_{B,1}$ and $S_{B,2}$ are triggered back to the original open-circuit position. Finally, at $T_{A_{10}}$ also S_A is switched back by the control timer to its original open-circuit position, and the circuit can repeat the described procedure. For proper operation, $T_{B_{01}} \geq T_s$, to allow to collect at least one sample needed to estimate t_0 , and $T_{A_{10}} \geq \tau_{cds}$ to avoid the detection of late multipath components corresponding to a previous transmission. In this way, repetitive transmission of pulses separated by at least $T_{A_{10}}$ is possible. Two other points require discussion. The threshold r_{TH} can be calculated from a noise only part of the received signal (this approach is used herein), or from the strongest path power value. In this last case, to first estimate the strongest path power, the same circuit can be used, with the logic part disabled. The proposed receiver in fact then becomes a strongest path power estimator, and a training transmission is required to perform this operation. The delay introduced by the F block should be smaller than the minimum time resolution allowed by the signal, which is approximately the inverse of the used bandwidth, to avoid the potential detection by the circuit of resolvable multipath components which follow the first peak and could have larger amplitude than it. However, due to the very simple operation performed by the logic part, this point does not seem a critical issue.

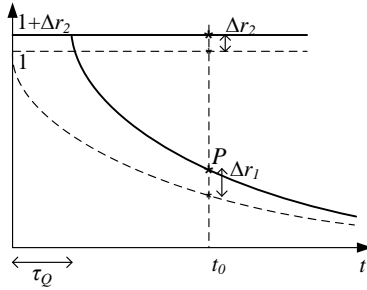


Figure 5.3: *Quantization error introduced by the proposed solution.*

Sources of impairment evaluation

There are two sources of inaccuracy specifically introduced by the described receiver implementation, which make TOA estimation with this solution different from that of a classical first peak detector based on a Nyquist sampled signal which allows perfect reconstruction of the received signal envelope. The first is the quantization error introduced by the two samplers, the second is due to possible fluctuations in the actual decay constant $\tau_{E,1}$ from its nominal value (typically caused by temperature variations). In the following, these sources of inaccuracy are evaluated.

By solving the equation:

$$\exp(-t_0/\tau_{E,1}) + \Delta r_1 = (1 + \Delta r_2) \exp(-(t_0 - \tau_Q)/(\tau_{E,1}(1 + \Delta\tau_{E,1}))) \quad (5.6)$$

in point P shown in Fig. 5.3, the error τ_Q in the TOA estimation introduced by the proposed solution can be determined. Δr_1 and Δr_2 are the sampling quantization errors of the samplers of $B1$ and $B2$, respectively, and $\Delta\tau_{E,1}$ is the relative error in the decay constant $\tau_{E,1}$. Under the hypothesis that $\tau_Q \ll \tau_{E,1}$ (this hypothesis is true, according to the values given in the following), and considering only the errors till the first order, τ_Q results in:

$$\tau_Q \approx \tau_{E,1}(-\Delta r_2 + \Delta r_1 \exp(t_0/\tau_{E,1}) - \Delta\tau_{E,1}/\tau_{E,1}t_0) \approx \tau_{E,1}(-\Delta r_2 + \Delta r_1 \exp(t_0/\tau_{E,1})) \quad (5.7)$$

since $\Delta\tau_{E,1}$ can be easily made negligible (if $\Delta\tau_{E,1} \leq 10^{-4}$, from (5.7)) with an inexpensive calibration step piloting the input with a known voltage. For evaluating τ_Q , we assume that the first peak power is approximately equal to the maximum ADC input level. In this case, fixing the interval of variation of the

ADC input between 0 and the estimated first peak power, the quantization errors Δr_1 and Δr_2 (normalized to the first peak power itself) are uniformly distributed random variables (r.v.'s) in $[-1/2^{N_s+1}, 1/2^{N_s+1}]$, where N_s is the number of bits of the ADC. τ_Q is then a zero mean r.v.. Applying the variance propagation law to the equation for τ_Q , approximated to the second order, and linearized around the mean of Δr_1 , Δr_2 , and t_0 , its variance is:

$$\sigma_{\tau_Q}^2 \approx \frac{\tau_{E,1}^2}{12 \cdot 2^{2N_s}} (1 + \exp(T_s/\tau_{E,1})) \quad (5.8)$$

The minimum of (5.8) with respect to $\tau_{E,1}$ can be obtained by differentiation. This gives the equation:

$$2(1 + \exp(T_s/\tau_{E,1})) - T_s/\tau_{E,1} \exp(T_s/\tau_{E,1}) = 0 \quad (5.9)$$

which can be numerically solved with respect to $T_s/\tau_{E,1}$, giving $T_s/\tau_{E,1} \approx 2.217$. By replacing this value in (5.8):

$$\sigma_{\tau_Q} \approx 0.42 \cdot T_s/2^{N_s} \quad (5.10)$$

which depends on the performance of the sampler. For example, with $T_s = 20$ ns (which corresponds to a sampling rate of 50 MHz) and $N_s = 8$, $\sigma_{\tau_Q} \approx 1$ cm, when expressed in units of range. Therefore, the proposed solution allows to significantly relax the hardware requirements for the receiver; in fact, a very simple signal processing is used and the sampling rate needed is of only a few tens of MHz, which can be achieved with inexpensive ADCs available in the market. This represents a significant improvement in complexity compared to Nyquist rate based approaches, which require an ADC sampling at several GHz; in this way, it is possible to solve the main implementation challenges which arise when UWB signals are used. At the same time, the error specifically introduced by the proposed implementation is in the order of a centimeter, thus negligible for practical system operation; this means that the final range error is comparable with that of an ideal first peak detector with perfect knowledge of the received signal envelope. This is a significant difference compared to e.g. traditional bin-energy based TOA estimation approaches [5], which achieve lower complexity sacrificing part of the potential accuracy available.

Capitalizing on this conclusion, in the next subsections, the performance of the TOA estimation strategy assuming an *ideal* first peak detector is evaluated.

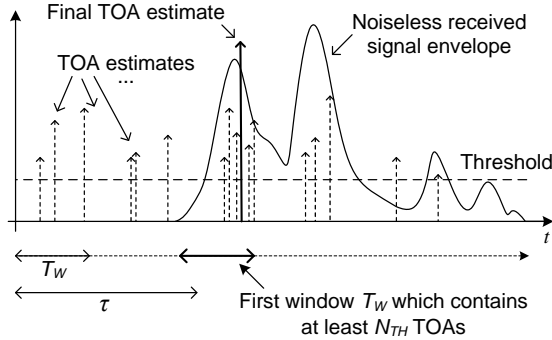


Figure 5.4: TOA estimation strategy.

5.2.2 TOA estimation strategy

The receiver proposed in Section 5.2.1 estimates the TOA directly from the received signal without further processing; for this reason, it is not possible to increase the effective signal to noise ratio by performing an average *before* TOA estimation to allow for performance and reliability flexibility. To address this issue, the following TOA estimation strategy is proposed; even if the approach is intended as a solution to address the specific requirements arising from the use of the proposed receiver concept, the analysis is general and can be used for other peak detection based TOA estimation algorithms.

A repetitive transmission of N pulses is performed. Each time the TOA of the received signal is estimated with the proposed receiver implementation. The N collected time estimates are temporally sorted. The strategy is to find the first time window of duration T_W and arbitrary starting time which contains at least N_{TH} TOAs, as shown in Fig. 5.4. The average of the TOAs which belong to this window is chosen as final TOA estimate.

Probabilities of early false alarm and missed detection

In the next subsections, the performance of the described solution is analyzed by evaluating the probability of early false alarm:

- $P_{EFA} \triangleq \Pr \{ \text{at least one time window of duration } T_W \text{ and arbitrary starting time which contains at least } N_{TH} \text{ TOAs exists in the initial noise only part of duration } \tau \text{ of the received signal} \}$

and the probability of missed detection:

- $P_{MD} \triangleq (1 - P_{EFA}) \cdot \Pr\{\text{in } N \text{ transmissions there are less than } N_{TH} \text{ TOAs in any time window of duration } T_W \text{ which contains the true TOA of the direct path}^1\}$.

If $P_{EFA} \ll 1$ then $P_{MD} \approx \Pr\{\text{in } N \text{ transmissions there are less than } N_{TH} \text{ TOAs in any time window of duration } T_W \text{ which contains the true TOA of the direct path}\}$. In this way, it is possible to evaluate the *reliability* of the TOA estimation. We will show that if the direct path is correctly detected, the range error results at centimeter level, as it can be expected from the use of very large bandwidths.

To simplify the analysis, limited to the theoretical evaluation of P_{EFA} , we assume the receiver implements a first crossing detection over a threshold r_{TH} , instead of a first peak detection. Due to the short duration of the used pulse, the results of the two cases differ in a negligible way. The threshold r_{TH} is calculated from the noise only part of the received signal at the matched filter output and is expressed as: $r_{TH} = k_{TH} \sigma_{n_{MF}}$, where k_{TH} is a real positive number and $\sigma_{n_{MF}}^2 = \int_{-\infty}^{\infty} N_0 |W(f)|^2 / E_w df = N_0$ is the variance of the noise $n_{MF}(t)$ at the unity gain matched filter output.

5.2.3 Performance evaluation - early false alarm

To calculate an exact expression for P_{EFA} is difficult; for this reason, an upper bound is determined. The first problem is that the duration τ of the noise only part of the received signal is a r.v. and it is unknown. Thus, a noise window $\tau_{MAX} = \max\{\tau\}$ is considered here, since P_{EFA} monotonically increases with τ . The actual value of $\max\{\tau\}$ depends on the particular choice of the parameters of the coarse acquisition step; for plotting the figures in this section, a choice of $\max\{\tau\} = 160$ ns is used, corresponding to the output of the coarse acquisition step. The second problem is related to the distribution of the TOA in τ , in case noise in this region is detected. Ref. [13] provides a framework to evaluate the probability $p_N(T_n)$ of first level crossing in a time window T_n for Gaussian noise and double-sided (symmetric about zero) threshold, while ref. [14] applies the results to UWB ranging. These results can be used in our analysis, observing that $p_N(T_n)$ also represents the probability of single-sided (above zero) first threshold

¹Due to multipath and eventual propagation through dielectric materials, the (unknown) true TOA of the direct path does not necessarily coincide with the TOA of the first peak of the received signal, even in noiseless conditions, as shown in the previous chapter.

crossing for the noise *envelope* at the matched filter output². From [13], the single-sided threshold first crossing probability in T_n for a Gaussian process is:

$$G(T_n) = 1 - \exp(-T_n/\rho) \quad (5.11)$$

with

$$\rho = 2\Phi(k_{TH})/\lambda \exp(k_{TH}^2/2) \quad (5.12)$$

and

$$\lambda = 2\sqrt{\int_{-\infty}^{\infty} f^2 S_{nw}(f) df / \int_{-\infty}^{\infty} S_{nw}(f) df} \quad (5.13)$$

where $\Phi(x) = \int_{-\infty}^x 1/\sqrt{2\pi} \exp(-\xi^2/2) d\xi$ and S_{nw} is the power spectral density at the matched filter output when in ingress only noise is present. From $G(T_n)$, an upper bound $\bar{p}_N(T_n)$ for the required probability can be immediately calculated as [13]:

$$p_N(T_n) \leq \bar{p}_N(T_n) = 1 - (1 - G(T_n))^2 \quad (5.14)$$

Observing that the Fourier transform of the considered pulse $w(t)$ in (5.3) is:

$$W(f) = A_0 T_g \sqrt{\pi/2} (\exp(-2T_g^2 \pi^2 (f - f_0)^2) + \exp(-2T_g^2 \pi^2 (f + f_0)^2)) \quad (5.15)$$

gives $\lambda = 2\sqrt{f_0^2 + 1/(8T_g^2 \pi^2)}$. By plotting the *cdf* of $p_N(T_n)$ (shown in Fig. 5.5) for the considered values of T_n , $p_N(T_n)$ approximately linearly increases with T_n when choosing $k_{TH} \approx 4$ or larger, showing that in case of TOA estimation in the time window T_n , it can be assumed uniformly distributed in $[0, T_n]$. This means that for $k_{TH} \geq 4$:

$$P_{EFA} \leq \sum_{n=N_{TH}}^N P_0(n) \binom{N}{n} \bar{p}_N(\tau_{MAX})^n (1 - \bar{p}_N(\tau_{MAX}))^{N-n} \quad (5.16)$$

where $P_0(n) = \Pr\{\text{given } n \text{ uniformly distributed r.v.'s in } [0, \tau_{MAX}], \text{ there exists at least one time window } T_W \text{ which contains at least } N_{TH} \text{ of them}\}$. A closed form expression for $P_0(n)$ is difficult to derive. For this reason, its value has been determined by simulation.

²In fact, it can be noted that a): the signal envelope is always larger than or equal to the absolute value of the signal itself, and b): if the envelope crosses a single-sided threshold in one point, also the signal crosses a double-sided threshold within a time interval equal to the inverse of the carrier f_0 , around that point. According to these points, and observing that the values of interest of T_n are $T_n \gg 1/f_0$, in a window T_n the double-sided first threshold crossing probability for the noise at the matched filter output is equal to the single-sided first threshold crossing probability of the noise envelope at the matched filter output. This justifies the use of the results in [13] for the considered problem.

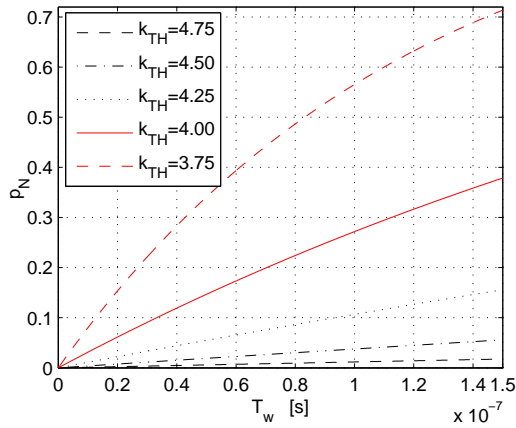


Figure 5.5: $p_N(T_w)$ vs. T_w for different k_{TH} .

In (5.16) there are 4 parameters which can be varied. T_W should be chosen the smallest possible, since P_{EFA} increases with it. The threshold k_{TH} is a parameter which affects both P_{EFA} and P_{MD} . Since only bounds for P_{EFA} and P_{MD} are given, it is not possible to find the k_{TH} which minimizes the overall probability of early false alarm and missed detection. However, in a relatively wide region of variation of k_{TH} (between about 3.5 and 5.5), the overall probability does not significantly change (using the corresponding set of system parameters); for this reason, $k_{TH} = 4.5$ is chosen. The other free parameters in (5.16) are N and N_{TH} . Varying both of them and calculating P_{EFA} for each pair (N, N_{TH}) , it is possible to determine a region in the plane (N, N_{TH}) which allows to satisfy a given P_{EFA} . Fig. 5.6 shows the region of the plane (N, N_{TH}) which satisfies the requirement $P_{EFA} \leq P_{EFA}^{req}$ for $P_{EFA}^{req} = 0.002, 0.01$ and 0.05 , as examples. Any of the points (N, N_{TH}) below the curve allows to have a P_{EFA} smaller than the target P_{EFA}^{req} (clearly, the farther the points are from the curve the lower the actual P_{EFA} is). As expected, the region of the plane becomes smaller for decreasing P_{EFA} ; however, significant variations in the target P_{EFA}^{req} can be obtained with limited variation in the parameters (N, N_{TH}) , since the plotted curves are very close each other. In this way, significant flexibility in the system reliability can be achieved.

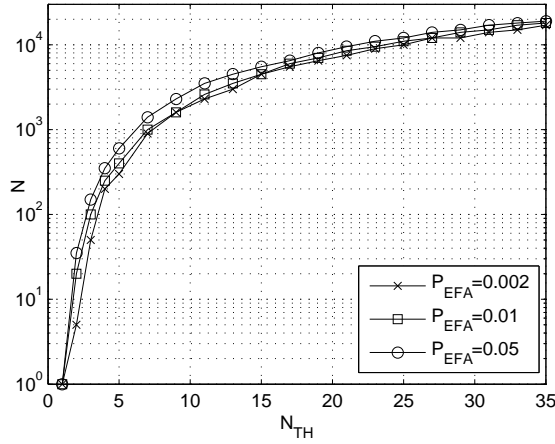


Figure 5.6: Region of the plane (N, N_{TH}) which satisfies the required $P_{EFA} \leq P_{EFA}^{req}$ (below the curves), for $P_{EFA}^{req} = 0.002, 0.01, 0.05$.

5.2.4 Performance evaluation - missed detection

From the definition of P_{MD} , the following upper bound is straightforward: $P_{MD} \leq \Pr \{ \text{in } N \text{ transmissions there are less than } N_{TH} \text{ TOA estimates in a particular time window } W_0 \text{ of duration } T_W \text{ which contains the true TOA of the direct path} \}$, since this last event includes that which specifies P_{MD} . This last upper bound for P_{MD} can be calculated as:

$$P_{MD} \leq \sum_{n=0}^{N_{TH}-1} \binom{N}{n} p_D^n (1-p_D)^{N-n} \quad (5.17)$$

with $p_D \triangleq \Pr \{ \text{in a given transmission, the signal in the chosen window } W_0 \text{ which contains the direct path crosses the threshold} \}$. If we are able to find a window W_0 which allows to easily calculate p_D , we have a bound also for P_{MD} .

In the previous chapter, the range error obtained from TOA estimation of the first peak of the channel has been modeled. It has been shown that the error depends on the distance itself; however, from the model we can state that, in noiseless conditions, the two events: $EV_1 = \{ \text{the smallest window } W_0 \text{ which contains the true TOA of the direct path crosses the threshold} \}$ and $EV_2 = \{ \text{the first peak of the channel crosses the threshold} \}$ are the same if and only if the same window W_0 starts in approximately $TOA_{true} - 1/B$ (the negative errors are limited to about $1/B$, since the pulse duration is approximately $2/B$) and has

width $T_W \approx 2/B + m_{\epsilon_{TOA}}$, where TOA_{true} is the true TOA of the direct path and $m_{\epsilon_{TOA}}$ is the bias in TOA estimation, as shown in Section 4.2³. From the proposed model, for $B = 3$ GHz, we find $T_W \approx 1$ ns for LOS, and $T_W \approx 1.5$ ns for NLOS. For this reason, we choose $T_W = 1.5$ ns. If this condition is satisfied, the two events EV_1 and EV_2 are the same, and we can state:

$$p_D = \Pr\{\text{the first peak of the channel crosses the threshold}\}.$$

These relations hold in noiseless conditions (in fact the proposed TOA based range error model has been derived with quasi noiseless measurements). However, it is easy now to derive a bound for p_D in noisy conditions: $p_D = \Pr\{\text{the signal in the chosen window } W_0 \text{ which contains the true TOA of the direct path crosses the threshold in noisy conditions}\} \geq \Pr\{\text{the first peak of the channel in noiseless conditions plus the noise crosses the threshold}\} = \Pr\{|a_{pk} + n_{MF}(\tau_{pk})| \geq k_{TH}\sigma_{n_{MF}}\}$, where a_{pk} is the first peak amplitude at the matched filter output in noiseless conditions, and τ_{pk} is the first peak time of arrival.

Defining $FPNR \triangleq E_w/(N_0 L_{FP})$ the first peak power to noise ratio as expected from the link budget and L_{FP} the first peak power path-loss⁴ as calculated in Section 5.4, results in:

$$\begin{aligned} p_D &\geq \Pr\{|a_{pk}/\sigma_{n_{MF}} + G_0| \geq k_{TH}\} = & (5.18) \\ &\Pr\{|\sqrt{FPNR \cdot S_{FP}} + G_0| \geq k_{TH}\} \geq \\ &\Pr\{\sqrt{FPNR \cdot S_{FP}} + G_0 \geq k_{TH}\} = \\ &1 - \Phi\left(k_{TH} - \sqrt{S_{FP} \cdot FPNR}\right) \end{aligned}$$

where G_0 is a standard Gaussian distributed random variable. Using (5.18), (5.17) becomes:

$$\begin{aligned} P_{MD} &\leq \sum_{n=0}^{N_{TH}-1} \binom{N}{n} \int_{s=-\infty}^{\infty} f_{S_{FP}}(s) (1 - \Phi(k_{TH} - \sqrt{s \cdot FPNR}))^n & (5.19) \\ &\Phi(k_{TH} - \sqrt{s \cdot FPNR})^{N-n} ds \end{aligned}$$

where $f_{S_{FP}}(s)$ is the *pdf* of S_{FP} .

³Note that in NLOS $m_{\epsilon_{TOA}}$ differs from $m(B_{if}, d)$, as defined in the previous chapter, due to the longer positive tail of S_{TOA} in this case (see eq. (5.9)).

⁴Note that L_{FP} usually differs from the total signal power path loss, as discussed in more detail in Chapter 3; this difference is neglected in the IEEE UWB channel models [16]-[17].

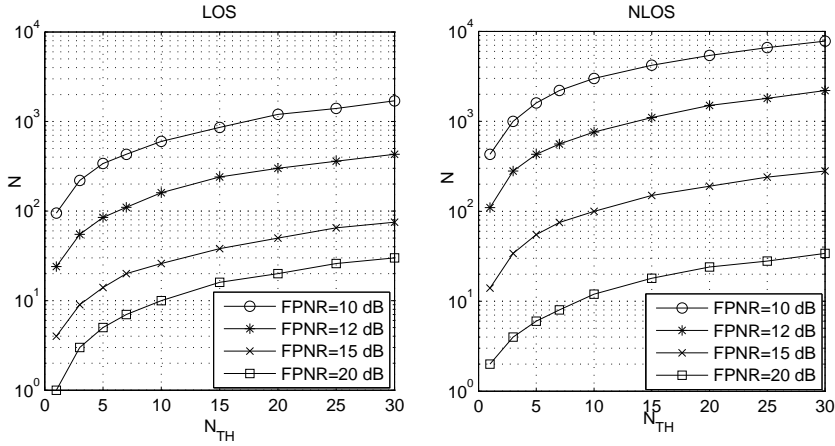


Figure 5.7: Regions (above the lines) of the plane (N, N_{TH}) which satisfy $P_{MD} \leq 0.01$ obtained by evaluating (5.19) with the model in Chapter 3 both for LOS (left), and for NLOS (right), and for different values of FPNR.

Fig. 5.7 shows an example of the regions (above the lines) of the plane (N, N_{TH}) which satisfy $P_{MD} \leq 0.01$ obtained by evaluating (5.19) with the model in Chapter 3 both for LOS (left), and for NLOS (right), and for different values of FPNR. It can be seen that, for the same FPNR and N_{TH} , due to the larger first path power fading, NLOS propagation requires a higher N for meeting a required P_{MD} ; this effect is particularly evident for small values of FPNR and becomes negligible for larger ones.

Global performance

Combining the requirements for P_{EFA} and P_{MD} , it is possible to determine the region (N, N_{TH}) which allows to satisfy both constraints. For example, from Figs. 5.6 and 5.7, it can be seen that for having $P_{EFA} \leq 0.01$ and $P_{MD} \leq 0.01$, choosing $N = 3$ and $N_{TH} = 2$, the minimum FPNR required by the proposed approach is 20 dB both for LOS and for NLOS. Having 10 dB of FPNR available requires at least $N = 500$ and $N_{TH} = 7$ for LOS, while $N = 4000$ and $N_{TH} = 15$ for NLOS (a smaller FPNR is possible, however this needs a consistent increase of N).

Achieved ranging accuracy

To realistically evaluate the achieved accuracy, the mean absolute range error which can be obtained with the proposed solution has been investigated using the collected measurements. For the simulation, one of the measured signals is randomly chosen from the total set of available measurements (which can be considered noise-free); the selected signal is filtered in the proper 3 GHz bandwidth and it is zero padded; the total frame duration is chosen $T_f = 800$ ns and $\tau = 160$ ns for coherence with the values given in the coarse acquisition part in Section 6.3; a signal format like in (5.1) is built. Noise is artificially added to have the proper value of FPNR, and the previously described TOA estimation strategy is implemented. The estimated distance with the proposed method is compared with the true one between transmitter and receiver, as measured. Results are averaged over 100 different measurements randomly chosen from the total set. Choosing a proper pair (N, N_{TH}) which allows to make negligible P_{EFA} and P_{MD} for FPNR = 10, 12, 15 and 20 dB, respectively (the corresponding values are reported in the legend of Fig. 5.8), it is possible to investigate the achievable accuracy of the proposed solution, when the direct path is correctly detected. Results are shown in Fig. 5.8; from the figure, centimeter level accuracy can be obtained with the proposed approach, when the FPNR satisfies the requirements from Figs. 5.6 and 5.7. This accuracy is similar to that achieved having perfect knowledge of the signal envelope. Similar accuracy has been found with simulations using the IEEE models (4 cm for CM3 and 7 cm for CM4). The range error in this last case is defined as the difference between the TOA of the first path of the (infinite bandwidth) channel impulse response and the TOA estimated from the received signal with the proposed solution. It is worthwhile to mention that in this way the additional delay introduced by e.g. propagation through dielectric materials, usually experienced in NLOS propagation, is not taken into account. This explains the smaller error in NLOS, when compared to results obtained with real measurements, in which the reference distance is the true one between transmitter and receiver, as measured.

5.2.5 Oscillator inaccuracies

In this subsection, impairments on the proposed solution due to deviations of the frequency output of the reference oscillators with respect to their nominal values, are evaluated. This is a very critical point for UWB systems, due to the extremely

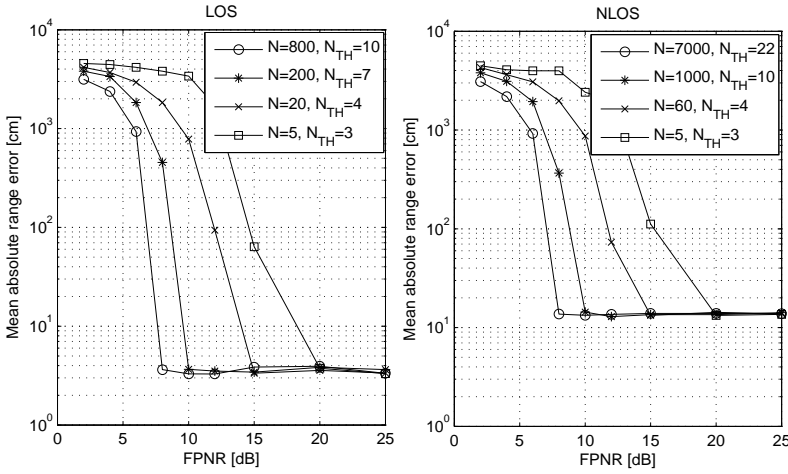


Figure 5.8: Mean absolute range error in cm vs. FPNR, both for LOS (left) and for NLOS (right) for different pairs of (N, N_{TH}) .

short time duration pulses used. The *relative* (unknown) deviation between the oscillator frequency of the transmitter, f_{os}^{TX} , and of the receiver, f_{os}^{RX} , is defined as:

$$\delta_{os} \triangleq \frac{f_{os}^{RX} - f_{os}^{TX}}{f_{os}^{REF}} = \frac{f_{os}^{RX} - f_{os}^{REF} - f_{os}^{TX} + f_{os}^{REF}}{f_{os}^{REF}} = \delta_{os}^{RX} - \delta_{os}^{TX} \quad (5.20)$$

where

$$\delta_{os}^{RX} \triangleq \frac{f_{os}^{RX} - f_{os}^{REF}}{f_{os}^{REF}} \quad (5.21)$$

is defined as the relative deviation of the receiver oscillator frequency with respect to the nominal value f_{os}^{REF} , and

$$\delta_{os}^{TX} \triangleq \frac{f_{os}^{TX} - f_{os}^{REF}}{f_{os}^{REF}} \quad (5.22)$$

is defined as the relative deviation of the transmitter oscillator frequency with respect to f_{os}^{REF} . δ_{os}^{TX} and δ_{os}^{RX} are assumed constant in the time interval in which the analysis is performed. Therefore, the underlying assumption made is that the transmitter and receiver oscillator frequencies only differ for a constant bias term⁵. Under this assumption, the generic k -th TOA estimate is affected by

⁵This assumption is introduced to simplify the theoretical analysis; however, it should be noted that the approach based on the statistical average described in Section 5.2.2 is inherently

an additional error due to oscillator inaccuracies equal to $((k-1)T_f + \tau_{TOA})\delta_{os}$, where τ_{TOA} is the estimated TOA. Thus, indicating with N_{TOA} the number of TOAs in the detected time window T_w containing the direct path, the different TOA estimates are affected each by an additional error equal to one different element of an equally random subset of N_{TOA} values in the series (the oscillator deviations in T_w are approximated to 0):

$$\{0, T_f\delta_{os}, 2T_f\delta_{os}, 3T_f\delta_{os}, \dots, (N-1)T_f\delta_{os}\} + \tau_0\delta_{os} \quad (5.23)$$

It is clear that the maximum error due to oscillator deviations is $NT_f\delta_{os}$ and for symmetry its average is $0.5NT_f\delta_{os}$. For example, assuming δ_{os} in absolute value smaller than 0.5 parts per million (ppm) (this is a value relatively easy to achieve with temperature compensated crystal oscillators available today in the market) and choosing $T_f = 800$ ns, the average introduced error $\mu_{\epsilon_{os}}$ is of about 3 cm for $N = 500$ and becomes negligible for $N \leq 100$. Therefore, for having e.g. $\mu_{\epsilon_{TOA}} \leq 3$ cm, FPNR ≈ 10 dB in LOS, and FPNR ≈ 12 dB in NLOS is required.

Oscillator inaccuracies statistical characterization

It is worth to note that a statistical characterization of the additional range error ϵ_{os} introduced by oscillator inaccuracies is not possible to derive exactly in the general case; for this reason, only the mean and the maximum value have been provided. However, we can observe that for the most interesting situation in which $N \gg N_{TOA}$ (this condition corresponds to the most critical situation of medium-low FPNR in which the considered error is not negligible), ϵ_{os} can be approximated as:

$$\epsilon_{os} \approx \frac{1}{N_{TOA}} \sum_{i=1}^{N_{TOA}} U_i NT_f \delta_{os} \quad (5.24)$$

where U_i are independent and uniformly distributed random variables in $[0,1]^3$. From the central limit theorem for the sum of independent and uniformly distributed random variables, the error can be approximated with a Gaussian distribution already for $N_{TOA} \geq 3$; the mean and standard deviation in this case are

robust to zero mean variations of the oscillator frequencies around their nominal value, since they are averaged out in the final TOA estimation, especially for large N .

³It is easy to see that this approximation is licit if: 1) the effect of oscillator frequency variation in a time window T_f can be neglected; 2) each of the N_{TOA} uniform random variables in $[0,1]$ can be located in a different of the N adjacent bins (with width $1/N$) in which the interval $[0,1]$ can be divided. The first condition is satisfied if $N \gg 1$, while the second if $N \gg N_{TOA} \geq 1$.

$\mu_{\epsilon_{os}} = 0.5NT_f\delta_{os}$ and $\sigma_{\epsilon_{os}} = 0.5/\sqrt{3N_{TOA}} NT_f |\delta_{os}|$, respectively. For convenience, in the remaining part of the paragraph, this approximation is used for the proposed derivations.

It is evident that the proposed solution allows to significantly relax the requirements on the oscillator accuracy, since a coherent average before the TOA estimation is not employed. On the contrary, performing an average on the received signal samples in order to increase the effective FPNR prior to TOA estimation, following traditional signal processing techniques, would have required a significantly higher accuracy of the oscillators, since, due to the short duration of the UWB pulses used, corresponding signal samples should differ of a very small fraction of a ns (at least smaller than 1/10 of the inverse of the central frequency) to be effectively summed coherently. Moreover, while for the proposed approach a further increase in the oscillators deviation only determines a corresponding increase in the additional range error (which is linearly proportional to δ_{os}), for traditional signal processing techniques an excessive increase in the absolute value of δ_{os} causes a complete degradation of the system performance, since different signal samples are not summed coherently anymore. Thus, the proposed solution makes the system particularly robust with respect to variations in the transmitter and receiver frequency oscillators compared to their nominal values.

Effect of oscillator inaccuracies on positioning

A last point is relevant to address in this section. In the previous part, the analysis has been restricted to the additional range error introduced by variations in the oscillators' frequencies during the transmission between a single transmitter and receiver. This is, however, only a basic step in order to calculate the position of the node to be located. In a positioning system, the actual error introduced in the range estimation by oscillator inaccuracies depends on the positioning system principle of operation itself. In the following, for illustrative purposes, we consider three different conceptual cases in which the positioning system relies on 1) tracking, 2) two way ranging [15], or 3) (self) navigation, respectively.

1) If the considered system uses a tracking approach in which the reference stations are synchronized and act as receivers, while the position of the transmitter needs to be determined (this is for example the case for most of the commercially available systems in the market), in each range measurement, ϵ_{os} is a different realization of a Gaussian random variable with mean and standard deviation equal respectively to $\mu_{\epsilon_{os}}$ and $\sigma_{\epsilon_{os}}$ (as for the case of transmission between a

single transmitter and receiver), since the total transmission lasts NT_f and all receivers share a common clock.

2) If the system makes use of a two way ranging approach, each range measurement between a pair of transceivers is calculated in a completely independent way with respect to the others. A complete transmission, in order to collect a range estimate between a single pair of transmitter and receiver, lasts in this case $2NT_f + T_{pt}$ [15], where T_{pt} is the processing time required in the receiver before replicating the transmission back to the transmitter. Thus, ϵ_{os} is in this case a Gaussian random variable with mean equal to $(NT_f + T_{pt} + 0.5NT_f)\delta_{os}^{TX} - T_{pt}\delta_{os}^{RX} = 3/2NT_f\delta_{os}^{TX} - T_{pt}\delta_{os}$ and standard deviation $\sigma_{\epsilon_{os}}$.

3) In the third scenario, the system uses a navigation approach in which the reference stations share a common clock and act as transmitters, while the position of the receiver needs to be determined (this is a basic approach conceptually equivalent to GPS). For simplicity, we can assume that N_{rs} reference stations transmit with a time division multiple access scheme, transmitting sequentially at contiguous intervals of time. In this case, the total transmission time to collect all ranges for a position fix is $N_{rs}NT_f$; ϵ_{os} for the i -th reference station (i between 1 and N_{rs}) is in this case a different realization of a Gaussian random variable with mean value $(1 + 2(i - 1))\mu_{\epsilon_{os}}$ and standard deviation $\sigma_{\epsilon_{os}}$.

The first and the third approach allow to compensate for the mean value of the considered errors. In fact, in both cases the mean error of ϵ_{os} in each range estimate can be treated in the positioning model - next to the ordinary clock offset - as an additional parameter (the reference stations share a common clock) depending on the unknown δ_{os} , which can be estimated by collecting an additional range measurement. This allows, after solving for the unknown δ_{os} , to consider ϵ_{os} in each range measurement as a different realization of a zero mean Gaussian random variable with standard deviation $\sigma_{\epsilon_{os}}$.

5.3 Coarse acquisition

In this section, a preliminary coarse acquisition strategy, required for proper operation of the receiver implementation as presented in Fig. 5.1, is described. With respect to the notation introduced in the beginning of Section 5.2, the purpose of this step is to provide an estimate T_0 of the frame starting time, such that $\tau_0 = T_0 + \tau$ and $0 \leq \tau \leq T_f - \tau_{cds}$. An energy based coarse acquisition is proposed and its performance evaluated and related to the relevant system and channel

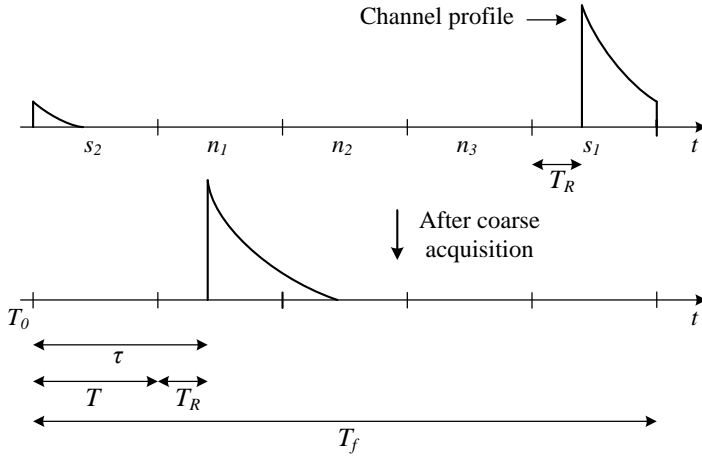


Figure 5.9: *Coarse acquisition step.*

parameters.

Fixing an arbitrary observation start-time and choosing a positive integer K which represents the number of time bins with duration $T = T_f/K$ in T_f , the following statistics are calculated:

$$E_k = \sum_{j=0}^{N_{CA}-1} \int_{kT+jT_f}^{(k+1)T+jT_f} r(t)^2 dt \quad (5.25)$$

for $k = 0..K - 1$. N_{CA} is the number of frames used in this step. The coarse estimation of the frame starting time is calculated as:

$$T_0 = T(\arg \max_k \{E_k\} - 1) \quad (5.26)$$

The rationale behind this strategy is the following. Assuming $T \approx \tau_{cds}$ (the appropriateness of this choice will be discussed in the following), in the most general situation, in a frame T_f there are two bins, called s_1 and s_2 , which contain the first and the last part of the useful signal, respectively, and $K - 2$ bins, $n_1..n_{K-2}$, containing only noise (see also Fig. 5.9). Since the strategy in (5.25), (5.26) performs a maximum energy detection (summed over N_{CA} frames), it is likely that the maximum energy bin is the one corresponding to s_1 or s_2 . The start-time of the signal with respect to T_0 (assumed for notational convenience equal to zero from this moment on) is then $\tau = T + T_R$ or $\tau = T_R$ if the maximum energy bin is s_1 or s_2 , respectively; T_R represents the delay of the first path from

T_0 modulo T , and it is a uniformly distributed r.v. in $[0, T]$. By imposing $K \geq 3$, we succeed (at least in noiseless conditions) in the coarse acquisition step, since the frame starts with a noise only part shorter than $2T$, and the useful signal part goes to zero before the end of the frame (since $T \approx \tau_{cds}$). As an example, Fig. 5.9 shows the described coarse acquisition step, for $K = 5$.

5.3.1 Coarse acquisition performance evaluation

The performance of the proposed scheme is evaluated in terms of probability of coarse acquisition P_{CA} , defined as the probability of having the energy in bins s_1 or s_2 greater than that in all the other bins. Defining $P_{s_1} \triangleq \Pr \{s_1 \text{ has the highest energy}\}$ and $P_{s_2} \triangleq \Pr \{s_2 \text{ has the highest energy}\}$, conditioned on a particular realization of T_R results in:

$$P_{CA} \triangleq P_{s_1} + P_{s_2} - P_{s_1 \cap s_2} \quad (5.27)$$

Since the two events: $\{s_1 \text{ has the highest energy}\}$ and $\{s_2 \text{ has the highest energy}\}$ are mutually exclusive⁶, the probability of the intersection of the two events $P_{s_1 \cap s_2} = \Pr \{\text{both } s_1 \text{ and } s_2 \text{ have the highest energy}\}$ is zero and 5.27 simply becomes:

$$P_{CA} \triangleq P_{s_1} + P_{s_2} \quad (5.28)$$

To theoretically evaluate (5.28), a statistical characterization of E_k in (5.25) is required. To this purpose, IEEE channel models [16] are difficult to analyze. For this reason, a simplified channel model composed of a single exponential decay and a dense path arrival rate is considered in this section. It will be shown that this assumption introduces negligible differences compared to results obtained using the IEEE models. A more convenient representation of the CIR becomes: $h(t) = \sum_{l=0}^{L-1} h_{R,l} \delta(t - \tau_{R,l})$. L is the number of *resolvable* multipath components; $\tau_{R,l} = \tau_{R,0} + lT_B$ is the delay of the l -th resolvable multipath component, with $T_B = 1/B$, $h_{R,l} = |h_{R,l}| \exp(j\phi_l)$ is the amplitude of the l -th resolvable multipath component, and $\phi_l \in \{0, \pi\}$ with equal probability. $|h_{R,l}|$ is usually modeled as a r.v. (e.g. Nakagami distributed [16]); however, to simplify the analytical

⁶In fact the punctual probability that the energy of bin s_1 (E_{s_1}) and of bin s_2 (E_{s_2}) is equal is zero, since E_{s_1} and E_{s_2} are two continuous and independent random variables (the bins s_1 and s_2 are disjoint (see also Fig. 5.9) and $T \gg 1/B$, meaning that the realization of the noise in each of the two bins can be considered independent). This means that *only one* of the two bins can have largest energy; this implies that the two events are mutually exclusive, and the requested probability can be calculated as the sum of P_{s_1} and P_{s_2} , separately considered.

derivation, $|h_{R,l}|$ is assumed deterministic with $h_{R,l}^2 = h_{R,0}^2 \exp(-lT_B/\alpha_{ch})$, where α_{ch} is the channel power decay constant and $h_{R,0}^2 = 1/PL_{TP} \cdot (1 - \exp(-T_B/\alpha_{ch}))$ for normalization; PL_{TP} is the total signal power path loss. In the link budget calculation, the *total* signal power fading S_{TP} can be included in this term. In this way, after normalizing to the total signal power, the small scale fading in $|h_{R,l}|$ results only in a relative variation in the energy of s_1 and s_2 with respect to each other; however, due to the large number of multipath components integrated, this variation can be neglected for the purpose of the analysis. Under this hypothesis, the energy in s_1 and s_2 is respectively:

$$E_{s_1} = \sum_{j=0}^{N_{CA}-1} \int_{t=T_{s_1}+jT_f}^{T_{s_1}+T+jT_f} (w(t) \otimes \sum_{l=0}^{L-1} h_{R,l} \delta(t - jT_f - T_{s_1} - T_R) + n(t))^2 dt \quad (5.29)$$

and:

$$E_{s_2} = \sum_{j=0}^{N_{CA}-1} \int_{t=T_{s_2}+jT_f}^{T_{s_2}+T+jT_f} (w(t) \otimes \sum_{l=0}^{L-1} h_{R,l} \delta(t - jT_f - T_{s_2} - T_R) + n(t))^2 dt \quad (5.30)$$

where T_{s_1} and T_{s_2} are the starting times of s_1 and s_2 , and \otimes represents the convolution operation. The energy in the remaining $K - 2$ noise only bins is:

$$E_{n_i} = \sum_{j=0}^{N_{CA}-1} \int_{T_{n_i}+jT_f}^{T_{n_i}+T+jT_f} n(t)^2 dt \quad (5.31)$$

for $i = 1..K - 2$, where T_{n_i} is the starting time of bin n_i .

E_{s_1} and E_{s_2} are non-central chi-square distributed r.v.'s with non-centrality parameter, respectively (an ideal rectangular receiver filter over the signal band is assumed):

$$\mu_{NC}(E_{s_1}) = \frac{N_{CA}}{N_0} \int_0^T \left(\sum_{l=0}^{L-1} h_{R,l} w(t - lT_B - T_R) \right)^2 dt = \quad (5.32)$$

$$\frac{N_{CA}E_r}{N_0} \left(1 - \exp\left(-\frac{T - T_R}{\alpha_{ch}}\right) \right)$$

$$\mu_{NC}(E_{s_2}) = \frac{N_{CA}}{N_0} \int_0^T \left(\sum_{l=0}^{L-1} h_{R,l} w(t - lT_B + T - T_R) \right)^2 dt = \quad (5.33)$$

$$\frac{N_{CA}E_r}{N_0} \left(\exp\left(-\frac{T - T_R}{\alpha_{ch}}\right) - \exp\left(-\frac{2T - T_R}{\alpha_{ch}}\right) \right)$$

Table 5.1: Mean and Variance of E_{s_1} , E_{s_2} and E_{n_i}

μ_{s_1}	$N_{CA}(MN_0 + E_r(1 - \exp(-(T - T_R)/\alpha_{ch})))$
$\sigma_{s_1}^2$	$N_{CA}(2MN_0^2 + 4N_0E_r(1 - \exp(-(T - T_R)/\alpha_{ch})))$
μ_{s_2}	$N_{CA}(MN_0 + E_r(\exp(-(T - T_R)/\alpha_{ch}) - \exp(-(2T - T_R)/\alpha_{ch})))$
$\sigma_{s_2}^2$	$N_{CA}(2MN_0^2 + 4N_0E_r(\exp(-(T - T_R)/\alpha_{ch}) - \exp(-(2T - T_R)/\alpha_{ch})))$
μ_{n_0}	$N_{CA}MN_0$
$\sigma_{n_0}^2$	$2N_{CA}MN_0^2$

where $E_r = E_w/PL_{TP}$ is the received energy in a single pulse transmission. E_{n_i} are central chi-square distributed r.v.'s. The mean and variance of a standard non-central chi-square r.v. (given by the sum of the squares of unit variance Gaussian r.v.'s) are given by $M + \mu_{NC}$ and $2M + 4\mu_{NC}$ respectively, where $M = 2BT + 1$ are the degrees of freedom of the signal in each bin. In this way, using (5.32) and (5.33), it is possible to immediately calculate μ_{s_1} , σ_{s_1} , μ_{s_2} , σ_{s_2} , μ_{n_0} , σ_{n_0} , which are the mean and standard deviation of E_{s_1} , E_{s_2} and E_{n_i} , respectively (for central chi-square r.v.'s, the same expressions are valid, considering $\mu_{NC} = 0$). These parameters are reported in Table 5.1. Since, as will be shown in the following, the M of interest are $M \geq 100$, E_{s_1} , E_{s_2} and E_{n_i} can be approximated with Gaussian distributions [19] (the approximation improves for larger N_{CA}). With the introduced notation, the expressions for P_{s_1} and P_{s_2} become:

$$P_{s_1} = \Pr \{E_{s_1} \geq \max \{E_{s_2}, E_{n_1}, \dots, E_{n_{K-2}}\}\} \quad (5.34)$$

$$P_{s_2} = \Pr \{E_{s_2} \geq \max \{E_{s_1}, E_{n_1}, \dots, E_{n_{K-2}}\}\} \quad (5.35)$$

Analytical evaluation of the statistics of the maximum energy bin

Reference [19] provides an iterative solution to determine the mean and standard deviation of the maximum of a set of Gaussian r.v.'s. However, the results are exact only for the case of two r.v.'s. For this reason, we propose here to solve the problem in two steps; (5.34)-(5.35) are respectively equivalent to:

$$P_{s_1} = \Pr \{E_{s_1} \geq \max \{E_{s_2}, E_{n_{MAX}}\}\} \quad (5.36)$$

$$P_{s_2} = \Pr \{E_{s_2} \geq \max \{E_{s_1}, E_{n_{MAX}}\}\} \quad (5.37)$$

with

$$E_{n_{MAX}} = \max \{E_{n_1}, \dots, E_{n_{K-2}}\} \quad (5.38)$$

Table 5.2: $\mu_{n_{MAX}}^{(0)}$ and $\sigma_{n_{MAX}}^{(0)}$ for different values of $K - 2$

$K - 2$	2	3	5	8	10	15	20
$\mu_{n_{MAX}}^{(0)}$	0.5642	0.8463	1.1630	1.4236	1.5387	1.7359	1.8675
$\sigma_{n_{MAX}}^{(0)}$	0.8256	0.7480	0.6690	0.6106	0.5868	0.5486	0.5251

Since $E_{n_1}, \dots, E_{n_{K-2}}$ are independent (the bins are disjoint and $T \gg 1/B$) and identically distributed (i.i.d.) Gaussian r.v.'s (according to the introduced approximation), the *pdf* of $E_{n_{MAX}}$ is [20]:

$$f_{n_{MAX}}(x) = (K - 2)(\Phi((x - \mu_{n_0})/\sigma_{n_0}))^{K-3} \phi((x - \mu_{n_0})/\sigma_{n_0})/\sigma_{n_0} \quad (5.39)$$

with $\phi(x) = 1/\sqrt{2\pi} \exp(-x^2/2)$ and $\Phi(x) = \int_{-\infty}^x \phi(\xi) d\xi$. The mean of $E_{n_{MAX}}$ is:

$$\mu_{n_{MAX}} = \int_{-\infty}^{\infty} x(K - 2)(\Phi((x - \mu_{n_0})/\sigma_{n_0}))^{K-3} \phi((x - \mu_{n_0})/\sigma_{n_0})/\sigma_{n_0} dx \quad (5.40)$$

With the change of variable $y = (x - \mu_{n_0})/\sigma_{n_0}$, results:

$$\mu_{n_{MAX}} = \mu_{n_0} + \mu_{n_{MAX}}^{(0)} \sigma_{n_0} \quad (5.41)$$

where $\mu_{n_{MAX}}^{(0)}$ is the mean of the maximum of $K - 2$ i.i.d. standard Gaussian r.v.'s. In a similar way, the standard deviation of $E_{n_{MAX}}$ is:

$$\sigma_{n_{MAX}} = \sigma_{n_{MAX}}^{(0)} \sigma_{n_0} \quad (5.42)$$

where $\sigma_{n_{MAX}}^{(0)}$ is the standard deviation of the maximum of $K - 2$ i.i.d. standard Gaussian r.v.'s. Thus, for calculating an exact expression for the mean and variance of $E_{n_{MAX}}$, only a parametrization of $\mu_{n_{MAX}}^{(0)}$ and $\sigma_{n_{MAX}}^{(0)}$ as a function of $K - 2$ is needed. Table 5.2 shows $\mu_{n_{MAX}}^{(0)}$ and $\sigma_{n_{MAX}}^{(0)}$ for different values of $K - 2$, determined by simulation. From simulations, $E_{n_{MAX}}$ can be approximated as a Gaussian r.v.⁷. The last step to evaluate (5.36)-(5.37) is to determine the pdf of $E_{MAX1} = \max\{E_{s_1}, E_{n_{MAX}}\}$ and of $E_{MAX2} = \max\{E_{s_2}, E_{n_{MAX}}\}$. From [19], E_{MAX1} and E_{MAX2} are approximated with Gaussian r.v.'s; considering for example E_{MAX2} , the exact expressions for its mean μ_{MAX2} and variance σ_{MAX2}^2 are, respectively:

$$\mu_{MAX2} = \mu_{s_2} \Phi(\beta_2) + \mu_{n_{MAX}} \Phi(-\beta_2) + \gamma_2 \phi(\beta_2) \quad (5.43)$$

⁷Note that for $K - 2 \rightarrow \infty$ it becomes an extreme value distribution, however, for $K - 2 \approx 10$ or smaller, which is the case of interest here, a Gaussian approximation provides accurate results.

$$\begin{aligned} \sigma_{MAX2}^2 = & (\mu_{s_2}^2 + \sigma_{s_2}^2)\Phi(\beta_2) + (\mu_{n_{MAX}}^2 + \sigma_{n_{MAX}}^2)\Phi(-\beta_2) + \\ & (\mu_{s_2} + \mu_{n_{MAX}})\gamma_2\phi(\beta_2) - \mu_{MAX2}^2 \end{aligned} \quad (5.44)$$

where $\gamma_2 = \sqrt{\sigma_{s_2}^2 + \sigma_{n_{MAX}}^2}$ and $\beta_2 = (\mu_{s_2} - \mu_{n_{MAX}})/\gamma_2$. Observing that, given a particular T_R , E_{s_1} and E_{MAX2} are independent (the bins are disjoint and $T \gg 1/B$), simply results:

$$P_{s_1} = 1 - \Phi((\mu_{s_1} - \mu_{MAX2})/\sqrt{\sigma_{s_1}^2 + \sigma_{MAX2}^2}) \quad (5.45)$$

In a similar way, the expression for P_{s_2} (which is specular) can be derived. These results are conditioned to a particular realization of T_R .

Coarse acquisition results

The final P_{CA} can be calculated by averaging over T_R :

$$P_{CA} = 1/T \int_{t=0}^T (P_{s_1} + P_{s_2}) dt \quad (5.46)$$

To obtain the presented results, $T \approx \tau_{cds}$ has been assumed. However, τ_{cds} is an environment and location dependent channel parameter, and in a real system it is not a-priori known. On the other hand, its exact knowledge is not required. In fact, every $T \geq \tau_{cds}$ satisfies the proposed approach. A choice of $T \leq \tau_{cds}$, while attractive since it allows to reduce the noise variance in each bin, needs more attention, since it could lead to a wrong coarse acquisition, due to the typically clustered nature of indoor UWB multipaths and to the fact that, if T is not large enough, the maximum energy bin could differ from s_1 or s_2 , even in noiseless conditions. Through simulations, we found that a choice of $T \geq 4\mu_{T_{med}}$ is enough for our purpose, where $\mu_{T_{med}}$ is the mean value of the channel mean excess delay T_{med} . $\mu_{T_{med}}$ is a large scale parameter which can be a-priori (approximately) known. Using the IEEE CM1 ÷ CM4 (residential and office environments), results in $\mu_{T_{med}}$ between about 9 ns (for CM3) and 20 ns (for CM2). A value of T which satisfies the previously introduced requirement is $T = 80$ ns. For the proposed simulation results, the frame period is chosen $T_f = 800$ ns (and accordingly $K = 10$); in this way, the condition which allows to avoid inter-frame interference $\tau_{cds} \leq T_f - \max\{\tau\} = T_f - 2T = 640$ ns is always satisfied for the considered channels. To calculate P_{CA} , knowledge of $\alpha_{ch} = T_{med}$ (this relation holds for an exponential decay) is required. In Fig. 5.10, results obtained both considering the real distribution of the mean excess delay (a lognormal distributed r.v. [21]),

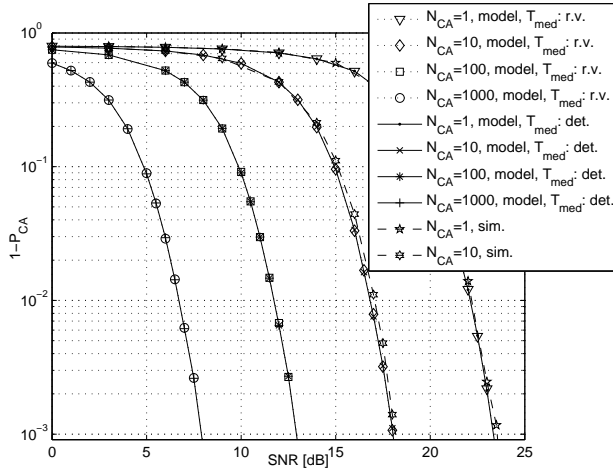


Figure 5.10: Performance of proposed coarse acquisition scheme for CM3.

and considering it deterministic and equal to its mean $\mu_{T_{med}}$ are plotted for CM3 (office LOS). The Signal to Noise Ratio (SNR) at the receiver is defined as:

$$SNR \triangleq 10 \log_{10} E_r/N_0 \quad (5.47)$$

The proposed analytical derivation is in good agreement with simulations using the IEEE models (due to the long simulation times required, results for only $N_{CA} = 1$ and $N_{CA} = 10$ are shown); the same good match can be found for the other IEEE channel models. No significant differences arise between curves obtained from the model using the complete distribution of T_{med} and only its mean. Thus, to correctly evaluate P_{CA} , the only channel parameter required is $\mu_{T_{med}}$; moreover, since its dependency is weak, only a coarse estimate of it is needed. From Fig. 5.10, it is possible to choose a proper value for N_{CA} , given the available SNR and the required P_{CA} .

5.4 Link Budget Evaluation

The main drawback of the proposed TOA estimation scheme is caused by the impossibility of increasing the FPNR by averaging before TOA estimation. This limits the maximum achievable distance. In this section, the link budget provided by the presented solution, under the realistic assumption that the transmitted signal satisfies the requirements imposed by FCC, is evaluated. In [1], the FCC

specifies UWB emission limits in terms of peak and average power (both EIRP). The peak transmitted power should be smaller than 0 dBm when measured with a spectrum analyzer in any 50 MHz bandwidth used by the signal, and the average transmitted power spectral density should be smaller than -41.3 dBm/MHz when measured in any 1 MHz bandwidth used by the signal. Both requirements affect the maximum effective power P_T^{MAX} which can be transmitted in a single pulse. If $T_f = 800$ ns, $1/T_f = 1.25$ MHz is much smaller than the 50 MHz resolution bandwidth used for the peak power measurement compliance; thus, from [22] the requirement on peak power gives:

$$P_T^{MAX} \leq 0.001 \cdot (B/(50 \cdot 10^6))^2 \approx 35.6 \text{ dBm} \quad (5.48)$$

For the average power requirement, an upper bound to P_T^{MAX} can be determined taking the asymptotic condition in which the pulse repetition frequency is much higher than the 1 MHz resolution bandwidth used for average power measurement compliance; this gives [22]:

$$P_T^{MAX} \leq 7.5 \cdot 10^{-8} (BT_f)^2 \approx 26.4 \text{ dBm} \quad (5.49)$$

The power of the noise in the receiver is

$$P_N = -174 \text{ dBm/Hz} + 10 \log_{10}(3 \cdot 10^9) \approx -79.2 \text{ dBm} \quad (5.50)$$

The link margin can then be calculated considering $P_T^{MAX} \approx 26.4$ dBm, a minimum $\text{FPNR}_{MIN} = 10$ dB and observing that the first peak path loss exponent n_{FP} is approximately 2 in LOS propagation. From the relation:

$$PL_{FP} = -10 \log_{10}((c/(4\pi f_0 d))^{n_{FP}}) \leq P_T^{MAX} - P_N - \text{FPNR}_{MIN} \quad (5.51)$$

results $d_{MAX} \approx 300$ m.

It is worth to note that while the fine TOA estimation is based on the first peak, which propagates with path loss exponent n_{FP} , the coarse acquisition step is based on the total signal, which propagates with path loss exponent n_{TP} . The model for n_{TP} proposed in Chapter 3 has been obtained by fitting the data with a reference distance $d_0 = 1$ m. This is equivalent to assuming that the total power propagates with path loss exponent 2 till d_0 (free space), and then from d_0 with path loss exponent n_{TP} . With similar motivations as those previously described, by imposing a maximum achievable distance of $d_{MAX} \approx 300$ m, the minimum N_{CA} required by the coarse acquisition step can be determined. The minimum SNR required to reach d_{MAX} is:

$$\text{SNR}_{d_{MAX}} = P_T^{MAX} - P_N - PL_{TP} \quad (5.52)$$

where

$$PL_{TP} = -10 \log_{10}((c/(4\pi f_0 d_0))^2 (d_0/d_{MAX})^{n_{TP}}) \quad (5.53)$$

Considering from the IEEE models the worse case (for LOS propagation) of $n_{TP} = 1.79$ for CM3, results $\text{SNR}_{d_{MAX}} \approx 15.6$ dB. From this value it is possible to calculate the minimum N_{CA} to achieve the target P_{CA} with the plots of Fig. 5.10. For example, if $1 - P_{CA} \leq 10^{-3}$, $N_{CA} \approx 40$ (not shown in Fig. 5.10) is enough for the purpose. It is worth to note that the curves in Fig. 5.10 have been derived without considering the fading in the total power. This can be taken into account by considering an additional fading margin of a few dB in the link budget analysis for the total power. In a similar way, the link margin for NLOS propagation can be evaluated. The main difference in this case is represented by the reduced coverage, which is strongly dependent on the environment; for example, using the channel parameters in Chapter 3, the maximum achievable distance in NLOS is reduced by a factor of about 5.

The suggested set of system parameters appears a reasonable choice for short to medium range indoor positioning applications; however, it is clear that the achieved maximum distance is not a strict limit, and significantly larger distances are possible with a different choice of the parameters of interest. In this evaluation, the receiver noise figure, which is approximately equal to the noise figure of the LNA, has been ignored. This can be accounted for by allocating a few additional dBs in the link budget for both total power and first path power.

5.5 Chapter summary

In this chapter, a low-complexity TOA estimation strategy has been proposed, and its performance evaluated. TOA estimation is performed using the receiver implementation proposed in Section 5.2.1. The receiver works for a large part in the analog domain, and requires a limited amount of processing to perform TOA estimation, still being able to fully exploit the very good multipath resolvability which comes from the extremely large bandwidth used. To allow for performance flexibility, a strategy to combine multiple TOA estimates has been suggested and evaluated. Upper bounds for the early false alarm and missed detection probabilities are derived; the expressions can be used for determining the system parameters to satisfy given reliability requirements. A range error standard deviation of a few centimeters can be reached in LOS, with sampling rates in the order of a few tens of MHz, thus allowing to solve one of the main techno-

logical challenges which make it difficult to practically realize UWB positioning systems. This accuracy has been obtained with simulations using IEEE channel models as well as with the collected UWB measurements as described in Chapter 2. For further validation, the implementation of the TOA estimation strategy on an acoustic test-bed developed during the research activity [23], has shown results consistent with theory. A preliminary coarse acquisition scheme, required by the suggested TOA estimation receiver for proper working, has then been presented. To keep the overall system complexity low, coarse acquisition is based on maximum energy bin detection. The analytical performance of the approach is derived and compared with simulations using the IEEE channel models. It is shown that the only channel parameter required to evaluate the strategy is the mean value of the channel mean excess delay.

The main drawback of the described solution is represented by the limit in the maximum achievable distance. However, it is shown that, satisfying the FCC limits imposed for UWB transmissions, it is possible to reach several hundreds of meters in LOS, making this solution ideal for low-cost, short to medium range coverage positioning systems which require centimeter level accuracy. Coverage in NLOS is reduced by a factor of about 5, depending on the particular propagation conditions.

Bibliography

- [1] Z.N. Low, J.H. Cheong, C.L. Law, W.T. Ng and F. Watanabe, "*Pulse detection algorithm for line-of-sight (LOS) UWB ranging applications*", IEEE Antennas and Wireless Propagation Letters, vol. 4, pp. 63-67, 2005.
- [2] C. Mazzucco, U. Spagnolini, G. Mulas, "*A ranging technique for UWB indoor channel based on power delay profile analysis*", IEEE VTC Spring 2004, vol 5, pp. 2595-2599, May 2004.
- [3] Joon-Yong Lee, R.A. Scholtz, "*Ranging in a dense multipath environment using an UWB radio link*", IEEE Journal on Selected Areas in Communications, vol. 20, no. 9, pp. 1677-1683, Dec. 2002.
- [4] A.A. D'Amico, U. Mengali, L. Taponecco, "*Energy-based TOA estimation*", IEEE Transaction on Wireless Communications, vol. 7, no. 3, pp. 838-847, Mar. 2008.

- [5] I. Guvenc, Z. Sahinoglu, "*Threshold-based TOA estimation for impulse radio UWB systems*", IEEE ICU 2005, pp. 420-425, Sept. 2005.
- [6] I. Guvenc, Z. Sahinoglu, P.V. Orlik, "*TOA estimation for IR-UWB systems with different transceiver types*", IEEE Transactions on Microwave Theory and Techniques, vol. 54, no. 4, pp. 1876-1886, Jun. 2006.
- [7] L. Stoica, A. Rabbachin, I. Oppermann, "*A low-complexity noncoherent IR-UWB transceiver architecture with TOA estimation*", IEEE Transactions on Microwave Theory and Techniques, vol. 54, no. 4, pp. 1637-1646, Jun. 2006.
- [8] C. Carbonelli, U. Mengali, "*Synchronization algorithms for UWB signals*", IEEE Transaction on Wireless Communications, vol. 7, no. 3, pp. 838-847, Mar. 2008.
- [9] S.R. Aedudodla, S. Vijayakumaran, T.F. Wong, "*Timing acquisition in ultra-wideband communication systems*", IEEE Transaction on Vehicular Technologies, vol. 54, no. 5, pp. 1570-1583, Sep. 2005.
- [10] A. Rabbachin, I. Oppermann, "*Synchronization analysis for UWB systems with a low-complexity energy collection receiver*", Joint UWBST & IWUWBS 2004, May 2004.
- [11] FCC, Office of Engineering and Technology, "*Revision of part 15 of the commissions rules regarding ultra-wideband transmission systems*", ET Docket, no. 98-153, 2002.
- [12] P.H. Young, "*Electronic communication techniques*", fifth edition, par. 5.6, Prentice Hall, 2004.
- [13] I.F. Blake, W.C. Lindsey, F. Watanabe, "*Level crossing problems for random processes*", IEEE Transaction on Information Theory, vol IT-19, no. 3, pp. 295-315, May 1973.
- [14] Joon-Yong Lee, Sungyul Yoo, "*Large error performance of UWB ranging in multipath and multiuser environments*", IEEE Transaction on Microwave Theory and Techniques, vol. 54, no. 4, pp. 1887-1895, Apr. 2006.
- [15] R. Roberts, "Ranging subcommittee final report", Nov 2004.
- [16] A.F. Molisch, D. Cassioli, C.C. Chong, S. Emami, A. Fort, B. Kannan, J. Karedal, J. Kunisch, H.G. Schantz, K. Siwiak and M.Z. Win, "*A comprehensive*

- standardized model for ultrawideband propagation channels*", IEEE Transaction on Antennas and Propagation, vol. 54, no. 11, pp. 3151-3166, Nov. 2006.
- [17] A.F. Molisch, "*Ultrawideband propagation channels-theory, measurements, and modeling*", IEEE Transaction on Vehicular Technologies, vol. 54, no. 5, pp. 1528-1545, Sept. 2005.
- [18] P.A. Humblet, M. Azizoglu, "*On the bit error rate of lightwave systems with optical amplifiers*", IEEE Journal of Lightwave Technology, vol. 9, no. 11, pp. 1576-1582, Nov. 1991.
- [19] C.E. Clark, "*The greatest of a finite set of random variables*", Operation Research, vol. 9, no. 2, pp. 145-162, Mar.-Apr. 1961.
- [20] A. Balakrishnan, A. Cohen, "*Order statistics and inference - estimation methods*", Academic Press, 1990.
- [21] I. Guvenc, C.C. Chong, F. Watanabe, "*NLOS identification and mitigation techniques for UWB localization systems*", IEEE WCNC 2007, pp. 1571-1576, Mar. 2007.
- [22] R.J. Fontana, E.A. Richley, "*Observations on Low Data Rate, Short Pulse UWB Systems*", IEEE ICUWB 2007, pp. 334-338, Sep. 2007.
- [23] G. Bellusci, J. Yan, G.J.M. Janssen, C.C.J.M. Tiberius, "*An Ultra-Wideband Positioning Demonstrator Using Audio Signals*", IEEE WPNC 2007, Mar. 2007.

Narrowband Interference Impairments on Low-Complexity TOA Estimation

The problem of interference is inherently related to wireless communications, due to the shared nature of the transmission medium, in which different technologies and systems need to coexist. However, this issue is particularly relevant for UWB communications, due to its unlicensed use of the radio resources. Interference caused *by* UWB to other licensed devices is addressed by the frequency regulators both prohibiting UWB emissions in particularly sensitive frequency bands (e.g. around 1.5 GHz, where GPS operates, or around 2.4 GHz (the industrial, scientific, and medical radio band)), and by strongly limiting emissions with masks inside the bandwidth in which UWB is allowed to operate, in terms of peak and average radiated power [1]. On the contrary, the effects of interference *to* UWB systems need to be carefully investigated for proper system design, parameters definition, and signal processing algorithms, since it could significantly affect overall performance.

Interference to UWB systems can be divided in two different types: from other UWB sources (multi-user interference), and from other radio systems. This differentiation reflects not only the conceptually diverse sources of the two types of interference, but also the significantly different characteristics and effects of them

on UWB system performance, as well as ways to evaluate and counteract caused impairments. The problem of multi-user interference (MUI) has received large attention in literature [2]-[10], and a variety of results has been published, ranging from the more simplistic Gaussian assumption for the multi-user interference, to more complex models which appear more accurate in realistic situations [9]-[10]. This interest is justified with the original idea of UWB as a multiple-access wireless data transmission technique; however, this issue appears less critical in the context of positioning applications, where the transmission is typically very low-data rate and duty-cycle, and a simple time division scheme combined with carrier sense multiple access protocols, can achieve good performance, getting around, or strongly mitigating this problem. Interference from other systems to UWB has started to receive attention in these last years; an overview of the problem is provided in [11], and other results are available e.g. in [12]-[16]. Considering the huge signal band used by UWB, other licensed devices have a relative bandwidth much smaller from their perspective; for this reason, this type of interference is usually referred to in the literature as *narrowband* interference (NBI), keeping in mind the particular meaning this term has in this context, which make this definition suitable also for traditional wideband signals (e.g. WiFi, or W-CDMA). The problem of NBI appears critical for ranging applications, since it is intuitively clear that it can not only affect the transmission efficiency (in terms of increased minimum SNR at receiver), but it can also lead to very large errors [8] in the detection of TOA, thus significantly affecting overall positioning performance. However, to the best of our knowledge, previous literature only focuses on communications applications [11]-[15] or bin energy based TOA estimation [16], while no results are available for NBI impairments on peak detection based TOA estimation techniques.

In this chapter, the effect of NBI on the accuracy of the TOA estimation approach proposed in Chapter 5 is addressed, and related impairments evaluated. While the analysis specifically focuses on the strategy described in the previous chapter, the approach employed is general, and can be applied to other first peak based TOA estimation algorithms. The solution proposed to evaluate the probability of early false alarm under NBI is based on the first threshold crossing probability evaluation for Gaussian processes and time varying boundaries [17]-[18]. Impairments on global TOA estimation performance and the coarse acquisition step are then evaluated.

6.1 Narrowband interference signal model

NBI is modeled as a single-tone continuous-wave signal:

$$i(t) = \alpha_I A_I \cos(2\pi f_I t + \theta_I) \quad (6.1)$$

where $A_I^2/2$ is the average NBI power, α_I is a Rayleigh distributed r.v. which accounts for the slowly-varying NBI fading, with $E[\alpha_I^2] = 1$, and θ_I is the random signal phase uniformly distributed in $[0, 2\pi]$. This is a common assumption which has been widely adopted in literature [11]-[12], since the modulation of a narrowband interferer signal can be realistically considered constant for several UWB frames; in this way, this approach can be used as a benchmark to compare NBI impairments on different techniques. However, the proposed framework can be extended to a wider range of interference sources, in particular single carrier amplitude modulated signals. In this case, it is possible to condition to a particular realization of the NBI signal in the total transmission duration NT_f , to calculate with the proposed approach the probabilities of interest, and to average over the different possible realizations. The approach is general and results in relatively compact formulas for the realistic case in which the NBI symbol duration is significantly (as found from simulations, 5 times or more) longer than T_f , but smaller than the total transmission duration NT_f . For conciseness, this issue is not addressed in this contribution.

To keep the analytical approach to the problem feasible, the phase in each frame is assumed independent from that in the other frames; this is reasonable, since $2\pi f_I T_f \approx 10^4$. On the contrary, a particular realization of α_I can be considered constant in all the frames belonging to one complete transmission, since the channel coherence time is usually significantly longer.

6.2 NBI impairments - TOA estimation

In this paragraph, the effect of NBI on the TOA estimation approach proposed in section 5.2, is evaluated.

6.2.1 Early False Alarm

The evaluation of the probability of early false alarm under NBI can be reconducted to the calculation of the probability of first crossing of a time varying

threshold for stationary Gaussian processes. A theoretical framework which provides an approximate solution to the problem is addressed in [17] (the analysis gives accurate results for first crossing probabilities in the considered time window T_n smaller than 0.1, which is the situation of interest here). Specific results for an asymptotically periodic threshold are reported in [18]. This is an interesting case for the considered problem, since a sinusoidal signal is a particular case of an asymptotically periodic threshold. The problem can be solved with an approach similar to that presented in Section 5.2.3, considering a periodic threshold ¹:

$$b(t) = i_{MF}(t) + r_{TH} \tag{6.2}$$

where:

$$i_{MF}(t) = i(t) \otimes w(-t)/\sqrt{E_w} = \frac{K_W(f_I)}{\sqrt{B}} \alpha_I A_I \cos(2\pi f_I t + \arg\{W(f_I)\}) \tag{6.3}$$

is the interference at the matched filter output. $K_W(f_I)$ is defined as $K_W(f_I) \triangleq |W(f_I)| / |W_{sinc}(f_I)|$ (and zero outside the band of interest); $W_{sinc}(f)$ is the Fourier transform of a *sinc* function (in the time domain) with a bandwidth B centered around f_0 , and energy E_w . Conditioned to a given value $n_{MF}(0) \leq b(0)$ of the noise at $t = 0$ at the matched filter output, from [18] the single-sided first crossing probability density function for $b(t)$ is:

$$g(t|n_{MF}(0)) = R[b(t)] \exp\left(-\int_0^t R[b(t')] dt'\right) \tag{6.4}$$

where $R[b(t)]$ is a periodic function given by:

$$R[b(t)] = \frac{\sqrt{-\ddot{\gamma}(0)}}{2\pi} \exp\left(\frac{-(r_{TH} + i_{MF}(t))^2}{2\sigma_{n_{MF}}^2}\right) \tag{6.5}$$

$$\left(\exp\left(\frac{i_{MF}^2(t)}{2\ddot{\gamma}(0)}\right) - i_{MF}(t) \sqrt{\frac{2\pi}{-\ddot{\gamma}(0)}} \left(1 - \Phi\left(\frac{i_{MF}(t)}{\sqrt{-\ddot{\gamma}(0)}}\right)\right)\right)$$

$\gamma(t)$ is the normalized autocorrelation function of $n_{MF}(t)$, and $\{\dot{\cdot}\}$ and $\{\ddot{\cdot}\}$ represent the first and second derivative of $\{\cdot\}$, respectively. The conditioned single-sided first crossing probability in T_n can be immediately calculated as

¹Note that the original problem requires to calculate the first time in $[0, \tau]$ in which $n_{MF}(t) + i_{MF}(t) = r_{TH}$; however, since the process is stationary and $i_{MF}(t) = -i_{MF}(t + \pi/(2\pi f_I))$, this is statistically equivalent to calculating the first time in $[0, \tau]$ in which $n_{MF}(t) = r_{TH} + i_{MF}(t)$.

$G(T_n|n_{MF}(0)) = \int_0^{T_n} g(t|n_{MF}(0))dt$, and the probability of single-sided first threshold crossing is:

$$\begin{aligned}
 G(T_n) &= \Pr\{n_{MF}(0) \geq b(0)\} + G(T_n|n_{MF}(0) \leq b(0)) \approx \tag{6.6} \\
 &\approx G(T_n|n_{MF}(0) \leq b(0)) = \int_{\theta=0}^{2\pi} \int_{n_{MF}(0)=-\infty}^{b(0)} G(T_n|n_{MF}(0)) f_{\theta_I}(\theta) f_{n_{MF}}(n) d\theta dn = \\
 &\quad \frac{1}{2\pi} \int_0^{2\pi} G(T_n|n_{MF}(0)) \Phi\left(\frac{r_{TH} + \alpha_I A_I K_W(f_I)/\sqrt{B} \cos\theta}{\sigma_{n_{MF}}}\right) d\theta
 \end{aligned}$$

where it has been used that $G(T_n|n_{MF}(0))$ does not depend on the particular $n_{MF}(0)$ (given $n_{MF}(0) \leq b(0)$) and therefore it can be taken out of the internal integral in the second line of (6.6). To calculate (6.6), $\Pr\{n_{MF}(0) \geq b(0)\}$ has been neglected; this is licit since it is significantly smaller than $G(T_n|n_{MF}(0) \leq b(0))$ (in fact, we are interested in T_n and r_{TH} such that $T_n B \gg 1$ and $G(T_n) \ll 1$, which makes crossing inside a window T_n much more likely than in $t = 0$). As for the case of absence of NBI, an upper bound for the required double-sided first crossing probability is:

$$p_N(T_n) \leq \bar{p}_N(T_n) = 1 - (1 - G(T_n))^2 \tag{6.7}$$

The upper bound for the final P_{EFA} under NBI is:

$$P_{EFA} \leq \sum_{n=N_{TH}}^N P_0(n) \binom{N}{n} \int_{\alpha=0}^{\infty} \bar{p}_N(\tau_{MAX})^n (1 - \bar{p}_N(\tau_{MAX}))^{N-n} f_{\alpha_I}(\alpha) d\alpha \tag{6.8}$$

It is interesting to compare the results which can be obtained from (6.4)-(6.6) for the particular case of $i(t) = 0$ with those of Section 5.2.3. Using the differentiation theorem:

$$\ddot{\gamma}(0) = -\frac{\int_{-\infty}^{\infty} (2\pi f)^2 S_{nw}(f) df}{\int_{-\infty}^{\infty} S_{nw}(f) df} = -2\pi^2 \lambda^2 \tag{6.9}$$

it follows that:

$$R[b(t)] = \frac{\lambda}{\sqrt{2}} \exp(-r_{TH}^2/2\sigma_{n_{MF}}^2) \tag{6.10}$$

becomes a constant. Thus, after some calculation:

$$G(T_n) = (1 - \exp(-T_n/\rho))\Phi(k_{TH}) \tag{6.11}$$

Observing that for the k_{TH} of interest $\Phi(k_{TH}) \approx 1$, this expression for $G(T_n)$ equals that provided in Section 5.2.3.

6.2.2 Missed Detection

With arguments similar to those discussed in Section 5.2.4, a lower bound for p_D conditioned to a particular realization of $i(t)$ is:

$$p_D \geq \Pr\{\sqrt{FPNR \cdot S_{FP}} + R_0 \geq k_{TH} + i_{MF}(t_{pk})/\sigma_{n_{MF}}\} = \quad (6.12)$$

$$1 - \Phi(k_{TH} + i_{MF}(t_{pk})/\sigma_{n_{MF}} - \sqrt{S_{FP} \cdot FPNR})$$

Averaging over θ_I results in:

$$p_D \geq \bar{p}_D = 1 - \frac{1}{2\pi} \int_0^{2\pi} \Phi(k_{TH} + \alpha_I A_I K(f_I)/(\sqrt{B}\sigma_{n_{MF}}) \cos \theta - \sqrt{S_{FP} \cdot FPNR}) d\theta \quad (6.13)$$

where \bar{p}_D is the lower bound of p_D . The upper bound for the final probability of missed detection can be written as:

$$P_{MD} \leq \sum_{n=0}^{N_{TH}-1} \binom{N}{n} \int_{s=0}^{\infty} \int_{\alpha=0}^{\infty} \bar{p}_D^n (1 - \bar{p}_D)^{N-n} f_{S_{FP}}(s) f_{\alpha_I}(\alpha) d\alpha ds \quad (6.14)$$

6.2.3 TOA performance evaluation under NBI

Given an NBI source, using (6.8), (6.14), it is possible to evaluate the impairments in P_{EFA} and P_{MD} , for a given set of (N, N_{TH}) and k_{TH} (for a definition of these parameters we refer to Section 5.2). To this purpose, first a criterion to choose the parameters of interest is required. In the following, an early false alarm threshold matching is used: keeping constant the other system parameters, the value of k_{TH} which allows to have the same early false alarm probability, is determined. Fig. 6.1 shows the values of k_{TH} which allow to have the same required bound on P_{EFA} as for the case of $k_{TH} = 4.5$ without NBI, for a given Interference to Noise Ratio (INR), defined as:

$$\text{INR} \triangleq \frac{A_I^2}{2N_0B} \quad (6.15)$$

Using the determined k_{TH} , the corresponding values of (N, N_{TH}) which allow to satisfy the requested P_{MD} are accordingly calculated. Fig. 6.2 shows the regions of the plane (N, N_{TH}) which satisfy $P_{EFA} \leq 0.01$ and $P_{MD} \leq 0.01$, for LOS propagation, and for different values of INR. In a similar way, results for the NLOS case (not shown here) can be calculated. The curve corresponding to the constraint for the P_{EFA} is the same as for the case without NBI, due to the early false alarm probability matching criterion used. By evaluating the variations in

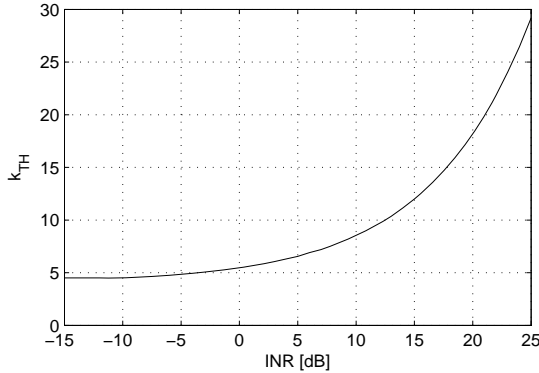


Figure 6.1: k_{TH} which allow to have the same \bar{p}_N as for the case of $k_{TH} = 4.5$ without NBI, and accordingly the same required bound on P_{EFA} , for a given value of INR.

the curve for P_{MD} for a given value of INR and FPNR, it is possible to know the corresponding impairment in terms of variations in the minimum required N (and N_{TH}) or FPNR. From the figure, an increase in INR determines an increase in the minimum required N for the same FPNR; e.g. of about 2 orders of magnitude for INR=30 dB and FPNR=12 dB (in fact, the minimum N increases from about 60 till about 7000 in the two cases; these values can be found by looking for the point (N, N_{TH}) with the minimum N which is both below the curve for P_{EFA} and above the curve for P_{MD} in the two cases, for the same FPNR). In a similar way, the impairments can also be evaluated in terms of increase in minimum required FPNR, for the same (N, N_{TH}) . For example, for $(N = 60, N_{TH} = 3)$, the minimum required FPNR in the absence of NBI is of about 12 dB (from Figs. 5.6, 5.7). An interference source with INR=30 dB requires an increase of the FPNR to about 20 dB (8 dB more), to meet the same performance requirements (from Fig. 6.2).

6.3 NBI impairments - coarse acquisition

For evaluating the performance of the coarse acquisition scheme under NBI, the same assumptions on the channel as in Section 5.3 are made. Conditioned to a particular realization of $i(t)$, E_{s_1} , E_{s_2} , and E_{n_i} for $i = 1..K-2$ are non-central chi-square distributed random variables with non centrality parameters, respectively

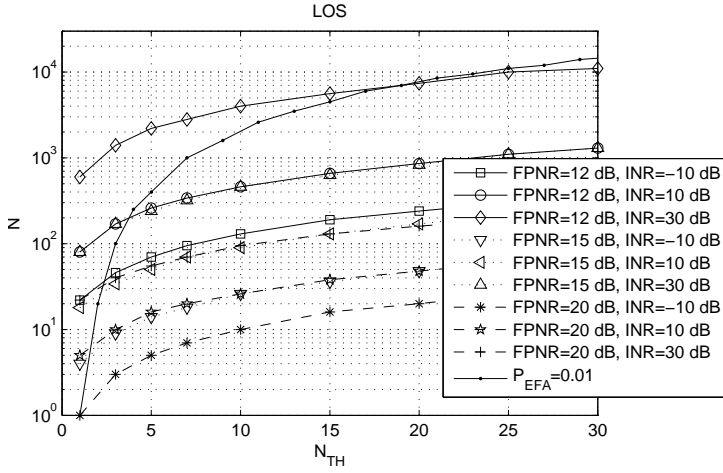


Figure 6.2: Regions of the plane (N, N_{TH}) which satisfy the required $P_{EFA} \leq 0.01$ and $P_{MD} \leq 0.01$, for different values of FPNR and INR, and for LOS propagation; these regions are determined as the portion of the plane below the curve for P_{EFA} and above the respective curve for P_{MD} .

[19]:

$$\mu_{NC}(E_{s_1}) = \frac{1}{N_0} \sum_{j=0}^{N_{CA}-1} \int_0^T \left(\sum_{l=0}^{L-1} c_j h_{R,l} w(t - lT_B - T_R) + i(t - T_{s_1} - jT_f) \right)^2 dt \quad (6.16)$$

$$\mu_{NC}(E_{s_2}) = \frac{1}{N_0} \sum_{j=0}^{N_{CA}-1} \int_0^T \left(\sum_{l=0}^{L-1} c_j h_{R,l} w(t - lT_B + T - T_R) + i(t - T_{s_2} - jT_f) \right)^2 dt \quad (6.17)$$

$$\mu_{NC}(E_{n_i}) = \frac{1}{N_0} \sum_{j=0}^{N_{CA}-1} \int_0^T i(t - T_{n_i} - jT_f)^2 dt \quad (6.18)$$

Before the expressions in (6.16)-(6.18) can be evaluated, we need to calculate:

$$\int_0^T i(t - t_g)^2 dt = \frac{\alpha_I^2 A_I^2}{2} \left(T + \frac{1}{4\pi f_I} \sin(4\pi f_I t + 2\theta_g) \Big|_0^T \right) \approx \frac{\alpha_I^2 A_I^2 T}{2} \quad (6.19)$$

where t_g is a generic time shift value and $\theta_g = \theta_I - 2\pi f_I t_g$, and it has been used $T \gg 1/(4\pi f_I)$, and:

$$\int_0^T \sum_{l=L_A}^{L_B-1} h_{R,l} w(t - lT_B) i(t - t_g) dt = \quad (6.20)$$

$$\alpha_I A_I \sum_{l=L_A}^{L_B-1} h_{R,l} \text{Re} \left\{ \int_{-\infty}^{\infty} w(t - lT_B) \exp(j2\pi f_I t + \theta_g) \right\} =$$

$$\alpha_I A_I |W(f_I)| \sum_{l=L_A}^{L_B-1} h_{R,l} \cos(2\pi f_I T_B l + \theta_W)$$

where $L_A = 0$ and $L_B = L_R$ for E_{s_1} , while $L_A = L_R$ and $L_B = L$ for E_{s_2} , with:

$$L_R \triangleq \text{round} \{L(T - T_R)/T\} \quad (6.21)$$

where $\text{round} \{\cdot\}$ denotes the closest integer to $\{\cdot\}$, and $\theta_W = \theta_g + \arg \{W(f_I)\}$. The fully-analytical solution proposed in the framework developed in [13], applied to the analysis of NBI for transmitted-reference and for energy detection [14] systems, assumes the term in (6.20) negligible. However, as shown in Fig. 6.5, this approach provides differences of several dB in the obtained results for large SNR and small N_{CA} (which are of interest for the described approach). Thus, a statistical characterization of (6.20) is proposed in the following.

6.3.1 Statistical characterization of the signal \times interference term

We define the stochastic part of (6.20) for s_1 and s_2 , respectively, as:

$$R_{s_1}(L_R) \triangleq \sum_{l=0}^{L_R-1} h_{R,l} \cos(2\pi f_I l T_B + \theta_{W_1}) = \quad (6.22)$$

$$|h_{R,0}| \sum_{l=0}^{L_R-1} \exp(j\phi_l) \exp(-lT_B/(2\alpha_{ch})) \cos(2\pi f_I T_B l + \theta_{W_1})$$

$$R_{s_2}(L_R) \triangleq \sum_{l=L_R}^{L-1} h_{R,l} \cos(2\pi f_I l T_B + \theta_{W_2}) = \quad (6.23)$$

$$|h_{R,0}| \sum_{l=L_R}^{L-1} \exp(j\phi_l) \exp(-lT_B/(2\alpha_{ch})) \cos(2\pi f_I T_B l + \theta_{W_2})$$

Conditioned on the random phase θ_I , $R_{s_1}(L_R)$ and $R_{s_2}(L_R)$ are linear combinations of L_R and $L - L_R$ independent random variables (ϕ_l are independent) with standard deviation $|h_{R,0}| \exp(-lT_B/(2\alpha_{ch})) \cos(2\pi f_I T_B l + \theta_{W_{(\cdot)}})$ for $l = 0..L_R - 1$ and $l = L_R..L - 1$, respectively (the standard deviation of $\exp(j\phi_l) = 1$). Observing that the Lyapunov conditions on the central limit theorem for the sum of independent but not identically distributed random variables are satisfied [20],

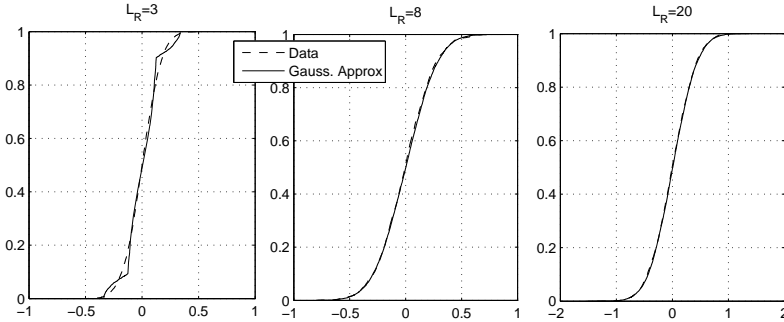


Figure 6.3: Empirical cdf of R_{s_1} and Gaussian approximation for $f_I = 4.6$ GHz and $\alpha_{ch} = 15$ ns, as an example, for $L_R = 3$, $L_R = 8$, and $L_R = 20$.

for L_R and $L - L_R$ large enough, $R_{s_1}(L_R)$ and $R_{s_2}(L_R)$ can be modeled as zero mean Gaussian distributed random variables. As an example, Fig. 6.3 shows the empirical cdf of R_{s_1} and the Gaussian approximation for $f_I = 4.6$ GHz and $\alpha_{ch} = 15$ ns, for $L_R = 3$, $L_R = 8$, and $L_R = 20$; it can be seen that already for $L_R \geq 8$ the approximation gives very good results (similarly, for $R_{s_2}(L_R)$, the Gaussian approximation is very good for $L - L_R \geq 8$). Considering that (6.20) gives a negligible contribution for values of L_R close to the low extrema for s_1 and s_2 , a Gaussian approximation can be used for $R_{s_{(\cdot)}}(L_R)$ for all values of L_R .

The variances of $R_{s_1}(L_R)$ and $R_{s_2}(L_R)$ are given, respectively, by:

$$\sigma_{R_{s_1}}^2(L_R) = h_{R,0}^2 \sum_{l=0}^{L_R-1} \exp(-lT_B/\alpha_{ch}) \cos^2(2\pi f_I T_B l + \theta_{W_1}) = \quad (6.24)$$

$$\frac{1}{2PL_{TP}} (1 - \exp(-T_B/\alpha_{ch}L_R)) + \frac{1}{2} h_{R,0}^2 \sum_{l=0}^{L_R-1} \exp(-lT_B/\alpha_{ch}) \cos(4\pi f_I T_B l + 2\theta_{W_1})$$

and:

$$\sigma_{R_{s_2}}^2(L_R) = h_{R,0}^2 \sum_{l=L_R}^{L-1} \exp(-lT_B/\alpha_{ch}) \cos^2(2\pi f_I T_B l + \theta_{W_2}) = \quad (6.25)$$

$$\frac{1}{2PL_{TP}} (\exp(-T_B/\alpha_{ch}L_R) - \exp(-T_B/\alpha_{ch}L)) +$$

$$\frac{1}{2} h_{R,0}^2 \sum_{l=L_R}^{L-1} \exp(-lT_B/\alpha_{ch}) \cos(4\pi f_I T_B l + 2\theta_{W_2})$$

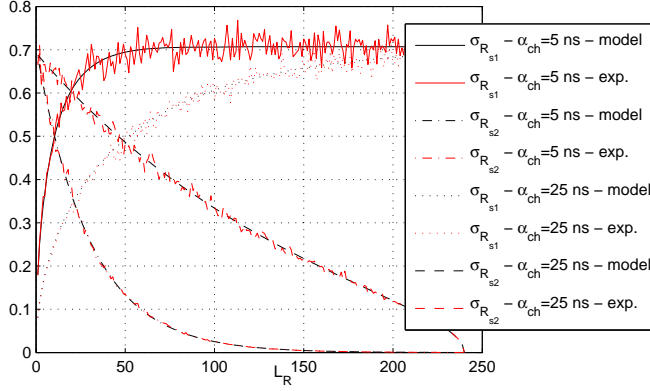


Figure 6.4: $\sigma_{R_{s_1}}(L_R)$ and $\sigma_{R_{s_2}}(L_R)$ for $f_I = 4.6$ GHz and $\alpha_{ch} = 5$ and 25 ns for comparison, both from simulations using (6.22), (6.23) and with the proposed model in (6.26)-(6.27).

By de-conditioning with respect to the random phase, the average variances of $R_{s(\cdot)}(L_R)$ are:

$$\sigma_{R_{s_1}}^2(L_R) = \frac{1}{2PL_{TP}} (1 - \exp(-T_B/\alpha_{ch}L_R)) \quad (6.26)$$

$$\sigma_{R_{s_2}}^2(L_R) = \frac{1}{2PL_{TP}} (\exp(-T_B/\alpha_{ch}L_R) - \exp(-T_B/\alpha_{ch}L)) \quad (6.27)$$

where it has been used $\int_{\theta=0}^{2\pi} \cos(4\pi f_I T_B l + 2\theta) = 0$. Given the other system parameters (which affect L and L_R), $\sigma_{R_{s(\cdot)}}(L_R)$ only depends on T_B/α_{ch} , and not on f_I . Fig. 6.4 shows $\sigma_{R_{s_1}}$ and $\sigma_{R_{s_2}}$ for $f_I = 4.6$ GHz and $\alpha_{ch} = 5$ and 25 ns for comparison, both from simulations using (6.22), (6.23) and with the proposed model in (6.26)-(6.27).

6.3.2 Probability of coarse acquisition under NBI

The probability of coarse acquisition is:

$$P_{CA} = \frac{1}{T} \int_{\alpha=0}^{\infty} \int_{t=0}^T (P_{s_1} + P_{s_2}) f_{\alpha_I}(\alpha) dt d\alpha \quad (6.28)$$

Fig. 6.5 shows the performance of the proposed coarse acquisition scheme under NBI, for CM3 and for $N_{CA} = 1$ and $N_{CA} = 100$, both from simulation using

the IEEE model, and with the proposed approach. Due to the long simulation time, curves obtained by simulation using the IEEE model are reported only for $N_{CA} = 1$. The proposed solution matches very well to the simulation results. On the contrary, neglecting the term in (6.20) introduces deviations of several dB in the obtained results for large SNR and small N_{CA} , as shown in Fig. 6.5 (see e.g. the curves for $N_{CA} = 1$ and INR=30 dB). In the reported plots, $f_I = 4.6$ GHz, since it corresponds to the maximum of $K_W(f_I)$, and represents the situation with the most severe performance impairments due to NBI. NBI can be counteracted by increasing the SNR or the minimum N_{CA} required; in this last case, for example for INR=30 dB, by increasing N_{CA} from 1 to 100, allows to gain about 17 dB in the minimum SNR needed to reach the target $1 - P_{CA} = 10^{-3}$. It is worthwhile to underline that for the results in Fig. 6.5, $c_j = 1$ has been chosen (therefore, no randomization code has been used). This choice clearly affects the specific value of the signal \times interference term, which in this case will be smaller in modulo by a factor $N_{CA}/|\sum_1^{N_{CA}} c_i|$, when a given random sequence $\{c_j\}$ is used (while the random code does not affect the other terms; see also Table 7.1); therefore, the proposed analysis represents in this case a worst case scenario; for example, for large N_{CA} and depending on the particular $\{c_j\}$ used, the signal \times interference term can be neglected (while in general it needs to be considered).

It is worthwhile to underline that the coarse acquisition step is significantly more sensitive to NBI than the TOA estimation strategy. For example, an increase in SNR of about 10 dB allows to compensate only an INR=10 dB, for $N_{CA} = 1$, as it can be seen by comparing results in Fig. 6.5 with those in Fig. 5.10. This is intuitively clear, since this approach is based on energy detection. Also in this case, as for the analysis without NBI, no significant difference arises by substituting α_{ch} with its mean value (not shown in the figure), representing that also under NBI the only channel parameter required for the evaluation of the proposed approach is the mean value of the channel mean excess delay.

6.4 Chapter summary

In this chapter, impairments due to narrowband interference on TOA estimation, have been evaluated. The solution proposed in Section 5.2 provides a fair robustness towards NBI, thanks to the repetitive transmission strategy adopted, which is inherently robust towards the occurrence of outliers in TOA estimation due to NBI. It is shown that an interference source with INR=30 dB requires an increase

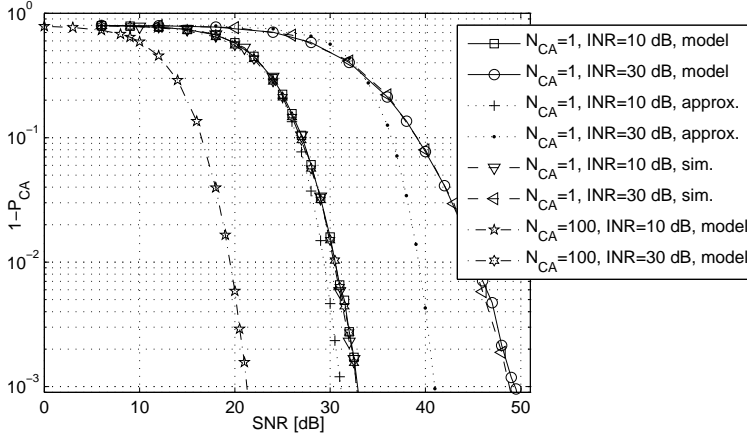


Figure 6.5: P_{CA} vs. SNR for different INR, for CM3 and for $N_{CA} = 1$ and $N_{CA} = 100$.

Table 6.1: Mean and Variance of E_{s_1} , E_{s_2} and E_{n_i}

μ_{s_1}	$N_{CA}(MN_0 + E_r(1 - \exp(-(T - T_R)/\alpha_{ch}))) + 2\alpha_I A_I \sqrt{E_r T_B} K_W(f_I) R_{s_1}(L_R) N_{CA} / \sum_1^{N_{CA}} c_j + \alpha_I^2 A_I^2 T/2$
$\sigma_{s_1}^2$	$N_{CA}(2MN_0^2 + 4N_0(E_r(1 - \exp(-(T - T_R)/\alpha_{ch}))) + 2\alpha_I A_I \sqrt{E_r T_B} K_W(f_I) R_{s_1}(L_R) N_{CA} / \sum_1^{N_{CA}} c_j + \alpha_I^2 A_I^2 T/2)$
μ_{s_2}	$N_{CA}(MN_0 + E_r(\exp(-(T - T_R)/\alpha_{ch}) - \exp(-(2T - T_R)/\alpha_{ch}))) + 2\alpha_I A_I \sqrt{E_r T_B} K_W(f_I) R_{s_2}(L_R) N_{CA} / \sum_1^{N_{CA}} c_j + \alpha_I^2 A_I^2 T/2$
$\sigma_{s_2}^2$	$N_{CA}(2MN_0^2 + 4N_0(E_r(\exp(-(T - T_R)/\alpha_{ch}) - \exp(-(2T - T_R)/\alpha_{ch}))) + 2\alpha_I A_I \sqrt{E_r T_B} K_W(f_I) R_{s_2}(L_R) N_{CA} / \sum_1^{N_{CA}} c_j + \alpha_I^2 A_I^2 T/2)$
μ_{n_0}	$N_{CA}(MN_0 + \alpha_I^2 A_I^2 T/2)$
$\sigma_{n_0}^2$	$N_{CA}(2MN_0^2 + 4N_0 \alpha_I^2 A_I^2 T/2)$

of only 8 dB in the FPNR (from FPNR=12 dB to 20 dB) to achieve the same performance as without NBI. The same analysis has been carried out also for the coarse acquisition step. It is shown that the signal \times interference term, which arises at the output of the energy detector, can be neglected only for large N_{CA} . On the contrary, for small N_{CA} and large SNR , neglecting this terms causes deviations of several dB with respect to experimental results; for this reason, a statistical characterization of this term is proposed. This situation is of particular interest for the proposed solution, due to the relatively high power which can be transmitted in a single pulse (see also Section 5.4). The evaluation of performance impairments on coarse acquisition due to NBI shows that the coarse acquisition is more sensitive to interference than the TOA estimation; this is intuitive, since coarse acquisition is based on energy detection. However, in this last case NBI impairments can be effectively compensated by increasing N_{CA} .

Bibliography

- [1] FCC, Office of Engineering and Technology, "*Revision of part 15 of the commissions rules regarding ultra-wideband transmission systems*", ET Docket, no. 98-153, 2002.
- [2] K. Witrisal, M. Pausini, A. Trindade, "*Multiuser interference and inter-frame interference in UWB transmitted reference systems*", Joint UWBST & IWUWBS, pp. 96-100, May 2004.
- [3] J.R. Foerster, "*The performance of a direct-sequence spread ultrawideband system in the presence of multipath, narrowband interference, and multiuser interference*", IEEE ICUWST, pp. 87-91, May 2002.
- [4] T. Erseghe, S. Tomasin, "*UWB WPAN receiver optimization in the presence of multiuser interference*", IEEE Transaction on Communications, vol. 57, no. 8, pp. 2369-2379, Aug. 2009.
- [5] N.C. Beaulieu, D.J. Young, "*Designing time-hopping ultrawide bandwidth receivers for multiuser interference environments*", Proceedings of the IEEE, vol. 97, no. 2, pp. 255-284, Feb. 2009.
- [6] Qing Zhou, F.C.M. Lau, "*Analytical performance of M-ary time-hopping orthogonal PPM UWB systems under multiple access interference*", IEEE Transaction on Communications, vol. 56, no. 11, pp. 1780-1784, Nov. 2008.

-
- [7] Bo Hu, N.C. Beaulieu, "Accurate performance evaluation of time-hopping and direct-sequence UWB systems in multi-user interference", IEEE Transaction on Communications, vol. 53, no. 6, pp. 1053-1062, Jun. 2005.
- [8] Joon-Yong Lee, Sungyul Yoo, "Large error performance of UWB ranging in multipath and multiuser environments", IEEE Transaction on Microwave Theory and Techniques, vol. 54, no. 4, pp. 1887-1895, Apr. 2006.
- [9] J. Fiorina, D. Domenicali, "The non validity of the gaussian approximation for multi-user interference in ultra wide band impulse radio: from an inconvenience to an advantage", IEEE Transactions on Wireless Communications, vol. 8, no. 11, pp. 5483 - 5489, Nov. 2009.
- [10] J. Fiorina, D. Panaitopol, D. Domenicali, "On the necessity of sensing the non Gaussianity of the interference: Application to uwb systems", IEEE CogART, pp. 96-99, Nov. 2009.
- [11] M. Chiani, A. Giorgetti, "Coexistence between UWB and narrow-band wireless communication systems", IEEE Proceedings, vol. 97, no.2, pp. 231-254, Feb. 2009.
- [12] A. Giorgetti, M. Chiani, M.Z. Win, "The effects of narrowband interference on wideband wireless communication systems", IEEE Transaction on Communications, vol. 53, no. 12, pp. 2139-2149, Dec. 2005.
- [13] T.Q.S. Quek, M.Z. Win, D. Dardari, "Unified analysis of UWB transmitted reference schemes in the presence of narrowband interference", IEEE Transaction on Wireless Communications, vol. 6, no. 6, pp. 2126-2139, Jun. 2007.
- [14] A. Rabbachin, T.Q.S. Quek, P.C. Pinto, I. Oppermann, M.Z. Win, "UWB energy detection in the presence of multiple narrowband interferers", IEEE ICUWB 2007, pp. 857-862, 24-26 Sep. 2007.
- [15] M. Pausini, G.J.M. Janssen, "On the narrowband interference in transmitted reference UWB receivers", IEEE ICU 2005, pp. 571-575, Sep. 2005.
- [16] D. Dardari, A. Conti, U. Ferner, A. Giorgetti, M.Z. Win, "Time-of-arrival estimation of UWB signals in the presence of narrowband and wideband interference", IEEE ICUWB 2007, pp. 71-76, Sep. 2007.
- [17] L.M. Ricciardi, S. Sato, "On the evaluation of first-passage-time densities for Gaussian processes", Signal Processing, vol. 11, no. 4, pp. 339-357, Dec. 1986.

- [18] E. di Nardo, A.G. Nobile, E. Pirozzi, L.M. Ricciardi, "*On the asymptotic behavior of first passage time densities for stationary gaussian processes and varying boundaries*", Methodology and Computing in Applied Probability, vol. 5, pp. 211-233, Jun. 2003.
- [19] P.A. Humblet, M. Azizoglu, "*On the bit error rate of lightwave systems with optical amplifiers*", IEEE Journal of Lightwave Technology, vol. 9, no. 11, pp. 1576-1582, Nov. 1991.
- [20] Kai Lai Chung, "*A Course in Probability Theory*", Academic Press, 2nd edition 2000.

Conclusions and Recommendations

Recent years have been characterized by a continuously increasing demand for positioning information. The inherent inability of GPS to provide satisfactory performance inside buildings, together with the need for *accurate indoor positioning* in emerging fields like wireless sensor networks, health-care, logistics, location based services, automation, gaming, entertainment, has driven the attention towards alternative technologies able to overcome the "indoor positioning bottleneck". Ultra-Wideband radio has been recognized as the ideal technology to that purpose due to its unique and unmatched spectral characteristics and the huge signal bandwidth used, which make these signals robust to the challenging indoor propagation conditions. At the time the research presented in this thesis was started, while a large number of related scientific contributions was already available in the literature, the relevance of several fundamental issues was not yet identified and many aspects were not fully understood. Providing an answer to several of those considered the most important ones, namely:

1. *identification of characteristic parameters of the UWB multipath channel for ranging based positioning in typical indoor environments, and development of statistical models based on measurements*
2. *use of the developed models for positioning applications and evaluation of achieved performance*

3. *development of new low-complexity receiver architectures and signal processing algorithms for extraction of the required channel parameters information*
4. *analysis of the narrowband interference impairments on ranging performance*

was the goal of this thesis. Based on the investigations and discussions in previous chapters, the most important findings and conclusions are presented in a summarized form in this chapter. Furthermore, a number of issues which remain unsolved, and which constitute a possible list of topics for future research, will be highlighted.

7.1 Conclusions

This thesis has specifically focused on physical layer aspects related to UWB radio signals when used for positioning applications based on *ranging*, since this appears the most promising solution for indoor applications demanding for centimeter level accuracy.

7.1.1 Channel characterization for positioning applications based on ranging

The use of extremely large bandwidths implies that the different paths which compose the received signal can be largely resolved, even in dense multipath environments. This makes it possible to use statistics which exhibit a dependency on the distance for ranging applications, since variations of these statistics are mainly related to the channel location dependency and not to the unresolvable multipath. In this way, their measures can be sufficiently reliably related to the distance traveled by the signal, provided that a model for them is available. This concept is defined as *statistics based ranging*. The statistics which are identified and modeled in this thesis are the total power (TP) of the received signal, and the power of the first path (FP) of the received signal.

Both for LOS and for NLOS, the global fading standard deviation strongly depends on the used bandwidth. This phenomenon is more accentuated in LOS, where the location dependency is weaker and therefore multipath represents a more significant part of the overall fading deviations. For example, in LOS decreasing the bandwidth from 7.5 GHz down to 1 GHz determines an increase in

the global fading standard deviation of a factor about 2 for TP and 3 for FP. For large bandwidths, FP exhibits a very small fading (down to about 0.6 dB).

When decreasing the used bandwidth, the fading also depends on the distance between transmitter and receiver.

This phenomenon is explainable due to the denser unresolvable multipath, which affects the received signal with increasing distance.

The global fading variations can be approximated as a lognormal r.v. for TP, while as a double-lognormal r.v. for FP in LOS and as a Nakagami r.v. for FP in NLOS.

The use of this simplified statistical characterization does not introduce any significant impairment in ranging performance, provided that the bandwidth and distance dependency are properly modeled.

A very small number of calibration measurements is needed to correctly estimate the channel path-loss exponent.

For example, 6 calibration measurements in LOS, and 13 in NLOS are sufficient to estimate with a relative error smaller than 0.1 in 99.9% of the cases the path-loss exponent for TP. The requirements for the channel fading standard deviation estimation are higher; however, an accurate estimate for it is usually not required for statistics based ranging.

7.1.2 Performance evaluation of ranging based positioning

Using the developed models, different solutions can be employed in order to improve the accuracy provided by traditional total power based ranging. Given the propagation condition (LOS or NLOS), actual improvements depend on the particular method used. A straightforward conclusion is that higher accuracy can be achieved with a larger amount of information used.

In LOS and for the full bandwidth, by differentiating and identifying the particular environment in which transmitter and receiver are placed and using a best linear unbiased estimator of the distance, it is possible to achieve with

the statistics based ranging approach a standard deviation range error of about 0.44 m for distances between transmitter and receiver up to 13 m.

Compared to results from the traditional signal strength approach on the same data (which provided a standard deviation range error of 1.07 m), this represents an improvement of a factor of about 2.5.

Knowledge of the model for the fading distance and bandwidth dependency can be used to mitigate the large positive errors which are the most consistent ones in power based ranging.

This allows to significantly improve the achieved performance compared to results without using any model knowledge; for example, for LOS, FP and 0.5 GHz bandwidth, the standard deviation range error decreases from about 3.42 m down to 1.76 m, i.e. a factor about 2 smaller.

For practical applications, it is often relevant to investigate the best compromise between complexity and performance. From this point of view, the most appealing solution appears to use statistics based ranging in LOS only, and to rely on the first path power statistic, in conjunction with the use of very large bandwidths. The use of large bandwidths has in fact two advantages: to make the used statistics very reliable, and to make the model characterization extremely simple (no distance dependency).

In LOS propagation, FP only is able to achieve a standard deviation range error of about 54 cm, and no a-priori information at all is required (in fact, its path loss exponent can be approximated with 2). This solution, combined with a good positioning system geometry and depending on the number of reference stations used, can provide a final positioning accuracy of a few decimeters for a system with maximum distance between transmitter and receiver up to 13 m.

To combine TP with FP appears especially advantageous in NLOS propagation (and in mixed LOS/NLOS positioning scenarios). When using also TP, knowledge of the channel parameters is needed. A very limited amount of calibration measurements is required to correctly estimate them; e.g. 10 random measurements

allow to make the additional range error due to incorrect parameters estimation smaller than 5%.

The first path power can be estimated in a low-complexity way with a similar receiver architecture as presented in Chapter 5. Since this approach does not rely on any accurate synchronization between transmitter and receiver, it is particularly suited for very low-complexity applications.

The biconical antennas used in this thesis for modeling purposes are omni-directional in their H plane, and have been placed at the same height at the transmitter and the receiver; in this way, it is possible to strongly mitigate the directional dependency of the antennas' transfer function, and to completely eliminate it along the direct ray between transmitter and receiver. This also means that, for statistics based ranging, achieved results are representative of systems which require positioning information in planes only (examples can be found e.g. in automation and robotics, specific wireless sensor networks applications, etc.). When using this solution for 3D positioning applications using commercially available antennas, the final accuracy will be inferior (or alternatively, to achieve the same accuracy, the maximum coverage needs to be decreased since the estimated distance standard deviation increases with distance, see e.g. eq. (3.12)).

For applications which demand for highly accurate positioning information, ranging based on TOA estimation is the most suitable option. In fact, when using the full bandwidth, a standard deviation range error of less than 2 cm in LOS has been achieved.

The error increases in NLOS due to the additional delay caused by propagation through dielectric materials and to the more dense multipath.

The TOA based range error can be modeled as a Gaussian distributed random variable in LOS, and as the combination of a Gaussian and an exponentially distributed random variable in NLOS.

The range error increases when decreasing the used bandwidth or when increasing the distance between transmitter and receiver, due to the more dense multipath.

Reliable (with 99% of correct detection rate) LOS/NLOS detection can be achieved using the TOA and the total power (or first path power) of the received signal.

This information can be used to improve in a significant way global positioning accuracy using weighted least squares methods, especially in mixed LOS/NLOS scenarios (improvements in this case are up to a factor 3).

Increasing the bandwidth above 2 GHz does not provide a significant improvement in the TOA estimation accuracy. Larger bandwidths are however beneficial for LOS/NLOS detection, since the TP and FP fading decrease in a noticeable way for bandwidths larger than 2 GHz.

7.1.3 Low complexity TOA estimation receiver architecture and signal processing

The TOA of the received signal can be estimated in a low-complexity way with a receiver which works for a large part in the analog domain and limits the digital processing to the last part of the architecture.

The proposed implementation consists of an analog peak detector followed by two RC filters with different time constants; from the two different exponentially decaying signals, the TOA of the first peak of the received signal is reconstructed.

The proposed solution requires simple signal processing and sampling rates in the order of only a few tens of MHz, about two orders of magnitude less than the Nyquist rate for UWB signals. In this way, it is possible to overcome the main limitations which make it difficult to practically build UWB receivers. At the same time, the achieved range error is at centimeter level since it is possible to fully exploit the extremely large signal bandwidth used.

Performance flexibility can be achieved with a statistical averaging strategy, which does not require any coherent processing on the received signals among multiple transmissions.

In this way, by means of repetitive transmissions, it is possible to tune the probabilities of early false alarm and missed detection to arbitrarily small values; at the same time, it is possible to allow power deviations of about 10 dB less than the minimum required one in case of single pulse transmission. The strategy is inherently robust towards oscillators' inaccuracies; for temperature compensated crystal oscillators available in the market, additional introduced errors are negligible up to 100 pulses transmission, with proper choice of the system parameters.

Satisfying FCC power limitations, the proposed solution can achieve a coverage of a few hundreds of meters in LOS.

Coarse acquisition based on energy detection is a viable solution to provide a preliminary coarse synchronization needed by the proposed TOA estimation receiver architecture. This solution well matches with the low-complexity framework developed. While it is in general more sensitive to noise, it allows to easily increase the effective SNR by averaging the collected energy samples over multiple transmissions.

7.1.4 impairments due to narrowband interference

The worldwide acceptance of UWB technology is strongly related to coexistence issues with other (licensed) existing narrowband systems sharing the same spectrum. Narrowband interference impairments on TOA estimation have been analyzed by evaluating the first threshold crossing probability for Gaussian processes and time varying boundaries.

The proposed TOA estimation strategy is particularly robust towards interference thanks to the repetitive transmission strategy adopted, which is inherently immune towards the occurrence of outliers in TOA estimation due to interferer signals.

An interference source of 30 dB above the noise, requires only about 8 dB of increase in the minimum required SNR.

The signal \times interference term, which arises at the output of the energy detector used in the coarse acquisition step, can be neglected only when large number N_{CA} of pulses is used.

On the contrary, for small N_{CA} and large SNR, neglecting this terms can introduce deviations of several dB with respect to experimental results; for this reason, a statistical characterization of this term is proposed. It is shown that a Gaussian approximation can be used for analysis purposes.

Coarse acquisition, being based on energy detection, is more sensitive to interference than the fine TOA estimation step; however, also in this last case NBI impairments can be effectively compensated by increasing N_{CA} .

7.2 Recommendations for future research

In the following, issues related to the work presented in this thesis which are relevant to address in future research, are shortly highlighted.

When using UWB for positioning applications, a particularly critical element of the overall system is represented by the antennas. As discussed in Chapter 3, the accuracy of the statistics based ranging approach can be significantly affected by the antennas directional gain dependency, resulting in potentially significant performance impairments. In the same way, the promise for centimeter level positioning accuracy achievable with TOA based ranging, risks to be partly voided by the directional dependency of the antennas phase center. The challenges in addressing the antennas directional non-idealities are exacerbated by the extremely large fractional bandwidth which characterizes UWB systems, and which requires a reconsideration of traditional antenna design schemes. It is the opinion of the author that advances with respect to this point might significantly improve effective UWB positioning systems accuracy.

In this thesis, a LOS/NLOS detection strategy has been proposed and validated based on the collected data. The proposed approach however, requires knowledge of the TOA of the received signal, and for this reason, while it can be used to improve positioning performance for TOA based systems, it is not suitable for statistics based ranging applications, since they do not rely on the TOA. On the other hand, a correct identification of the proper propagation condition is

fundamental for this approach, in order to choose the proper channel parameters. For this reason, it is recommended to address this issue at the positioning level, when a redundant data-set of range measurements is available.

A statistical channel characterization is inherently related to the specific typology of the environment for which the model is developed. The models proposed in Chapter 2-4 are representative for UWB indoor office propagation. At the time of writing, no results were available for UWB channel characterization for positioning applications in other environments, e.g. the industrial ones, which typically exhibit a significantly different behavior, due to the large presence of metallic infrastructure. Therefore, it is suggested to address this issue in future UWB channel measurement campaigns.

The contribution of Chapter 5 has been to develop a new concept and principle of implementation of a receiver architecture for low-complexity TOA estimation. A circuit implementation of the proposed solution is encouraged.

The analysis of narrowband interference on TOA estimation has focused on a single tone and a single interferer source. It would be very interesting to extend the analysis to more realistic signal formats (e.g. OFDM signals) and to multiple interferer sources.

The analysis of multi-user interference on the TOA estimation approach proposed in Chapter 5 has not been addressed, since in most positioning applications, due to the low rate transmission, the probability of collisions, even in multi-user scenarios, can be neglected. However, it would be interesting to investigate eventual impairments on the proposed TOA strategy due to multi-user interference.



List of Abbreviations

ADC	Analog to Digital Converter
AOA	Angle of Arrival
AWGN	Additive White Gaussian Noise
BLUE	Best Linear Unbiased Estimator
cdf	Cumulative Density Function
CDMA	Code Division Multiple Access
CEPT	European Conference of Postal and Telecommunications Administrations
CIR	Channel Impulse Response
CM	Channel Model
EFA	Early False Alarm
EIRP	Equivalent Isotropically Radiated Power
FCC	Federal Communications Commission
FFT	Fast Fourier Transform
FP	First path Power
FPNR	First path Power to Noise Ratio
GBIP	General Purpose Information Bus
GLRT	Generalized Likelihood Ratio Test
GPS	Global Positioning System
IEEE	Institute of Electrical and Electronics Engineers
IF	Inverse Filtering

INR	Interference to Noise Ratio
LNA	Low Noise Amplifier
LOS	Line of Sight
LS	Least Squares
KS	Kolmogorov Smirnov
MAP	Maximum a Posteriori
MD	Missed Detection
MF	Matched Filter
MUI	Multi User Interference
NLOS	Non Line of Sight
NBI	Narrowband Interference
OFDM	Orthogonal Frequency Division Multiplexing
PL	Path Loss
PSD	Power Spectral Density
RF	Radio Frequency
RMS	Root Mean Square
SNR	Signal to Noise Ratio
TDOA	Time Difference of Arrival
TOA	Time of Arrival
TP	Total Power
UWB	Ultra Wideband
Wi-Fi	Wireless Fidelity
W-CDMA	Wideband Code Division Multiple Access
WLS	Weighted Least Squares

List of symbols

Text notations

\mathbf{X}	boldfaced uppercase letters denote matrices
\mathbf{x}	boldfaced lowercase letters denote row vectors
\mathbf{X}^T	transposition of matrix \mathbf{X}
$\det\{\mathbf{X}\}$	determinant of matrix \mathbf{X}
$\ \mathbf{x}\ $	norm of vector \mathbf{x}
$E\{\cdot\}$	statistical expectation operator
$f_X(x)$	probability density function of a random variable X whose sample values equals x
$F_X(x)$	cumulative density function of a random variable X whose sample values equals x
$\phi_X(x)$	Probability density function of a Standard Gaussian random variable X whose sample values equals x
$\Phi_X(x)$	Cumulative density function of a Standard Gaussian random variable X whose sample values equals x
$F_X(x H)$	conditional cumulative density function of a random variable X whose sample values equals x , given that the hypothesis H is true
\hat{x}	estimate of random variable x
$mean\{\cdot\}$	mean of enclosed random variable
$var\{\cdot\}$	variance of enclosed random variable

μ_x	mean of random variable x (alternative representation)
σ_x^2	variance of random variable x (alternative representation)
\bar{x}	expected value of random variable x (alternative representation)
$round\{\cdot\}$	closest integer to the quantity enclosed
$ \cdot $	absolute value of the quantity enclosed
$[a, b]$	closed interval of variation of the given variable
$\delta(t)$	Dirac delta function
$x[n]$	n -th sample of continuous signal $x(t)$ corresponding to $x(nT_S)$
$\tilde{x}(t)$	envelope of time domain signal $x(t)$
\ln	natural logarithm
$\log 10$	base 10 logarithm
\otimes	convolution operation
\triangleq	by definition equal to
j	imaginary unit
$Re\{\cdot\}$	real part of the complex scalar enclosed within
$\arg\{\cdot\}$	phase angle of the complex scalar enclosed within

Lowercase symbols

a_{pk}	first peak amplitude
$a_{R,l}$	amplitude of l -th resolvable multipath component
c	speed of light in air
c_j	j -th element of a random polarity code
d	distance between transmitter and receiver
d_0	reference distance between transmitter and receiver
f_0	central frequency of the spectrum
f_H	upper frequency of the -10 dB emission spectrum
f_I	narrowband interferer frequency
f_L	lower frequency of the -10 dB emission spectrum
f_{os}	oscillator frequency
f_{pr}	pulse generator repetition frequency
f_S	sampling rate
$h(t)$	channel impulse response
$h_l(t)$	amplitude of l -th channel multipath component
$h_{sys}(t)$	measurement system impulse response

$i(t)$	narrowband interferer
$i_{MF}(t)$	narrowband interferer at the matched filter output
k_{PL}	exponential term modeling the path loss frequency dependency
k_{TH}	threshold for TOA estimation
m	Nakagami m-factor
n	path-loss exponent
$n(t)$	Gaussian additive white Gaussian noise
$n_{MF}(t)$	noise at the matched filter output
$p(t)$	signal generator output
p_{nc}	probability of positioning algorithm non-convergency
$r(t)$	received signal
$w(t)$	transmitted pulse
$w_l(t)$	distorted pulse received along the l -th multipath component

Uppercase symbols

A_I	narrowband interferer amplitude
B	signal bandwidth
B_c	signal effective bandwidth
B_f	signal fractional bandwidth
B_{if}	(inverse filtered) signal bandwidth
B_R	(spectrum analyzer) resolution bandwidth
E_0	standard exponential random variable
E_k	energy in bin k
E_w	energy of transmitted pulse $w(t)$
FP	first path power
G_0	standard Gaussian random variable
$H(f)$	channel frequency response
K	number of time bins in T_f
L	number of resolvable multipath components
L_{ch}	number of channel multipath components
M	degrees of freedom of
N	number of repetitive transmissions for TOA estimation
N_0	noise power spectral density
N_m	number of measurements used to estimate the channel parameters

N_p	number of range estimates used for positioning
N_{rs}	number of reference stations
N_S	bit of resolutions of ADC
$N_{s,os}$	maximum number of samples which can be recorded by the oscilloscope
N_{TH}	minimum number of TOA estimates in time window T_W to detect it
N_{TOA}	number of TOA estimates in time window T_W
$N_{w,os}$	number of adjacent time windows recorded to collect a single channel measurement
P_{CA}	probability of coarse acquisition
$P(d)$	power at distance d
P_{EFA}	probability of early false alarm
PL	path loss
$PL(d)$	path loss distance dependent component
$PL(f)$	path loss frequency dependent component
P_{MD}	probability of missed
P_{meas}	EIRP measured signal power
P_T	EIRP transmitted signal power
$Q(x)$	Q function of standard Gaussian random variable evaluated at x
$R(f)$	frequency response of the received signal
RX	receiver
S	random variations of the considered statistic around its model fit
S_M	random variations of power around its model fit due to multipath
S_L	random variations of power around its model fit due to location dependency
T	bin time duration
T_0	coarse estimate of the frame starting time
T_f	frame repetition period
T_{md}	maximum measurable delay of the oscilloscope
T_{oti}	overlap time interval between adjacent time windows recorded by the oscilloscope

TP	total signal power
T_{pr}	pulse generator period
T_{pt}	processing time at receiver
$T_{s,os}$	maximum time window which can be recorded by the oscilloscope
T_S	sampling period
T_{vs}	virtual sampling period of the oscilloscope
T_W	time window for detection of TOA
TX	transmitter
$W(f)$	frequency spectrum of transmitted pulse $w(t)$

Greek symbols

α_{ch}	channel power decay constant
α_I	narrowband interference fading
δ_{os}	relative deviation of transmitter and receiver oscillators frequencies
ϵ	range error
$\phi_l(t)$	phase of the l -th channel multipath component
$\Gamma\{\cdot\}$	Gamma function of the positive real enclosed
$\kappa(z[n])$	kurtosis of samples $z[n]$
μ_{NC}	Chi-square non centrality parameter
τ	TOA of the received signal after coarse acquisition
τ_0	TOA of the received signal
τ_{cds}	channel delay spread
τ_E	envelope detector time constant
τ_D	differentiator time constant
$\tau_l(t)$	delay of the l -th channel multipath component
τ_{pk}	first peak time of arrival
τ_Q	quantization error in TOA estimation
$\tau_{R,l}$	delay of l -th resolvable multipath component
Ω	amplitude mean square of a Nakagami random variable
ξ_{KS}	Kolmogorov Smirnov significance level
$\zeta_l(t)$	distortion undergone by the l -th channel multipath component



Publications by the Author

Patents, Journals and Letters

- [J.1] G. Bellusci, G.J.M. Janssen, "*Method and Device for Signal Time-of-Arrival Determination*", International Patent no. WO/2010/131966, May 2010.
- [J.2] G. Bellusci, G.J.M. Janssen, J. Yan, C.C.J.M. Tiberius, "*Performance Evaluation of Low-Complexity Receiver Concept for TOA Based UWB Ranging*", submitted to IEEE Transaction on Wireless Communications.
- [J.3] G. Bellusci, G.J.M. Janssen, J. Yan, C.C.J.M. Tiberius, "*Modeling Distance and Bandwidth Dependency of TOA-Based UWB Ranging Error for Positioning*", Hindawi Research Letters in Communications, 2009.
- [J.4] J. Yan, C.C.J.M. Tiberius, P.J.G. Teunissen, G. Bellusci, G.J.M. Janssen, "*A Framework for Low-Complexity Least-Squares Localization with High Accuracy*", accepted for publication, IEEE Transaction on Signal Processing.

Conference Papers

- [C.1] G. Bellusci, G.J.M. Janssen, J. Yan, C.C.J.M. Tiberius, "*A Low-Complexity UWB Receiver Concept for TOA Based UWB Ranging*", Invited Paper, IEEE ICUWB 2009, Vancouver.
- [C.2] J. Yan, C.C.J.M. Tiberius, G. Bellusci, G.J.M. Janssen, "*A Novel Non-Iterative Localization Solution*", IEEE GLOBECOM 2009, Honolulu.

- [C.3] G. Bellusci, G.J.M. Janssen, J. Yan, C.C.J.M. Tiberius, "*A Sub-Sampling Receiver Architecture for Ultra-Wideband Time of Arrival Based Indoor Ranging*", ION GNSS 2009, Savannah.
- [C.4] J. Yan, G. Bellusci, "*Low-complexity Ultra-Wideband Indoor Positioning*", ION GNSS 2009, Savannah.
- [C.5] J. Yan, C.C.J.M. Tiberius, G. Bellusci, G.J.M. Janssen, "*Low Complexity Improvement on Linear Least-Squares Localization*", IEEE ICCS 2008, Guangzhou.
- [C.6] G. Bellusci, G.J.M. Janssen, J. Yan, C.C.J.M. Tiberius, "*A New Approach to Low-Complexity Indoor LOS Range Estimation*", IEEE PIMRC 2008, Cannes.
- [C.7] G. Bellusci, G.J.M. Janssen, J. Yan, C.C.J.M. Tiberius, "*Model of the Distance and Bandwidth Dependency of TOA-Based UWB Ranging Error*", IEEE ICUWB 2008, Hannover.
- [C.8] G. Bellusci, G.J.M. Janssen, J. Yan, C.C.J.M. Tiberius, "*Low Complexity Ultra-Wideband Ranging in Indoor Multipath Environments*", IEEE-ION PLANS 2008, Monterey (Best Paper Award).
- [C.9] J. Yan, C.C.J.M. Tiberius, G. Bellusci, G.J.M. Janssen, "*Feasibility of Gauss-Newton Method for Indoor Positioning*", IEEE-ION PLANS 2008, Monterey.
- [C.10] G. Bellusci, G.J.M. Janssen, J. Yan, C.C.J.M. Tiberius, "*Novel Ultra-Wideband Low-Complexity Ranging Using Different Channel Statistics*", IEEE WCNC 2008, Las Vegas.
- [C.11] J. Yan, G. Bellusci, C.C.J.M. Tiberius, G.J.M. Janssen, "*Analyzing non-Linearity Effect for Indoor Positioning Using an Acoustic Ultra-Wideband System*", IEEE WPNC 2008, Hannover.
- [C.12] G. Bellusci, J. Yan, G.J.M. Janssen, C.C.J.M. Tiberius, "*An Ultra-Wideband Positioning Demonstrator Using Audio Signals*", IEEE WPNC 2007, Hannover.
- [C.13] Z. Irahhtauten, G. Bellusci, G.J.M. Janssen, H. Nikookar, C.C.J.M. Tiberius, "*Investigation of UWB Ranging in Dense Indoor Multipath Environments*", IEEE ICCS 2006, Singapore.

Relation to this Thesis

This thesis is based, in part, on previously published results as listed above. The following table provides a good overview of the major and minor relations between these publications and the chapter of this thesis.

Table 7.1: *Relations between the publication and the chapters of this thesis: ●: major relation; ○: minor relation.*

Publication	Ch. 2	Ch. 3	Ch. 4	Ch. 5	Ch. 6
J.1			○	●	
J.2		○	○	●	●
J.3	○		●		
J.4	○	○			
C.1			○	●	
C.2	○	○			
C.3			○	●	
C.4	○	○			
C.5	○	○			
C.6	●	●			
C.7	●		●		
C.8	●	●			
C.9	○	○			
C.6	●	●			
C.11	○	○			
C.11	○	○			
C.13	○		○		

Samenvatting (Summary in Dutch)

Binnenshuisplaatsbepaling heeft recentelijk veel belangstelling gekregen van zowel het onderzoek als de industrie. Logistiek, gezondheidszorg, het volgen van personen en objecten, spellen en entertainment zijn enkele voorbeelden van toepassingen die kunnen profiteren van nauwkeurige informatie over de locatie. Echter binnenshuis zijn bestaande oplossingen, zoals bijvoorbeeld GPS, niet beschikbaar, onbetrouwbaar of onnauwkeurig. Daarom moeten hiervoor alternatieve oplossingen worden bedacht.

De afgelopen jaren is UWB gidentificeerd als een ideale kandidaat voor binnenshuisplaatsbepaling. Het gebruik van UWB pulsen korter dan een nanoseconde en met een bandbreedte van enkele GHz geeft unieke mogelijkheden om de verschillende gereflecteerde componenten, waaruit een ontvangen signaal bestaat, van elkaar te onderscheiden. Hierdoor kan het aankomsttijdstip, de relevante informatie voor plaatsbepaling, nauwkeurig worden geschat en kan centimeter nauwkeurigheid in de positie worden bereikt, zelfs in omgevingen met veel reflecties. Voordat de mogelijkheden van deze technologie volledig benut kunnen worden moeten er echter nog een aantal zaken worden opgelost:

- UWB signalen vertonen complexe voortplantingsverschijnselen. De grote bandbreedte van deze signalen zorgt er voor dat verschillende frequentiecomponenten van het signaal op een andere wijze reageren op de omgeving. Daarom zijn nieuwe propagatiemodellen, die de interactie van de zich voortplantende golven met de omgeving beschrijven en voorspellen, van essentieel belang; immers het radiokanaal is het belangrijkste element in de bepaling

van de prestaties van het systeem. Beschikbare kanaalmodellen zijn ontwikkeld met het oog op communicatie en missen daarom relevante informatie voor plaatsbepaling.

- Soortgelijke afwegingen gelden ook voor het merendeel van de bekende schattingsalgoritmen voor de aankomsttijd, aangezien deze meestal worden gezien als een simpele uitbereiding van de bekende schattingstechnieken voor de kanaal-impulsresponsie die zijn ontwikkeld voor communicatietoepassingen, waarbij de aankomsttijd van het ontvangen signaal wordt bepaald als een nevenproduct. Deze methoden zijn inherent suboptimaal aangezien ze de unieke eigenschappen van UWB niet meenemen en zich niet focussen op de voor plaatsbepaling relevante informatie. Daarnaast zijn ze lastig voor UWB te implementeren omdat de vereiste hardware en signaalverwerking nog heel complex zijn.

Op grond van bovenstaande motivaties kunnen de originele bijdragen van deze thesis in twee delen worden onderverdeeld. In het eerste deel van deze thesis wordt een nieuw model voorgesteld voor de kanaalkarakterisatie met het oog op het bepalen van de afstand. Dit model kan op vele manieren worden toegepast. Gebruikmakend van het concept van statistische afstandsbepaling kan worden aangetoond dat deze methode de unieke eigenschappen van UWB benut en in staat is om decimeter nauwkeurigheid te bereiken. Dit is een significante verbetering ten opzichte van traditionele methoden terwijl de de hier voorgestelde methode een vergelijkbare complexiteit heeft. Daarnaast is een model ontwikkeld voor het bepalen van de fout in de afstandsbepaling op basis van de aankomsttijd en is er een analyse gemaakt van de invloed van de relevante systeemp parameters op deze fout, zoals de bandbreedte en de afstand tussen zender en ontvanger. Aangetoond is dat met kennis van het kanaalmodel de uiteindelijke positienauwkeurigheid aanzienlijk kan worden verbeterd door gebruikt te maken van de gewogen kleinste-kwadratenmethode. Tenslotte is een LOS/NLOS detectiestrategie ontwikkeld en gevalideerd op de verzamelde testdata. Het tweede deel van dit verslag behandelt een nieuw concept voor de schatting van de aankomsttijd van een signaal en de implementatie hiervan. Deze oplossing benadrukt de unieke eigenschappen van UWB signalen en is in staat om centimeter nauwkeurigheid te halen met een lage complexiteit en sample rates in de orde van enkele tientallen MHz. Hiermee kunnen de beperkingen, die realisatie van een UWB plaatsbepalingssysteem beletten, worden omzeild. In deze context is ook een methode ontwikkeld om de invloed van smalbandige interferentie te evalueren. Aangetoond is dat het

voorgestelde systeem een redelijke resistentie tegen interferentie heeft, waardoor het kan werken in frequentiebanden waarin ook andere systemen actief zijn.

Giovanni Bellusci

April 2010



Acknowledgments

I am indebted to a number of people who directly or indirectly contributed to the work which has been presented in this thesis.

First of all, I would like to sincerely thank my supervisor, Dr. Gerard Janssen for his supervision during these years, for his constructive criticism, for having allowed and encouraged me to conduct my research autonomously and independently, and for the reading and valuable suggestions of the original draft of this thesis. I would also like to express my gratitude for the other people involved in the "HERE" project: a deep thank goes to Dr. Christian Tiberius, for his constant availability and the numerous valuable discussions which helped in improving the content and quality of the work here presented; special thanks to my colleague, Junlin Yan, for his professionalism and friendship, and for the fruitful cooperation. I would also like to owe my gratitude to my promotor, Prof. Ignaas Niemegeers, for giving me the opportunity to pursue my Ph.D. with the Wireless and Mobile Communications group.

Thanks to all my colleagues from the WMC, NAS, and IRCTR groups for their inspiring atmosphere; a particular note is for Zoubir Irahhauteu, for his support in developing the UWB measurement set-up and performing the measurements. I would like to thank Marjon, Laura, Wendy, Dominique, Rowena and Stefanie for their constant help with the administrative matters.

I am especially thankful to all the friends I had the pleasure to meet during my stay in Delft. These years have been an intense and stimulating experience, and it has been a pleasure to share all the moments with you.

Finally, my deepest and sincere gratitude is for my parents, for their uncon-

ditional love, and for their generosity in always giving me the trust, freedom and possibility of expressing myself... Thank You!

Giovanni Bellusci

April 2010



Curriculum Vitae

Giovanni Bellusci was born in Terlizzi (BA), Italy, on July 25, 1981. He obtained the B.Sc. and M.Sc. degrees (both *cum laude*) from the university of Pisa, Italy, in 2003 and 2005, respectively. He carried out his M.Sc. thesis with the Digital Transmissions group of the University of Pisa, working on synchronization algorithms for transmitted reference UWB systems. During the university years, he was also student at "Sant'Anna School of Advanced Studies", after obtaining a five years duration scholarship.

In February 2006 he joined the Wireless and Mobile Communications Group of the Delft University of Technology, where he worked till March 2010 towards his Ph.D. degree; here he has been involved in the project "HERE: Indoor Positioning Using Ultra-Wideband Radio Signals". During this activity, he authored one patent and several scientific contributions; he received the best paper award at the IEEE/ION PLANS Conference 2008, and he was awarded as best Ph.D. student in Telecommunications 2009, from the Dutch Engineering organization KIVI Niria.

